Yang Lu
Trippstadter Straße 121
D–67663 Kaiserslautern

Contributions to the application of adaptive antennas and CDMA code pooling in the TD-CDMA downlink

Beim Fachbereich Elektrotechnik
der Universität Kaiserslautern
zur Verleihung des akademischen Grades
Doktor–Ingenieur (Dr.–Ing.)
eingereichte Dissertation

von

Dipl.–Ing. Yang Lu

Vorwort

Die vorliegende Arbeit entstand in der Zeit von April 1999 bis Oktober 2001 im Rahmen meiner Tätigkeit als wissenschaftlicher Mitarbeiter von Prof. Dr.-Ing. Habil. P.W. Baier am Lehrstuhl für hochfrequente Signalübertragung und -verarbeitung der Universität Kaiserslautern. Ich möchte all jenen danken, die mich während der Entstehung dieser Arbeit unterstützt haben.

Mein besonderer Dank ergeht an Prof. P. W. Baier für die Anregung, die Betreuung und die Förderung meiner Arbeit. Durch seine stete Diskussionsbereitschaft sowie durch zahlreiche Ratschläge und Hinweise hat er wesentlich zum Gelingen dieser Arbeit beigetragen.

Herrn Prof. Dr.-Ing. F. Jondral danke ich für das Interesse an dieser Arbeit und für die Übernahme des Korreferats. Weiterhin danke ich dem Vorsitzenden der Promotionskommission, Herrn Prof. Dr.-Ing. R. Urbansky.

Bei der Universität Kaiserslautern möchte ich mich für die Benutzung leistungsfähiger Rechnersysteme des Regionalen Hochschulrechenzentrums Kaiserslautern (RHRK) bedanken. Den Mitarbeitern des RHRK danke ich auch für die Beratung und Hilfestellung in Rechnerfragen.

Die in der vorliegenden Arbeit enthaltenen Ergebnisse entstanden größtenteils im Rahmen von Projekten, die durch die Deutsche Forschungsgemeinschaft (DFG) gefördert wurden, wofür ich mich bedanken möchte. Im Rahmen dieser Förderung entstand auch eine Zusammenarbeit zu der Arbeitsgruppe Prof. Dr.techn. J.A. Nosseks, Technische Universität München, woraus wichtige Hinweise für meine Arbeit resultierten.

Den jetzigen und den ehemaligen Kollegen am Lehrstuhl für hochquente Signalübertragung und -verarbeitung danke ich für eine angenehme Arbeitsatmosphäre und für viele fruchtbare Diskussionen, die mir oftmals weitergeholfen haben. Ein besonderer Dank ergeht an Herrn Dipl.-Ing. J. Clos für die Unterstützung am Anfang meiner Tätigkeit am Lehrstuhl sowie an Herrn Dipl.-Ing. M. Meurer für die zahlreichen gewinnbringenden Dialoge wissenschaftlichen Inhalts. Eine weitere Dank ergeht an die Studenten, die im Rahmen von Diplomarbeiten unter meiner Anleitung Beiträge zu dieser Arbeit geleistet haben.

Nicht zuletzt möchte ich bei meiner Familie, insbesondere meiner Frau, und meinen Freunden bedanken, die mir immer ein großer Rückhalt waren. Ganz besonders herzlich

bedanke ich meinen Eltern. Sie haben mir das Studium in Deutschland ermöglicht und mich immer nach besten Kräften unterstützen. Ihnen widme ich diese Arbeit.

Düsseldorf, im Januar 2002

Yang Lu

Contents

Chapter 1

Introduction

1.1 Air interface technologies for 3rd generation mobile radio systems

Compared to 2rd generation (2G) mobile radio systems, especially to the successful Global System for Mobile Communications (GSM), which is closely related to the urge for voice communication anywhere, anytime and with anyone [HWB00], 3rd generation (3G) mobile radio systems will offer multimedia services with high user data rates such as audio/video, wireless e-mail, Web browsing, e-commerce and so forth. In order to support these applications, advanced air interface technologies are required. Air interface technologies of mobile radio systems are utilized to fulfill the following tasks:

- Generation of the transmission signals at the transmitter.

- Transmission of the generated signals over the mobile radio channel.

- Estimation of the transmitted signals at the receiver.

In 1998 the five standards developing organizations of Europe, the United States, Japan, Korea and China have agreed to create the Third Generation Partnership Project (3GPP) for the production of 3G mobile system specifications with a view to harmonizing proposals of the regional standardization bodies. It is agreed by 3GPP [3G99] to use the UMTS Terrestrial Radio Access (UTRA) and the evolved GSM network subsystem in the UMTS core network. According to [HWB00] the key decisions of 3GPP on the standards of radio and network technologies are the following:

- Use CDMA for UTRA.

- Build the UMTS Terrestrial Radio Access Network (UTRAN) on the Asynchronous Transfer Mode (ATM).

- Reuse and enhance existing GSM network elements for the UMTS core network.

UTRA consists of the two radio interface modes

- Frequency Division Duplex (FDD) and

- Time Division Duplex (TDD),

where UTRA FDD uses Wideband Code Division Multiple Access (WCDMA) and UTRA TDD uses Time Division Code Division Multiple Access (TD-CDMA). The FDD mode with WCDMA is a pure CDMA-based system and requires paired frequency bands, whereas the TDD mode with TD-CDMA is based on a combination of TDMA (Time Division Multiple Access) and CDMA (Code Division Multiple Access) and is suited for the application in unpaired frequency bands. The parameters of these two transmission modes have been so well harmonized that a common definition of the higher layers should be possible [3G99]. In UTRA, the different service needs can be supported by a combination of FDD and TDD. The FDD mode is claimed to be advantageous for applications in public macro and micro cell environments with high mobility, whereas the TDD is suitable for public micro and pico cell environments with high traffic density [Haa00]. In this thesis only the air interface TD-CDMA is studied.

The structure of the frame and time slot, the latter termed also burst, of TD-CDMA is shown in Fig. 1.1 [Kle96, Ste96, Bla98, May99, Pap00]. From the figure it is seen that in each partial frequency band B and time slot, there are K_s burst signals, i.e., physical channels, each using a specific spreading code.

The burst signal structure of TD-CDMA is shown in Fig. 1.2 [Kle96, Ste96, Bla98, May99, Pap00]. Each time slot of the physical channel k_s, $k_s = 1 \ldots K_s$, consists of two data blocks, a midamble and a guard interval. Each data block of a TDMA burst signal contains N data symbols, and each symbol is spread by a specific CDMA code, which is Q chips long. The midamble and the guard interval contain L_m and L_g chips, respectively.

It is also seen from Fig. 1.1 that, for a fixed modulation scheme and a fixed channel coding rate, the minimal supportable user data rates in TD-CDMA are achieved, when only a single time slot is assigned to the corresponding user within the TDMA frame, and within this time slot a single burst signal. User data rates higher than the minimal supportable user data rates can be supported by using the following approaches:
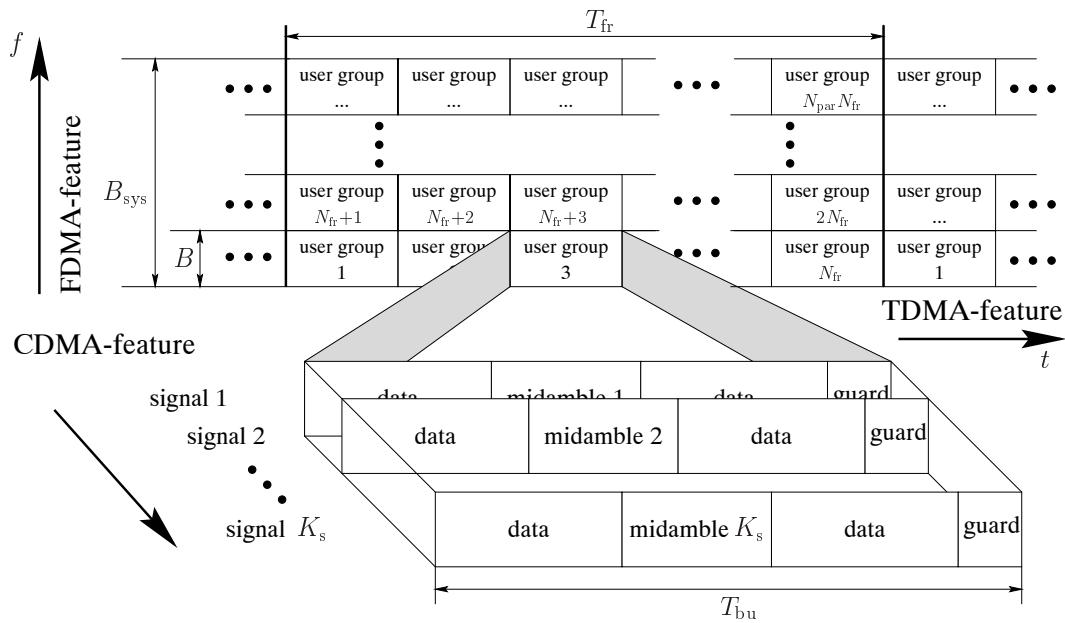
Fig. 1.1: Frame and burst structure of TD-CDMA [Kle96, Ste96, Bla98, May99, Pap00]
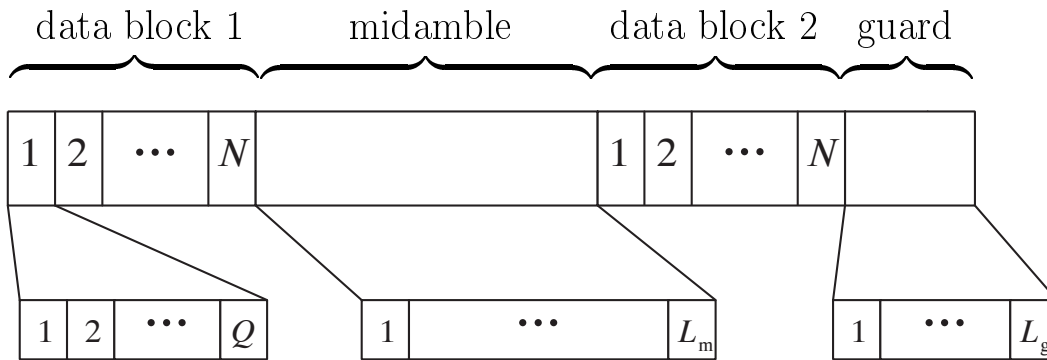
Fig. 1.2: Burst signal structure of TD-CDMA [Kle96, Ste96, Bla98, May99, Pap00]

1. Increasing the number of utilized time slots per user, which is termed time slot pooling.

2. Increasing the number of simultaneously utilized burst signals per user, which is termed CDMA code pooling and will be intensively studied in this thesis.

3. Combining the approaches 1 and 2.

The transmission quality of a mobile radio system is limited by the multiple access interference (MAI) [Lee89]. Thanks to the TDMA component of TD-CDMA, rather few

of user signals are simultaneously active. Therefore, TD-CDMA easily lends itself to the application of multi-user detection (MUD) or joint detection (JD) and of adaptive antennas. JD, by eliminating intracell MAI, i.e., the interference from/to other mobile stations (MS) served by the same base station (BS), considerably enhances system performance [Kle96].

Due to the reciprocity theorem, in TD-CDMA the channel impulse responses valid in uplink and downlink are at least approximately the same, because both links use the same frequency band. Consequently, the channel impulse response estimates obtained at the BS during uplink reception can be directly used for performing downlink beam forming. Therefore, TD-CDMA is, as compared with WCDMA, more suitable for utilizing adaptive transmit antennas. In the following section a brief introduction into the utilization of adaptive transmit antennas in mobile radio systems is given.

1.2 Adaptive transmit antennas in the downlink of mobile radio systems

Since, on the one hand, the number of subscribers to wireless services has enormously increased in the last few years and, on the other hand, 3G mobile radio systems will have to cope with multimedia services with high user data rates, the need for new techniques to improve spectrum utilization is important. Spectrum has become expensive. For instance, in the recent spectrum auction in Germany, companies spent 100 billion DM on UMTS licenses. In order to get a reasonable return on investment, the spectrum obtained through the auction must be used as efficiently as possible. Therefore, 3G mobile radio systems should be designed with a view to achieving high spectrum efficiency.

One approach to a substantial capacity enhancement of 3G mobile radio systems is the use of cell site adaptive antennas. The investigations of using adaptive antennas for mobile radio systems have been the subject of research activities in different research groups over the world in the last few years to overcome the problem of limited available bandwidth by increasing spectrum efficiency [Win84, SBEM90, AMVW91, BS92a, BS92b, MO94, BA94, NPK94, FCB93, ZO95, God97a, God97b, LR99, SOY⁻99, THGM99, GF97, LCL99, Zet86].

In contrast to free space propagation, in which there is only a direct path from the transmitter to the receiver without attenuating objects and multipath reflections, the mobile radio channel is an unpredictable and difficult communications medium. The main

characteristics of the mobile radio channel are shadowing and multipath propagation. Shadowing is caused by obstacles blocking the transmission path and results in slow variations of the powers of the received signals. Therefore, shadowing is also referred to as slow fading [Lee89]. The variation of the received signal powers due to shadowing can often be approximated by a log-normal distribution. Multipath propagation arises from scattering by buildings and other objects and causes differences in the propagation time delays. This scattering produces rapid random amplitude and phase variations in the received signals. Measurements confirm that the fast variations can be approximately characterized by a Rayleigh distribution. Therefore, fast fading is referred to as Rayleigh fading [Lee89]. In addition, the differences in the time delays due to the multipath propagation causes transmitted data impulses to overlap, resulting in intersymbol interference (ISI).

Each of the available frequency bands in mobile radio systems should be reused in order to utilize the assigned spectrum more efficiently. In consequence, the MSs simultaneously using the same partial frequency band B interfere with each other. This multiple access interference is termed co-channel interference.

In order to mitigate the impacts of the unfavorable channel properties and of multiple access interference in mobile radio systems, adaptive antennas can be utilized. An adaptive antenna consists of an array of antenna elements and a real-time signal processor. The potential and the key benefits of using adaptive transmit antennas in the downlink can be classified into the following two categories:

- For a given transmit signal power at the BS, adaptive transmit antennas provide an increase of the receive signal power at the MS. In the other words, for a certain receive signal power at the MS adaptive transmit antennas allow a reduction of the transmit power at the BS, thereby lowering the total co-channel interference in the system.

- Adaptive transmit antennas can be used to spatially separate the signals sent by the BS to the different MSs. This effect is termed signal separation and leads to reduce the power of the interfering signal received at the MSs.

Due to the benefits mentioned above, adaptive transmit antennas help to reduce the outage probability and the bit error rate (BER) for a given system load in terms of the number of the simultaneously active MSs in mobile radio systems. From the cellular network operators' point of view, for a given required quality of service (QoS), adaptive

transmit antennas allow to increase the number the simultaneously active MSs and allow frequency bands to be reused more often in mobile radio systems.

In the uplink of CDMA mobile radio systems the spatial and temporal signal processing can be jointly performed at the BSs [Koh94, IK96]. Considering TD-CDMA, mature algorithms of such a joint spatial and temporal signal processing for the uplink are available in [BSP97, Bla98, PFBB99, Pap00]. The application of these algorithms shows that the system performance of the TD-CDMA uplink can be considerably enhanced by using adaptive antennas. Since this thesis focuses on the study of the application of adaptive transmit antennas in the TD-CDMA downlink, the principal approach and the beam forming strategies to exploit the potential of adaptive transmit antennas in the TD-CDMA downlink are described in what follows.

A section of a cellular network with one reference cell and six adjacent cells is shown in Fig. 1.3. In the reference cell, considering the TD-CDMA downlink, a total number K of MSs are served by the BS with K_s CDMA codes in each partial frequency band B and time slot, see also Fig. 1.1. In contrast to the uplink, when adaptive transmit antennas are utilized at the BS, the spatial signal processing has to be done at the BS, whereas the temporal signal processing is performed at each MS μ_k, $k = 1 \ldots K$. The downlink spatial signal processing of TD-CDMA consists in weighting the transmit signals and feeding them into the K_a transmit antenna elements, see Fig. 1.4. As stated in Section 1.1, in each partial frequency band B and time slot the transmitter simultaneously generates K_s CDMA signals, see Fig. 1.1. If a single omnidirectional antenna is utilized at the BS, all K_s CDMA signals are first added and then fed to this antenna. In the case of a BS with an antenna array of K_a transmit antenna elements, as shown in Fig. 1.4, each of the K_s CDMA signals is first fed into one of the K_s input ports of a weighting network. In this network K_a versions of each CDMA signal k_s are generated by weighting each CDMA signal k_s with the K_a components $\underline{w}_{k_a}^{(k_s)}$, $k_a = 1 \ldots K_a$, of the weight vector

$$\underline{\mathbf{w}}^{(k_s)} = (\underline{w}_1^{(k_s)} \ldots \underline{w}_{K_a}^{(k_s)})^{\mathrm{T}}, \ k_s = 1 \ldots K_s. \tag{1.1}$$

At each of the K_a output ports of the weighting network a linear combination of the K_s input signals appears, which is fed to the corresponding transmit antenna element and transmitted to MS μ_k, $k = 1 \ldots K$. Now, the crucial question is how the antenna weight vectors $\underline{\mathbf{w}}^{(k_s)}$, $k_s = 1 \ldots K_s$, of (1.1), should be chosen in order to optimize the TD-CDMA downlink performance. In what follows, two common algorithms for determining the antenna weight vectors $\underline{\mathbf{w}}^{(k_s)}$, $k_s = 1 \ldots K_s$, of (1.1) are briefly described.

- Maximizing the carrier power C algorithm
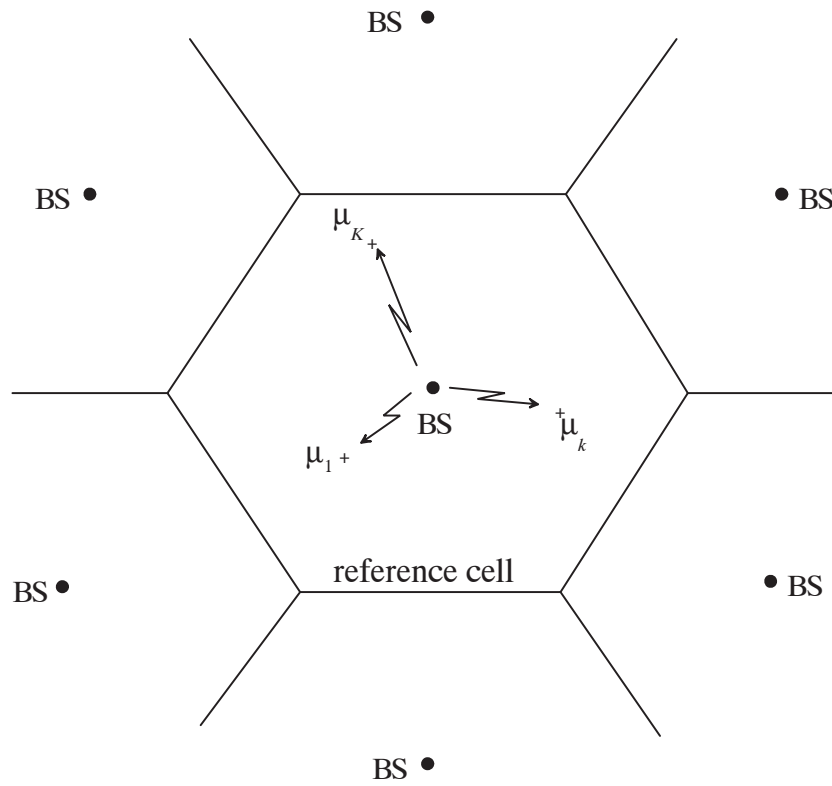
Fig. 1.3: Section of a cellular network with one reference cell and six adjacent cells
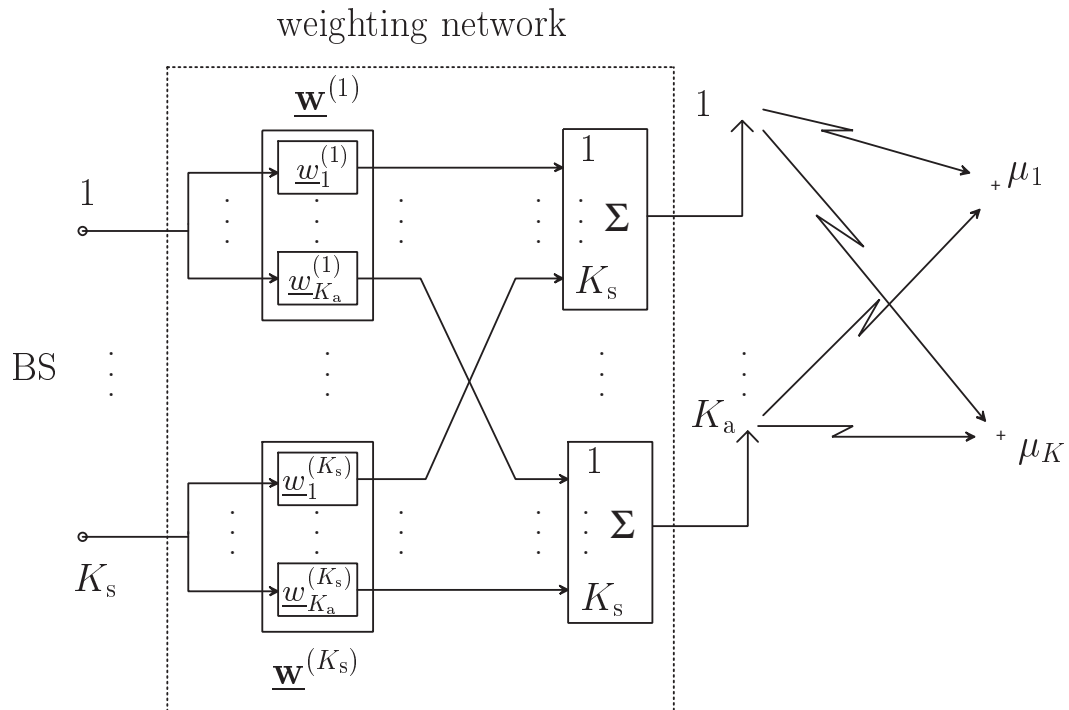
Fig. 1.4: Downlink transmission with adaptive transmit antennas

Considering the cellular network and the downlink transmission with adaptive transmit antennas shown in Figs. 1.3 and 1.4, the BS at the reference cell transmits a CDMA signal k_s to serve MS μ_k. The algorithm determines the antenna weight vector $\underline{\mathbf{w}}^{(k_s)}$, $k_s = 1 \dots K_s$, of (1.1) related to this CDMA signal used to serve MS μ_k in such a way that for a given transmit power, the carrier power C of the desired CDMA signal received at MS μ_k is maximized [LB00a]. This algorithm is termed maximizing C (MC) algorithm. A performance analysis and an application of this algorithm can be found in [LB00b].

- Maximizing the ratio of the carrier power C to the total interference power I algorithm

An algorithm to maximize the ratio of the carrier power C to the total interference power I is proposed in [SB97]. To clarify this algorithm, suppose that the BS at the reference cell transmits a CDMA signal k_s to serve MS μ_k, see Fig. 1.3. Again the carrier power C is defined as the power of the corresponding desired CDMA signal k_s received at MS μ_k. The CDMA signal k_s transmitted to serve MS μ_k causes undesired signals received at other MSs $\mu_{k'}$, $k' \neq k$, located in all cells of the cellular network including or excluding the reference cell. The sum of the powers of these signals is considered as the total interference power I. The interfering CDMA signal caused by the CDMA signal k_s transmitted by the BS in the reference cell to serve MS μ_k also in the reference cell and received at another MS $\mu_{k'}$, $k' \neq k$, in the reference cell is referred to as intracell interference. The interfering signal received at another MS $\mu_{k'}$, $k' \neq k$, not being located in the reference cell is referred to as intercell interference. Whether both intracell and intercell interference or only intercell interference should be taken into account to calculate the total interference power I when utilizing the algorithm for determining the antenna weight vectors $\underline{\mathbf{w}}^{(k_s)}$, $k_s = 1 \dots K_s$, of (1.1), depends on the considered mobile radio system. In the thesis the TD-CDMA mobile radio system is considered as a target system. Therefore, only the intercell interference is taken into account, because the intracell interference can be eliminated by JD [Kle96]. According to the algorithm, the antenna weight vectors $\underline{\mathbf{w}}^{(k_s)}$, $k_s = 1 \dots K_s$, of (1.1) related to CDMA signal k_s, $k_s = 1 \dots K_s$, used to serve MS μ_k are determined in such a way that the ratio of the carrier power C to the total interference power I is maximized. A performance analysis and an application of the algorithm are described in [Sch01]. It should be noted that the ratio of the carrier power C to the total interference power I discussed above is not the true carrier-to-interference ratio (C/I) observed at MS μ_k. Therefore, it is termed pseudo C/I ratio and is designated by $(C/I)_P$ throughout the thesis. Consequently, the algorithm is termed maximizing pseudo carrier-to-interference ratio $(C/I)_P$ (MPCI) algorithm.

Having given an overview of air interface technologies for 3G mobile radio systems in Section 1.1 and discussed the use of adaptive transmit antennas in the downlink of mobile radio systems in Section 1.2, the goals and the contents of the thesis are presented in the following two sections.

1.3   Goals of the thesis

As stated in Section 1.2, the use of adaptive transmit antennas for the TD-CDMA uplink was substantially investigated to a satisfactory extent [BSP97, Bla98, PFBB99, Pap00]. In contrast to the advanced state-of-the-art, the application of adaptive transmit antennas in the TD-CDMA downlink has not yet been extensively studied. Although algorithms for determining the antenna weight vectors $\underline{\mathbf{w}}^{(k_\mathrm{s})}$, $k_\mathrm{s} = 1 \ldots K_\mathrm{s}$, of (1.1) were presented in [Sch01], the research of [Sch01] focused mainly on the utilizing of adaptive transmit antennas on the system level. From this point of view, the aim of this thesis is to extend the research of [Sch01] on the system level and to deliver contributions to the application of adaptive transmit antennas in connection with CDMA code pooling in the TD-CDMA downlink on the link level. To this purpose, the following goals are pursued:

- Developing a concept of utilizing adaptive transmit antennas for the TD-CDMA downlink both on the system level and link level.

- Investigating the performance of this concept in connection with CDMA code pooling on the link level.

- Performing these investigations based on computer simulations.

The main work tasks of the thesis are described as follows:

- In the investigation and analysis of the performance of systems with adaptive transmit antennas for the TD-CDMA downlink on the system level and link level, channel models have a particular relevance. Widely known and used channel models are, for instance, the COST207 [COS89], the ITU [ITU98] and the 3GPP channel models [3G99], which statistically describe the fading effects of the channels. However, these channel models do not provide any directional characteristics of the propagation paths. Therefore, channel models including the directional characteristics, known as directional channel models, will be developed for both system level and link level simulations. Furthermore, in order to investigate the impact of co-channel interference on the system performance, multi-user scenarios will be generated.

- As stated in Section 1.2, in the TD-CDMA uplink the spatial and temporal signal processing can be jointly performed at the BS, whereas in the TD-CDMA downlink the spatial signal processing has to be performed at the BS and the temporal signal processing at the MS. In this thesis, spatial signal processing algorithms for determining the antenna weight vectors $\underline{\mathbf{w}}^{(k_\mathrm{s})}$, $k_\mathrm{s} = 1 \ldots K_\mathrm{s}$, of (1.1) will be developed. These algorithms can also be considered as beam forming algorithms [SB97, Sch01]. Based on these algorithms, the system performance on the system level and link level will be extensively studied.

- A favorite data detection scheme for TD-CDMA is JD, which, by eliminating intra-cell interference, considerably enhances system performance [Naß95, Kle96, Bla98, Pap00]. If conventional JD [Kle96, Bla98, Pap00] is performed at a certain MS μ_k, $k = 1 \ldots K$, both the desired and the undesired CDMA signals arriving at this MS are jointly detected. As mentioned in Section 1.2, the use of suitable algorithms for determining the antenna weight vectors $\underline{\mathbf{w}}^{(k_\mathrm{s})}$, $k_\mathrm{s} = 1 \ldots K_\mathrm{s}$, of (1.1) enables the CDMA signals to be transmitted in a directionally selective manner. This means that the CDMA signals being of interest to a certain MS μ_k, $k = 1 \ldots K$, arrive with more power at this MS than the other undesired CDMA signals. From this point of view, all or one part of the CDMA signals not being of interest to MS μ_k can be excluded from the JD process performed at this MS. This data detection concept is termed partial joint detection (PJD). In the thesis, it will be investigated, how many and which of the undesired CDMA signals arriving at a certain MS μ_k, $k = 1 \ldots K$, should be excluded from JD in order to obtain the maximal possible data transmission quality in terms of the coded BER for a given signal-to-noise ratio (SNR).

- The rapid growth of the demand for Internet/Web access requires higher user data rates transmission in future mobile radio systems. As stated in Section 1.1, in TD-CDMA higher user data rates can be supported by CDMA code pooling. In the case of using this concept, the number of CDMA codes assigned to a specific MS takes values between two and the total number K_s of the available CDMA codes. Each of the K_s CDMA codes assigned to the considered MS determines one CDMA signal. When performing JD at the receiver, each of the CDMA signals experiences a specific SNR degradation [Kle96]. The differences between the SNR degradations of different CDMA signals can be interpreted as a more or less explicit mismatch between the corresponding CDMA codes and the common channel impulse responses. This mismatch is termed CDMA-code/channel mismatch by the author. In the thesis, a forward error correction (FEC) channel coding rate adaptation scheme will be developed which allows to mitigate the impact of the CDMA-code/channel mismatch. As the basic idea of this concept, the channel coding rates of the CDMA signals with larger SNR degradations are chosen lower than those of the CDMA

signals with smaller SNR degradations. In addition or alternatively to this scheme, power control rationales for eliminating the SNR differences of the CDMA signals used to serve a certain MS will also be studied in the link level considerations. In these studies the SNR at the input as well as at the output of the joint detector will be considered.

- In the downlink, the achieved transmission quality is mainly determined by the C/I at the MSs. The C/I at the MS falling short of the required C/I is not acceptable, whereas exceeding the required C/I means to waste capacity. In order to circumvent such an imbalance, appropriate power control scheme is considered. From a system level point of view, the aim of the considered power control is to adjust the transmit powers of all MSs in each burst in such a way that the C/I at each MS in the cellular network attains the same possibly highest level. This power control scheme is termed C/I balancing [SB97, Sch01]. One problem occurring when performing C/I balancing is that, due to C/I balancing, the power differences of the signals transmitted to serve all MSs in a burst may amount to more than 60dB. Such high dynamics cannot be tackled in practical applications due to the nonlinearity and the limited dynamics of the RF amplifiers and other RF components. Consequently, the dynamics of the transmit powers have to be limited within a range of 20dB. Therefore, dynamics constraint algorithms will be developed.

- The computer simulations for investigating the performance of mobile radio systems tend to be time consuming and complex. Therefore, an efficient simulation concept for investigating the performance of the TD-CDMA downlink with adaptive transmit antennas in terms of coded BER to reduce the simulation time and the complexity will be developed in this thesis. The idea of this concept is to achieve an approximation of the coded BER based on the SNR degradation [Kle96, Pap00]. Furthermore, the performance with respect to the simulation time and the accuracy will be compared with that of the conventional simulation concept.

- The traditional channel estimation scheme in mobile radio systems requires training signals, which reduces the effective transmission rate. Based on the orthogonality of signal and noise subspaces, a blind channel estimation concept which needs only one training signal will be developed in this thesis. The performance of this channel estimation concept will be investigated.

- Finally, the spectrum efficiency [Lee89, Ste96, Bla98] in the downlink of TD-CDMA mobile radio system will be investigated.

1.4   Contents of the thesis

Following the goals discussed in Section 1.3, this thesis consists of eight chapters, whose contents are outlined in this section.

First, Chapter 2 deals with directional channel models. A brief introduction is given in Section 2.1. In Section 2.2 a directional channel model including the slow fading and the directional characteristics based on Hata-like propagation gain model [Ste96, Sch01] for system level simulations is introduced. Section 2.3 focuses on directional channel models for link level simulations. In Section 2.3.1 a directional channel model based on the well-known non-directional 3GPP channel model is introduced. Therefore, this directional channel model is termed modified 3GPP channel model in the thesis. Following the approach of [Bla98], another directional channel model based on randomly distributed scattering points around the MSs and near the BS is presented in Section 2.3.2. Therefore, this directional channel model is termed scattering point based channel model in the thesis. The directional channel model based on scattering points is utilized in link level simulations to study the concept CDMA code pooling, whereas the modified 3GPP channel model is suitable for link level simulations to investigate and analyze the effect of co-channel interference resulting in multi-user scenarios.

Chapter 3 focuses on system level simulations. After a brief introduction given in Section 3.1, Section 3.2 describes the considered cellular network consisting of a certain number of identical hexagonal cells. Two algorithms for determining the antenna weight vectors $\underline{\mathbf{w}}^{(k_s)}$ of (1.1) are presented in Section 3.3. The one maximizing the carrier power C at each MS for a given transmit power at the BS is discussed in 3.3.1. The other maximizing the pseudo carrier-to-interference ratio $(C/I)_{\mathrm{P}}$, is described in 3.3.2. Section 3.4 discusses the centralized power control (CPC) scheme [GVGZ94] to balance the C/I of all MSs in the cellular network and consequently, to achieve a equal and possibly highest level of C/I. Finally, the simulation results in terms of the cumulative distribution functions (CDF) of the C/I without and with dynamics constraint of the transmit powers are shown in Section 3.5.1 and 3.5.2, respectively.

In contrast to system level simulations, in link level simulations only an isolated cell consisting of one BS and a number K of MSs is taken into consideration. Data transmission between the BS and the MSs in the isolated cell is simulated. The intercell interference is modeled as white Gaussian noise. The system performance in terms of the coded BER depending on the SNR at the input of the joint detector is investigated in Chapter 4. After an introduction given in Section 4.1, a downlink transmission model based on the characteristics of the used transmit antennas and the properties of the

directional mobile radio channels is described in Section 4.2. If a number K_s of CDMA signals are available to carry the data with a number K_a of transmit antenna elements from the BS to the MSs, the data transmission between the BS and a certain MS μ_k, $k = 1 \ldots K$, can be modeled as a network with K_s input ports and one output port. This network consists of two partial networks described in Sections 4.2.1 and 4.2.2, respectively:

- A linear weighting network with K_s input ports and K_a output ports. This network introduced in Section 1.2, see Fig. 1.4, can perform the linear combinations of the K_s CDMA signals utilizing the antenna weight vectors $\underline{\mathbf{w}}^{(k_\mathrm{s})}$, $k_\mathrm{s} = 1 \ldots K_\mathrm{s}$, of (1.1).

- A network with K_a input ports and one output port modeling the transmission between the inputs of the K_a BS transmit antenna elements and the antenna output of MS μ_k, $k = 1 \ldots K$.

As stated in Section 1.2, the minimal supportable user data rates in TD-CDMA are achieved, if a MS μ_k, $k = 1 \ldots K$, is assigned a single time slot within each frame, and, within this time slot, a single CDMA code, see Fig. 1.1. It has also been mentioned that user data rates higher than the minimal supportable user data rates can be achieved by CDMA code pooling. The mathematical fundamentals of CDMA code pooling are studied in Section 4.3. A number of quantities, vectors, matrices for treating data transmission and detection in the TD-CDMA downlink with adaptive transmit antennas are introduced in Section 4.4. The mathematical description of the two algorithms maximizing the carrier power C and maximizing the carrier-to-interference ratio $(C/I)_\mathrm{p}$ to determine the antenna weight vectors $\underline{\mathbf{w}}^{(k_\mathrm{s})}$ of (1.1) are presented in Section 4.5.

Section 4.6 deals with data detection concept, which is first briefly introduced in Section 4.6.1. As mentioned in Section 1.3, the obvious data detection scheme in TD-CDMA is JD [Kle96]. In the case of conventional JD [Naß95, Kle96, Bla98, Pap00], at each MS not only the CDMA signals transmitted by the BS for this MS, but also the CDMA signals transmitted for all other MSs supported by the same BS are jointly detected. This data detection scheme is discussed in Section 4.6.2. When adaptive transmit antennas are utilized at the BSs, transmitted CDMA signals, by virtue of the directional selectivity of the antenna system, arrive with more or less reduced power at those MSs for which they are not meant. This observation led to PJD, see also Section 1.3. In PJD, at each MS only a part of all transmitted CDMA signals, of course including those being of interest to the specific MS, are jointly detected. This scheme is studied in Section 4.6.3. The optimization of the signal-to-noise-plus-interference ratio (SNIR) with PJD is discussed in Section 4.7. After providing a mathematical description of the effective noise plus interference power in PJD in Section 4.7.1, an algorithm for optimizing the SNIR is

proposed in Section 4.7.2. Then, the application of the SNIR maximization is illustrated by means of an example in Section 4.7.3. In Section 4.7.4, it will be shown that, if the SNR at the input of the joint detector at MS μ_k is below a threshold termed critical SNR, the performance of PJD is better than that of conventional JD. The critical SNR valid for MS μ_k is designated as $\gamma_{\text{crit}}^{(k)}$.

One of the standard performance criteria for mobile radio systems is the coded BER. Traditionally, the coded BER performance of mobile radio systems is investigated by computer simulations such as the well-known Monte-Carlo-Simulation. As a disadvantage of this method in the case of TD-CDMA with JD, a large number of experiments are required, which are usually computationally expensive due to complex matrix calculations and inversions required by JD. In Section 4.8 a more efficient simulation concept is proposed, which yields estimates of the coded BER. After a brief introduction in Section 4.8.1, the coded BER is determined for systems without and with adaptive transmit antennas in Section 4.8.2 and 4.8.3, respectively.

With the algorithms for determining the antenna weight vectors $\underline{\mathbf{w}}^{(k_s)}$ of (1.1) described in Section 4.5 and the data detection schemes discussed in Section 4.4 simulations are performed in order to investigate the performance of systems with adaptive transmit antennas. The simulation results and the discussions are the contents of Section 4.9. First, the considered simulation parameters are summarized in Section 4.9.1. Then, as measures for the algorithms, antenna patterns, signal separation and transmit power reduction are investigated and the simulation results are discussed in Sections 4.9.2, 4.9.3 and 4.9.4, respectively. The average coded BERs depending on the average SNR at the input of the joint detector when performing conventional JD and PJD are presented in Section 4.9.5.

When performing traditional channel estimation training signals are required [Ste95], which result in reduction of the effective transmission rate. Therefore, a blind channel estimation concept is proposed in Chapter 5. The basic idea behind this concept is to estimate the channel impulse responses based on the orthogonality of the signal and the noise subspaces.

As stated in Section 1.2, higher user date rate is one of the necessary requirements for future mobile radio systems to support the applications such as Web browsing and wireless internet access. To this purpose, CDMA code pooling is considered. This concept results in multi-channel transmission, which will be discussed in Chapter 6. Section 6.1 provides a brief introduction. A simplified additive white Gaussuian noise (AWGN) multi-channel model describing the signal transmission between the BS and MS μ_k, $k = 1 \dots K$, is derived in Section 6.2. Based on this model a concept to maximize the total channel capacity with constant input SNR averaged over all CDMA signals received at this MS

is presented in Section 6.3.1 and the corresponding results are shown in Section 6.3.2. Section 6.4 deals with CDMA-code/channel mismatch mentioned in Section 1.2 and start with an introduction in Section 6.4.1. Under consideration of both single-direction and multi-direction channel models the SNR degradations are mathematically analyzed in Sections 6.4.2 and 6.4.3, respectively. For mitigating the impact of the CDMA-code/channel mismatch on the system performance, different concepts are developed.

- First, as discussed in Section 1.1, the N data symbols of each burst signal within a time slot, see Fig. 1.4, will be transmitted by using a user specific CDMA code. Now, if these N data symbols are transmitted by using different CDMA codes, this concept is termed CDMA code interleaving. It will be studied in Section 6.5.1.

- Second, two power control rationales for mitigating the effect of CDMA-code/channel mismatch are presented in Section 6.5.2.

These concepts are discussed in detail in Section 6.5 and the simulation results concerning these concepts are shown and discussed in Section 6.5.3.

Adaptive data rate schemes are of interest to improve the performance of data transmission over mobile radio channels with time variant SNR due to fading and time variant interference in mobile radio channels. In the case of FEC coded transmission the information data rate can be adapted by properly choosing

1. the modulation scheme, that is the symbol alphabet, or

2. the FEC coding rate.

These two approaches can be followed either excluding or in combination. In Section 6.6, an adaptive data rate approach with fixed modulation scheme QPSK and varied channel coding rate is discussed.

In Chapter 7 the spectrum efficiency of the TD-CDMA downlink utilizing adaptive transmit antennas is investigated. Section 7.1 provides the definition of the spectrum efficiency and the simulation method. The corresponding simulation result in terms of the outage probability is presented in Section 7.2.

Finally, Chapter 8 summarizes the results of Chapters 2 to 7 in English and German and concludes the thesis.

Chapter 2

Directional channel models

2.1   Introduction

As stated in Chapter 1, in order to exploit the potential of utilizing adaptive transmit antennas in the TD-CDMA downlink, the performance of spatial signal processing in terms of the algorithms for determining the antenna weight vectors $\underline{\mathbf{w}}^{(k_{\mathrm{s}})}$ of (1.1) and the performance of temporal signal processing in terms of the data detection algorithms should be investigated. To this purpose, realistic and simply generated directional channel models are required. As already mentioned in Section 1.4, in the present chapter, a channel model including the slow fading and the directional characteristics considered for system level simulations is presented in Section 2.2. In Section 2.3 two different directional channel models for link level simulations including the fast fading and the directional characteristics are presented. A certain MS is designated by the symbol μ_m in the system level considerations, and by the symbol μ_k in the link level considerations. These designations are chosen in order to harmonize the designations in this thesis with those used in other publications of the Research Group for RF Communications at University of Kaiserslautern as for instance [Kle96, Ste96, Bla98, May99, Web00, Pap00, Sch01, Ost01].

2.2   Directional system level channel model

Fig. 2.1 shows a finite cellular scenario of identical hexagonal cells considered for system level simulations. In this cellular scenario, each BS is located in the center of the

- **BS**

+ **MS**
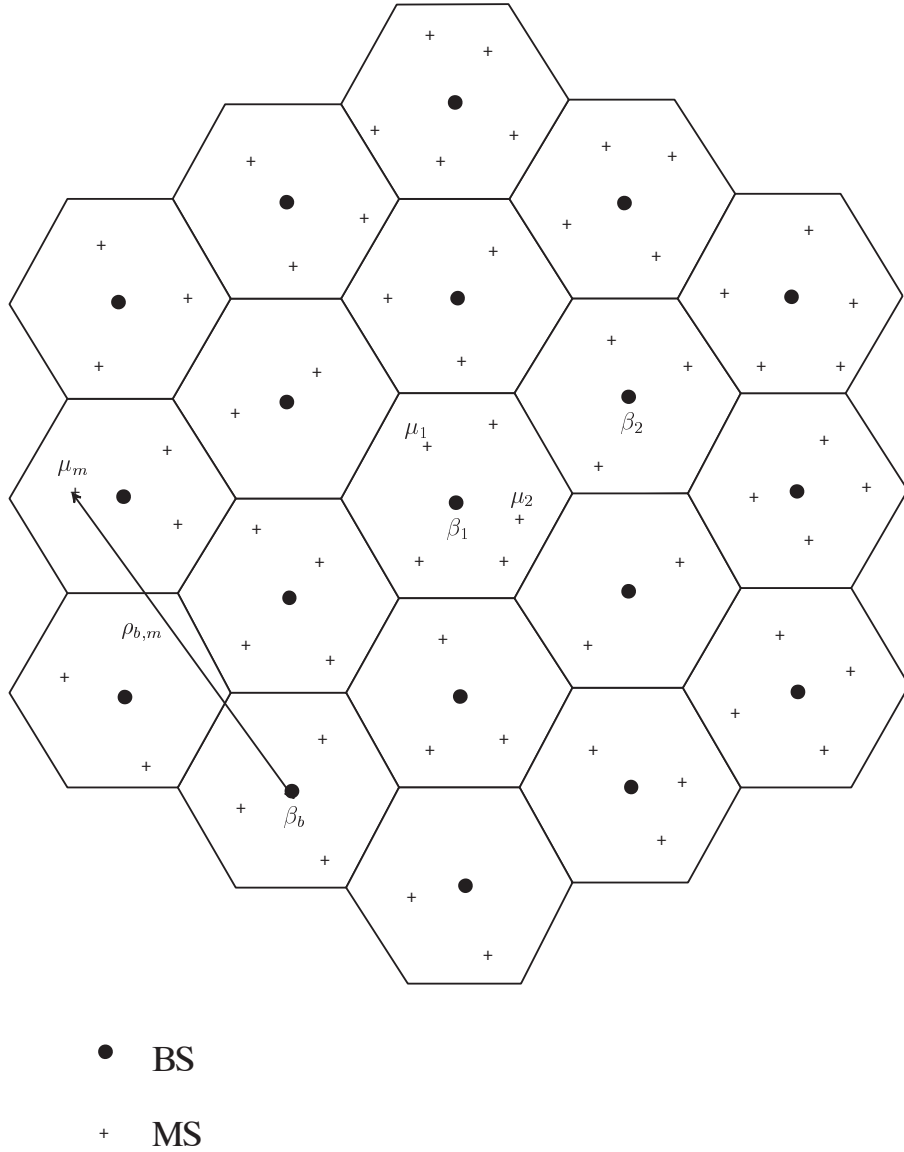
Fig. 2.1: Model scenario for system level simulations

corresponding cell. The BSs form the set

$$\mathbb{B} = \left\{ \beta_1 \ \ldots \ \beta_b \ \ldots \ \beta_{|\mathbb{B}|} \right\}, \tag{2.1}$$

where the cardinality $|\mathbb{B}|$ of $\mathbb{B}$ is the total number of the BSs or the cells in the cellular scenario. The MSs are randomly distributed over the cellular scenario and form the set

$$\mathbb{M} = \left\{ \mu_1 \ \ldots \ \mu_m \ \ldots \ \mu_{|\mathbb{M}|} \right\}, \tag{2.2}$$

where the cardinality $|\mathbb{M}|$ of $\mathbb{M}$ is the total number of the MSs in the cellular scenario. In the considered channel model for system level simulations it is assumed that only one

relevant propagation path from BS β_b, $b = 1 \ldots |\mathbb{B}|$, to MS μ_m, $m = 1 \ldots |\mathbb{M}|$, exists. This propagation path originates in the line-of-sight (LOS) from BS β_b, $b = 1 \ldots |\mathbb{B}|$, to MS μ_m, $m = 1 \ldots |\mathbb{M}|$. The assumption holds if the largest amount of the received signal power at the BS is impinging from a small angular range around the LOS [KMT⁻96, SB97]. For each propagation path from BS β_b, $b = 1 \ldots |\mathbb{B}|$, to MS μ_m, $m = 1 \ldots |\mathbb{M}|$, see Fig. 2.1, a propagation gain $g_{b,m}$ can be determined by applying a Hata-like propagation gain model, which also accounts for shadowing effects, as described in the following. According to [Ste96, Sch01], $g_{b,m}$ depends on the geometrical length $\rho_{b,m}$ of the propagation path from BS β_b, $b = 1 \ldots |\mathbb{B}|$, to MS μ_m, $m = 1 \ldots |\mathbb{M}|$, see Fig. 2.1, on the attenuation coefficient α, and on the shadowing factor represented by a random variable $\xi_{b,m}$ as follows:

$$g_{b,m} = \frac{1}{\xi_{b,m} \rho_{b,m}^{\alpha}}. \tag{2.3}$$

$\xi_{b,m}$ in (2.3) is log-normal distributed and can be derived from a Gaussian random variable $\chi_{b,m}$ with zero mean and standard deviation σ by the transformation

$$\xi_{b,m} = 10^{-\chi_{b,m}/10}. \tag{2.4}$$

The Gaussian random variable $\chi_{b,m}$ in (2.4) is termed the logarithmic shadowing factor of the propagation path from BS β_b, $b = 1 \ldots |\mathbb{B}|$, to MS μ_m, $m = 1 \ldots |\mathbb{M}|$ [MS99]. Moreover, from the locations of the BSs and the MSs in the cellular scenario, the direction of departure (DOD) and the direction of arrival (DOA) pertaining to the propagation path from BS β_b, $b = 1 \ldots |\mathbb{B}|$, to MS μ_m, $m = 1 \ldots |\mathbb{M}|$, can be determined at BS β_b and MS μ_m, respectively.

In summary, the system level directional channel model for the propagation from BS β_b, $b = 1 \ldots |\mathbb{B}|$, to MS μ_m, $m = 1 \ldots |\mathbb{M}|$, is characterized by

- a single relevant propagation path from BS β_b, $b = 1 \ldots |\mathbb{B}|$, to MS μ_m, $m = 1 \ldots |\mathbb{M}|$,

- a corresponding propagation gain $g_{b,m}$ of (2.3), and

- a DOD and a DOA at BS β_b, $b = 1 \ldots |\mathbb{B}|$, and MS μ_m, $m = 1 \ldots |\mathbb{M}|$, respectively.

2.3   Directional link level channel models

2.3.1   Modified 3GPP channel model

As stated in Section 1.3, the well-known 3GPP channel model [3G99] does not provide the directional characteristics for the taps introduced in this channel model. Therefore,

the 3GPP channel model is not suitable for investigating the performance of the spatial signal processing when utilizing adaptive transmit antennas. From this viewpoint, a simple, but nevertheless realistic and simply established modified 3GPP channel model is proposed in this section. The main idea behind establishing this modified 3GPP channel model is to assign an individual directional characteristic to each tap of the original 3GPP channel model. Obviously, in the most simplest way, the directional characteristics could be chosen from an uniform distribution on the interval $[0, 2\pi)$. In this section, a more realistic approach is introduced. In order to clarify this approach, the key parameters are introduced based on a configuration of a single cell multi-user scenario as shown in Fig. 2.2. This scenario allows to investigate the performance of the algorithms for determining the antenna weight vectors $\underline{\mathbf{w}}^{(k_\mathrm{s})}$ of (1.1) aiming at suppressing and mitigating co-channel interference when utilizing adaptive transmit antennas at the BS.

In the model scenario shown in Fig. 2.2, all K MSs are uniformly spaced over the angular domain Ω. MSs μ_k, $k = 1 \ldots K$, are assumed to be shifted in azimuth by the angles $\varphi^{(k)}$, $k = 1 \ldots K$, relative to the Reference Direction (RD). Therefore, the LOSs from the BS to MSs μ_k, $k = 1 \ldots K$, are given by $\varphi^{(k)}$, $k = 1 \ldots K$. The angular range around the LOS, also referred to as the angular spread, pertaining to each MS is assumed to be the same and is characterized by the angle β. The angular separation of two adjacent MSs is

$$\Delta\varphi = \begin{cases} \frac{\Omega}{K} & \text{if} \quad \Omega = 2\pi, \\ \frac{\Omega}{K-1} & \text{else.} \end{cases} \tag{2.5}$$

With $\varphi^{(1)}$ the LOS from the BS to MS μ_1, the LOS from the BS to any MS μ_k becomes

$$\varphi^{(k)} = (k-1)\Delta\varphi + \varphi^{(1)}, \ k = 1 \ldots K. \tag{2.6}$$

Now, consider the case that the BS transmits a signal to serve MS μ_k, see Fig. 2.2, over a directional channel containing a certain number K_e of propagation paths. At the BS the DODs of the transmitted signal are assumed to be distributed in the angular range β around the LOS from the BS to MS μ_k. Then each of the K_e propagation paths can be viewed as caused by a virtual scattering point situated in the range β. Using scattering points to generate directional channel model will be described in detail in Section 2.3.2. Therefore, the directional characteristic belonging to each of the K_e propagation paths can be characterized by an azimuthal angle $\varphi^{(k,k_\mathrm{e})}$, $k_\mathrm{e} = 1 \ldots K_\mathrm{e}$, relative to the RD in the interval $[\varphi^{(k)} - \frac{\beta}{2}, \varphi^{(k)} + \frac{\beta}{2}]$. How the K_e propagation paths from the BS to MS μ_k are determined and how the directional characteristics in terms of $\varphi^{(k,k_\mathrm{e})}$ are assigned to the corresponding propagation paths from the BS to MSs μ_k, $k = 1 \ldots K$, will be described in the following.

Suppose that the original 3GPP channel model has L_a propagation paths. In order to generate a modified 3GPP channel model which includes DODs and angular spread
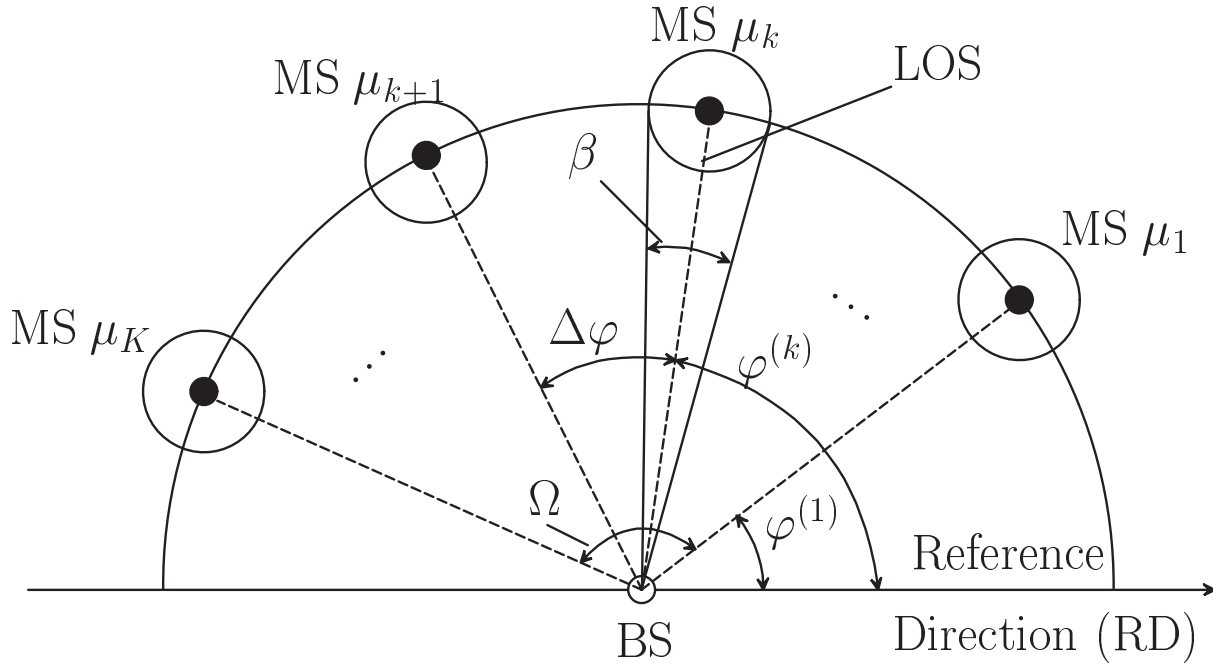
Fig. 2.2: Model scenario for link level simulations

β, each of the L_a propagation paths is split up into two partial propagation paths. This leads to the total number

$$K_e = 2L_a \tag{2.7}$$

of the propagation paths of the modified 3GPP channel model. The assignment of the directional characteristics to the K_e partial propagation paths is shown in Fig. 2.3. The directions of the two splitted partial propagation paths are assumed to be symmetrically arranged with respect to the LOS from the BS to MS μ_k. For instance, consider $\varphi^{(k,k_e)}$ and $\varphi^{(k,k_e+1)}$ in Fig. 2.3. Then, the difference between the directions of two adjacent partial propagation paths is, with the angular spread β,

$$\Delta\beta = \frac{\beta}{K_e - 1}. \tag{2.8}$$

Finally, with the LOS from the BS to MS μ_k characterized by $\varphi^{(k)}$ of (2.6), the angular spread β and $\Delta\beta$ of (2.8), the direction assigned to propagation path k_e in the modified 3GPP channel model considered for MS μ_k takes the form

$$\varphi^{(k,k_e)} = \varphi^{(k)} - \frac{\beta}{2} + (k_e - 1)\frac{\beta}{K_e - 1}, \quad k_e = 1 \ldots K_e. \tag{2.9}$$
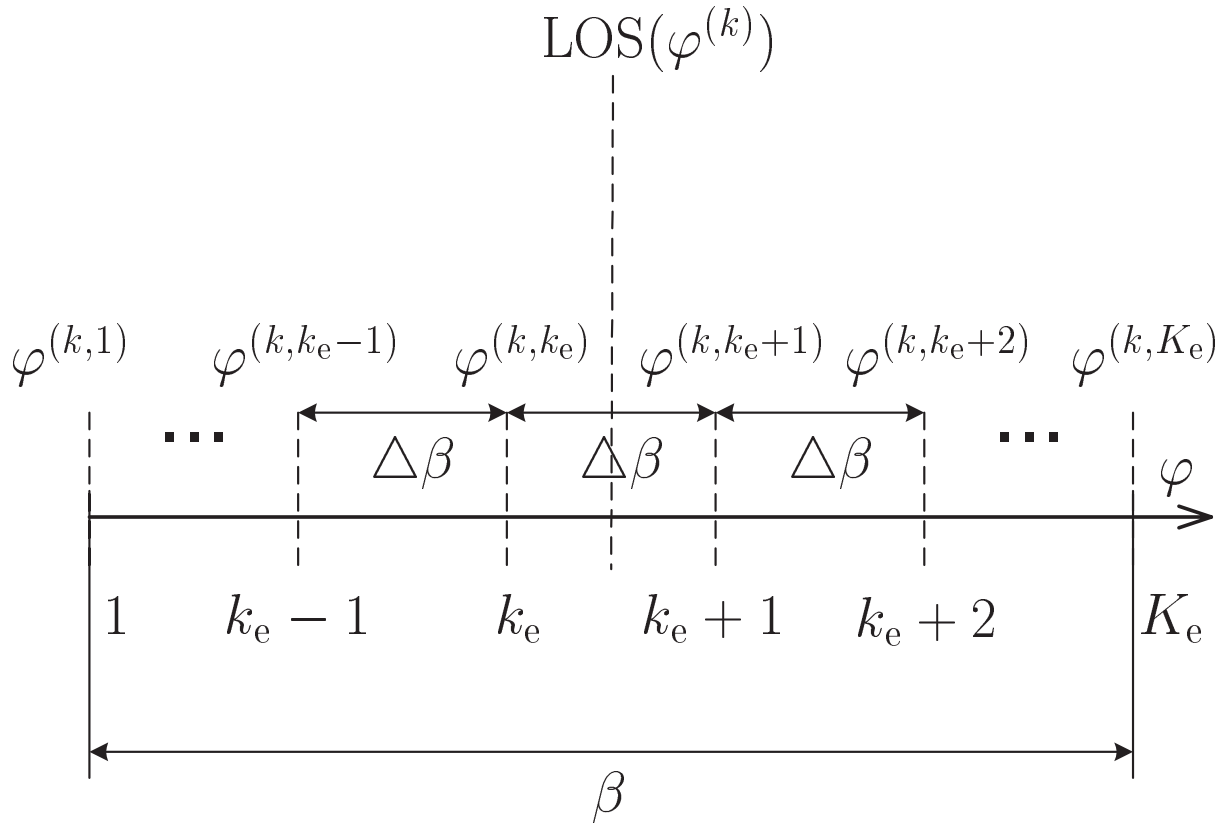
Fig. 2.3: Assignment of the directions to the partial propagation paths of the modified 3GPP channel model valid for MS μ_k

It should be noted that $\varphi^{(k,k_e)}$ of (2.9) assigned to partial propagation path k_e obtained by splitting a certain propagation path of the original 3GPP channel model should be close to the user specific LOS $\varphi^{(k)}$ of (2.6), if the relative delay of this original propagation path of the 3GPP channel models is small.

The value of the angular spread β heavily depends on the propagation environments. In [Bla98] it is shown that in small cells the value of β is large while in large cells it is small. This observation allows to consider different propagation environments, e.g., large or small cells, by choosing the value of β correspondingly.

In Summary, the modified 3GPP channel model derived from the original 3GPP channel model can be characterized by

- a number K_e of propagation paths, see (2.7), and

- a number K_e of corresponding directions $\varphi^{(k,k_e)}$, $k_e = 1 \ldots K_e$, of (2.9).

The main advantages of the modified 3GPP channel model are the following:

Tab. 2.1: Propagation conditions for multipath fading environments [3G99]

relative delay /ns	average power /dB
0	0
260	-3
521	-6
781	-9

- It is simple to generate, because only a few parameters are required. This allows extensive simulations in a short time.

- It reflects the essential physical propagation mechanisms including the angular spread.

Based on the propagation conditions for multipath fading environments of the 3GPP channel model case 3 [3G99] as shown in Fig. 2.1, the directions $\varphi^{(k,k_e)}$, $k_e = 1 \ldots K_e$, of (2.9) of the modified 3GPP directional channel model valid for MS μ_1 with $\varphi^{(1)} = 0°$ and $\beta = 30°$ can be determined according to (2.9) as shown in Tab. 2.2.

Tab. 2.2: Examplary directional channel model derived from the 3GPP channel model case 3; $\varphi^{(k)} = 0°$, $\beta = 30°$ and $K_e = 8$

k_e	relative delay /ns	$\varphi^{(k,k_e)}$	k_e	relative delay /ns	$\varphi^{(k,k_e)}$
1	781	$-15°$	5	0	$2.14°$
2	521	$-10.71°$	6	260	$6.43°$
3	260	$-6.43°$	7	521	$10.71°$
4	0	$-2.14°$	8	781	$15°$

The channel impulse response valid for each of the L_a propagation paths introduced in the original 3GPP channel model can be obtained by low-pass filtering utilizing a low-pass filter of bandwidth $2f_c$ and subsequent sampling with the sampling frequency f_c, where f_c is the chip rate. Considering the modified 3GPP channel model, the channel impulse responses valid for the two splitted propagation paths originating in the corresponding propagation path of the 3GPP channel model, are assumed to be exactly identical. Each is equal to one half of the channel impulse responses derived from the corresponding original propagation path of the 3GPP channel model. This assumption means that the modified 3GPP channel model and the original 3GPP channel model lead to the same channel impulse response, if a single omnidirectional antenna is utilized at the BS.

2.3.2   Channel model based on scattering points

In this section, a directional channel model based on randomly distributed scattering points, which are concentrated in scattering areas, is described. When establishing this channel model, an approach similar to which is presented in [Bla98] is followed. This channel model is suitable for the case that only two MSs are supported by the BS, while CDMA code pooling is applied.

Fig. 2.4 shows this channel model. The two MSs μ_1 and μ_2 lie in the center of a scattering area each, and a third scattering area is located near the BS. Each of the three scattering areas has the diameter D and contains the same number of randomly distributed scattering points. The total number of scattering points of the channel model valid for each MS is K_e, and the individual scattering point is marked by its number $k_e = 1 \ldots K_e$. All K_e scattering points are assumed to have the same scattering coefficient. The angular separation between the two MSs μ_1 and μ_2 is $\Delta\varphi$ and the two MSs μ_1 and μ_2 lie symmetrically to the connecting line between the BS and the center of the scattering area close to the BS. The distance between the BS and the MSs is termed d, and the distance between the BS and the center of the scattering area close to the BS is $0.3d$. Single point scattering is assumed for each propagation path from the BS to the MSs μ_1 and μ_2, and the LOS is excluded. The scattering points around each MS are assumed to be relevant only for this MS. This means that no propagation paths leading from the BS to MS μ_1 over scattering points around MS μ_2 are considered. Additionally, there are no other objects except for the corresponding scattering points on each propagation path between the BS and MSs μ_1 and μ_2.

In addition to the parameters introduced above, the remaining important parameters for generating the scattering point based channel model are defined in Fig. 2.5. The azimuthal angle between the x-axis and propagation path k_e at BS is $\varphi_e^{(k,k_e)}$ and at MS μ_k is $\varphi_s^{(k,k_e)}$. The velocity of MS μ_k is $v^{(k)}$ and the moving direction is characterized by the azimuthal angle $\varphi_v^{(k)}$. The distances from the BS to scattering point k_e and from scattering point k_e to MS μ_k are termed $r_1^{(k,k_e)}$ and $r_2^{(k,k_e)}$, respectively. Therefore, the propagation path from the BS over scattering point k_e to MS μ_k has the total length

$$l^{(k,k_e)} = r_1^{(k,k_e)} + r_2^{(k,k_e)}, \ \ k = 1 \ldots K, \ \ k_e = 1 \ldots K_e. \tag{2.10}$$

With the velocity c_0 of light, the delay of propagation path k_e from the BS to the MS μ_k becomes

$$\tau^{(k,k_e)} = \frac{l^{(k,k_e)}}{c_0} = \frac{r_1^{(k,k_e)} + r_2^{(k,k_e)}}{c_0}, \ \ k = 1 \ldots K, \ \ k_e = 1 \ldots K_e. \tag{2.11}$$
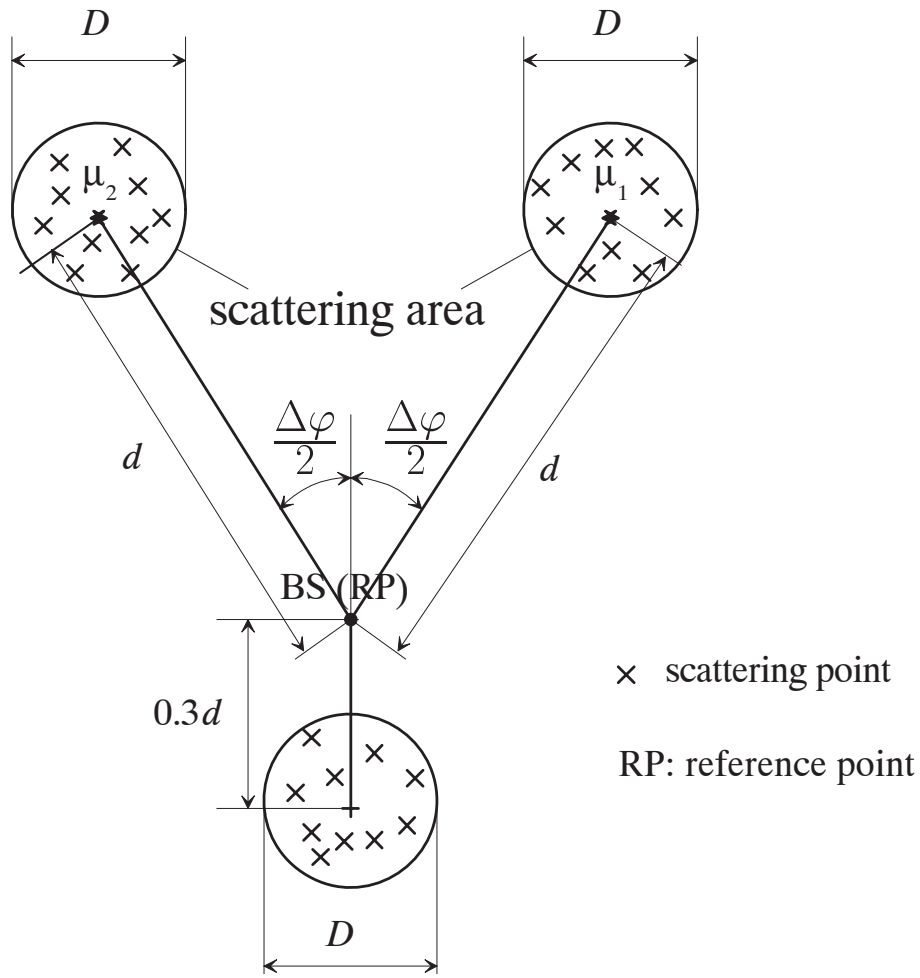
Fig. 2.4: A simple directional channel model based on scattering points considered in link level simulations

Following [Fuh97, Bla98] the relative amplitude of the signal received at MS μ_k over propagation path k_e from the BS to MS μ_k is assumed to take the value

$$a^{(k,k_e)} = \frac{1}{r_1^{(k,k_e)} r_2^{(k,k_e)}}, \quad k = 1 \ldots K, \ k_e = 1 \ldots K_e. \tag{2.12}$$

Furthermore, with the carrier wavelength λ, the angles $\varphi_s^{(k,k_e)}$ and $\varphi_v^{(k)}$ and the velocity $v^{(k)}$ of MS μ_k, see Fig. 2.5, the Doppler shift

$$f_D^{(k,k_e)} = \frac{v}{\lambda} \cos(\varphi_s^{(k,k_e)} - \varphi_v^{(k)}), \quad k = 1 \ldots K, \ k_e = 1 \ldots K_e, \tag{2.13}$$

of propagation path k_e from the BS to MS μ_k is introduced. Then, with the delay $\tau^{(k,k_e)}$ of (2.11), the relative amplitude $a^{(k,k_e)}$ of (2.12) and the Doppler shift $f_D^{(k,k_e)}$ of (2.13) related to propagation path k_e from the BS to MS μ_k, the non-bandlimited directional
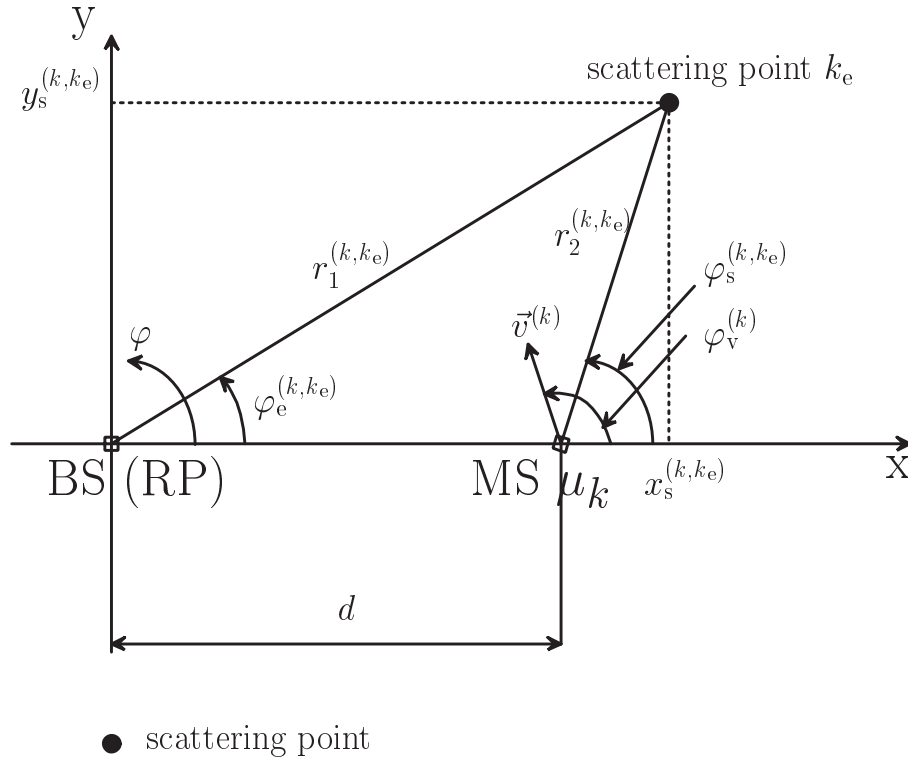
Fig. 2.5: Parameters for generating the scattering point based channel model

channel impulse response of propagation path k_e from the BS to MS μ_k becomes

$$
\begin{aligned}
\underline{h}_\mathrm{d}^{(k,k_\mathrm{e})}(\tau, t, \varphi) \;\; = \;\; & \frac{1}{r_1^{(k,k_\mathrm{e})} r_2^{(k,k_\mathrm{e})}} \exp(-\mathrm{j}2\pi f_\mathrm{c} \tau^{(k,k_\mathrm{e})}) \exp(\mathrm{j}2\pi f_\mathrm{D}^{(k,k_\mathrm{e})} t) \\
& \delta(\tau - \tau^{(k,k_\mathrm{e})}) \delta(\varphi - \varphi_\mathrm{e}^{(k,k_\mathrm{e})}).
\end{aligned} \tag{2.14}
$$

Similar to generating the modified 3GPP channel model introduced in Section 2.3.1, the directional channel impulse responses $\underline{\mathbf{h}}_\mathrm{d}^{(k,k_\mathrm{e})}$ valid for propagation path k_e from the BS to MS μ_k are obtained by low-pass filtering the non-bandlimited directional channel impulse responses $\underline{h}_\mathrm{d}^{(k,k_\mathrm{e})}(\tau, t, \varphi)$ of (2.14), originating in the propagation environment of Fig. 2.4 by a low-pass filter of bandwidth $2f_\mathrm{c}$ and subsequent sampling with the sampling frequency f_c, where f_c is the chip rate. Each directional channel impulse response $\underline{\mathbf{h}}_\mathrm{d}^{(k,k_\mathrm{e})}$ is represented by W samples, with the first sample corresponding to the shortest delay between the BS and MS μ_k. Non zero sample values beyond said W sample values are set to zero.

Chapter 3

System level considerations

3.1   Introduction

As stated in Section 1.3, in order to assess the performance of mobile radio systems with adaptive transmit antennas in accordance with the spatial signal processing, computer simulations have to be performed on the system level. In system level simulations the transmission quality in terms of C/I at each MS μ_m in a cellular scenario consisting of a certain number of identical hexagonal cells, see Fig. 2.1, is investigated. Then, the statistic of C/I, i.e., the CDF Prob($C/I \leq \Gamma$), is determined by C/I balancing. To this purpose, a two-step simulation procedure is applied [SB97, Sch01]:

- First, the antenna weight vectors

$$\mathbf{\underline{w}}_{b,m} = (\underline{w}_{b,m,1} \ldots \underline{w}_{b,m,K_\mathrm{a}})^\mathrm{T} \tag{3.1}$$

  related to the signal transmitted by BS β_b, $b = 1 \ldots |\mathbb{B}|$, in the cellular scenario to serve MS μ_m, $m = 1 \ldots |\mathbb{M}|$, are determined by applying the MC or MPCI algorithm as discussed in Section 1.2.

- Second, in order to achieve the same and highest possible C/I, the CPC algorithm [GVGZ94] mentioned in Section 1.4 is used to balance C/I by adjusting the transmit powers for all MSs μ_m, $m = 1 \ldots |\mathbb{M}|$, in the cellular scenario.

This chapter provides a comprehensive view of the concept and is organized as follows. The considered cellular scenario and the mathematical descriptions of the carrier power

C_m and the total interference power I_m related to a certain MS μ_m, $m = 1 \ldots |\mathbb{M}|$, in the cellular scenario are presented in Section 3.2. Section 3.3 focuses on the algorithms for determining the antenna weight vectors $\underline{\mathbf{w}}_{b,m}$ of (3.1). The MC algorithm is discussed in Section 3.3.1, whereas Section 3.3.2 deals with the MPCI algorithm. In Section 3.4, the C/I balancing concept is presented. The obtained simulation results in terms of the CDF of C/I are given in Section 3.5. The results shown in Section 3.5.1 are valid for the case without transmit power limitations, whereas the results obtained with constraining the transmit power dynamics are shown in Section 3.5.2. Note that the concept CDMA code pooling is excluded in system level simulations discussed in this thesis. This concept could be included in further research on investigating the TD-CDMA downlink with adaptive transmit antennas on the system level.

3.2   Considered cellular scenario

As shown in Fig. 2.1 and stated in Section 2.2, the cellular scenario considered in the thesis for system level simulations consists of a number of identical hexagonal cells. As also mentioned earlier, each of the $|\mathbb{B}|$ BSs is located in the center of the corresponding cell, whereas the $|\mathbb{M}|$ MSs are randomly distributed over the cellular scenario. The average number of MSs per cell is termed $\bar{K}$. An uniform linear array (ULA) of K_a omnidirectional transmit antenna elements with half wavelength inter-element distance is used at each BS, whereas each MS has only a single omnidirectional receive antenna. For the following mathematical analysis it is useful to introduce the relation [Ste96]

$$m \mapsto z(m), \ m = 1 \ldots |\mathbb{M}|, \ z(m) = 1 \ldots |\mathbb{B}|, \tag{3.2}$$

which uniquely assigns MS μ_m to BS $\beta_{z(m)}$. As stated in Section 1.2, co-channel interference occurs because of the simultaneous use of the same partial frequency band B, see Fig. 1.1, to serve different MSs μ_m, $m = 1 \ldots |\mathbb{M}|$, in the cellular scenario. With the relation (3.2), the interference situation of MS μ_m, $m = 1 \ldots |\mathbb{M}|$, can be mathematically described as follows. When BS $\beta_{z(m)}$ serves MS μ_m, the signal transmitted by BS $\beta_{z(m)}$ to MS μ_m is received not only by MS μ_m, but also by the $(|\mathbb{M}| - 1)$ other MSs $\mu_{\tilde{m}}$, $\tilde{m} \neq m$. Each MS μ_m, $m = 1 \ldots |\mathbb{M}|$, is in a specific interference situation. The set consisting of all those MS $\mu_{\tilde{m}}$, $\tilde{m} = 1 \ldots |\mathbb{M}|$, with $\beta_{z(\tilde{m})}$ being an interfering BS for the considered MS μ_m is given by [Ste96]

$$\mathbb{I}_m = \{\mu_{\tilde{m}} \setminus \mu_m\}. \tag{3.3}$$

The set $\mathbb{I}_m$ of (3.3) depends on the data detection scheme applied in the mobile radio system. As mentioned in Section 1.2, if JD is used in TD-CDMA, intracell interference is
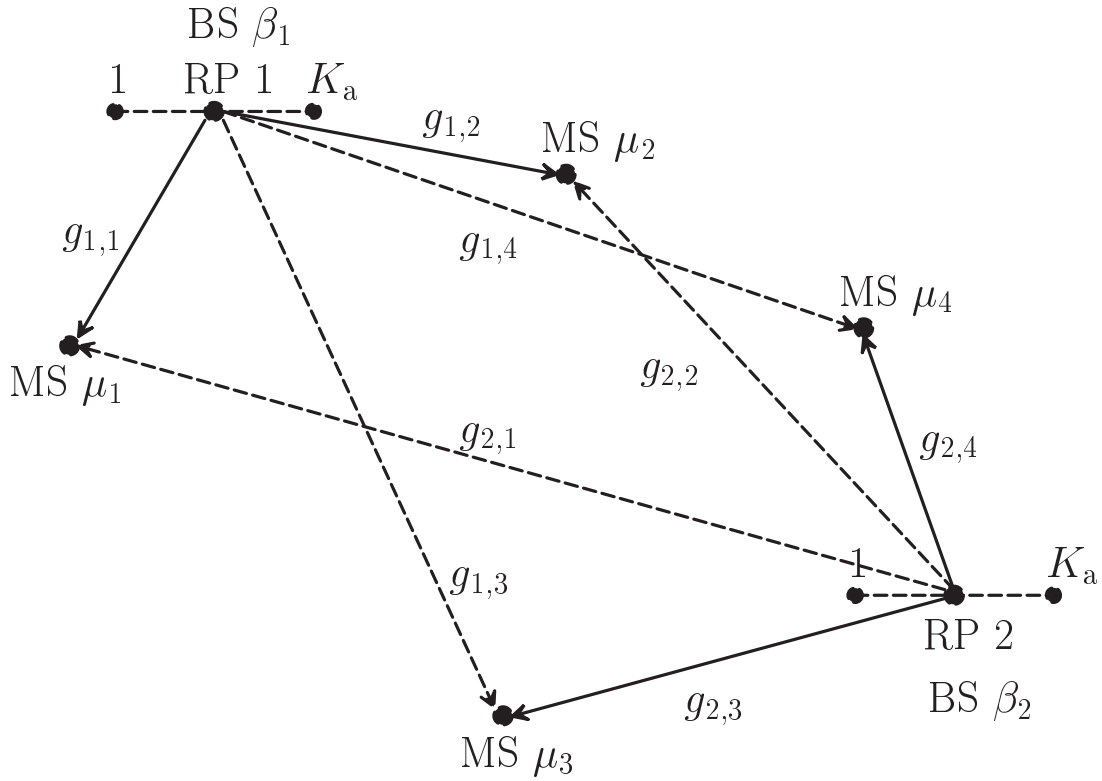
Fig. 3.1: Exemplary scenario with two BSs, each using K_a transmit antenna elements, and four MSs, each using a single omnidirectional antenna

eliminated. Therefore, in this case, (3.3) can be redefined by a disjunct set

$$\mathbb{I}_m = \left\{ \mu_{\tilde{m}} \setminus \mu_m \bigcap z(\tilde{m}) \neq z(m) \right\}. \tag{3.4}$$

The set $\mathbb{I}_m$ of (3.4) will be utilized throughout the thesis, because JD is considered as the data detection scheme in the TD-CDMA downlink.

In order to clarify the user specific interference situation characterized by the set $\mathbb{I}_m$ of (3.4), a simple, but nevertheless illustrative scenario with four MSs and two BSs is shown in Fig. 3.1. MSs μ_1 and μ_2 are served by BS β_1 and MSs μ_3 and μ_4 by BS β_2. Each of the four MSs uses a single omnidirectional receive antenna, whereas each of the two BSs has an ULA of K_a transmit antenna elements. A certain propagation gain $g_{b,m}$ is assigned to the propagation path from BS β_b, $b = 1, 2$, to MS μ_m, $m = 1 \ldots 4$. Considering this

simple scenario, the relation of (3.2) becomes

$$z(m) = \begin{cases} 1 & \text{for } m = 1, \ 2, \\ 2 & \text{for } m = 3, \ 4, \end{cases} \tag{3.5}$$

and the user specific interference situation at MS μ_1 can be characterized by

$$\mathbb{I}_1 = \{\mu_3, \ \mu_4\}. \tag{3.6}$$

The propagation gain $g_{b,m}$ of (2.3) related to the propagation path from a certain BS $\beta_{z(m)}$, which serves MS μ_m, to a certain MS $\mu_{\tilde{m}}$ can be denoted with the relation (3.2) as $g_{z(m),\tilde{m}}$. As in Section 2.2, see (2.3), $g_{z(m),\tilde{m}}$ depends on the geometrical length $\rho_{z(m),\tilde{m}}$ of the propagation path from BS $\beta_{z(m)}$ to MS $\mu_{\tilde{m}}$, see Fig. 2.1, on the attenuation coefficient α and on a shadowing factor which is represented by a log-normal distributed random variable $\xi_{z(m),\tilde{m}}$. As also mentioned in Section 2.2, the log-normal distributed random variable $\xi_{z(m),\tilde{m}}$ can be derived from a Gaussian random variable $\chi_{z(m),\tilde{m}}$ with zero mean and standard deviation σ via the transformation of (2.4). Therefore, the propagation gain related to the propagation path form BS $\beta_{z(m)}$ to MS $\mu_{\tilde{m}}$ becomes

$$g_{z(m),\tilde{m}} = \frac{1}{\xi_{z(m),\tilde{m}} \rho_{z(m),\tilde{m}}^{\alpha}}. \tag{3.7}$$

In a system with K_{a} transmit antenna elements at each BS and a single omnidirectional receive antenna at each MS, a certain MS receives K_{a} different, but statistical not independent signals. When the same signal is transmitted from different transmit antenna elements at a certain BS, in a sufficiently large distance the signals from the different transmit antenna elements only differ in phase advance. The phase advance can be determined by the geometry of the transmit antenna elements and the LOS from the BS to the MS. The parameters for determining the phase advance are shown in Fig. 3.2. BS $\beta_{z(m)}$ utilizes an ULA of K_{a} transmit antenna elements with half wavelength inter-element distance. The distance between the RP and transmit antenna element k_{a} is given by $l^{(k_{\mathrm{a}})}$, $k_{\mathrm{a}} = 1 \dots K_{\mathrm{a}}$. The LOS from the RP at BS $\beta_{z(m)}$ to MS $\mu_{\tilde{m}}$ is characterized by the azimuthal angle $\varphi_{z(m),\tilde{m}}$ related to the RL. With the wavelength λ, the azimuthal angle $\varphi_{z(m),\tilde{m}}$, the distance $l^{(k_{\mathrm{a}})}$ and the azimuthal angle

$$\alpha^{(k_{\mathrm{a}})} = \begin{cases} 0° & \text{for antenna element } k_{\mathrm{a}} \text{ on the right side of RP,} \\ 180° & \text{for antenna element } k_{\mathrm{a}} \text{ on the left side of RP,} \end{cases} \tag{3.8}$$

the phase advance

$$\psi_{z(m),\tilde{m},k_{\mathrm{a}}} = \frac{2\pi}{\lambda} l^{(k_{\mathrm{a}})} \cos\left(\varphi_{z(m),\tilde{m}} - \alpha^{(k_{\mathrm{a}})}\right) \tag{3.9}$$

$$\text{LOS to MS } \mu_{\tilde{m}}$$

RP: reference point at BS $\beta_{z(m)}$

RL: reference line at BS $\beta_{z(m)}$

Fig. 3.2: Parameters for determining the phase advance $\psi_{z(m),\tilde{m},k_\mathrm{a}}$ of (3.9)

is obtained. Now, suppose that BS $\beta_{z(m)}$ serves MS μ_m by transmitting a signal with the amplitude $\underline{a}_m$. With the propagation gain $g_{z(m),\tilde{m}}$ of (3.7) the signal received at MS $\mu_{\tilde{m}}$ has the power

$$R_{z(m),\tilde{m}} = \frac{1}{2}|\underline{a}_m|^2 g_{z(m),\tilde{m}}, \tag{3.10}$$

when a single omnidirectional transmit antenna would be used at BS $\beta_{z(m)}$. In this case the carrier power C_m of the signal transmitted by BS $\beta_{z(m)}$ to serve MS μ_m becomes at MS μ_m

$$C_m = R_{z(m),m} = \frac{1}{2}|\underline{a}_m|^2 g_{z(m),m}. \tag{3.11}$$

Furthermore, under the assumption that the signals transmitted by BS $\beta_{z(m)}$ and received at MSs $\mu_{\tilde{m}}$, $\mu_{\tilde{m}} \in \mathbb{I}_m$, see (3.4), are uncorrelated, with the set $\mathbb{I}_m$ of (3.4), the total interference power generated by BS $\beta_{z(m)}$ when serving MS μ_m is given by

$$I_m = \sum_{\tilde{m}|\mu_{\tilde{m}} \in \mathbb{I}_m} R_{z(m),\tilde{m}}. \tag{3.12}$$

Now, suppose that an antenna array of K_a transmit antenna elements is used at BS $\beta_{z(m)}$, $m = 1 \ldots |\mathbb{M}|$. With $\underline{a}_{m,k_\mathrm{a}}$ the amplitude of the signal transmitted from transmit antenna element k_a to MS μ_m, and with the phase advance $\psi_{z(m),m,k_\mathrm{a}}$ of (3.9), the carrier power

C_m of the signal transmitted by BS $\beta_{z(m)}$ and received at MS μ_m becomes

$$C_m = \frac{1}{2} | \sum_{k_a=1}^{K_a} \sqrt{g_{z(m),m}} \mathrm{e}^{\mathrm{j}\psi_{z(m),m,k_a}} \underline{a}_{m,k_a} |^2.$$ (3.13)

Similarly, the total interference power of the signals transmitted by BS $\beta_{z(m)}$ to serve MS μ_m, but received at all MSs $\mu_{\tilde{m}}$, $\mu_{\tilde{m}} \in \mathbb{I}_m$, see (3.4), takes the form

$$I_m = \frac{1}{2} \sum_{\tilde{m}|\mu_{\tilde{m}}\in\mathbb{I}_m} | \sum_{k_a=1}^{K_a} \sqrt{g_{z(m),\tilde{m}}} \mathrm{e}^{\mathrm{j}\psi_{z(m),\tilde{m},k_a}} \underline{a}_{\tilde{m},k_a} |^2.$$ (3.14)

I_m of (3.14) is the total power of the signal received at the MSs forming the set $\mathbb{I}_m$ of (3.4), when BS $\beta_{z(m)}$ serves MS μ_m.

3.3 Algorithms for determining the antenna weights

3.3.1 The MC algorithm

With the antenna weight vector $\underline{\mathbf{w}}_{z(m),m}$ of (3.1) and the amplitude $\underline{a}_m$ of the transmitted signal, the amplitude

$$\underline{a}_{m,k_a} = \underline{w}_{z(m),m,k_a} \underline{a}_m$$ (3.15)

of the weighted signal at transmit antenna element k_a is obtained. Then, the total transmit power

$$T_m = \frac{1}{2} \sum_{k_a=1}^{K_a} |\underline{a}_{m,k_a}|^2$$ (3.16)

at BS $\beta_{z(m)}$ holds. The MC algorithm to determine the antenna weight vectors $\underline{\mathbf{w}}_{z(m),m}$ of (3.1) for MS μ_m, $m = 1 \ldots |\mathbb{M}|$, served by BS $\beta_{z(m)}$ is performed in such a way that the ratio of the carrier power C_m of (3.13) of the signal received at MS μ_m to the total transmit power T_m of (3.16) at BS $\beta_{z(m)}$ is maximized. Under the assumption that amplitude $\underline{a}_m$ in (3.15) has the magnitude one, substituting $\underline{a}_{m,k_a}$ of (3.15) into (3.13) and (3.16) yields the ratio

$$\frac{C_m}{T_m} = \frac{| \sum_{k_a=1}^{K_a} \sqrt{g_{z(m),m}} \mathrm{e}^{\mathrm{j}\psi_{z(m),m,k_a}} \underline{w}_{z(m),m,k_a} |^2}{| \sum_{k_a=1}^{K_a} \underline{w}_{z(m),m,k_a} |^2}$$ (3.17)

of the carrier power C_m of (3.13) of the signal received at MS μ_m to the total transmit power T_m of (3.16) at BS $\beta_{z(m)}$. Now, with the vector

$$\underline{\mathbf{y}}_{z(m),m} = \sqrt{g_{z(m),m}}(\mathrm{e}^{\mathrm{j}\psi_{z(m),m,1}} \ldots \mathrm{e}^{\mathrm{j}\psi_{z(m),m,K_{\mathrm{a}}}})^{\mathrm{T}} \tag{3.18}$$

and the matrix

$$\underline{\mathbf{X}}_m = \underline{\mathbf{y}}_{z(m),m}^* \underline{\mathbf{y}}_{z(m),m}^{\mathrm{T}}, \tag{3.19}$$

(3.17) can be rewritten in the form

$$\frac{C_m}{T_m} = \frac{\underline{\mathbf{w}}_{z(m),m}^{*\mathrm{T}} \underline{\mathbf{y}}_{z(m),m}^* \underline{\mathbf{y}}_{z(m),m}^{\mathrm{T}} \underline{\mathbf{w}}_{z(m),m}}{\underline{\mathbf{w}}_{z(m),m}^{*\mathrm{T}} \underline{\mathbf{w}}_{z(m),m}} = \frac{\underline{\mathbf{w}}_{z(m),m}^{*\mathrm{T}} \underline{\mathbf{X}}_m \underline{\mathbf{w}}_{z(m),m}}{\underline{\mathbf{w}}_{z(m),m}^{*\mathrm{T}} \underline{\mathbf{w}}_{z(m),m}}. \tag{3.20}$$

(3.20) is a standard quadratic form. For a given propagation gain $g_{z(m),m}$ of (3.7) of the propagation path from BS $\beta_{z(m)}$ to MS μ_m and the phase advance $\psi_{z(m),m,k_{\mathrm{a}}}$ of (3.9), the antenna weight vector $\underline{\mathbf{w}}_{z(m),m}$ of (3.1) valid for MS μ_m which maximizes the ratio (3.20) is the eigenvector belonging to the largest eigenvalue of the matrix $\underline{\mathbf{X}}_m$ of (3.19) [ZF84]. Furthermore, with the restraint

$$\underline{\mathbf{w}}_{z(m),m}^{*\mathrm{T}} \underline{\mathbf{w}}_{z(m),m} = 1, \ m = 1 \ldots |\mathbb{M}|, \tag{3.21}$$

the antenna weight vector $\underline{\mathbf{w}}_{z(m),m}$ of (3.1) valid for MS μ_m is uniquely determined. It can be seen from (3.17) that, when utilizing the MC algorithm for determining the antenna weight vector $\underline{\mathbf{w}}_{z(m),m}$ of (3.1) valid for MS μ_m only the propagation gain $g_{z(m),m}$ of (3.7) and the DOD pertaining to the LOS from BS $\beta_{z(m)}$ to MS μ_m are required.

3.3.2   The MPCI algorithm

In Section 3.2, if BS $\beta_{z(m)}$ transmits a signal to serve MS μ_m utilizing an antenna array of K_{a} transmit antenna elements, the carrier power C_m of (3.13) of the desired signal received at MS μ_m and the total interference power I_m of (3.14) of the signals simultaneously received at other MSs $\mu_{\tilde{m}}$, $\mu_{\tilde{m}} \in \mathbb{I}_m$, see (3.4), are given. Based on these expressions, the pseudo carrier-to-interference ratio

$$\left(\frac{C}{I}\right)_{\mathrm{p},m} = \frac{C_m}{I_m} = \frac{\left|\sum\limits_{k_{\mathrm{a}}=1}^{K_{\mathrm{a}}} \sqrt{g_{z(m),m}}\mathrm{e}^{\mathrm{j}\psi_{z(m),m,k_{\mathrm{a}}}}\underline{a}_{m,k_{\mathrm{a}}}\right|^2}{\sum\limits_{\tilde{m}|\mu_{\tilde{m}} \in \mathbb{I}_m} \left|\sum_{k_{\mathrm{a}}=1}^{K_{\mathrm{a}}} \sqrt{g_{z(m),\tilde{m}}}\mathrm{e}^{\mathrm{j}\psi_{z(m),\tilde{m},k_{\mathrm{a}}}}\underline{a}_{\tilde{m},k_{\mathrm{a}}}\right|^2} \tag{3.22}$$

valid for MS μ_m served by BS $\beta_{z(m)}$ can be formed. With the vector

$$\underline{\mathbf{y}}_{z(m),\tilde{m}} = \sqrt{g_{z(m),\tilde{m}}}(\mathrm{e}^{\mathrm{j}\psi_{z(m),\tilde{m},1}} \ldots \mathrm{e}^{\mathrm{j}\psi_{z(m),\tilde{m},K_{\mathrm{a}}}})^{\mathrm{T}}, \tag{3.23}$$

the matrix

$$\underline{\mathbf{Y}}_m = \sum_{\tilde{m}|\mu_{\tilde{m}} \in \mathbb{I}_m} \underline{\mathbf{y}}^*_{z(m),\tilde{m}} \underline{\mathbf{y}}^{\mathrm{T}}_{z(m),\tilde{m}}, \tag{3.24}$$

the vector $\underline{\mathbf{y}}_{z(m),m}$ of (3.18) and the matrix $\underline{\mathbf{X}}_m$ of (3.19), (3.22) can be rewritten as

$$(\frac{C}{I})_{\mathrm{p},m} = \frac{\underline{\mathbf{w}}^{*\mathrm{T}}_{z(m),m} \underline{\mathbf{y}}^*_{z(m),m} \underline{\mathbf{y}}^{\mathrm{T}}_{z(m),m} \underline{\mathbf{w}}_{z(m),m}}{\underline{\mathbf{w}}^{*\mathrm{T}}_{z(m),m} \underline{\mathbf{y}}^*_{z(m),\tilde{m}} \underline{\mathbf{y}}^{\mathrm{T}}_{z(m),\tilde{m}} \underline{\mathbf{w}}_{z(m),m}} = \frac{\underline{\mathbf{w}}^{*\mathrm{T}}_{z(m),m} \underline{\mathbf{X}}_m \underline{\mathbf{w}}_{z(m),m}}{\underline{\mathbf{w}}^{*\mathrm{T}}_{z(m),m} \underline{\mathbf{Y}}_m \underline{\mathbf{w}}_{z(m),m}}. \tag{3.25}$$

(3.25) is a standard quadratic form and is bounded by the minimal and maximal eigen-values of the matrix pair $(\underline{\mathbf{Y}}_m, \underline{\mathbf{X}}_m)$. Consequently, the antenna weight vector $\underline{\mathbf{w}}_{z(m),m}$ of (3.1) which maximizes (3.25) is equal to the eigenvector belonging to the maximal eigen-value of the matrix pair $(\underline{\mathbf{Y}}_m, \underline{\mathbf{X}}_m)$ [ZF84]. Similar to (3.20), with the restraint given in (3.21), the antenna weight vector $\underline{\mathbf{w}}_{z(m),m}$ of (3.1) in (3.25) valid for MS μ_m is uniquely determined. For determining the antenna weight vector $\underline{\mathbf{w}}_{z(m),m}$ of (3.1) valid for MS μ_m served by BS $\beta_{z(m)}$, $m = 1 \ldots |\mathbb{M}|$ when using (3.25), the following knowledge is required at BS $\beta_{z(m)}$:

- The propagation gain $g_{z(m),m}$ of (3.7) for the propagation path from BS $\beta_{z(m)}$ to MS μ_m, which is necessary for determining the matrix $\underline{\mathbf{X}}_m$ of (3.19), as well as the propagation gains $g_{z(m),\tilde{m}}$ of (3.7) for the propagation paths from BS $\beta_{z(m)}$ to the other MSs $\mu_{\tilde{m}}$, $\mu_{\tilde{m}} \in \mathbb{I}_m$, see (3.4), are required. This later mentioned propagation gains are necessary for determining the matrix $\underline{\mathbf{Y}}_m$ of (3.24).

- The DOD pertaining to the LOS from BS $\beta_{z(m)}$ to MS μ_m, which is necessary for determining the matrix $\underline{\mathbf{X}}_m$ of (3.19), as well as the DODs pertaining to the LOSs from BS $\beta_{z(m)}$ to the other MSs $\mu_{\tilde{m}}$, $\mu_{\tilde{m}} \in \mathbb{I}_m$, see (3.4), are required. These DODs are needed for determining the matrix $\underline{\mathbf{Y}}_m$ of (3.24).

Therefore, compared with the MC algorithm, see (3.20), the MPCI algorithm requires more knowledge for determining the antenna weight vectors $\underline{\mathbf{w}}_{z(m),m}$, $m = 1 \ldots |\mathbb{M}|$, of (3.1).

3.4   C/I balancing

In Section 3.1 the MC and MPCI algorithms for determining the antenna weight vectors $\underline{\mathbf{w}}_{z(m),m}$ of (3.1) valid for MS μ_m, $m = 1 \ldots |\mathbb{M}|$, are discussed. In this section, the power control algorithm of the two-step approach mentioned in Section 3.1 is presented.

A specially interesting power control algorithm has been introduced in [Ste96, Sch01], which utilizes the concept of the CPC [GVGZ94] algorithm as mentioned in Section 1.4. The idea behind this algorithm is that the transmit powers T_m, $m = 1\ldots|\mathbb{M}|$, of (3.16), are adjusted in such a way that each MS μ_m, $m = 1\ldots|\mathbb{M}|$, in the cellular scenario attains the same and highest possible C/I. Following [Sch01], the mathematical details of the CPC algorithm are discussed in what follows for the convenience of the readers.

With the antenna weight vectors $\underline{\mathbf{w}}_{z(m),m}$, $m = 1\ldots|\mathbb{M}|$, of (3.1) determined by applying the MC or MPCI algorithm introduced in Section 3.3, a propagation gain

$$g_{\mathrm{mod},z(m),\tilde{m}} = |\sum_{k_{\mathrm{a}}=1}^{K_{\mathrm{a}}} \sqrt{g_{z(m),\tilde{m}}}\mathrm{e}^{\mathrm{j}\psi_{z(m),\tilde{m},k_{\mathrm{a}}}}\underline{w}_{z(m),\tilde{m},k_{\mathrm{a}}}|^2 \tag{3.26}$$

for the propagation path from BS $\beta_{z(m)}$ to MS $\mu_{\tilde{m}}$ is introduced and is termed modified propagation gain. With the transmit powers T_m, $m = 1\ldots|\mathbb{M}|$, of (3.16) and the modified propagation gains $g_{\mathrm{mod},z(m),\tilde{m}}$ of (3.26) the carrier-to-interference ratio

$$(\frac{C}{I})_m = \gamma_m = \frac{T_m g_{\mathrm{mod},z(m),m}}{\sum\limits_{\tilde{m}|\mu_{\tilde{m}}\in\mathbb{I}_m} T_{\tilde{m}} g_{\mathrm{mod},z(\tilde{m}),m}} \tag{3.27}$$

valid for MS μ_m, $m = 1\ldots|\mathbb{M}|$, is obtained. Transforming (3.27) yields

$$\sum_{\tilde{m}|\mu_{\tilde{m}}\in\mathbb{I}_m} T_{\tilde{m}} g_{\mathrm{mod},z(\tilde{m}),m} = \frac{1}{\gamma_m} T_m g_{\mathrm{mod},z(m),m}. \tag{3.28}$$

Now, following [Ste96, Sch01], the following matrix and vector formalisms are introduced:

- Matrix $\mathbf{W}$ of dimension $|\mathbb{M}|\times|\mathbb{M}|$ contains the modified propagation gains $g_{\mathrm{mod},z(\tilde{m}),m}$ of (3.26) of the interferers.

- Matrix $\mathbf{V}$ of dimension $|\mathbb{M}|\times|\mathbb{M}|$ contains the modified propagation gains $g_{\mathrm{mod},z(m),m}$ of (3.26) of the carrier.

- Vector

$$\mathbf{t} = (T_1 \ldots T_{|\mathbb{M}|})^{\mathrm{T}} \tag{3.29}$$

of dimension $|\mathbb{M}| \times 1$ contains the transmit powers T_m of (3.16) for all MSs μ_m, $m = 1\ldots|\mathbb{M}|$, which are to be determined for the C/I balancing purpose.

- Diagonal matrix Λ of dimension $|\mathbb{M}| \times |\mathbb{M}|$ contains the reciprocal values of $1/\gamma_m$, $m = 1\ldots|\mathbb{M}|$.

With these matrix and vector formalisms, the linear system of equations (3.28) takes the form

$$\mathbf{Wt} = \Lambda \mathbf{Vt}. \tag{3.30}$$

Because the C/I balancing means to make all diagonal elements of the matrix Λ equal, the matrix Λ can be reduced to a signal value $1/\gamma$ and (3.30) becomes

$$\mathbf{Wt} = \frac{1}{\gamma}\mathbf{Vt}. \tag{3.31}$$

With the matrices $\mathbf{W}$ and $\mathbf{V}$, the vector $\mathbf{t}$ of (3.29) can be calculated by solving an eigenvalue problem [Ste96, Sch01]. The eigenvalue problem has only one solution termed matrix root with the matching eigenvector containing only non-negative elements [Min88]. The matching eigenvector contains the number $|\mathbb{M}|$ of the transmit powers T_m, $m = 1 \ldots |\mathbb{M}|$, of (3.16).

For instance, with the exemplary scenario consisting of two BSs and four MSs shown in Fig. 3.1, the matrices $\mathbf{W}$ and $\mathbf{V}$ in (3.31) become

$$\mathbf{W} = \begin{pmatrix} 0 & 0 & g_{\mathrm{mod},1,3} & g_{\mathrm{mod},1,4} \\ 0 & 0 & g_{\mathrm{mod},1,3} & g_{\mathrm{mod},1,4} \\ g_{\mathrm{mod},2,1} & g_{\mathrm{mod},2,2} & 0 & 0 \\ g_{\mathrm{mod},2,1} & g_{\mathrm{mod},2,2} & 0 & 0 \end{pmatrix}, \tag{3.32}$$

and

$$\mathbf{V} = \begin{pmatrix} g_{\mathrm{mod},1,1} & 0 & 0 & 0 \\ 0 & g_{\mathrm{mod},1,2} & 0 & 0 \\ 0 & 0 & g_{\mathrm{mod},2,3} & 0 \\ 0 & 0 & 0 & g_{\mathrm{mod},2,4} \end{pmatrix}, \tag{3.33}$$

respectively.

3.5   Simulation results

3.5.1   Unlimited transmit power dynamics

In order to quantitatively assess the algorithms introduced in Sections 3.3 and 3.4, simulations are performed on the system level. In these simulations a large number of random

Tab. 3.1: Simulation parameters

standard deviation σ	8dB
attenuation coefficient α	4
reuse factor r	1
number $|\mathbb{B}|$ of the BSs in the cellular scenario	19, 37, 61
average number $\bar{K}$ of the MSs per cell	1, 2, 4, 8
number K_{a} of transmit antenna elements	1, 2, 4, 8

deployments of MSs in the cellular scenario is considered. As stated in Section 1.2, only the intercell interference is considered in system level simulations, since the intracell interference can be eliminated by JD. In the present section, simulation results are valid for the case that the dynamics of the transmit power are unlimited. The chosen simulation parameters are given in Tab. 3.1.

First, the influence of K_{a} on the CDF of C/I is investigated. Simulations were done by utilizing the MPCI algorithm for determining the antenna weight vector $\underline{\mathbf{w}}_{b,m}$ of (3.1) valid for each MS μ_m, $m = 1 \ldots |\mathbb{M}|$, of the cellular scenario served by BS β_b, $b = 1 \ldots |\mathbb{B}|$. Figs. 3.3 to 3.6 show the obtained CDF of C/I for different values of $\bar{K}$. The parameter in each figure is K_{a}. The expectation of C/I increases as K_{a} increases. However, this expectation is not proportional to K_{a}. The variance of C/I becomes slightly larger with increasing K_{a} due to the reduction of interferer diversity [BKNS94].

The influence of $\bar{K}$ on the CDF of C/I can also be observed from Figs. 3.3 to 3.6. As to be expected, the expectation of C/I decreases as $\bar{K}$ increases. For instance, in the case $K_{\mathrm{a}} = 2$, for each doubling of $\bar{K}$ C/I decreases by about 2dB. This is due to the fact that a larger number $\bar{K}$ of the MSs per cell produces more interference.

In Fig. 3.7 it is shown how the CDF of C/I depends on the choice of the algorithm utilized to determine the antenna weight vectors $\underline{\mathbf{w}}_{b,m}$ of (3.1). As mentioned in Section 3.3, two considered algorithms are the MC and MPCI algorithms. Fig. 3.7 shows that the MPCI algorithm performs slightly better than the MC algorithm. However, as stated in Section 3.3, less knowledge to determine the antenna weight vectors $\underline{\mathbf{w}}_{b,m}$ of (3.1) is required when performing the MC algorithm as compared with performing the MPCI algorithm.

The influence of the system size in terms of the number $|\mathbb{B}|$ of BSs on the CDF of C/I is shown in Fig. 3.8. This figure shows the CDF of C/I with $|\mathbb{B}|$ as the parameter for $\bar{K} = 2$ and $K_{\mathrm{a}} = 4$. C/I decreases with increasing $|\mathbb{B}|$. This degradation is expected because the number of interfering signals increases as $|\mathbb{B}|$ increases. However, the difference of CDF of C/I for different $|\mathbb{B}|$ is rather small.
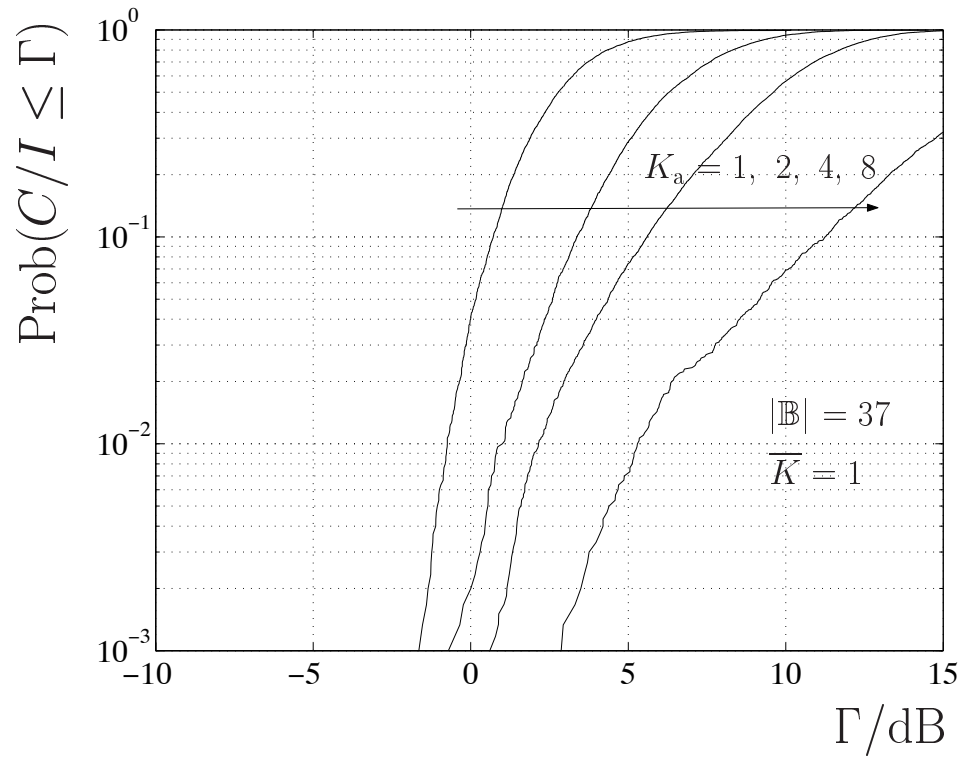
Fig. 3.3: CDF of C/I using the MPCI algorithm; $|\mathbb{B}| = 37$, $\bar{K} = 1$; parameter: K_a
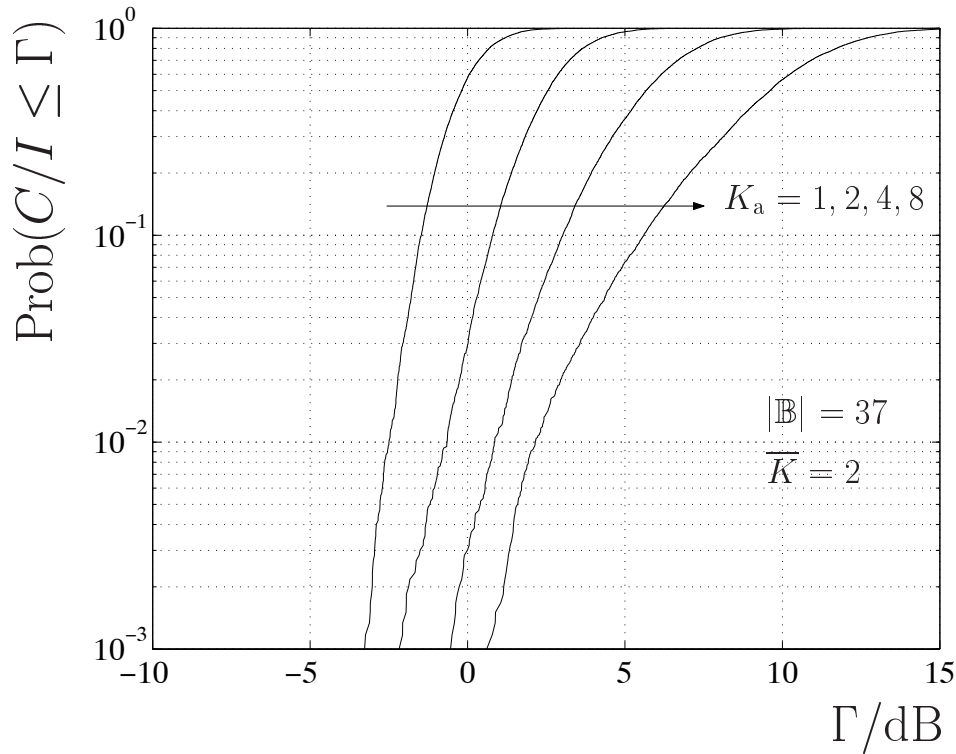
Fig. 3.4: CDF of C/I using the MPCI algorithm; $|\mathbb{B}| = 37$, $\bar{K} = 2$; parameter: K_a
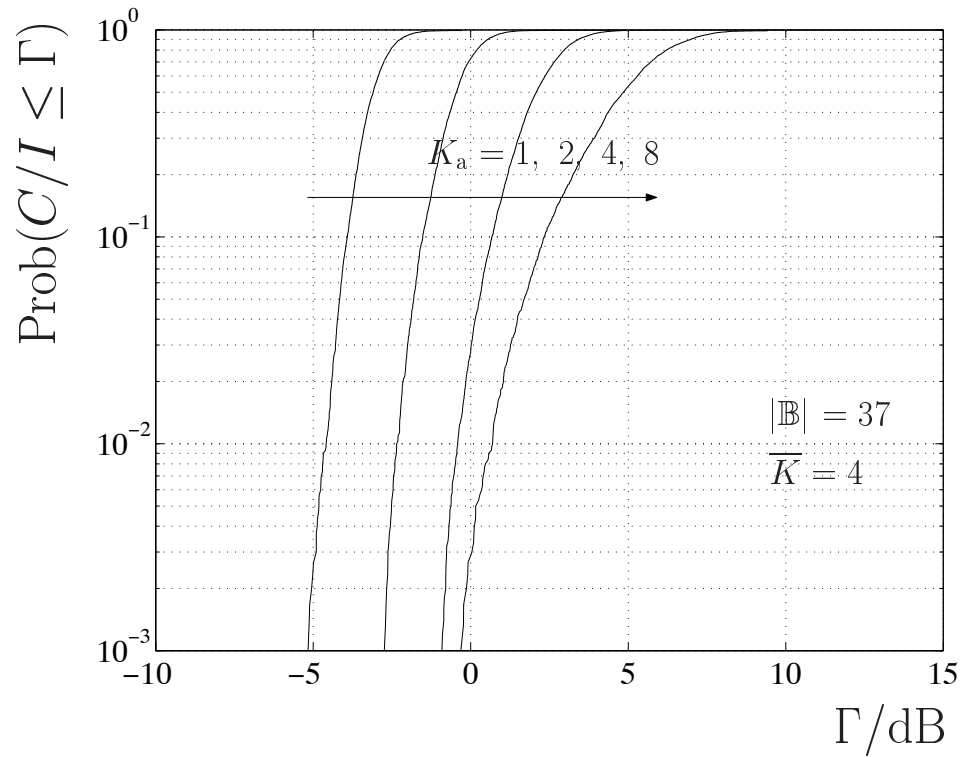
Fig. 3.5: CDF of C/I using the MPCI algorithm; $|\mathbb{B}| = 37$, $\bar{K} = 4$; parameter: K_{a}
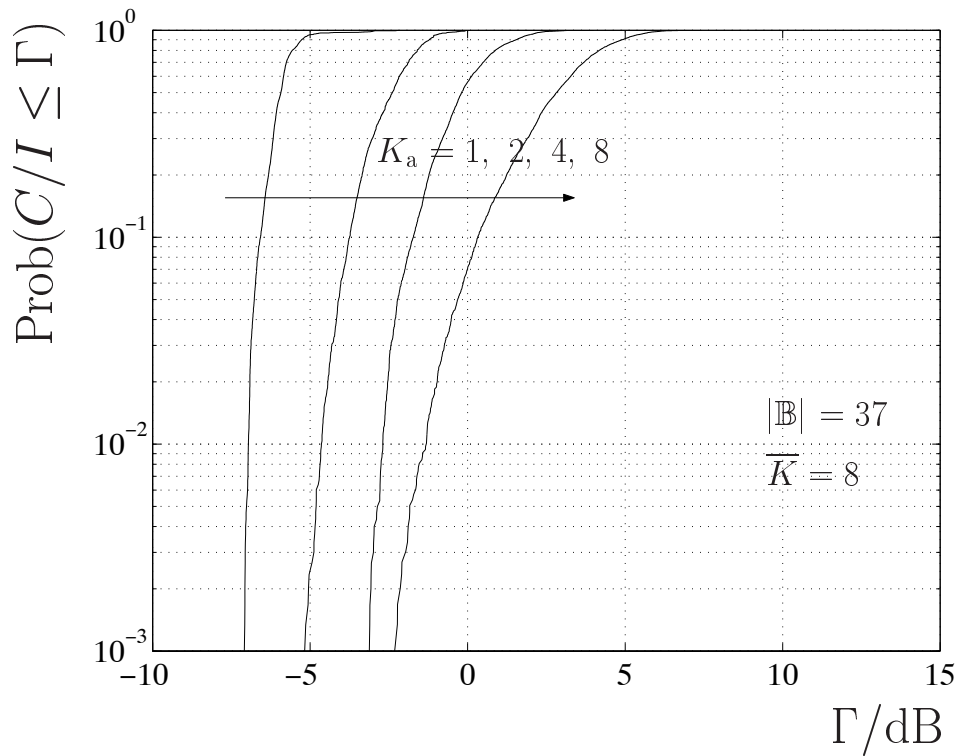
Fig. 3.6: CDF of C/I using the MPCI algorithm; $|\mathbb{B}| = 37$, $\bar{K} = 8$; parameter: K_{a}
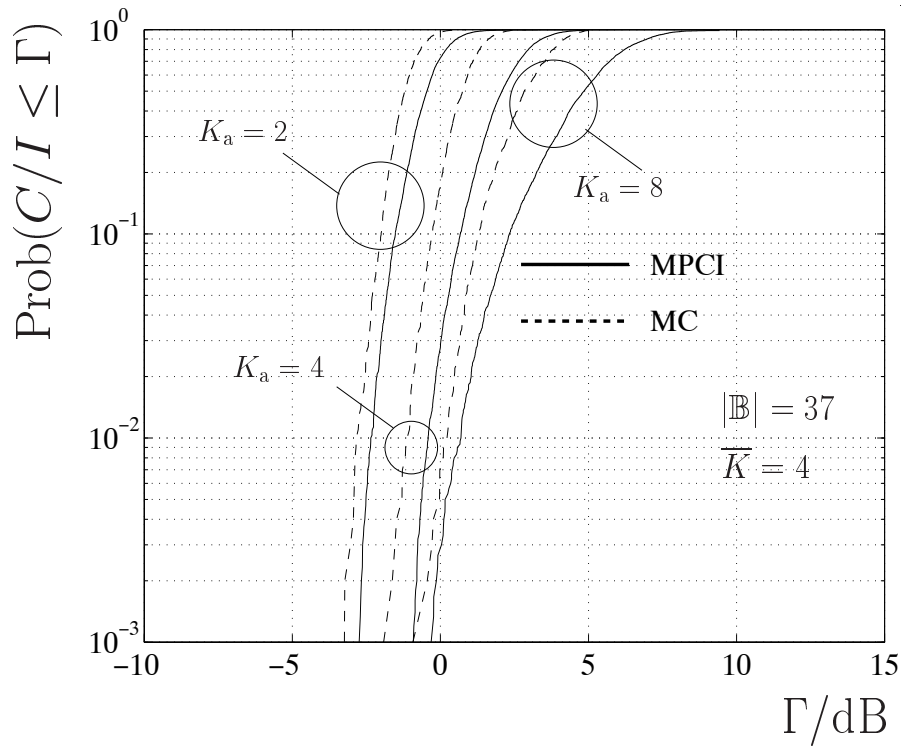
Fig. 3.7: CDF of C/I using the MC and MPCI algorithms; $|\mathbb{B}| = 37$ and $\bar{K} = 4$; parameter: K_{a}
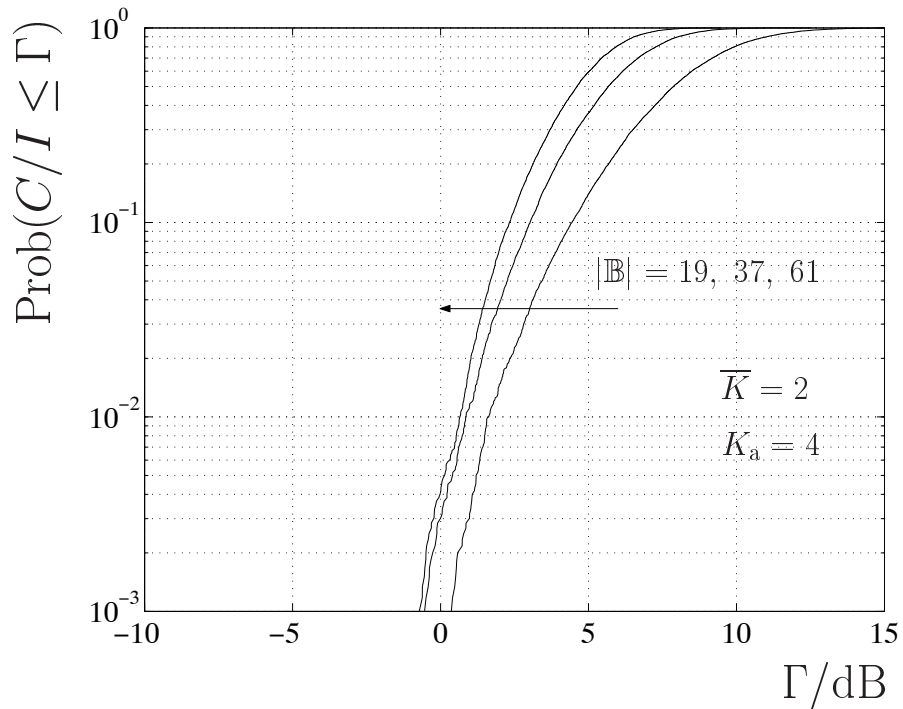
Fig. 3.8: CDF of C/I using the MPCI algorithm; $\bar{K} = 2$ and $K_{\mathrm{a}} = 4$; parameter: $|\mathbb{B}|$

3.5.2   Limited transmit power dynamics

Generally, the powers T_m, $m = 1 \ldots |\mathbb{M}|$, in (3.29) of the signals transmitted for the MSs μ_m, $m = 1 \ldots |\mathbb{M}|$, in one burst, which are obtained after C/I balancing, may take values in the range from zero to infinity. As an example, T_m for all MSs μ_m, $m = 1 \ldots |\mathbb{M}|$, in one burst with $|\mathbb{B}| = 37$, $\bar{K} = 2$ and $K_a = 4$ are shown in Figs. 3.9 to 3.14. The utilized algorithm for determining the antenna weight vectors $\underline{\mathbf{w}}_{b,m}$ of (3.1) is the MPCI algorithm. The terms LP, CP and HP appearing in the captions of these figures will be explained below. The figures show that the dynamics of the transmit powers exceed 70dB. However, as already stated in Chapter 1, because of the nonlinearities of amplifiers and other RF components, the dynamics of the transmit powers in reality should be restricted to 20dB. With $T_{\max}$ and $T_{\min}$ being the maximum and minimum transmit powers, respectively, the limited transmit power band is given by

$$10\log(\frac{T_{\max}}{T_{\min}}) = 20\text{dB}. \tag{3.34}$$

In order to satisfy (3.34), procedures should be developed to get, instead of the vector $\mathbf{t}$ of (3.29) of transmit powers T_m, a vector

$$\mathbf{t}^{'} = (T_1^{'} \ldots T_{|\mathbb{M}|}^{'})^{\text{T}} \tag{3.35}$$

of modified transmit powers $T_m^{'}$, derived from $\mathbf{t}$. After having obtained the modified transmit powers $T_m^{'}$, $m = 1 \ldots |\mathbb{M}|$, in (3.35), the carrier-to-interference ratio γ_m of (3.27) at each MS μ_m, $m = 1 \ldots |\mathbb{M}|$, can then be calculated by substituting T_m in (3.27) by $T_m^{'}$.

As procedures to determine $T_m^{'}$ in (3.35), an algorithm based on clipping and an algorithm based on suppression will be presented.

The basic idea behind the clipping algorithm is to simply restrict the transmit powers T_m in (3.29) in the limited 20dB transmit power band of (3.34) depending on whether the value of T_m is larger than $T_{\max}$ or smaller than $T_{\min}$ in (3.34). The clipping algorithm is described as follows:

$$T_m^{'} = \begin{cases} T_{\min} & \text{for } T_m \leq T_{\min}, \\ T_m & \text{for } T_{\min} < T_m < T_{\max}, \\ T_{\max} & \text{for } T_m \geq T_{\max}. \end{cases} \tag{3.36}$$

This algorithm gives the vector $\mathbf{t}^{'}$ of the modified transmit powers $T_m^{'}$, see (3.35). A question still open is how the limiting values $T_{\min}$ and $T_{\max}$ in (3.34) and (3.36) should be chosen. Up to now, see (3.34) it has only been stated that $T_{\max}/T_{\min} = 100$ should hold. There are infinitely many possibilities to select $T_{\min}$ and $T_{\max}$ of (3.34). Three different

approaches to determine $T_{\min}$ and $T_{\max}$ will be studied in what follows. These approaches are based on the fact that, when performing C/I balancing as described in Section 3.4, the dynamically not considered transmit powers fulfill the condition

$$\tilde{T}_{\min} \le T_m \le \tilde{T}_{\max}, \tag{3.37}$$

where usually $\tilde{T}_{\min}$ and $\tilde{T}_{\max}$ differ in much more than 20dB, see Figs. 3.9 to 3.14. The three considered approaches are termed low power (LP), centered power (CP) and high power (HP) approach, respectively. With

$$\bar{T} = \frac{1}{|\mathbb{M}|} \sum_{m=1}^{|\mathbb{M}|} T_m \tag{3.38}$$

the transmit power averaged over all T_m, $m = 1 \ldots |\mathbb{M}|$, in the vector $\mathbf{t}$ of (3.29), with $\tilde{T}_{\min}$ and $\tilde{T}_{\max}$ in (3.37) and $T_{\min}$ and $T_{\max}$ in (3.34), these three approaches can be described as follows:

LP:

$$T_{\min} = \tilde{T}_{\min}, \ T_{\max} = 100 T_{\min}. \tag{3.39}$$

CP:

$$T_{\min} = \bar{T}/10, \ T_{\max} = 10\bar{T}. \tag{3.40}$$

HP:

$$T_{\max} = \tilde{T}_{\max}, \ T_{\min} = T_{\max}/100. \tag{3.41}$$

As an example, the transmit powers T_m' in (3.35) obtained when using clipping and CP are shown in Fig. 3.10.

An alternative to the clipping approach described above is an approach based on compression. This approach can be described as follows:

- Arrange the transmit powers T_m, $m = 1 \ldots |\mathbb{M}|$, in the vector $\mathbf{t}$ of (3.29) obtained after C/I balancing for unlimited dynamics in ascending order.

- Calculate the differences

$$\Delta T_m = T_{m+1} - T_m, \ m = 1 \ldots (|\mathbb{M}| - 1) \tag{3.42}$$

  between adjacent transmit powers.

- With $\tilde{T}_{\max}$ and $\tilde{T}_{\min}$ in (3.37) and $T_{\max}$ and $T_{\min}$ in (3.34) compute the quantity

$$\Delta \tilde{T} = \frac{T_{\max} - T_{\min}}{\tilde{T}_{\max} - \tilde{T}_{\min}}. \tag{3.43}$$

In (3.43) $T_{\max}$ and $T_{\min}$ are determined according to (3.39), (3.40) and (3.41) depending on which one of the approaches LP, CP or HP is chosen.

- With ΔT_m of (3.42) and $\Delta \tilde{T}$ of (3.43) introduce the modified differences

$$\Delta T'_m = \Delta T_m \Delta \tilde{T}. \tag{3.44}$$

- With $\Delta T'_m$ of (3.44) form the modified transmit powers T'_m in (3.35) according to

$$
\begin{aligned}
T'_1 &= \tilde{T}_{\min}, \\
T'_m &= T'_{m-1} + \Delta T'_{m-1} = T'_{m-1} + \Delta T_{m-1} \Delta \tilde{T}, \; m = 2 \ldots (|\mathbb{M}| - 1).
\end{aligned} \tag{3.45}
$$

Examples for the transmit powers T'_m in (3.35) for all MSs μ_m, $m = 1 \ldots |\mathbb{M}|$, obtained by compression are shown in Figs. 3.12 to 3.14.

It has to be expected that constraining the transmit power dynamics leads to a less favorable CDF of C/I as compared to the situation without such a constraint. Also, the CDF of C/I obtained under restricted transmit power dynamics depends on whether LP, CP or HP and whether clipping or compression are chosen. Figs. 3.15 and 3.16 show the CDF of C/I obtained when using different schemes of dynamics constraint. For the sake of comparison the CDF of C/I for the case of unlimited transmit power dynamics is also shown in Figs. 3.15 and 3.16. The considered algorithm to determine the antenna weight vectors $\underline{\mathbf{w}}_{b,m}$, $b = 1 \ldots |\mathbb{B}|$, $m = 1 \ldots |\mathbb{M}|$, of (3.1) is the MPCI algorithm. According to Fig. 3.15, in the case of clipping the approach CP is the most favorable. According to Fig. 3.16, in the case of compression, the performance of the three approaches LP, CP and HP is virtually equal. A comparison of the curves in Fig. 3.15 with those of Fig. 3.16 shows that compression outperforms clipping.
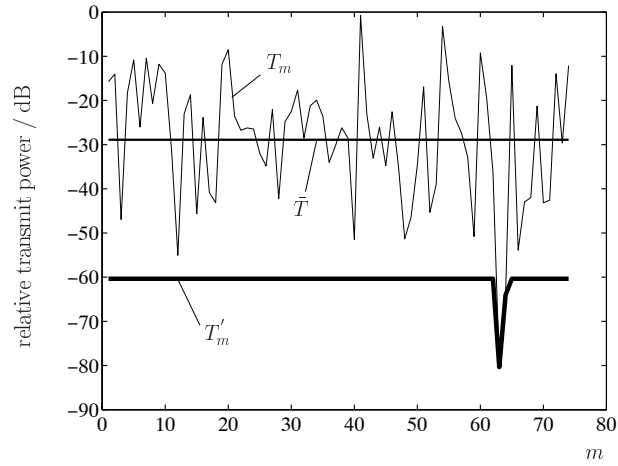
Fig. 3.9: Relative transmit powers without (——) and with (━━) power constraint by clipping; selection of $T_{\min}$ and $T_{\max}$: LP; $|\mathbb{B}| = 37$, $\bar{K} = 2$ and $K_a = 4$
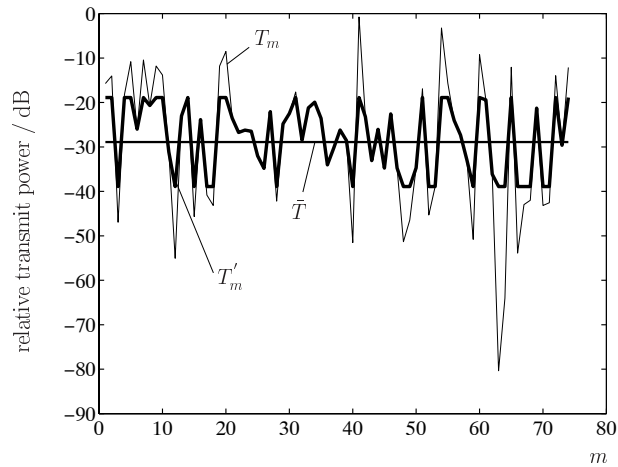
Fig. 3.10: Relative transmit powers without (——) and with (━━) power constraint by clipping; selection of $T_{\min}$ and $T_{\max}$: CP; $|\mathbb{B}| = 37$, $\bar{K} = 2$ and $K_a = 4$
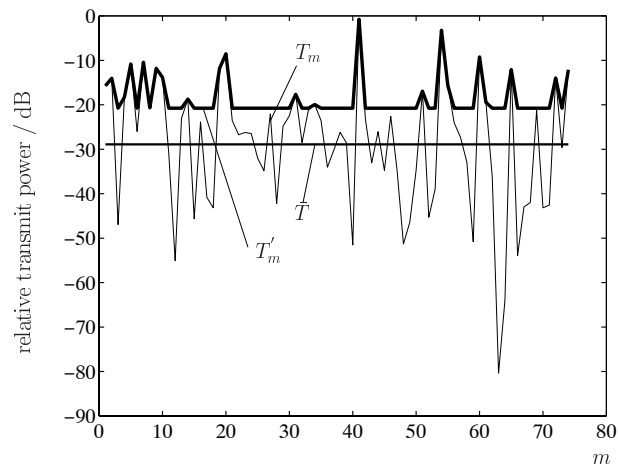
Fig. 3.11: Relative transmit powers without (——) and with (━━) power constraint by clipping; selection of $T_{\min}$ and $T_{\max}$: HP; $|\mathbb{B}| = 37$, $\bar{K} = 2$ and $K_a = 4$
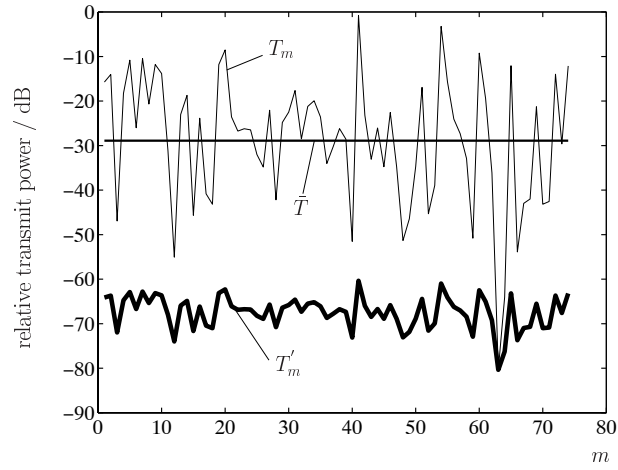
Fig. 3.12: Relative transmit powers without (——) and with (▬) power constraint by compression; selection of $T_{\min}$ and $T_{\max}$: LP; $|\mathbb{B}| = 37$, $\bar{K} = 2$ and $K_a = 4$
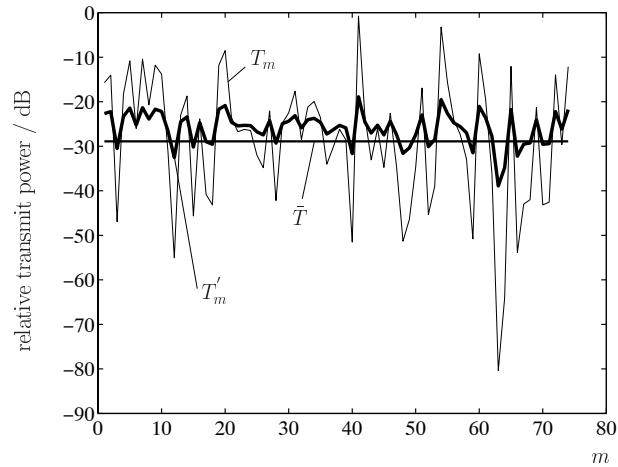
Fig. 3.13: Relative transmit powers without (——) and with (▬) power constraint by compression; selection of $T_{\min}$ and $T_{\max}$: CP; $|\mathbb{B}| = 37$, $\bar{K} = 2$ and $K_a = 4$
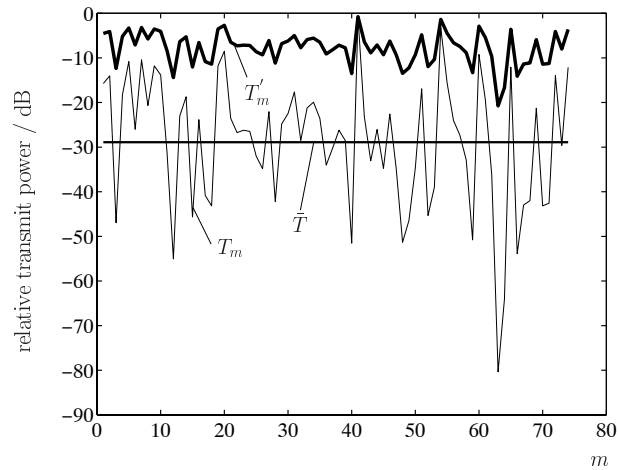
Fig. 3.14: Relative transmit powers without (——) and with (▬) power constraint by compression; selection of $T_{\min}$ and $T_{\max}$: HP; $|\mathbb{B}| = 37$, $\bar{K} = 2$ and $K_a = 4$
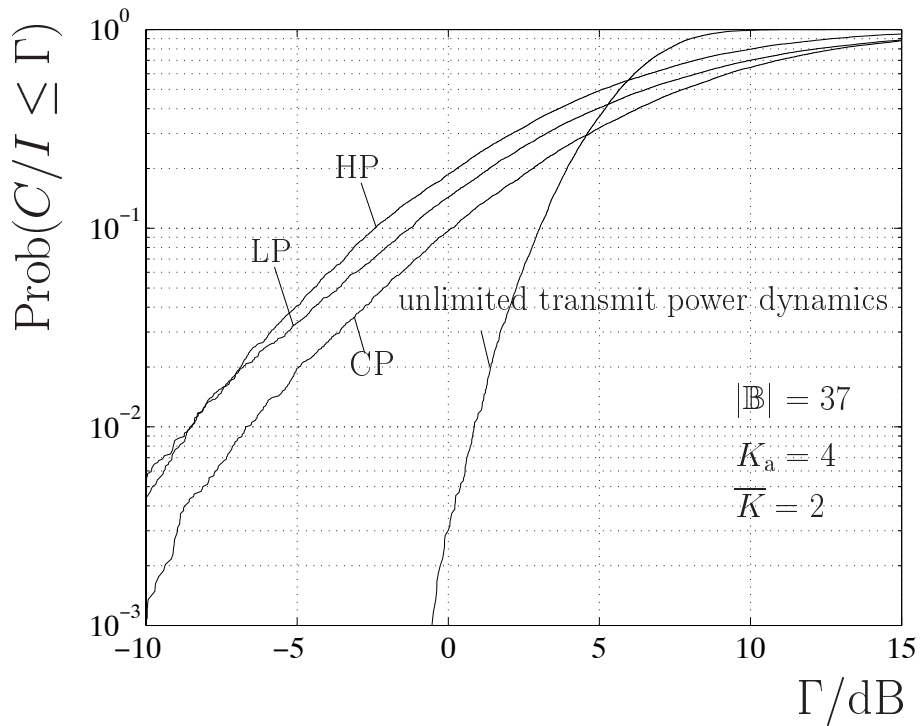
Fig. 3.15: CDF of C/I by clipping with different selections of T_{min} and T_{max}: LP, CP and HP; $|\mathbb{B}| = 37$, $\bar{K} = 2$ and $K_a = 4$
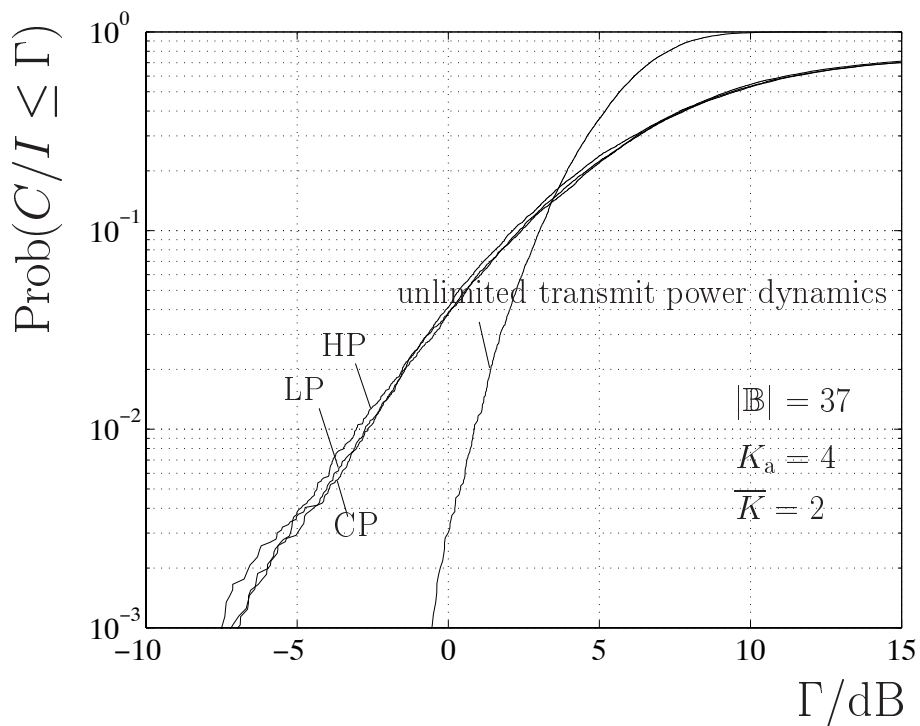
Fig. 3.16: CDF of C/I by compression with different selections of T_{min} and T_{max}: LP, CP and HP; $|\mathbb{B}| = 37$, $\bar{K} = 2$ and $K_a = 4$

Chapter 4

Link level considerations

4.1   Introduction

In Chapter 3, the investigations of the TD-CDMA downlink with adaptive transmit antennas are focused on the system level. The obtained simulation results show that the system performance in terms of the CDF of C/I can be significantly improved with increasing number K_a of transmit antenna elements, see for instance Figs. 3.3 to 3.6. In this chapter adaptive transmit antennas are considered on the link level. The key benefits of using adaptive transmit antennas, see Section 1.2, will be quantitatively demonstrated. Moreover, it will be shown that in connection with PJD adaptive transmit antennas can significantly reduce the coded BER for a given SNR at the input of the joint detector.

The present chapter is organized as follows. A transmission model which allows the inclusion and consideration of adaptive transmit antennas in the TD-CDMA downlink is introduced in Section 4.2. In Section 4.3, mathematical descriptions are presented to clarify the assignment of CDMA codes to MSs when utilizing CDMA code pooling. Then, a comprehensive description of the data transmission between the BS and the MS in the downlink is provided in Section 4.4. Next, the MC and MPIC algorithms, which were already introduced in Chapter 3 for system level considerations, are described in Section 4.5 with respect to the specific aspects of link level considerations. The conventional JD and PJD schemes are discussed in Section 4.6 followed by the description of a procedure for optimization of the SNIR when performing PJD in Section 4.7. In order to reduce the complexity of the computer simulations an efficient simulation concept for investigating the coded BER is introduced and its performance is compared with that obtained by using the common computer simulation techniques in Section 4.8. Finally, simulation results are
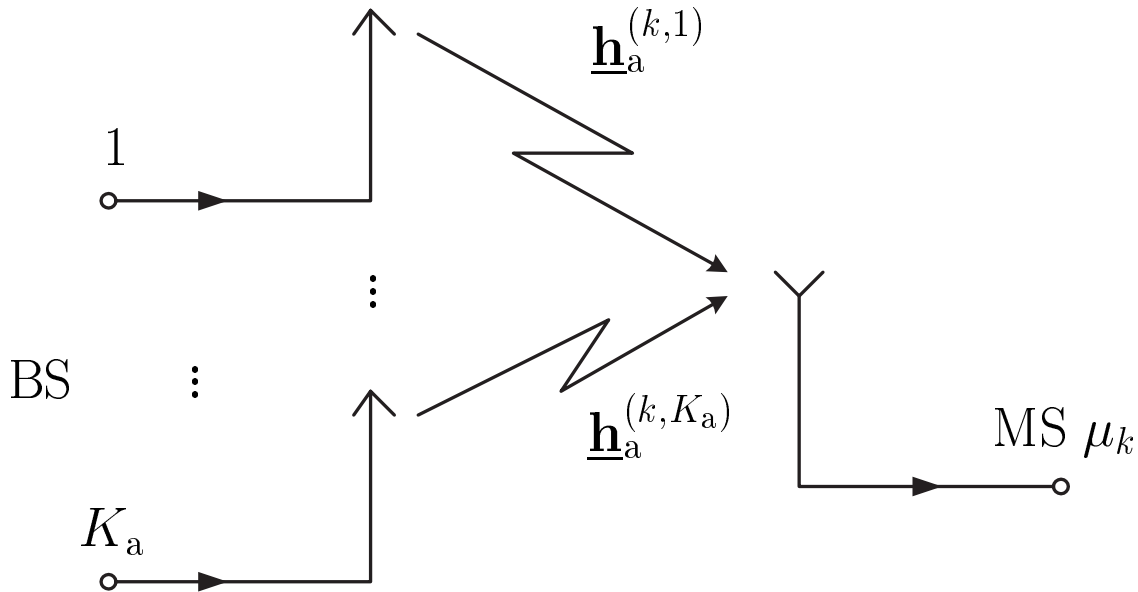
Fig. 4.1: Network with K_a input ports and one output port modeling the channel between the inputs of the K_a BS transmit antenna elements and the output of the receive antenna of MS μ_k

presented and discussed in Section 4.9. Throughout the following chapters, signals and channel impulse responses are presented in the time discrete equivalent low-pass domain, if not otherwise stated.

4.2   Transmission model of the TD-CDMA downlink with adaptive transmit antennas

4.2.1   Channels between the ports of the transmit antennas and the port of the receive antenna

A network with K_a input ports and one output port modeling the channel between the inputs of the K_a BS transmit antenna elements and the output of the receive antenna of MS μ_k is shown in Fig. 4.1. In this network the channel impulse responses

$$\underline{\mathbf{h}}_\mathrm{a}^{(k,k_\mathrm{a})} = (\underline{h}_{\mathrm{a},1}^{(k,k_\mathrm{a})} \ldots \underline{h}_{\mathrm{a},W}^{(k,k_\mathrm{a})})^\mathrm{T}, \ k_\mathrm{a} = 1 \ldots K_\mathrm{a}, \ k = 1 \ldots K, \tag{4.1}$$

of dimension W characterizes signal transmission between the input of transmit antenna element k_a and the output of the receive antenna of MS μ_k. In total $K_\mathrm{a} \cdot K$ channel impulse responses $\underline{\mathbf{h}}_\mathrm{a}^{(k,k_\mathrm{a})}$ of (4.1) exist, which are termed antenna element specific channel impulse

DOD k_d leading to MS μ_k

AE 1

$\underline{\mathbf{h}}_\mathrm{d}^{(k,k_\mathrm{d})}$

$\underline{a}_{k_\mathrm{a}}^{(k,k_\mathrm{d})} \cdot \underline{\mathbf{h}}_\mathrm{d}^{(k,k_\mathrm{d})}$

RP

AE k_a

AE K_a
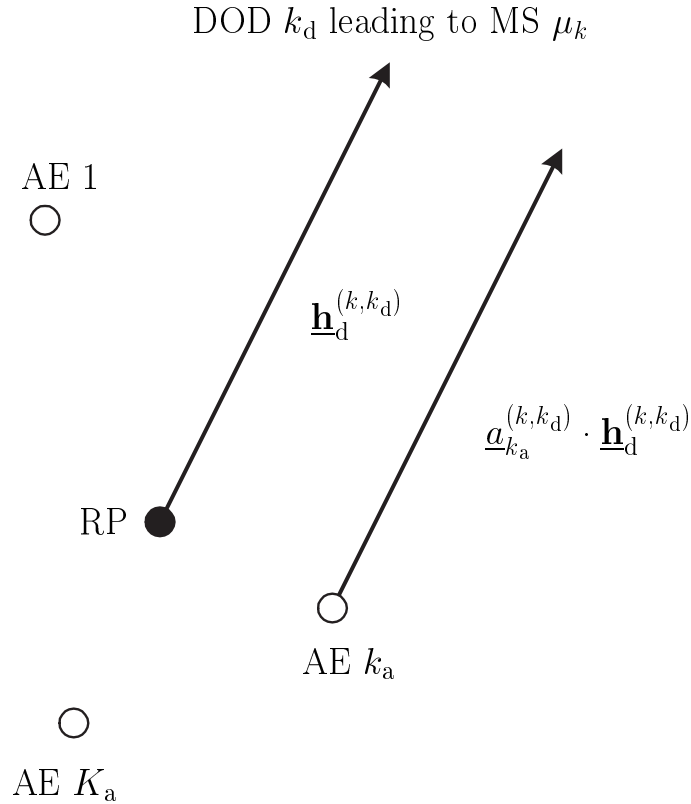
Fig. 4.2: Transmit antenna arrangement at the BS with reference point (RP) and antenna elements (AE)

responses, and which describe, under consideration of the characteristics of the transmit antenna elements, the complicated mechanism of multipath wave propagation between BS and MS μ_k in a condensed form. The transmit antenna configuration is assumed to be a micro structure [BBS97]. This means that the K_a transmit antenna elements are so closely spaced that, if they are all fed with the same signal, the waves launched by the individual transmit antenna elements in a certain direction lead to received signals at an MS antenna output which only differ in their carrier phases and amplitudes from each other.

In the transmit antenna arrangement, which may be linear, two-dimensional or three-dimensional, and which may consist of non-directional or directional antenna elements, a reference point RP is introduced, see Fig. 4.2. It is assumed that the number of DODs into which a wave can be transmitted by the BS in order to generate, via scattering at the various objects of the propagation environment, a signal of significant intensity at the MS μ_k, $k = 1 \ldots K$, has a finite value K_d. Without restricting generality, for each of the K MSs the same number K_d of relevant DODs is assumed, which has to be chosen sufficiently large in order to comply with the prevailing propagation environment. However, the K_d DODs themselves may differ from one MS to another MS. Each of the K_d DODs leading

from transmit antenna element k_a and bearing to MS μ_k is characterized by a complex steering factor $\underline{a}_{k_\mathrm{a}}^{(k,k_\mathrm{d})}$, $k_\mathrm{d} = 1 \ldots K_\mathrm{d}$, $k = 1 \ldots K$. In order to clarify the meaning of these factors, let us assume that in the RP a fictitious omnidirectional transmit antenna is placed, which is fed with a signal $\underline{\mathbf{s}}$. With this signal, a wave launched in DOD k_d bearing to MS μ_k generates the signal $\underline{\mathbf{s}}^{(k)}$ at the receive antenna output at MS μ_k. Now, if the same signal $\underline{\mathbf{s}}$ would be fed into transmit antenna element k_a, the wave launched into the same DOD would generate, with the complex steering factor $\underline{a}_{k_\mathrm{a}}^{(k,k_\mathrm{d})}$, the signal $\underline{a}_{k_\mathrm{a}}^{(k,k_\mathrm{d})} \cdot \underline{\mathbf{s}}^{(k)}$ at the receive antenna output at MS μ_k. $\underline{a}_{k_\mathrm{a}}^{(k,k_\mathrm{d})}$ depends on the characteristic, the location and the orientation of transmit antenna element k_a as well as on DOD k_d leading from transmit antenna element k_a to MS μ_k. For given values of k_d and k the K_a factors $\underline{a}_{k_\mathrm{a}}^{(k,k_\mathrm{d})}$, $k_\mathrm{a} = 1 \ldots K_\mathrm{a}$, can be compiled in a column vector of dimension K_a termed steering vector [MM80, GC81, NPK94]

$$\mathbf{a}^{(k,k_\mathrm{d})} = (\underline{a}_1^{(k,k_\mathrm{d})} \ldots \underline{a}_{K_\mathrm{a}}^{(k,k_\mathrm{d})})^\mathrm{T}, \; k_\mathrm{d} = 1 \ldots K_\mathrm{d}, \; k = 1 \ldots K. \tag{4.2}$$

Each of the K_d DODs leading from the RP to MS μ_k, see Fig. 4.2, is characterized by a directional channel impulse response

$$\mathbf{h}_\mathrm{d}^{(k,k_\mathrm{d})} = (\underline{h}_{\mathrm{d},1}^{(k,k_\mathrm{d})} \ldots \underline{h}_{\mathrm{d},W}^{(k,k_\mathrm{d})})^\mathrm{T}, \; k_\mathrm{d} = 1 \ldots K_\mathrm{d}, \; k = 1 \ldots K, \tag{4.3}$$

of dimension W. With the steering factors $\underline{a}_{k_\mathrm{a}}^{(k,k_\mathrm{d})}$ of (4.2) the directional channel impulse responses $\mathbf{h}_\mathrm{d}^{(k,k_\mathrm{d})}$ of (4.3) are related to the antenna element specific channel impulse responses $\mathbf{h}_\mathrm{a}^{(k,k_\mathrm{a})}$ of (4.1) as follows:

$$\mathbf{h}_\mathrm{a}^{(k,k_\mathrm{a})} = (\underline{h}_{\mathrm{a},1}^{(k,k_\mathrm{a})} \ldots \underline{h}_{\mathrm{a},W}^{(k,k_\mathrm{a})})^\mathrm{T} = \sum_{k_\mathrm{d}=1}^{K_\mathrm{d}} \mathbf{h}_\mathrm{d}^{(k,k_\mathrm{d})} \underline{a}_{k_\mathrm{a}}^{(k,k_\mathrm{d})}, \; k_\mathrm{a} = 1 \ldots K_\mathrm{a}, \; k = 1 \ldots K. \tag{4.4}$$

As shown in Fig. 4.3, based on (4.4) the network of Fig. 4.1 can be broken up into three partial networks, which represent the K_a transmit antenna elements, the radio channel and the receive antenna at MS μ_k, respectively. In case the actually occurring number of the relevant directional channel impulse responses is for some MS smaller than the predetermined value K_d, this can be considered in (4.4) by setting a corresponding number of the K_d directional channel impulse responses $\mathbf{h}_\mathrm{d}^{(k,k_\mathrm{d})}$ of (4.3) zero for this MS.

4.2.2   Channels between transmitter output and receiver input

As shown in [3G99], in each TDMA burst the TD-CDMA transmitter simultaneously generates K signals, see also Fig. 1.1, which are discernible by their individual CDMA codes [KKB96]

$$\underline{\mathbf{c}}^{(k_\mathrm{s})} = (\underline{c}_1^{(k_\mathrm{s})} \ldots \underline{c}_Q^{(k_\mathrm{s})})^\mathrm{T}, \; k_\mathrm{s} = 1 \ldots K_\mathrm{s}, \tag{4.5}$$
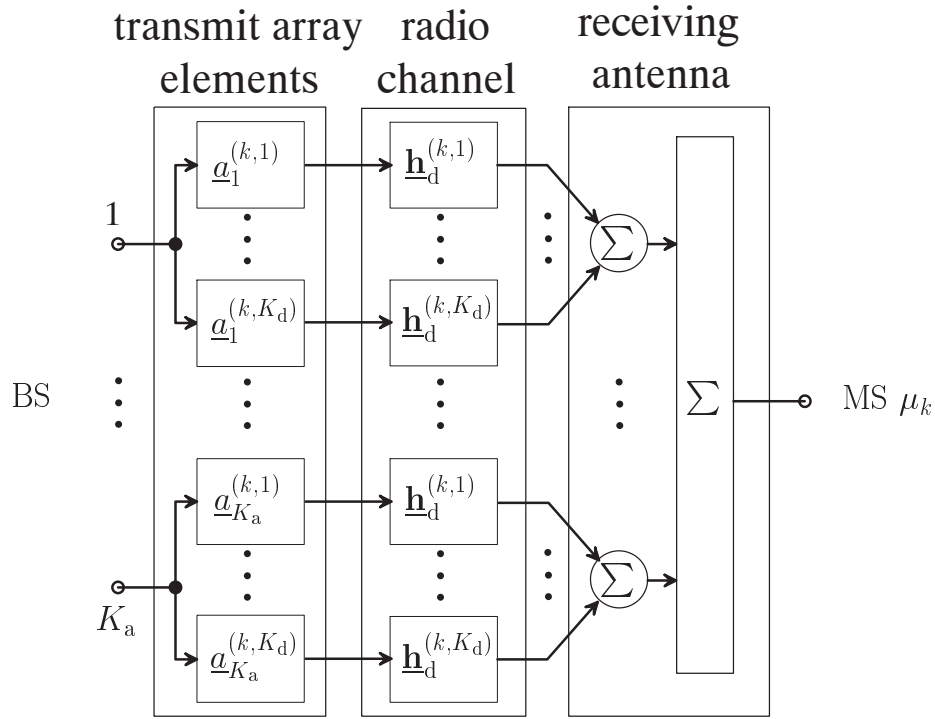
Fig. 4.3: Detailed description of the network of Fig. 4.1
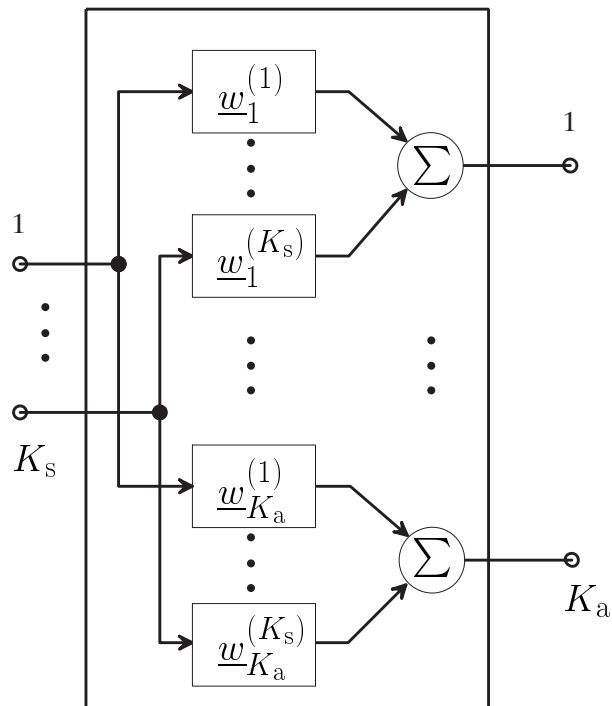
Fig. 4.4: Network with K_s input ports and K_a output ports performing the linear combination of the K signals utilizing the antenna weight vector $\underline{\mathbf{w}}^{(k_\mathrm{s})}$ of (4.7) at the BS

of dimension Q. Each of these signals carries a partial data vector

$$\underline{\mathbf{d}}^{(k_{\mathrm{s}})} = (\underline{d}_1^{(k_{\mathrm{s}})} \ldots \underline{d}_N^{(k_{\mathrm{s}})})^{\mathrm{T}}, \ k_{\mathrm{s}} = 1 \ldots K_{\mathrm{s}}, \tag{4.6}$$

of dimension N. In the case of a BS with a single omnidirectional transmit antenna, these K_{s} signals would be first added and then fed to the antenna. If the BS employs an antenna array of K_{a} transmit antenna elements, each of the K_{s} signals is first fed into one of the K_{s} input ports of a linear weighting network with K_{s} input ports and K_{a} output ports, see Fig. 4.4. At each of the K_{a} output ports of this network a linear combination of the K_{s} input signals appears, which is fed to the corresponding transmit antenna element. These linear combinations are determined by the K_{s} signal specific weight vectors

$$\underline{\mathbf{w}}^{(k_{\mathrm{s}})} = (\underline{w}_1^{(k_{\mathrm{s}})} \ldots \underline{w}_{K_{\mathrm{a}}}^{(k_{\mathrm{s}})})^{\mathrm{T}}, \ k_{\mathrm{s}} = 1 \ldots K_{\mathrm{s}}, \tag{4.7}$$

of dimension K_{a}, see Fig. 4.4. Each antenna weight vector $\underline{\mathbf{w}}^{(k_{\mathrm{s}})}$ of (4.7) is assigned to one of the K_{s} signals generated by the transmitter and containing the corresponding CDMA code $\underline{\mathbf{c}}^{(k_{\mathrm{s}})}$ of (4.5). In order to model the transmission channel between the K_{s} transmitter outputs and the receiver input, the networks of Figs. 4.3 and 4.4 have to be concatenated as shown in Fig. 4.5, which results in a network with K_{s} input ports and one output port.

The K_{a} antenna element specific channel impulse responses $\underline{\mathbf{h}}_{\mathrm{a}}^{(k,k_{\mathrm{a}})}$ of (4.1) related to MS μ_k can be arranged in the antenna element specific channel impulse response matrix

$$\underline{\mathbf{H}}_{\mathrm{a}}^{(k)} = (\underline{\mathbf{h}}_{\mathrm{a}}^{(k,1)} \ldots \underline{\mathbf{h}}_{\mathrm{a}}^{(k,K_{\mathrm{a}})}). \tag{4.8}$$

Then, the channel impulse response between input port k_{s} and the single output port of the network of Fig. 4.5 becomes, with $\underline{\mathbf{w}}^{(k_{\mathrm{s}})}$ of (4.7),

$$\underline{\mathbf{h}}^{(k,k_{\mathrm{s}})} = (\underline{h}_1^{(k,k_{\mathrm{s}})} \ldots \underline{h}_W^{(k,k_{\mathrm{s}})})^{\mathrm{T}} = \underline{\mathbf{H}}_{\mathrm{a}}^{(k)} \underline{\mathbf{w}}^{(k_{\mathrm{s}})}, \ k = 1 \ldots K, \ k_{\mathrm{s}} = 1 \ldots K_{\mathrm{s}}. \tag{4.9}$$

This channel impulse response is termed signal specific, because it is determined by the antenna weight vector $\underline{\mathbf{w}}^{(k_{\mathrm{s}})}$ of (4.7). The question still open is how the antenna weight vectors $\underline{\mathbf{w}}^{(k_{\mathrm{s}})}$ of (4.7) should be chosen in a beneficial way. This question will be answered in Section 4.5.

4.3 CDMA code pooling

High user data rates are required in future mobile radio systems. As already stated in Chapter 1, in TD-CDMA high user data rates can be supported by assigning more than one TDMA time slot within a TDMA frame and/or more than one CDMA code within
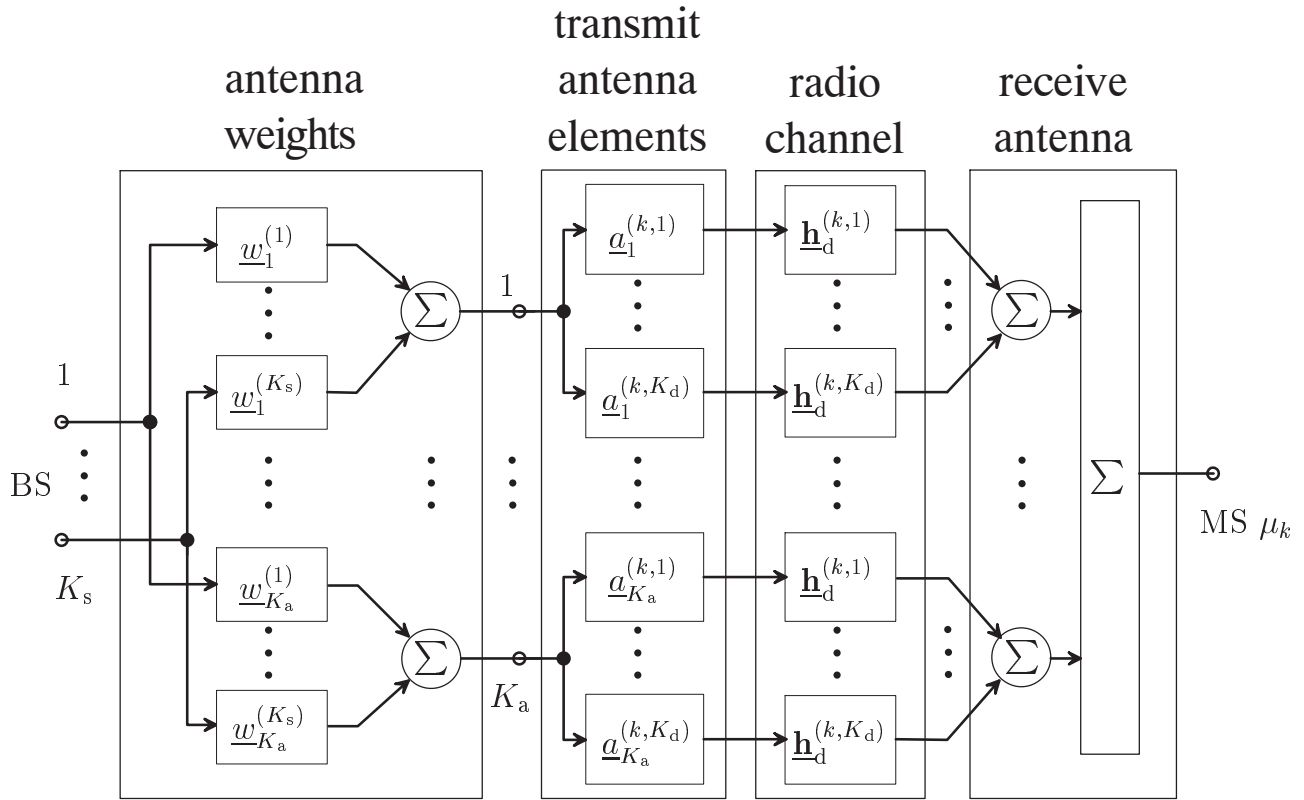
Fig. 4.5: Network with K_s input ports and one output port between the BS transmitter and the receiver of MS μ_k

this TDMA time slot to a user. The use of multi time slot within a TDMA frame to enable high data rate services has been considered in the General Packet Radio Service (GPRS) for GSM system, which proposes to use each time slot of a frame employed by GSM to support transmission rates as high as 115 kbits/s [AC99]. CDMA code pooling, the use of more than one CDMA code within a TDMA time slot to serve a certain MS μ_k, is described in the following.

Suppose a BS supports K MSs μ_k, $k = 1 \ldots K$, in the TD-CDMA downlink by

$$K_s \geq K \tag{4.10}$$

CDMA codes $\underline{\mathbf{c}}^{(k_s)}$, $k_s = 1 \ldots K_s$, of dimension Q, see (4.5), which form the set

$$\mathbb{C} = \left\{ \underline{\mathbf{c}}^{(1)} \ \ldots \ \underline{\mathbf{c}}^{(k_s)} \ \ldots \ \underline{\mathbf{c}}^{(K_s)} \right\}. \tag{4.11}$$

Each of the K_s CDMA codes $\underline{\mathbf{c}}^{(k_s)}$ contained in the set $\mathbb{C}$ of (4.11) is utilized by the BS to generate CDMA signal k_s to be transmitted via the adaptive transmit antenna, see Fig. 4.4. If CDMA code pooling is not applied, there is a one-to-one relation between CDMA codes and MSs, that is, each of the K MSs utilizes exactly one of the K_s CDMA codes

$\underline{c}^{(k_s)}$, $k_s = 1 \ldots K_s$, of (4.5), and, consequently, the number K of the MSs supportable in one TDMA time slot equals K_s. In the case of CDMA code pooling, more than one of the K_s CDMA codes $\underline{c}^{(k_s)}$, $k_s = 1 \ldots K_s$, of (4.5) are assigned, at least to some of the MSs μ_k, $k = 1 \ldots K$. This assignment can be described by the relation

$$k_s \mapsto y(k_s), \ y(k_s) \in \{1 \ldots K\}, \ k_s = 1 \ldots K_s, \tag{4.12}$$

which uniquely assigns CDMA code $\underline{c}^{(k_s)}$ of (4.5) to MS $\mu_{y(k_s)}$. In this case, by virtue of (4.12), several values k_s may lead to the same value $y(k_s)$. With $y(k_s)$ of (4.12) all CDMA codes, which are used to spectrally spread the signals intended for MS μ_k, constitute the set

$$\mathbb{C}^{(k)} = \bigcup_{\forall \ k_s | y(k_s) = k} \{\underline{c}^{(k_s)}\} \tag{4.13}$$

of cardinality $K_s^{(k)}$. Consequently, with $\mathbb{C}$ of (4.11) and $\mathbb{C}^{(k)}$ of (4.13) the CDMA codes not being of interest to MS μ_k constitute the set

$$\overline{\mathbb{C}^{(k)}} = \mathbb{C} \setminus \mathbb{C}^{(k)} \tag{4.14}$$

of cardinality $K_s - K_s^{(k)}$. It is to see from (4.13) that

$$\sum_{k=1}^{K} K_s^{(k)} = K_s \tag{4.15}$$

holds.

In order to illustrate the meaning of (4.12), (4.13) and (4.14), an exemplary assignment of the CDMA codes to the MSs when applying CDMA code pooling is shown in Fig. 4.6 for $K_s = 16$ and $K = 4$. Each of the four MSs is served by the BS by assigning more than one CDMA code. Obviously, MS μ_4 has the highest user data rates in this example. Now, $y(k_s)$ of (4.12) becomes

$$y(k_s) = \begin{cases} 1 & \text{if} \quad k_s = 5, 6, \\ 2 & \text{if} \quad k_s = 1, 2, 3, 4, \\ 3 & \text{if} \quad k_s = 7, 8, 9, \\ 4 & \text{if} \quad k_s = 10, 11, 12, 13, 14, 15, 16, \end{cases} \tag{4.16}$$

and $\mathbb{C}^{(k)}$, $k = 1 \ldots 4$, of (4.13) takes the form

$$\begin{aligned}
\mathbb{C}^{(1)} &= \left\{ \underline{c}^{(5)} \ \underline{c}^{(6)} \right\}, \\
\mathbb{C}^{(2)} &= \left\{ \underline{c}^{(1)} \ \underline{c}^{(2)} \ \underline{c}^{(3)} \ \underline{c}^{(4)} \right\}, \\
\mathbb{C}^{(3)} &= \left\{ \underline{c}^{(7)} \ \underline{c}^{(8)} \ \underline{c}^{(9)} \right\}, \\
\mathbb{C}^{(4)} &= \left\{ \underline{c}^{(10)} \ \underline{c}^{(11)} \ \underline{c}^{(12)} \ \underline{c}^{(13)} \ \underline{c}^{(14)} \ \underline{c}^{(15)} \ \underline{c}^{(16)} \right\}.
\end{aligned} \tag{4.17}$$

16 CDMA codes $\underline{\mathbf{c}}^{(1)} \ldots \underline{\mathbf{c}}^{(16)}$
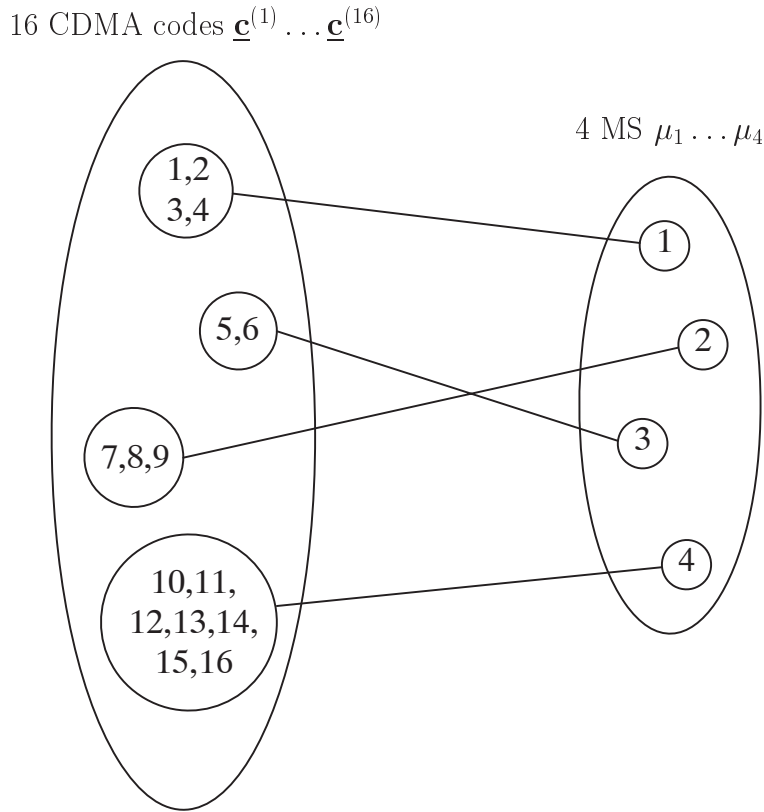
Fig. 4.6: Exemplary assignment of CDMA codes to MSs when applying CDMA code pooling; $K_{\mathrm{s}} = 16$ and $K = 4$

4.4 Data transmission

As fundamentals for treating data transmission and detection in the TD-CDMA uplink with adaptive receive antennas a number of quantities, vectors, matrices as well as data detection algorithms are available [Naß95, Ste96, Kle96, Bla98, Pap00]. In this thesis, these fundamentals are adapted in such a way that they become applicable to the TD-CDMA downlink with adaptive transmit antennas. The notations used in this thesis are listed in Tab. 4.1. Based on these notations the mathematical description of the data transmission in the TD-CDMA downlink with adaptive transmit antennas is given in this section.

With the CDMA codes $\underline{\mathbf{c}}^{(k_{\mathrm{s}})}$ of (4.5) the CDMA code matrices

$$
\begin{aligned}
\underline{\mathbf{C}}^{(k_{\mathrm{s}})} &= (\underline{C}_{l,w}^{(k_{\mathrm{s}})}),\ l = 1 \ldots Q + W - 1,\ w = 1 \ldots W,\ k_{\mathrm{s}} = 1 \ldots K_{\mathrm{s}}, \\
\underline{C}_{l,w}^{(k_{\mathrm{s}})} &= \begin{cases} \underline{c}_{l-w+1}^{(k_{\mathrm{s}})} & \text{if} \quad 1 \le l - w + 1 \le Q, \\ 0 & \text{else} \end{cases}
\end{aligned}
\tag{4.18}
$$

of dimension $(Q + W - 1) \times W$ can be formed. Then, with the CDMA code matrix $\underline{\mathbf{C}}^{(k_{\mathrm{s}})}$

Tab. 4.1: Notations

N	Number of data symbols per half-burst and one CDMA code.
$\underline{\mathbf{c}}^{(k_s)}$	CDMA code valid for CDMA signal k_s, $k_s = 1 \ldots K_s$, has the dimension $Q \times 1$
$\underline{\mathbf{d}}^{(k_s)}$	Partial coded data vector conveyed by means of CDMA code $\underline{\mathbf{c}}^{(k_s)}$, $k_s = 1 \ldots K_s$. $\underline{\mathbf{d}}^{(k_s)}$ is a $N \times 1$ vector.
$\underline{\mathbf{d}}$	Total coded data vector. $\underline{\mathbf{d}}$ is a vector which is obtained by stacking the K_s partial coded data vectors $\underline{\mathbf{d}}^{(k_s)}$, $k_s = 1 \ldots K_s$, and has the dimension $NK_s \times 1$.
$\underline{\mathbf{h}}^{(k,k_s)}$	Signal specific channel impulse response valid for CDMA signal k_s, $k_s = 1 \ldots K_s$, and MS μ_k, $k = 1 \ldots K$, has the dimension $W \times 1$
$\underline{\mathbf{b}}^{(k,k_s)}$	Composite channel impulse response valid for CDMA signal k_s, $k_s = 1 \ldots K_s$, and MS μ_k, $k = 1 \ldots K$, has the dimension $(Q + W - 1) \times 1$
$\underline{\mathbf{A}}^{(k,k_s)}$	Partial system matrix valid for CDMA signal k_s, $k_s = 1 \ldots K_s$, and MS μ_k, $k = 1 \ldots K$. $\underline{\mathbf{A}}^{(k,k_s)}$ has the dimension $(NQ + W - 1) \times N$ and is constituted by the CDMA code $\underline{\mathbf{c}}^{(k_s)}$ and the signal specific channel impulse response $\underline{\mathbf{h}}^{(k,k_s)}$
$\underline{\mathbf{A}}^{(k)}$	Total system matrix of the considered TDMA burst valid for MS μ_k, has the dimension $(NQ + W - 1) \times K_s N$.
$\underline{\mathbf{n}}^{(k)}$	Interference representing intercell interference plus thermal noise at MS μ_k. $\underline{\mathbf{n}}^{(k)}$ is an $(NQ + W - 1) \times 1$ vector. The components of $\underline{\mathbf{n}}^{(k)}$ are assumed to be independent complex Gaussian variables with variance $\sigma^{(k)2}$ of real and imaginary parts.
$\underline{\mathbf{e}}^{(k)}$	Total received signal at MS μ_k. $\underline{\mathbf{e}}^{(k)}$ is an $(NQ + W - 1) \times 1$ vector.

of (4.18) and the signal specific channel impulse responses $\underline{\mathbf{h}}^{(k,k_s)}$ of (4.9) the composite channel impulse responses

$$\underline{\mathbf{b}}^{(k,k_s)} = \underline{\mathbf{C}}^{(k_s)} \underline{\mathbf{h}}^{(k,k_s)} = \underline{\mathbf{C}}^{(k_s)} \underline{\mathbf{H}}_a^{(k)} \underline{\mathbf{w}}^{(k_s)}, \; k = 1 \ldots K, \; k_s = 1 \ldots K_s, \qquad (4.19)$$

of dimension $Q + W - 1$ between input port k_s and the output port of the network of Fig. 4.5 are obtained. $\underline{\mathbf{b}}^{(k,k_s)}$ of (4.19) carries the partial data vectors $\underline{\mathbf{d}}^{(k_s)}$ of (4.6) as shown in [Kle96]. In contrast to the uplink case, the composite channel impulse responses $\underline{\mathbf{b}}^{(k,k_s)}$ of (4.19) depend on the choice of the K_s antenna weight vectors $\underline{\mathbf{w}}^{(k_s)}$ of (4.7). Therefore, the performance of the TD-CDMA downlink depends on the antenna weight vectors $\underline{\mathbf{w}}^{(k_s)}$ of (4.7). With $\underline{\mathbf{b}}^{(k,k_s)}$ of (4.19), the partial system matrix

$$\begin{aligned}
\underline{\mathbf{A}}^{(k,k_s)} &= (\underline{A}_{i,n}^{(k,k_s)}), \; i = 1 \ldots NQ + W - 1, \; n = 1 \ldots N, \\
\underline{A}_{i,n}^{(k,k_s)} &= \begin{cases} \underline{b}_{i-(n-1)Q}^{(k,k_s)} & \text{if} \quad 1 \le i - (n-1)Q \le Q + W - 1, \\ 0 & \text{else} \end{cases}
\end{aligned} \qquad (4.20)$$

valid for MS μ_k and CDMA signal k_s associated with CDMA code $\underline{\mathbf{c}}^{(k_s)}$ of (4.5) can be formed. $\underline{\mathbf{A}}^{(k,k_s)}$ of (4.20) has dimension $(NQ + W - 1) \times N$. In Fig. 4.7 the structure
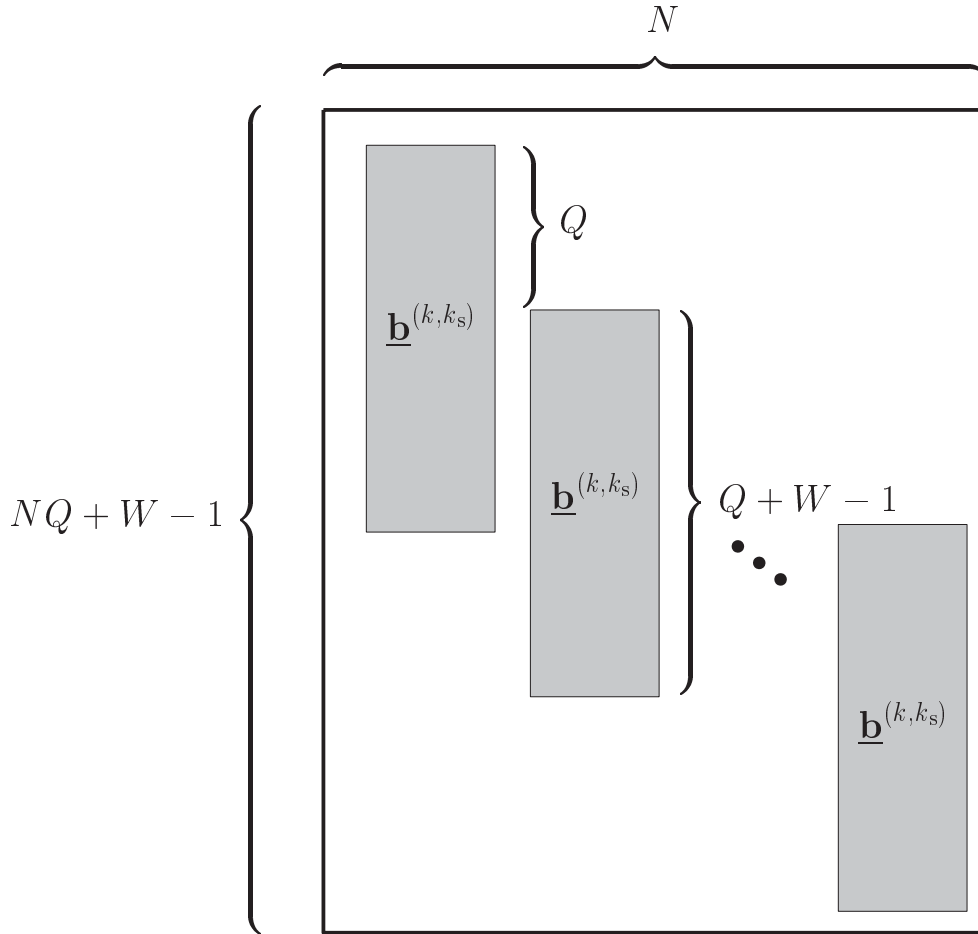
Fig. 4.7: Structure of the partial system matrix $\underline{\mathbf{A}}^{(k,k_s)}$ of (4.20), see also [Kle96, Naß95, Pap00]; white areas: zero elements

of $\underline{\mathbf{A}}^{(k,k_s)}$ of (4.20) is shown [Kle96, Pap00]. The partial system matrices $\underline{\mathbf{A}}^{(k,k_s)}$ of (4.20) can be stacked to form the total system matrix

$$\underline{\mathbf{A}}^{(k)} = (\underline{\mathbf{A}}^{(k,1)} \ldots \underline{\mathbf{A}}^{(k,K_s)}) \qquad (4.21)$$

valid for MS μ_k. $\underline{\mathbf{A}}^{(k)}$ of (4.21) has the dimensions $(NQ + W - 1) \times K_s N$.

With the vectors $\underline{\mathbf{d}}$ and $\underline{\mathbf{n}}^{(k)}$ introduced in Tab. 4.1 and with the total system matrix $\underline{\mathbf{A}}^{(k)}$ of (4.21) the received signal

$$\underline{\mathbf{e}}^{(k)} = (\underline{\mathbf{A}}^{(k,1)} \ldots \underline{\mathbf{A}}^{(k,K_s)})\underline{\mathbf{d}} + \underline{\mathbf{n}}^{(k)} = \underline{\mathbf{A}}^{(k)}\underline{\mathbf{d}} + \underline{\mathbf{n}}^{(k)} \qquad (4.22)$$

appearing at the output of the network of Fig. 4.5 and, consequently, at the receiver input of MS μ_k, is obtained. For instance, in the case Q equal to 3, W equal to 4 and K_a

equal to 2, the composite channel impulse response $\underline{\mathbf{b}}^{(k,k_s)}$ of (4.19) becomes

$$
\begin{pmatrix}
\underline{b}_1^{(k,k_s)} \\
\underline{b}_2^{(k,k_s)} \\
\underline{b}_3^{(k,k_s)} \\
\underline{b}_4^{(k,k_s)} \\
\underline{b}_5^{(k,k_s)} \\
\underline{b}_{Q+W-1}^{(k,k_s)}
\end{pmatrix}
=
\begin{pmatrix}
\underline{c}_1^{(k_s)} & 0 & 0 & 0 \\
\underline{c}_2^{(k_s)} & \underline{c}_1^{(k_s)} & 0 & 0 \\
\underline{c}_Q^{(k_s)} & \underline{c}_2^{(k_s)} & \underline{c}_1^{(k_s)} & 0 \\
0 & \underline{c}_Q^{(k_s)} & \underline{c}_2^{(k_s)} & \underline{c}_1^{(k_s)} \\
0 & 0 & \underline{c}_Q^{(k_s)} & \underline{c}_2^{(k_s)} \\
0 & 0 & 0 & \underline{c}_Q^{(k_s)}
\end{pmatrix}
\begin{pmatrix}
\underline{h}_{a,1}^{(k,1)} & \underline{h}_{a,1}^{(k,K_a)} \\
\underline{h}_{a,2}^{(k,1)} & \underline{h}_{a,2}^{(k,K_a)} \\
\underline{h}_{a,3}^{(k,1)} & \underline{h}_{a,3}^{(k,K_a)} \\
\underline{h}_{a,W}^{(k,1)} & \underline{h}_{a,W}^{(k,K_a)}
\end{pmatrix}
\begin{pmatrix}
\underline{w}_1^{(k_s)} \\
\underline{w}_{K_a}^{(k_s)}
\end{pmatrix}. \quad (4.23)
$$

Furthermore, with N equal to 3 and K_s equal to 2 the received signal $\underline{\mathbf{e}}^{(k)}$ of (4.22) takes the form

$$
\begin{pmatrix}
\underline{e}_1^{(k)} \\
\underline{e}_2^{(k)} \\
\underline{e}_3^{(k)} \\
\underline{e}_4^{(k)} \\
\underline{e}_5^{(k)} \\
\underline{e}_6^{(k)} \\
\underline{e}_7^{(k)} \\
\underline{e}_8^{(k)} \\
\underline{e}_9^{(k)} \\
\underline{e}_{10}^{(k)} \\
\underline{e}_{11}^{(k)} \\
\underline{e}_{NQ+W-1}^{(k)}
\end{pmatrix}
=
\begin{pmatrix}
\underline{b}_1^{(k,1)} & 0 & 0 & \underline{b}_1^{(k,K_s)} & 0 & 0 \\
\underline{b}_2^{(k,1)} & 0 & 0 & \underline{b}_2^{(k,K_s)} & 0 & 0 \\
\underline{b}_3^{(k,1)} & 0 & 0 & \underline{b}_3^{(k,K_s)} & 0 & 0 \\
\underline{b}_4^{(k,1)} & \underline{b}_1^{(k,1)} & 0 & \underline{b}_4^{(k,K_s)} & \underline{b}_1^{(k,K_s)} & 0 \\
\underline{b}_5^{(k,1)} & \underline{b}_2^{(k,1)} & 0 & \underline{b}_5^{(k,K_s)} & \underline{b}_2^{(k,K_s)} & 0 \\
\underline{b}_{Q+W-1}^{(k,1)} & \underline{b}_3^{(k,1)} & 0 & \underline{b}_{Q+W-1}^{(k,K_s)} & \underline{b}_3^{(k,K_s)} & 0 \\
0 & \underline{b}_4^{(k,1)} & \underline{b}_1^{(k,1)} & \underline{b}_1^{(k,K_s)} & \underline{b}_4^{(k,K_s)} & \underline{b}_1^{(k,K_s)} \\
0 & \underline{b}_5^{(k,1)} & \underline{b}_2^{(k,1)} & \underline{b}_2^{(k,K_s)} & \underline{b}_5^{(k,K_s)} & \underline{b}_2^{(k,K_s)} \\
0 & \underline{b}_{Q+W-1}^{(k,1)} & \underline{b}_3^{(k,1)} & \underline{b}_3^{(k,K_s)} & \underline{b}_{Q+W-1}^{(k,K_s)} & \underline{b}_3^{(k,K_s)} \\
0 & 0 & \underline{b}_4^{(k,1)} & 0 & 0 & \underline{b}_4^{(k,K_s)} \\
0 & 0 & \underline{b}_5^{(k,1)} & 0 & 0 & \underline{b}_5^{(k,K_s)} \\
0 & 0 & \underline{b}_{Q+W-1}^{(k,1)} & 0 & 0 & \underline{b}_{Q+W-1}^{(k,K_s)}
\end{pmatrix}
$$

$$
\begin{pmatrix}
\underline{d}_1^{(1)} \\
\underline{d}_2^{(1)} \\
\underline{d}_N^{(1)} \\
\underline{d}_1^{(K_s)} \\
\underline{d}_2^{(K_s)} \\
\underline{d}_N^{(K_s)}
\end{pmatrix}
+
\begin{pmatrix}
\underline{n}_1^{(k)} \\
\underline{n}_2^{(k)} \\
\underline{n}_3^{(k)} \\
\underline{n}_4^{(k)} \\
\underline{n}_5^{(k)} \\
\underline{n}_6^{(k)} \\
\underline{n}_7^{(k)} \\
\underline{n}_8^{(k)} \\
\underline{n}_9^{(k)} \\
\underline{n}_{10}^{(k)} \\
\underline{n}_{11}^{(k)} \\
\underline{n}_{NQ+W-1}^{(k)}
\end{pmatrix}. \quad (4.24)
$$

An alternative description of the partial system matrix $\underline{\mathbf{A}}^{(k,k_s)}$ of (4.20) can be obtained based on the channel impulse response matrix

$$
\underline{\tilde{\mathbf{H}}}^{(k,k_\mathrm{s})} =
\begin{pmatrix}
\underline{h}_1^{(k,k_\mathrm{s})} & 0 & \ldots & 0 \\
\underline{h}_2^{(k,k_\mathrm{s})} & \underline{h}_1^{(k,k_\mathrm{s})} & \ldots & 0 \\
\vdots & \vdots & \vdots & \vdots \\
\underline{h}_W^{(k,k_\mathrm{s})} & \underline{h}_{W-1}^{(k,k_\mathrm{s})} & \ldots & 0 \\
0 & \underline{h}_W^{(k,k_\mathrm{s})} & \ldots & 0 \\
\vdots & \vdots & \ldots & \vdots \\
0 & 0 & \ldots & \underline{h}_1^{(k,k_\mathrm{s})} \\
0 & 0 & \ldots & \underline{h}_2^{(k,k_\mathrm{s})} \\
\vdots & \vdots & \ldots & \vdots \\
0 & 0 & \vdots & \underline{h}_W^{(k,k_\mathrm{s})}
\end{pmatrix},
\tag{4.25}
$$

$$
\underline{\tilde{H}}_{n+w-1,n}^{(k,k_\mathrm{s})} =
\begin{cases}
\underline{h}_w^{(k,k_\mathrm{s})} & \text{if} \quad \begin{aligned} & w = 1\ldots W, \\ & n = 1\ldots N, \\ & k = 1\ldots K, \end{aligned} \\
0 & \text{else}
\end{cases}
\tag{4.26}
$$

containing the signal specific channel impulse response $\underline{\mathbf{h}}^{(k,k_\mathrm{s})}$ of (4.9) and the CDMA code matrix

$$
\underline{\tilde{\mathbf{C}}}^{(k_\mathrm{s})} =
\begin{pmatrix}
\underline{c}_1^{(k_\mathrm{s})} & 0 & \ldots & 0 \\
\underline{c}_2^{(k_\mathrm{s})} & 0 & \ldots & 0 \\
\vdots & \vdots & \vdots & \vdots \\
\underline{c}_Q^{(k_\mathrm{s})} & 0 & \ldots & 0 \\
0 & \underline{c}_1^{(k_\mathrm{s})} & \ldots & 0 \\
0 & \underline{c}_2^{(k_\mathrm{s})} & \ldots & 0 \\
\vdots & \vdots & \vdots & \vdots \\
0 & \underline{c}_Q^{(k_\mathrm{s})} & \vdots & 0 \\
\vdots & \vdots & \ldots & \vdots \\
0 & 0 & \ldots & \underline{c}_1^{(k_\mathrm{s})} \\
0 & 0 & \ldots & \underline{c}_2^{(k_\mathrm{s})} \\
\vdots & \vdots & \ldots & \vdots \\
0 & 0 & \ldots & \underline{c}_Q^{(k_\mathrm{s})}
\end{pmatrix},
\tag{4.27}
$$

$$
\underline{\tilde{C}}_{(n-1)Q+q,n}^{(k_\mathrm{s})} =
\begin{cases}
\underline{c}_q^{(k_\mathrm{s})} & \text{if} \quad \begin{aligned} & q = 1\ldots Q, \\ & n = 1\ldots N, \\ & k_\mathrm{s} = 1\ldots K_\mathrm{s}, \end{aligned} \\
0 & \text{else}
\end{cases}
\tag{4.28}
$$

containing the CDMA code $\underline{\mathbf{c}}^{(k_\mathrm{s})}$ of (4.5). With $\otimes$ denoting the Kronecker product, N the number of symbols in each data section of the burst and $\mathbf{I}^{(N \times N)}$ the $N \times N$ identity matrix, the CDMA code matrix $\underline{\tilde{\mathbf{C}}}^{(k_\mathrm{s})}$ of (4.27) can be expressed in the form

$$\underline{\tilde{\mathbf{C}}}^{(k_\mathrm{s})} = \mathbf{I}^{(N \times N)} \otimes \underline{\mathbf{c}}^{(k_\mathrm{s})}, \ \ k_\mathrm{s} = 1 \ldots K_\mathrm{s}. \tag{4.29}$$

Now, with $\underline{\tilde{\mathbf{H}}}^{(k,k_\mathrm{s})}$ of (4.25) and $\underline{\tilde{\mathbf{C}}}^{(k_\mathrm{s})}$ of (4.27)

$$\mathbf{A}^{(k,k_\mathrm{s})} = \underline{\tilde{\mathbf{H}}}^{(k,k_\mathrm{s})} \underline{\tilde{\mathbf{C}}}^{(k_\mathrm{s})}, \ \ k = 1 \ldots K, \ k_\mathrm{s} = 1 \ldots K_\mathrm{s}, \tag{4.30}$$

and

$$\mathbf{A}^{(k)} = (\mathbf{A}^{(k,1)} \ldots \mathbf{A}^{(k,K_\mathrm{s})}) = \left(\ \tilde{\mathbf{H}}^{(k,1)} \underline{\tilde{\mathbf{C}}}^{(1)} \ldots \tilde{\underline{\mathbf{H}}}^{(k,K_\mathrm{s})} \underline{\tilde{\mathbf{C}}}^{(K_\mathrm{s})} \ \right), \ k = 1 \ldots K, \tag{4.31}$$

hold for the partial system matrix $\mathbf{A}^{(k,k_\mathrm{s})}$ of (4.20) and for the total system matrix $\mathbf{A}^{(k)}$ of (4.21), respectively.

It should be noted that, for describing data transmission, in the case of the uplink, only one total system matrix $\underline{\mathbf{A}}$ of dimension $K_\mathrm{a}(NQ + W - 1) \times K_\mathrm{s}N$ is required, whereas in the case of downlink K total system matrices $\underline{\mathbf{A}}^{(k)}$, $k = 1 \ldots K$, of (4.21) or (4.31) each of dimension $(NQ + W - 1) \times K_\mathrm{s}N$ are necessary.

4.5 Algorithms for determining the antenna weights

4.5.1 The MC algorithm

In Section 3.3, the MC and MPCI algorithms have been introduced for system level considerations. In Sections 4.5.1 and 4.5.2, these algorithms will be derived for the link level. In the system level considerations of Section 3.3 the considered interference was restricted to the intercell interference, whereas in the present link level considereations only intracell interference plays a role. In the following derivations the CDMA codes $\underline{\mathbf{c}}^{(k_\mathrm{s})}$, $k_\mathrm{s} = 1 \ldots K_\mathrm{s}$, of (4.5) and the signal specific channel impulse responses $\underline{\mathbf{h}}^{(k,k_\mathrm{s})}$, $k = 1 \ldots K$, $k_\mathrm{s} = 1 \ldots K_\mathrm{s}$ of (4.9) have to be taken into account.

As in the system level considerations of Section 3.3, the main idea of the MC algorithm is that, for a given transmit power, the antenna weight vectors $\underline{\mathbf{w}}^{(k_\mathrm{s})}$, $k_\mathrm{s} = 1 \ldots K_\mathrm{s}$, of (4.7) related to the CDMA codes $\underline{\mathbf{c}}^{(k_\mathrm{s})}$, $k_\mathrm{s} = 1 \ldots K_\mathrm{s}$, of (4.5) assigned to MS μ_k, $k = 1 \ldots K$, are chosen in such a way that the power of the corresponding CDMA signal k_s received

at MS μ_k is maximized [LB00b]. Let us assume that CDMA signal k_s associated with CDMA code $\underline{\mathbf{c}}^{(k_s)}$ of (4.5) and carrying a single data symbol is fed into input port k_s of the network of Fig. 4.5. The magnitude of this data is one and the transmit antenna elements are perfectly decoupled. Then, the total energy radiated by the K_a transmit antenna elements due to feeding the CDMA signal based on $\underline{\mathbf{c}}^{(k_s)}$ into port k_s of the network of Fig. 4.5 becomes

$$T^{(k_s)} = \frac{1}{2}\underline{\mathbf{c}}^{(k_s)^{*T}}\underline{\mathbf{c}}^{(k_s)}\underline{\mathbf{w}}^{(k_s)^{*T}}\underline{\mathbf{w}}^{(k_s)}. \tag{4.32}$$

With the composite channel impulse response $\underline{\mathbf{b}}^{(k,k_s)}$ of (4.19), the energy of $\underline{\mathbf{b}}^{(k,k_s)}$ of (4.19) observed at the receiver input at MS μ_k becomes

$$R^{(k,k_s)} = \frac{1}{2}\underline{\mathbf{b}}^{(k,k_s)^{*T}}\underline{\mathbf{b}}^{(k,k_s)} = \frac{1}{2}\underline{\mathbf{w}}^{(k_s)^{*T}}\underline{\mathbf{H}}_a^{(k)^{*T}}\underline{\mathbf{C}}^{(k_s)^{*T}}\underline{\mathbf{C}}^{(k_s)}\underline{\mathbf{H}}_a^{(k)}\underline{\mathbf{w}}^{(k_s)}. \tag{4.33}$$

Furthermore, let us assume that it is intended to serve MS $\mu_{y(k_s)}$ by sending CDMA signal k_s based on $\underline{\mathbf{c}}^{(k_s)}$, see (4.12). Then, the desired energy received at MS $\mu_{y(k_s)}$ and generated by sending this signal is obtained by setting k_s equal to $y(k_s)$ in (4.33), which results in

$$R^{(k,y(k_s))} = \frac{1}{2}\underline{\mathbf{w}}^{(k_s)^{*T}}\underline{\mathbf{H}}_a^{(y(k_s))^{*T}}\underline{\mathbf{C}}^{(k_s)^{*T}}\underline{\mathbf{C}}^{(k_s)}\underline{\mathbf{H}}_a^{(y(k_s))}\underline{\mathbf{w}}^{(k_s)}. \tag{4.34}$$

Now, the criterion proposed by the author to determine the antenna weight vectors $\underline{\mathbf{w}}^{(k_s)}$, $k_s = 1 \ldots K_s$, of (4.7) consists in maximizing the ratio

$$\frac{R^{(y(k_s),k_s)}}{T^{(k_s)}} = \frac{\underline{\mathbf{w}}^{(k_s)^{*T}}\underline{\mathbf{H}}_a^{(y(k_s))^{*T}}\underline{\mathbf{C}}^{(k_s)^{*T}}\underline{\mathbf{C}}^{(k_s)}\underline{\mathbf{H}}_a^{(y(k_s))}\underline{\mathbf{w}}^{(k_s)}}{\underline{\mathbf{c}}^{(k_s)^{*T}}\underline{\mathbf{c}}^{(k_s)}\underline{\mathbf{w}}^{(k_s)^{*T}}\underline{\mathbf{w}}^{(k_s)}} = \frac{\underline{\mathbf{w}}^{(k_s)^{*T}}\underline{\mathbf{Y}}^{(y(k_s),k_s)}\underline{\mathbf{w}}^{(k_s)}}{\underline{\mathbf{w}}^{(k_s)^{*T}}\underline{\mathbf{w}}^{(k_s)}} \tag{4.35}$$

of the desired received energy $R^{(k,y(k_s))}$ of (4.34) to the total transmitted energy $T^{(k_s)}$ of (4.32). The antenna weight vectors $\underline{\mathbf{w}}^{(k_s)}$ of (4.7) can be determined by

$$\underline{\mathbf{w}}^{(k_s)} = \arg\max_{\underline{\mathbf{w}}^{(k_s)}}\frac{\underline{\mathbf{w}}^{(k_s)^{*T}}\underline{\mathbf{Y}}^{(y(k_s),k_s)}\underline{\mathbf{w}}^{(k_s)}}{\underline{\mathbf{w}}^{(k_s)^{*T}}\underline{\mathbf{w}}^{(k_s)}}, \ k_s = 1 \ldots K_s. \tag{4.36}$$

For a given CDMA code $\underline{\mathbf{c}}^{(k_s)}$ of (4.5) and a given antenna element specific channel impulse response matrix $\underline{\mathbf{H}}_a^{(y(k_s))}$ of (4.8) the antenna weight vector $\underline{\mathbf{w}}^{(k_s)}$ of (4.7) which maximizes the ratio (4.35) is the eigenvector belonging to the largest eigenvalue of the matrix $\underline{\mathbf{Y}}^{(y(k_s),k_s)}$ in (4.35) [ZF84]. Similar to (3.21), with the restraint

$$\underline{\mathbf{w}}^{(k_s)^{*T}}\underline{\mathbf{w}}^{(k_s)} = 1, \ k_s = 1 \ldots K_s, \tag{4.37}$$

$\underline{\mathbf{w}}^{(k_s)}$, $k_s = 1 \ldots K_s$, of (4.7) satisfying (4.36) is uniquely determined.

4.5.2   The MPCI algorithm

In contrast to the MC algorithm, the MPCI algorithm aims at maximizing the pseudo carrier-to-interference ratio $(C/I)_\mathrm{P}$, see Section 3.3. In the case considered in Section 4.5.1 the sum of the energies of CDMA signal k_s transmitted by the BS to serve MS μ_k and received at other MSs $\mu_{k'}$, $k' \neq k$, is

$$\sum_{\forall\ k|k\neq y(k_\mathrm{s})} R^{(k,k_\mathrm{s})} = \frac{1}{2}\underline{\mathbf{w}}^{(k_\mathrm{s})*\mathrm{T}} \sum_{\forall\ k|k\neq y(k_\mathrm{s})} \underline{\mathbf{H}}_\mathrm{a}^{(k)*\mathrm{T}} \underline{\mathbf{C}}^{(k_\mathrm{s})*\mathrm{T}} \underline{\mathbf{C}}^{(k_\mathrm{s})} \underline{\mathbf{H}}_\mathrm{a}^{(k)} \underline{\mathbf{w}}^{(k_\mathrm{s})}$$

$$= \frac{1}{2}\underline{\mathbf{w}}^{(k_\mathrm{s})*\mathrm{T}} \sum_{\forall\ k|k\neq y(k_\mathrm{s})} \underline{\mathbf{Y}}^{(k,k_\mathrm{s})} \underline{\mathbf{w}}^{(k_\mathrm{s})}. \tag{4.38}$$

According to the criterion of the MPCI algorithm for determining the antenna weight vectors $\underline{\mathbf{w}}^{(k_\mathrm{s})}$, $k_\mathrm{s} = 1 \ldots K_\mathrm{s}$, of (4.7) and with the relation (4.12), the pseudo carrier-to-interference ratio

$$\frac{R^{(y(k_\mathrm{s}),k_\mathrm{s})}}{\displaystyle\sum_{\forall\ k|k\neq y(k_\mathrm{s})} R^{(k,k_\mathrm{s})}} = \frac{\underline{\mathbf{w}}^{(k_\mathrm{s})*\mathrm{T}} \underline{\mathbf{Y}}^{(y(k_\mathrm{s}),k_\mathrm{s})} \underline{\mathbf{w}}^{(k_\mathrm{s})}}{\underline{\mathbf{w}}^{(k_\mathrm{s})*\mathrm{T}} \displaystyle\sum_{\forall\ k|k\neq y(k_\mathrm{s})} \underline{\mathbf{Y}}^{(k,k_\mathrm{s})} \underline{\mathbf{w}}^{(k_\mathrm{s})}} = \frac{\underline{\mathbf{w}}^{(k_\mathrm{s})*\mathrm{T}} \underline{\mathbf{Y}}^{(y(k_\mathrm{s}),k_\mathrm{s})} \underline{\mathbf{w}}^{(k_\mathrm{s})}}{\underline{\mathbf{w}}^{(k_\mathrm{s})*\mathrm{T}} \underline{\mathbf{Y}}_\mathrm{I}^{(k,k_\mathrm{s})} \underline{\mathbf{w}}^{(k_\mathrm{s})}} \tag{4.39}$$

is to be maximized. The antenna weight vector $\underline{\mathbf{w}}^{(k_\mathrm{s})}$, $k_\mathrm{s} = 1 \ldots K_\mathrm{s}$, of (4.7) to be determined is given by

$$\underline{\mathbf{w}}^{(k_\mathrm{s})} = \arg \max_{\underline{\mathbf{w}}^{(k_\mathrm{s})}} \frac{\underline{\mathbf{w}}^{(k_\mathrm{s})*\mathrm{T}} \underline{\mathbf{Y}}^{(y(k_\mathrm{s}),k_\mathrm{s})} \underline{\mathbf{w}}^{(k_\mathrm{s})}}{\underline{\mathbf{w}}^{(k_\mathrm{s})*\mathrm{T}} \underline{\mathbf{Y}}_\mathrm{I}^{(y(k_\mathrm{s}),k_\mathrm{s})} \underline{\mathbf{w}}^{(k_\mathrm{s})}}, \ k_\mathrm{s} = 1 \ldots K_\mathrm{s}. \tag{4.40}$$

Similar to (3.25), $\underline{\mathbf{w}}^{(k_\mathrm{s})}$ of (4.7) satisfying (4.40) is the eigenvector belonging to the maximal eigenvalue of the matrix pair $(\underline{\mathbf{Y}}_\mathrm{I}^{(y(k_\mathrm{s}),k_\mathrm{s})}, \underline{\mathbf{Y}}^{(y(k_\mathrm{s}),k_\mathrm{s})})$ [ZF84]. Furthermore, with the restraint (4.37), $\underline{\mathbf{w}}^{(k_\mathrm{s})}$ of (4.7) is uniquely determined.

The determination of the antenna weight vectors $\underline{\mathbf{w}}^{(k_\mathrm{s})}$, $k_\mathrm{s} = 1 \ldots K_\mathrm{s}$, of (4.7), with the MC and MPCI algorithms depends not only on the antenna element specific channel impulse response matrix $\underline{\mathbf{H}}_\mathrm{a}^{(y(k_\mathrm{s}))}$ of (4.8), but also on the utilized CDMA code $\underline{\mathbf{c}}^{(k_\mathrm{s})}$ of (4.5). Therefore, a renewed determination of $\underline{\mathbf{w}}^{(k_\mathrm{s})}$ of (4.7) is required if $\underline{\mathbf{c}}^{(k_\mathrm{s})}$ of (4.5) is changed, even if $\underline{\mathbf{H}}_\mathrm{a}^{(y(k_\mathrm{s}))}$ of (4.8) remains unaltered. Only for CDMA codes $\underline{\mathbf{c}}^{(k_\mathrm{s})}$ of (4.5) with perfect autocorrelation properties, which would mean that with $\underline{\mathbf{C}}^{(k_\mathrm{s})}$ of (4.18) the matrix $\underline{\mathbf{C}}^{(k_\mathrm{s})*\mathrm{T}} \underline{\mathbf{C}}^{(k_\mathrm{s})}$ would be, up to a factor, the identity matrix, $\underline{\mathbf{w}}^{(k_\mathrm{s})}$ of (4.7) would not depend on $\underline{\mathbf{c}}^{(k_\mathrm{s})}$ of (4.5).

4.6 Data detection

4.6.1 Introduction

In general, for CDMA-based systems data detection schemes can be divided into

- single-user detection (SUD) schemes, and

- multi-user detection (MUD) schemes.

The SUD schemes need no information regarding the other simultaneously active interfering users in the system and are often implemented by matched filters (MF) [Pro95]. The MUD schemes can be divided into interference cancellation (IC) and joint detection (JD). The first category is characterized by the regeneration and subtraction of the estimated data and consists of three subcategories:

- Successive Interference Cancellation (SIC) [DGE92, PH93, PH94b, PH94a, Vit90, WBOW00],

- Parallel Interference Cancellation (PIC) [VA90, YKI93, DSR98, BN99, WOWB01], and

- Hybrid Interference Cancellation (HIC) [Sun98, KA98].

In JD the front of the receiver is traditionally a bank of MF filters followed by filters that perform linear algorithms [Kle96, BBNS94, PV97, KA00], which are usually computationally expensive due to complex matrix calculations and inversions. JD can be divided into three subcategories:

- Maximum Likelihood Sequence Estimator (MLSE) [Ver86],

- Zero Forcing Block Linear Equalizer (ZF-BLE) [KB93, KKB93, KKB94], and

- Minimum Mean Square Error detector (MMSE) [RB98].

In this thesis JD performed by ZF-BLE is considered. Therefore, the terms JD and ZF-BLE are used synonymously in the following.

4.6.2 Conventional joint detection

According to (4.21) and (4.22) the signal $\underline{\mathbf{e}}^{(k)}$ received at MS μ_k, $k = 1 \dots K$, is a linear combination of the CDMA signals transmitted by the BS to MS μ_k and the other CDMA signals also transmitted by the same BS to serve the other MSs $\mu_{k'}$, $k' \neq k$, but received at MS μ_k, and the intercell interference characterized by $\underline{\mathbf{n}}^{(k)}$, see Tab. 4.1. Following (4.22), the signal $\underline{\mathbf{e}}^{(k)}$ received at MS μ_k can be written as

$$
\begin{aligned}
\underline{\mathbf{e}}^{(k)} &= (\underline{\mathbf{A}}^{(k,1)} \dots \underline{\mathbf{A}}^{(k,K_{\mathrm{s}})})(\underline{\mathbf{d}}^{(1)^{\mathrm{T}}} \dots \underline{\mathbf{d}}^{(K_{\mathrm{s}})^{\mathrm{T}}})^{\mathrm{T}} + \underline{\mathbf{n}}^{(k)} \\
&= \underline{\mathbf{A}}^{(k,1)}\underline{\mathbf{d}}^{(1)} + \dots + \underline{\mathbf{A}}^{(k,K_{\mathrm{s}})}\underline{\mathbf{d}}^{(K_{\mathrm{s}})} + \underline{\mathbf{n}}^{(k)}.
\end{aligned}
\tag{4.41}
$$

Furthermore, with the relation (4.12) describing the assignment of CDMA codes $\underline{\mathbf{c}}^{(k_{\mathrm{s}})}$ of (4.5) to MS μ_k, $k = 1 \dots K$, the signal $\underline{\mathbf{e}}^{(k)}$ of (4.41) received at MS μ_k can be rewritten in the form

$$
\underline{\mathbf{e}}^{(k)} = \sum_{\forall k_{\mathrm{s}} | y(k_{\mathrm{s}}) = k} \underline{\mathbf{A}}^{(k,k_{\mathrm{s}})}\underline{\mathbf{d}}^{(k_{\mathrm{s}})} + \sum_{\forall k_{\mathrm{s}} | y(k_{\mathrm{s}}) \neq k} \underline{\mathbf{A}}^{(k,k_{\mathrm{s}})}\underline{\mathbf{d}}^{(k_{\mathrm{s}})} + \underline{\mathbf{n}}^{(k)},
\tag{4.42}
$$

where the first term $\sum_{\forall k_{\mathrm{s}} | y(k_{\mathrm{s}}) = k} \underline{\mathbf{A}}^{(k,k_{\mathrm{s}})}\underline{\mathbf{d}}^{(k_{\mathrm{s}})}$ on the right side of (4.42) is the sum of the desired CDMA signals and the second term $\sum_{\forall k_{\mathrm{s}} | y(k_{\mathrm{s}}) \neq k} \underline{\mathbf{A}}^{(k,k_{\mathrm{s}})}\underline{\mathbf{d}}^{(k_{\mathrm{s}})}$ on the right site of (4.42) is the sum of the undesired CDMA signals received at MS μ_k.

As stated in Chapter 1, the term conventional JD means that not only the CDMA signals transmitted by the BS for MS μ_k, but also the CDMA signals transmitted for all the other MSs $\mu_{k'}$, $k' \neq k$, supported by the same BS and received at MS μ_k are jointly detected at MS μ_k. When performing conventional JD, with the covariance matrix

$$
\underline{\mathbf{R}}_{\mathrm{n}}^{(k)} = \mathrm{E}\left\{\underline{\mathbf{n}}^{(k)}\underline{\mathbf{n}}^{(k)^{*\mathrm{T}}}\right\}, \quad k = 1 \dots K,
\tag{4.43}
$$

of $\underline{\mathbf{n}}^{(k)}$ in (4.42) the estimate

$$
\begin{aligned}
\hat{\underline{\mathbf{d}}} &= \underbrace{(\underline{\mathbf{A}}^{(k)^{*\mathrm{T}}}\underline{\mathbf{R}}_{\mathrm{n}}^{(k)^{-1}}\underline{\mathbf{A}}^{(k)})^{-1}\underline{\mathbf{A}}^{(k)^{*\mathrm{T}}}\underline{\mathbf{R}}_{\mathrm{n}}^{(k)^{-1}}}_{\underline{\mathbf{M}}^{(k)}}\underline{\mathbf{e}}^{(k)} \\
&= \underline{\mathbf{d}} + \underline{\mathbf{M}}^{(k)}\underline{\mathbf{n}}^{(k)} = \underline{\mathbf{d}} + \underline{\mathbf{n}}_{\mathrm{out}}^{(k)}
\end{aligned}
\tag{4.44}
$$

of the total coded data vector $\underline{\mathbf{d}}$, see Tab. 4.1, is obtained at the receiver output of MS μ_k [Kle96]. The JD process is transparent for the total coded data vector $\underline{\mathbf{d}}$ in (4.44). The effect of the JD process is to transform the input intercell interference vector $\underline{\mathbf{n}}^{(k)}$ to the output intercell interference vector $\underline{\mathbf{n}}_{\mathrm{out}}^{(k)}$ according to [Kle96, Pap00]. This transformation depends on the matrix $\underline{\mathbf{M}}^{(k)}$ in (4.44) containing the information on the CDMA codes

$\underline{\mathbf{c}}^{(k_{\mathrm{s}})}$, $k_{\mathrm{s}} = 1 \ldots K_{\mathrm{s}}$, of (4.5), the antenna weight vectors $\underline{\mathbf{w}}^{(k_{\mathrm{s}})}$, $k_{\mathrm{s}} = 1 \ldots K_{\mathrm{s}}$, of (4.7), and the signal specific channel impulse responses $\underline{\mathbf{h}}^{(k,k_{\mathrm{s}})}$, $k = 1 \ldots K$, $k_{\mathrm{s}} = 1 \ldots K_{\mathrm{s}}$, of (4.9), but not on the kind of the channel encoder, the interleaving and the modulation.

The application of JD in TD-CDMA mobile radio systems considerably enhances system performance by eliminating intracell interference [Kle96]. However, the power of $\underline{\mathbf{n}}_{\mathrm{out}}^{(k)}$ in (4.44) at the output of the joint detector at MS μ_k is increased when performing JD. This effect can be quantified by the SNR degradation δ of the JD. According to [Kle96] the SNR degradation

$$\delta = \frac{\gamma_{\mathrm{MF}}}{\gamma_{\mathrm{JD}}} \tag{4.45}$$

is defined as the ratio of the SNR γ_{MF} at the output of the matched filter to the SNR γ_{JD} at the output of the joint detector. As shown in [Kle96], within the burst the SNR degradation differs from one symbol to another symbol. With $[\cdot]_{i,i}$ designating the i-th diagonal element of the matrix brackets and with $\underline{\mathbf{A}}^{(k)}$ of (4.21), the SNR degradation $\delta_i^{(k)}$ valid for i-th symbol of $\underline{\mathbf{d}}$ in (4.44) at the output of the joint detector at MS μ_k becomes [Kle96]

$$\delta_i^{(k)} = (\underline{\mathbf{A}}^{(k)*\mathrm{T}} \underline{\mathbf{A}}^{(k)})_{i,i} (\underline{\mathbf{A}}^{(k)*\mathrm{T}} \underline{\mathbf{A}}^{(k)})_{i,i}^{-1}, \ i = 1 \ldots K_{\mathrm{s}}N, \ k = 1 \ldots K. \tag{4.46}$$

The center symbol of all N symbols related to CDMA code $\underline{\mathbf{c}}^{(k_{\mathrm{s}})}$ of (4.5) has the largest SNR degradation [Kle96, BWW99], which is given by

$$\begin{aligned} \delta^{(k,k_{\mathrm{s}})} &= \mathrm{diag}(\underline{\mathbf{A}}^{(k)*\mathrm{T}} \underline{\mathbf{A}}^{(k)})_{N/2+(k_{\mathrm{s}}-1)N} \mathrm{diag}(\underline{\mathbf{A}}^{(k)*\mathrm{T}} \underline{\mathbf{A}}^{(k)})_{N/2+(k_{\mathrm{s}}-1)N}^{-1}, \\ &\quad k = 1 \ldots K, \ k_{\mathrm{s}} = 1 \ldots K_{\mathrm{s}}. \end{aligned} \tag{4.47}$$

The SNR degradations $\delta^{(k,k_{\mathrm{s}})}$ of (4.47) will be investigated in Section 6.4 in detail.

An approximate formula to estimate the SNR degradation δ of (4.45) is provided in [BWW99]. With the number K_{s} of the CDMA signals included in the JD process and the dimension Q of the CDMA codes $\underline{\mathbf{c}}^{(k_{\mathrm{s}})}$, $k_{\mathrm{s}} = 1 \ldots K_{\mathrm{s}}$, of (4.5), also referred to as processing gain, the SNR degradations δ of (4.45) can be approximated by

$$\delta = \frac{Q + 1}{Q - K_{\mathrm{s}} + 1}, \ K_{\mathrm{s}} > 1, \ Q \geq K_{\mathrm{s}}. \tag{4.48}$$

For a given Q the SNR degradation δ of (4.48) decreases as K_{s} decreases. This means that the smaller the number K_{s} of CDMA signals included in the JD process is, the smaller the SNR degradation δ of (4.48) is, and, consequently, the better the system performance becomes. In Fig. 4.8 the SNR degradation δ of (4.48) is shown versus the number K_{s} of the CDMA signals included in the JD process with $Q = 16$. It is observed that, if the system is fully loaded, this means $K_{\mathrm{s}} = Q = 16$, the SNR degradation δ of (4.48) is 12.3dB, whereas δ of (4.48) is only 2.76dB for $K_{\mathrm{s}} = 8$. This is one of the observations leading to PJD, which is discussed in the next section.
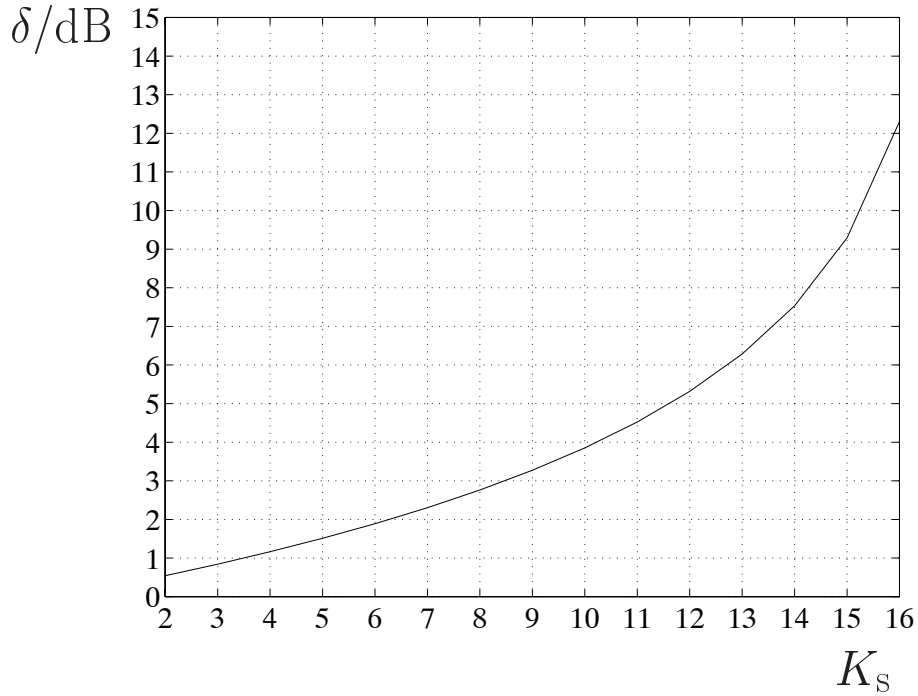
Fig. 4.8: δ of (4.48) versus K_s; $Q = 16$

4.6.3 Partial Joint Detection (PJD)

As mentioned in Chapter 1, if adaptive transmit antennas are utilized at the BS, transmitted CDMA signals not being of interest to a certain MS μ_k arrive with a more or less reduced power at this MS because of the spatial selectivity enabled by the adaptive transmit antennas. From this viewpoint, PJD is taken into account, in which at MS μ_k only a subset of all transmitted CDMA signals, of course including those being of interest to MS μ_k, that is, $\sum_{\forall k_\mathrm{s}|y(k_\mathrm{s})=k} \underline{\mathbf{A}}^{(k,k_\mathrm{s})}\underline{\mathbf{d}}^{(k_\mathrm{s})}$ in (4.42), are jointly detected. In this case, as opposed to conventional JD, two effects occur:

- Because not all K_s CDMA signals are included in the JD process at MS μ_k, the intercell interference enhancement quantified by SNR degradation δ of (4.45) is reduced, see also Fig. 4.8.

- A subset of the undesired CDMA signals, that is, a part of the signals $\sum_{\forall k_\mathrm{s}|y(k_\mathrm{s})\neq k} \underline{\mathbf{A}}^{(k,k_\mathrm{s})}\underline{\mathbf{d}}^{(k_\mathrm{s})}$ in (4.42), excluded from the JD process now emerges as an additional intracell interference.

As shown in [LB00b], the first, beneficial effect has more and more advantages over the second, detrimental effect as the number K_a of transmit antenna elements is increased.

This is due to the fact that the power of the additional intracell interfering CDMA signals coming up by being excluded from the JD process when performing PJD becomes smaller with increasing K_a. However, the question is how many and which of the undesired CDMA signals $\sum_{\forall k_\mathrm{s}|y(k_\mathrm{s})=k} \underline{\mathbf{A}}^{(k,k_\mathrm{s})}\underline{\mathbf{d}}^{(k_\mathrm{s})}$ in (4.42) should be excluded from the JD process at MS μ_k in order to maximize the effective SNIR. This question will be answered in the next section.

4.7 SNIR optimization in PJD

4.7.1 Effective noise plus interference power in PJD

It is desirable to concisely designate, among all CDMA codes $\underline{\mathbf{c}}^{(k_\mathrm{s})} \in \overline{\mathbb{C}^{(k)}}$, see (4.14), those CDMA codes the CDMA signals of which should be included/not included in the PJD process at a certain MS μ_k, $k = 1\ldots K$. To this purpose, to each of the $K_\mathrm{s} - K_\mathrm{s}^{(k)}$ CDMA codes $\underline{\mathbf{c}}^{(k_\mathrm{s})}$ of (4.5) being the basis for a CDMA signal undesired at MS μ_k a coefficient $\alpha^{(k,k_\mathrm{s})}$ is assigned. The superscript k_s of the coefficients $\alpha^{(k,k_\mathrm{s})}$ can take the values

$$k_\mathrm{s} \in \{1\ldots K_\mathrm{s}\}|y(k_\mathrm{s}) \neq k. \tag{4.49}$$

The values of the coefficients $\alpha^{(k,k_\mathrm{s})}$ are determined as follows:

$$\alpha^{(k,k_\mathrm{s})} = \begin{cases} 0 & \text{if the CDMA signal } k_\mathrm{s} \text{ related to CDMA code } \underline{\mathbf{c}}^{(k_\mathrm{s})} \\ & \text{is included in PJD at MS } \mu_k, \\ 1 & \text{else.} \end{cases} \tag{4.50}$$

The noise power at the receiver input of MS μ_k, which represents the intercell interference in an interference limited cellular system, see Section 1.2, is designated as $\sigma^{(k)^2}$, see Tab. 4.1. For each pair of a CDMA code $\underline{\mathbf{c}}^{(k_\mathrm{s})}$ of (4.5) and a MS μ_k a composite channel impulse response $\underline{\mathbf{b}}^{(k,k_\mathrm{s})}$ of (4.19) is determined by the CDMA code $\underline{\mathbf{c}}^{(k_\mathrm{s})}$ of (4.5), the antenna weight vector $\underline{\mathbf{w}}^{(k_\mathrm{s})}$ of (4.7) with which the CDMA signals generated at the BS are fed to the K_a BS transmit antenna elements, see Fig. 4.5, and the antenna element specific channel impulse response $\underline{\mathbf{h}}_\mathrm{a}^{(k,k_\mathrm{a})}$ of (4.4) of the radio channels between the BS transmit antenna element k_a and the receive antenna of MS μ_k [LB00b]. Now, with the coefficients $\alpha^{(k,k_\mathrm{s})}$ of (4.50) and the symbolism

$$\sum_{\forall\ k_\mathrm{s}|y(k_\mathrm{s})\neq k} \cdots = \sum_{\mathrm{undes}} \cdots \tag{4.51}$$

-"undes" stands for undesired- and under the assumption that each transmitted symbol has the magnitude one, the noise plus interference power at the receiver input of MS μ_k can be expressed as

$$N_{\text{in}}^{(k)} = \sigma^{(k)2} + \frac{1}{2Q} \sum_{\text{undes}} \alpha^{(k,k_{\text{s}})} \left| \underline{\mathbf{b}}^{(k,k_{\text{s}})} \right|^2 . \tag{4.52}$$

The terms $\sigma^{(k)2}$ and $\frac{1}{2Q} \sum\limits_{\text{undes}} \alpha^{(k,k_{\text{s}})} \left| \underline{\mathbf{b}}^{(k,k_{\text{s}})} \right|^2$ on the right side of (4.52) represent the intercell interference power and the intracell interference power, respectively. The total number of CDMA signals included in the PJD process at MS μ_k is

$$\tilde{K}_{\text{s}}^{(k)} = K_{\text{s}} - \sum_{\text{undes}} \alpha^{(k,k_{\text{s}})} \geq K_{\text{s}}^{(k)} . \tag{4.53}$$

Due to the intercell interference enhancement quantified by the SNR degradation δ of (4.45), when performing PJD, the effective noise plus interference power $N^{(k)'}$ at the receiver input of MS μ_k is larger than $N_{\text{in}}^{(k)}$ of (4.52). As mentioned in Section 4.6.2, δ can be approximated by (4.48). Through substituting K_{s} in (4.48) by $\tilde{K}_{\text{s}}^{(k)}$ of (4.53), the SNR degradation $\delta^{(k)}$ valid for MS μ_k, $k = 1 \ldots K$, can be expressed as

$$\delta^{(k)} = \frac{Q+1}{Q+1-\tilde{K}_{\text{s}}^{(k)}} = \frac{Q+1}{Q+1-K_{\text{s}}+\sum\limits_{\text{undes}} \alpha^{(k,k_{\text{s}})}} . \tag{4.54}$$

With $N_{\text{in}}^{(k)}$ of (4.52) and $\delta^{(k)}$ of (4.54) the effective noise plus interference power at the receiver input of MS μ_k becomes

$$N^{(k)'} = \delta^{(k)} N_{\text{in}}^{(k)} = \frac{Q+1}{Q+1-K_{\text{s}}+\sum\limits_{\text{undes}} \alpha^{(k,k_{\text{s}})}} \left(\sigma^{(k)2} + \frac{1}{2Q} \sum_{\text{undes}} \alpha^{(k,k_{\text{s}})} \left| \underline{\mathbf{b}}^{(k,k_{\text{s}})} \right|^2 \right) . \tag{4.55}$$

It is observed from (4.55) that, if more and more of the CDMA signals not being of interest to MS μ_k are excluded from the PJD process performed at MS μ_k, $\delta^{(k)}$ of (4.54) decreases and $N_{\text{in}}^{(k)}$ of (4.52) increases. This is the quantitative manifestation of the beneficial and detrimental effects, respectively, mentioned in Section 4.6.3.

With the input SNR

$$\gamma^{(k,k_{\text{s}})} = \frac{|\underline{\mathbf{b}}^{(k,k_{\text{s}})}|^2}{2Q\sigma^{(k)2}}, \ k_{\text{s}} = 1 \ldots K_{\text{s}}, \ k = 1 \ldots K, \tag{4.56}$$

valid for CDMA signal k_{s} associated with CDMA code $\underline{\mathbf{c}}^{(k_{\text{s}})}$ of (4.5) and received at MS μ_k the normalized effective noise plus interference power

$$N^{(k)} = N^{(k)'}/\sigma^{(k)2} = \frac{Q+1}{Q+1-K_{\text{s}}+\sum\limits_{\text{undes}} \alpha^{(k,k_{\text{s}})}} \left(1 + \sum_{\text{undes}} \alpha^{(k,k_{\text{s}})} \gamma^{(k,k_{\text{s}})} \right) \tag{4.57}$$

at the receiver input of MS μ_k can be obtained from (4.55).

4.7.2   Maximizing the SNIR

In the previous section the normalized effective noise plus interference power $N^{(k)}$, $k = 1 \ldots K$, of (4.57) at the receiver input of MS μ_k, $k = 1 \ldots K$, has been described for the case when PJD is applied. Now, a procedure for maximizing the SNIR will be presented in this section. The maximization of the SNIR at the receiver input of MS μ_k mentioned in Section 4.6.3 as the goal of the investigations in the present section is equivalent to minimizing $N^{(k)}$ of (4.57) by excluding a suitable subset of the $K_{\mathrm{s}} - K_{\mathrm{s}}^{(k)}$ CDMA signals not being of interest to MS μ_k from the PJD process performed at MS μ_k. However, the question is, how this subset should be composed. This question can be solved by analyzing the structure of $N^{(k)}$ of (4.57), which leads to the following observation: Let us start with including the selection of $K_{\mathrm{s}} - K_{\mathrm{s}}^{(k)}$ CDMA signals not being of interest to MS μ_k in the JD process performed at MS μ_k. If in the following step one element of this selection should be additionally excluded from the JD process, this element should always be the undesired CDMA signal with the smallest $\gamma^{(k,k_{\mathrm{s}})}$ of (4.56). Doing so, if it is possible to reduce $N^{(k)}$ of (4.57) at all, the maximum conceivable decrease of $N^{(k)}$ can be achieved. Based on this observation a procedure for determining the optimum subset can be established, see Fig. 4.9. To this purpose the $K_{\mathrm{s}} - K_{\mathrm{s}}^{(k)}$ CDMA signals not being of interest to MS μ_k are sorted in ascending order of their $\gamma^{(k,k_{\mathrm{s}})}$ of (4.56). The designation

$$i = \sum_{\mathrm{undes}} \alpha^{(k,k_{\mathrm{s}})} \tag{4.58}$$

for the number of excluded undesired CDMA signals and $N^{(k)}(i)$ for the corresponding normalized effective noise plus interference power $N^{(k)}$ of (4.57) when excluding the first i CDMA signals of the sorted list from JD process at MS μ_k of (4.57) are introduced. Then, the optimum subset of undesired CDMA signals to be excluded from the JD process at MS μ_k can be determined as follows:

1. Set $i = 0$ and calculate $N^{(k)}(0)$.

2. Set $i = i + 1$ and calculate $N^{(k)}(i)$.

3. Compare $N^{(k)}(i)$ with $N^{(k)}(i-1)$.

4. If $N^{(k)}(i) < N^{(k)}(i-1)$ is true then return to step 2, otherwise $i-1$ is the number of undesired CDMA signals which form the subset to be determined.

Concerning the procedure for determining the optimum subset of undesired CDMA signals to be excluded from the PJD process to maximize the SNIR at MS μ_k, see Fig.
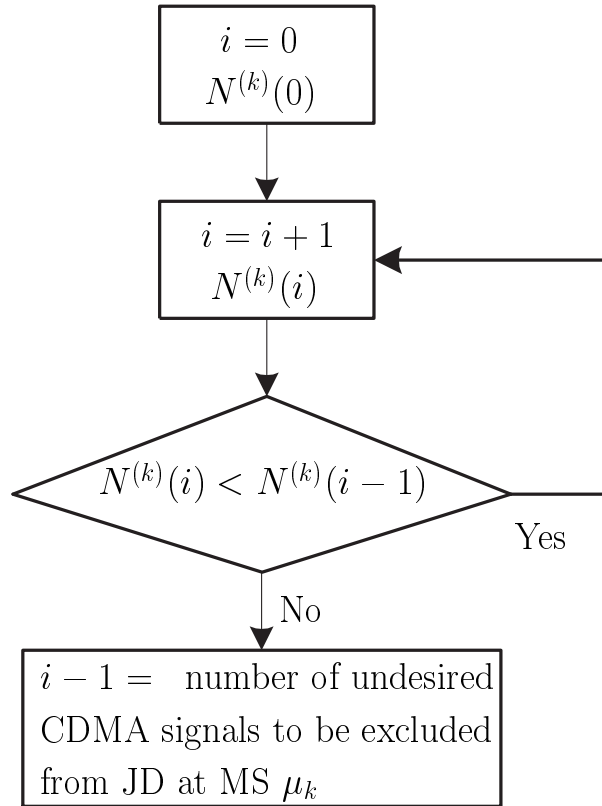
Fig. 4.9: Procedure to determine the CDMA signals undesired and to be excluded from the JD process at MS μ_k

4.9, there may be a question, why the procedure can be immediately finished when the value of $N^{(k)}(i)$ larger than that of $N^{(k)}(i-1)$. In the other words, are there any local minimums in the optimum process. In order to answer this question and in order to prove the correctness of the procedure, a mathematical analysis is given in what follows.

As mentioned above, at the beginning of the procedure the $K_{\mathrm{s}} - K_{\mathrm{s}}^{(k)}$ CDMA signals not being of interest to MS μ_k are sorted with respect to $\gamma^{(k,k_{\mathrm{s}})}$ of (4.56) in ascending order. For notational convenience, the sorted input SNRs $\gamma^{(k,k_{\mathrm{s}})}$ valid for the corresponding received CDMA signals associated with CDMA codes $\underline{\mathbf{c}}^{(k_{\mathrm{s}})}$ of (4.5), but not being of interest to MS μ_k are given by $\gamma^{(k)}(i)$, $i = 1 \ldots K_{\mathrm{s}} - K_{\mathrm{s}}^{(k)}$ with the relation

$$\gamma^{(k)}(i-1) < \gamma^{(k)}(i) < \gamma^{(k)}(i+1), \ i = 2 \ldots K_{\mathrm{s}} - K_{\mathrm{s}}^{(k)}. \tag{4.59}$$

With $N^{(k)}$ of (4.57) at the receiver input of MS μ_k, the normalized effective noise plus interference power

$$N^{(k)}(i-1) = \frac{Q+1}{Q+1-K_{\mathrm{s}}+i-1}(1 + \sum_{j=1}^{i-1} \gamma^{(k)}(j)) \tag{4.60}$$

valid for the $(i-1)$-th step of the procedure, the normalized effective noise plus interference power

$$N^{(k)}(i) = \frac{Q+1}{Q+1-K_{\mathrm{s}}+i}(1+\sum_{j=1}^{i}\gamma^{(k)}(j)) \tag{4.61}$$

valid for the i-th step of the procedure, and the normalized effective noise plus interference power

$$N^{(k)}(i+1) = \frac{Q+1}{Q+1-K_{\mathrm{s}}+i+1}(1+\sum_{j=1}^{i+1}\gamma^{(k)}(j)) \tag{4.62}$$

valid for the $(i+1)$-th step of the procedure are obtained, respectively. In order to answer the question mentioned above, let us assume that

$$N^{(k)}(i) > N^{(k)}(i-1) \tag{4.63}$$

holds. Now, it should be proved, whether

$$N^{(k)}(i+1) < N^{(k)}(i) \tag{4.64}$$

is possible or not.

First, suppose that (4.64) is possible. Then, after doing some mathematical calculations by plugging (4.60), (4.61) and (4.62) into (4.63) and (4.64),

$$\gamma^{(k)}(i) > \frac{1+\sum_{j=1}^{i-1}\gamma^{(k)}(j)}{Q+1-K_{\mathrm{s}}+i-1}, \tag{4.65}$$

and

$$\gamma^{(k)}(i+1) < \frac{1+\sum_{j=1}^{i}\gamma^{(k)}(j)}{Q+1-K_{\mathrm{s}}+i} \tag{4.66}$$

hold. Substituting (4.65) and (4.66) into (4.59) yields

$$\underbrace{\frac{1+\sum_{j=1}^{i-1}\gamma^{(k)}(j)}{Q+1-K_{\mathrm{s}}+i-1}}_{X} < \gamma^{(k)}(i) < \gamma^{(k)}(i+1) < \underbrace{\frac{1+\sum_{j=1}^{i}\gamma^{(k)}(j)}{Q+1-K_{\mathrm{s}}+i}}_{Y}. \tag{4.67}$$

Following (4.67), the difference

$$
\begin{aligned}
Y - X &= \frac{(Q+1-K_{\mathrm{s}}+i-1)(1+\sum_{j=1}^{i}\gamma^{(k)}(j)) - (Q+1-K_{\mathrm{s}}+i)(1+\sum_{j=1}^{i-1}\gamma^{(k)}(j))}{(Q+1-K_{\mathrm{s}}+i-1)(Q+1-K_{\mathrm{s}}+i)} \\
&= \frac{(Q+1-K_{\mathrm{s}}+i)\gamma^{(k)}(i) - (1+\sum_{j=1}^{i}\gamma^{(k)}(j))}{(Q+1-K_{\mathrm{s}}+i-1)(Q+1-K_{\mathrm{s}}+i)}
\end{aligned}
\tag{4.68}
$$

between Y and X in (4.67) should be larger than zero. Therefore,

$$\gamma^{(k)}(i) > \frac{1 + \sum_{j=1}^{i} \gamma^{(k)}(j)}{Q + 1 - K_{\mathrm{s}} + i} \tag{4.69}$$

must be satisfied. Compare (4.66) with (4.69), we have

$$\gamma^{(k)}(i) > \gamma^{(k)}(i+1), \tag{4.70}$$

which is incompatible with (4.59). Therefore, (4.64) cannot be hold, if (4.63) holds. This means that there is only a global minimum in the optimum procedure. In consequence, the SNIR maximizing procedure can be immediately terminated if the $N^{(k)}(i)$ is larger than $N^{(k)}(i-1)$.

4.7.3   Example

In this section, a simple, but, nevertheless, illustrative example for the application of the SNIR maximization procedure developed in Section 4.7.2 is given. In this example it will be studied how $N^{(k)}$ of (4.57) depends on the number i, see (4.58), of CDMA signals not being of interest to MS μ_k and excluded from the PJD process at this MS. To perform the procedure for maximizing the SNIR at a certain MS μ_k, see Fig. 4.9, only the knowledge of the input intercell interference power $\sigma^{(k)2}$, see Tab. 4.1, and of the composite channel impulse responses $\underline{\mathbf{b}}^{(k,k_{\mathrm{s}})}$ of (4.19) is required at MS μ_k, whereas knowledge about the antenna system utilized at the BS is not needed. The knowledge required at MS μ_k can be readily obtained from the channel estimates [Ste95] which are anyhow required at MS μ_k. In the case of time variant channels the described procedure has to be run through anew in each TD-CDMA burst. In different bursts the subset of CDMA signals not being of interest to MS μ_k and not included in the PJD process may differ depending on the composite channel impulse responses $\underline{\mathbf{b}}^{(k,k_{\mathrm{s}})}$ of (4.19) of the undesired CDMA signals and the intercell interference power power $\sigma^{(k)2}$, see Tab. 4.1.

With the symbolism

$$\sum_{\forall\ k_{\mathrm{s}}|y(k_{\mathrm{s}})=k} \cdots = \sum_{\mathrm{des}} \cdots \tag{4.71}$$

-"des" stands for desired-, and with the input SNRs $\gamma^{(k,k_{\mathrm{s}})}$ of (4.56) the SNRs

$$\gamma^{(k)}_{\mathrm{des}} \quad = \frac{1}{K^{(k)}_{\mathrm{s}}} \sum_{\mathrm{des}} \gamma^{(k,k_{\mathrm{s}})} = \frac{\sum_{\mathrm{des}} |\underline{\mathbf{b}}^{(k,k_{\mathrm{s}})}|^2}{2Q\sigma^{(k)2} K^{(k)}_{\mathrm{s}}} \tag{4.72}$$

Tab. 4.2: Values of $|\underline{\mathbf{b}}^{(1,k_{\mathrm{s}})}|^2$ valid for CDMA codes $\underline{\mathbf{c}}^{(9)} \ldots \underline{\mathbf{c}}^{(16)}$ at MS μ_1

	$|\underline{\mathbf{b}}^{(1,k_{\mathrm{s}})}|^2$			
$k_{\mathrm{s}} = 9 \ldots 12$	0.428	0.516	0.641	1.076
$k_{\mathrm{s}} = 13 \ldots 16$	1.214	1.217	1.712	1.832

at the input of the joint detector averaged over the $K_{\mathrm{s}}^{(k)}$ CDMA signals received and being of interest to MS μ_k are given. Now, the ratio

$$r^{(k)} = \frac{(\sum_{\mathrm{undes}} |\underline{\mathbf{b}}^{(k,k_{\mathrm{s}})}|^2)/(K_{\mathrm{s}} - K_{\mathrm{s}}^{(k)})}{(\sum_{\mathrm{des}} |\underline{\mathbf{b}}^{(k,k_{\mathrm{s}})}|^2)/K_{\mathrm{s}}^{(k)}} \tag{4.73}$$

of the average energies of the composite channel impulse responses $\underline{\mathbf{b}}^{(k,k_{\mathrm{s}})}$ of (4.19) of CDMA signals not being of interest and being of interest to MS μ_k, respectively, is introduced. $r^{(k)}$ of (4.73) is termed signal separation ratio. Because of the use of adaptive transmit antennas at the BS, $r^{(k)}$ of (4.73) is between one and zero and decreases with increasing number K_{a} of transmit antenna elements [LB00b]. Therefore, $r^{(k)}$ of (4.73) is a measure for the signal separation offered by the use of adaptive transmit antennas.

It is assumed in this example that the values of $\gamma_{\mathrm{des}}^{(k)}$ of (4.72) and of the quantities $|\underline{\mathbf{b}}^{(k,k_{\mathrm{s}})}|^2$ of the composite channel impulse responses $\underline{\mathbf{b}}^{(k,k_{\mathrm{s}})}$ of (4.19) belonging to the CDMA signals not being of interest to MS μ_k are known at MS μ_k. Then, with $\gamma_{\mathrm{des}}^{(k)}$ of (4.72) and $r^{(k)}$ of (4.73) the received intercell interference power can be determined as

$$\sigma^{(k)2} = \frac{\sum_{\mathrm{undes}} |\underline{\mathbf{b}}^{(k,k_{\mathrm{s}})}|^2}{2Q\gamma_{\mathrm{des}}^{(k)}r^{(k)}(K_{\mathrm{s}} - K_{\mathrm{s}}^{(k)})}. \tag{4.74}$$

With $\sigma^{(k)2}$ of (4.74) and the quantities $|\underline{\mathbf{b}}^{(k,k_{\mathrm{s}})}|^2$ of the CDMA signals not being of interest to MS μ_k the effective noise plus interference power $N^{(k)'}$ of (4.55) and consequently, the normalized effective noise plus interference power $N^{(k)}$ of (4.57) can be determined depending on the value i of (4.58).

In what follows, with the average input SNR $\gamma_{\mathrm{des}}^{(k)}$ of (4.72) of the CDMA signals being of interest to MS μ_k as a parameter, it will be shown how $N^{(k)}$ of (4.57) depends on the number i, see (4.58), of CDMA signals not being of interest to MS μ_k and excluded from the PJD process at MS μ_k. In the simulations, the values

$$\begin{aligned} K &= 2, K_{\mathrm{s}} = 16, r^{(1)} = 0.5, \\ K_{\mathrm{s}}^{(1)} &= K_{\mathrm{s}}^{(2)} = K_{\mathrm{s}}/2 = 8, \end{aligned} \tag{4.75}$$
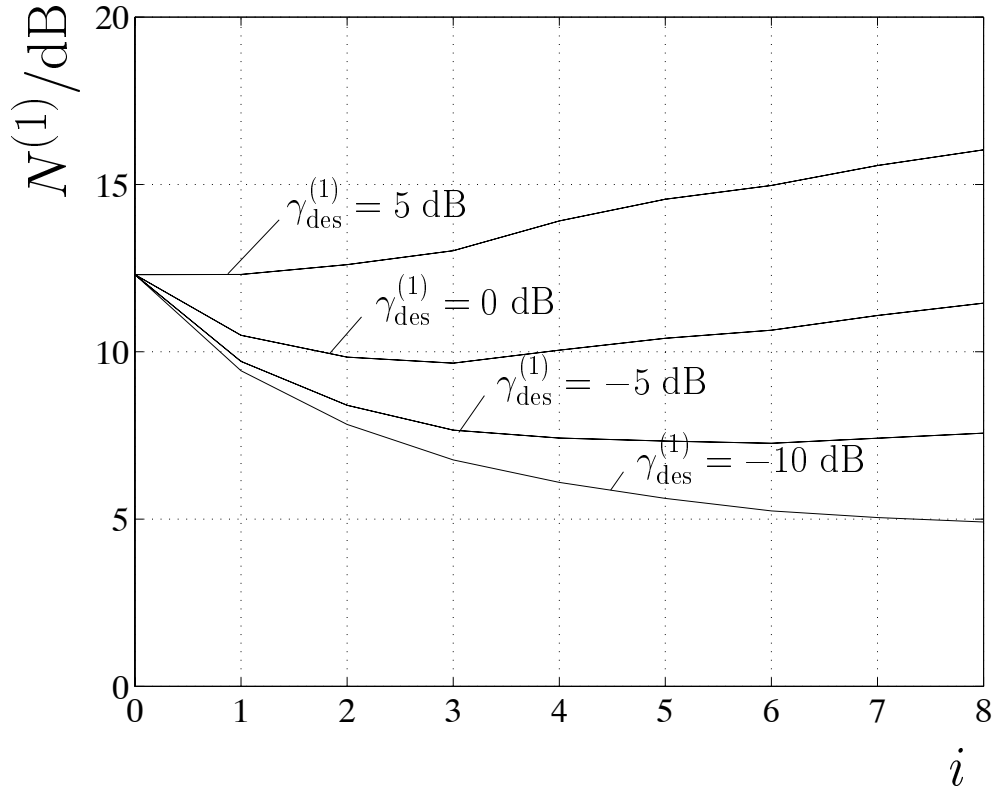
Fig. 4.10: $N^{(1)}$ of (4.57) versus the number i of (4.58) of undesired CDMA signals excluded from the JD process at MS μ_1; parameter: $\gamma_{\text{des}}^{(1)}$ of (4.72)

are assumed, where the first eight CDMA codes $\underline{\mathbf{c}}^{(1)} \ldots \underline{\mathbf{c}}^{(8)}$ are assigned to MS μ_1. Furthermore, it is assumed that $|\underline{\mathbf{b}}^{(1,k_{\text{s}})}|^2$, $k_{\text{s}} = 9 \ldots 16$, take the values given in Tab. 4.2. For this case $N^{(1)}$ of (4.57) is depicted versus i of (4.58) in Fig. 4.10 with $\gamma_{\text{des}}^{(1)}$ of (4.72) as a parameter. The graphics in Fig. 4.10 show that for large values of $\gamma_{\text{des}}^{(1)}$ all undesired CDMA signals should be included in the JD process at MS μ_k, whereas for small values of $\gamma_{\text{des}}^{(1)}$ all these signals should be excluded from the JD process. For intermediate values of $\gamma_{\text{des}}^{(1)}$, in the case of Fig. 4.10 for instance for $\gamma_{\text{des}}^{(1)}$ equal to 0dB and -5dB, $N^{(1)}$ of (4.57) becomes minimum for a certain value of i between zero and eight.

4.7.4   Critical input SNR

A procedure to optimize the SNIR at the input of the joint detector of a certain MS μ_k when performing PJD was introduced in the previous section. It can be seen from (4.57) that, in order to implement the procedure at MS μ_k, the signal specific channel impulse responses $\underline{\mathbf{h}}^{(k,k_{\text{s}})}$ of (4.9) and the CDMA codes $\underline{\mathbf{c}}^{(k_{\text{s}})}$ of (4.5) related to all undesired CDMA signals should be known at MS μ_k. In the case of the downlink, all CDMA signals transmitted by the BS from transmit antenna element k_{a} to MS μ_k travel over the common

channel characterized by the antenna element specific channel impulse response $\underline{\mathbf{h}}_{\mathrm{a}}^{(k,k_{\mathrm{a}})}$ of (4.1). However, the signal specific channel impulse responses $\underline{\mathbf{h}}^{(k,k_{\mathrm{s}})}$ of (4.9) differ from one CDMA signal to another CDMA signal due to the different antenna weight vectors $\underline{\mathbf{w}}^{(k_{\mathrm{s}})}$ of (4.7), see (4.9). Therefore, at each MS μ_k channel estimation should be performed for both desired and undesired CDMA signals in order to perform the procedure to optimize the SNIR. This observation leads to increase the complexity of the signal processing at MS μ_k. To avoid this increase of complexity, a suboptimal approach is considered, in which all $K_{\mathrm{s}} - K_{\mathrm{s}}^{(k)}$ undesired CDMA signals arriving at MS μ_k are excluded from the JD process. In this case, see the example given in Fig. 4.10, the normalized effective noise plus interference power $N^{(k)}$ of (4.57) at MS μ_k can be larger or smaller than that obtained by applying conventional JD depending on the average input SNR $\gamma_{\mathrm{des}}^{(k)}$ of (4.72). The objective of this section is to theoretically determine a critical input SNR $\gamma_{\mathrm{crit}}^{(k)}$, below which the normalized effective noise plus interference power $N^{(k)}$ of (4.57) is smaller than that obtained by applying conventional JD at MS μ_k. To this purpose, two extreme cases are considered in what follows:

- First, all $K_{\mathrm{s}} - K_{\mathrm{s}}^{(k)}$ CDMA signals not being of interest to MS μ_k, $k = 1 \ldots K$, are included in the JD process at MS μ_k, which is the case of conventional JD and is termed case 1 in what follows.

- Second, all $K_{\mathrm{s}} - K_{\mathrm{s}}^{(k)}$ CDMA signals not being of interest to MS μ_k, $k = 1 \ldots K$, are excluded from the JD process at MS μ_k. This is termed case 2 in the following.

According to (4.50), with $\sum\limits_{\mathrm{des}}$ of (4.71) the values of

$$\sum_{\mathrm{des}} \alpha^{(k,k_{\mathrm{s}})} = \begin{cases} 0 & \text{(case 1)}, \\ K_{\mathrm{s}} - K_{\mathrm{s}}^{(k)} & \text{(case 2)} \end{cases} \tag{4.76}$$

for cases 1 and 2 can be determined. Then, following (4.57), (4.72) and (4.73) the normalized effective noise plus interference power is

$$N^{(k)} = \begin{cases} Q + 1 & \text{(case 1)}, \\ \dfrac{Q+1}{Q+1-K_{\mathrm{s}}^{(k)}} (1 + r^{(k)}(K_{\mathrm{s}} - K_{\mathrm{s}}^{(k)})\gamma_{\mathrm{des}}^{(k)}) & \text{(case 2)}. \end{cases} \tag{4.77}$$

With the values of $K, K_{\mathrm{s}}, K_{\mathrm{s}}^{(1)}$ given in (4.75) the normalized effective noise plus interference power $N^{(1)}$ of (4.77) is shown versus $\gamma_{\mathrm{des}}^{(1)}$ of (4.72) in Fig. 4.11 for both case 1 and case 2 mentioned above. The parameter of the curves for case 2 is the signal separation ratio $r^{(1)}$ of (4.73). From the figure it is observed that there is an intersection point between the curve obtained for case 1 and each of the curves obtained for case 2, which
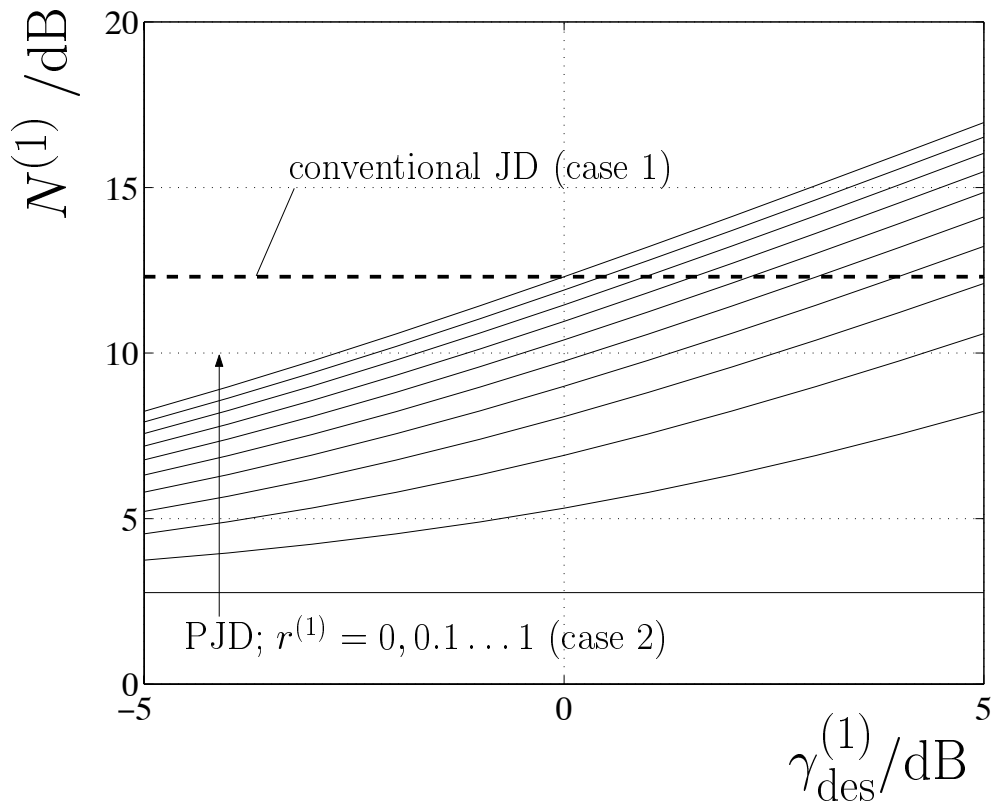
Fig. 4.11: $N^{(1)}$ of (4.57) versus $\gamma_{\text{des}}^{(1)}$ of (4.72); parameter: $r^{(1)}$ of (4.73)

corresponds to a $r^{(1)}$ of (4.73) in the range of 0.1 to 1. The value $\gamma_{\text{des}}^{(1)}$ of (4.72) corre-
sponding to each of the intersection points is defined as the critical input SNR $\gamma_{\text{crit}}^{(1)}$ valid
for MS μ_1. $\gamma_{\text{crit}}^{(1)}$ decreases with increasing $r^{(1)}$. For values $\gamma_{\text{des}}^{(1)}$ below $\gamma_{\text{crit}}^{(1)}$ the normalized
effective noise plus interference power $N^{(1)}$ of (4.77) obtained for case 2 is lower than that
obtained for case 1. Furthermore, in the case of perfect separation, i.e., $r^{(1)}$ equal to zero,
$N^{(1)}$ obtained for case 2 would not depend on the input SNR $\gamma_{\text{des}}^{(1)}$ and is approximately
9dB lower than that obtained for case 1.

Now, an analytical analysis for determining the critical input SNRs $\gamma_{\text{crit}}^{(k)}$, $k = 1 \ldots K$,
is presented. First, with the input SNRs $\gamma_{\text{des}}^{(k)}$ of (4.72) and the effective noise plus inter-
ference powers $N^{(k)'}$ of (4.55) the SNIRs

$$\gamma_{\text{out}}^{(k)} = \frac{\gamma_{\text{des}}^{(k)} Q}{N^{(k)'}} = \frac{(\sum\limits_{\text{des}} |\underline{\mathbf{b}}^{(k,k_{\text{s}})}|^2)/2K_{\text{s}}^{(k)}}{N^{(k)'}}, \; k = 1 \ldots K, \tag{4.78}$$

at the output of the joint detector at MS μ_k are introduced. Then, when case 2 is considered, according to (4.56) and (4.73), the input SNIRs

$$
\begin{aligned}
\gamma^{(k,k_s)} &= \frac{|\underline{\mathbf{b}}^{(k,k_s)}|^2}{2Q\sigma^{(k)2} + (\sum_{\text{undes}} |\underline{\mathbf{b}}^{(k,k_s)}|^2)} \\
&= \frac{|\underline{\mathbf{b}}^{(k,k_s)}|^2}{2Q\sigma^{(k)2} + r^{(k)}(K_s - K_s^{(k)})(\sum_{\text{des}}|\underline{\mathbf{b}}^{(k,k_s)}|^2)/K_s^{(k)}}
\end{aligned}
\tag{4.79}
$$

valid for the desired CDMA signals associated with the CDMA codes $\underline{\mathbf{c}}^{(k_s)}$ of (4.5) received at MS μ_k are given by taking the additional intracell interference into account. By substituting (4.55) and (4.57) in (4.78) the output SNIRs of (4.78) become

$$
\gamma_{\text{out}}^{(k)} = \frac{(\sum_{\text{des}}|\underline{\mathbf{b}}^{(k,k_s)}|^2)/K_s^{(k)}}{2Q\sigma^{(k)2} + r^{(k)}(K_s - K_s^{(k)})(\sum_{\text{des}}|\underline{\mathbf{b}}^{(k,k_s)}|^2)/K_s^{(k)}}Q\frac{Q + 1 - K_s^{(k)}}{Q + 1}.
\tag{4.80}
$$

For case 1, the output SNIRs of (4.78) take the form

$$
\gamma_{\text{out}}^{(k)} = \frac{(\sum_{\text{des}}|\underline{\mathbf{b}}^{(k,k_s)}|^2)/K_s^{(k)}}{2Q\sigma^{(k)2}}Q\frac{Q + 1 - K_s}{Q + 1}.
\tag{4.81}
$$

From (4.80) and (4.81) follows the abscissa value

$$
\gamma_{\text{crit}}^{(k)} = \frac{1}{(Q - K_s + 1)r^{(k)}}, \ \ k = 1 \ldots K,
\tag{4.82}
$$

at which the plots of the two functions (4.80) and (4.81) intersect. For fixed values of Q and K_s, $\gamma_{\text{crit}}^{(k)}$ of (4.82) increases with decreasing $r^{(k)}$ of (4.73). If Q and K_s attain the same value, $\gamma_{\text{crit}}^{(k)}$ of (4.82) becomes reciprocal to $r^{(k)}$. If $r^{(k)}$ is assumed to be one, $\gamma_{\text{crit}}^{(k)}$ is 0dB in this case.

In Fig. 4.12 $\gamma_{\text{out}}^{(k)}$ of (4.80) and (4.81) for cases 2 and 1, respectively, are depicted versus $\gamma_{\text{des}}^{(k)}$ of (4.72) with $K_s^{(k)}$ as parameter. $r^{(k)}$, K_s and Q are assumed to be 0.5, 16 and 16, respectively. The intersection point of the two functions (4.80) and (4.81) is independent of $K_s^{(k)}$ and occurs at a critical SNR $\gamma_{\text{crit}}^{(k)} = 3$dB. For values $\gamma_{\text{des}}^{(k)}$ of (4.72) below $\gamma_{\text{crit}}^{(k)}$ of (4.82), $\gamma_{\text{out}}^{(k)}$ of (4.80) obtained for case 2 is larger than $\gamma_{\text{out}}^{(k)}$ of (4.81) obtained for case 1.

In Figs. 4.13 and 4.14 $\gamma_{\text{out}}^{(k)}$ of (4.80) and (4.81) for cases 2 and 1, respectively, are depicted versus $\gamma_{\text{des}}^{(k)}$ of (4.72) with $K_s^{(k)}$ as parameter. The figures are valid for $K_s = 16$, $Q = 16$ and $K_s^{(k)} = 8$. Fig. 4.13 holds for $r^{(k)}$ of (4.73) varying from 0.0 to 0.1 with an increment of 0.01 and Fig. 4.14 for $r^{(k)}$ of (4.73) varying from 0.1 to 1 with an increment of 0.1. As to be expected, Figs. 4.13 and 4.14 show that $\gamma_{\text{crit}}^{(k)}$ of (4.82) increases
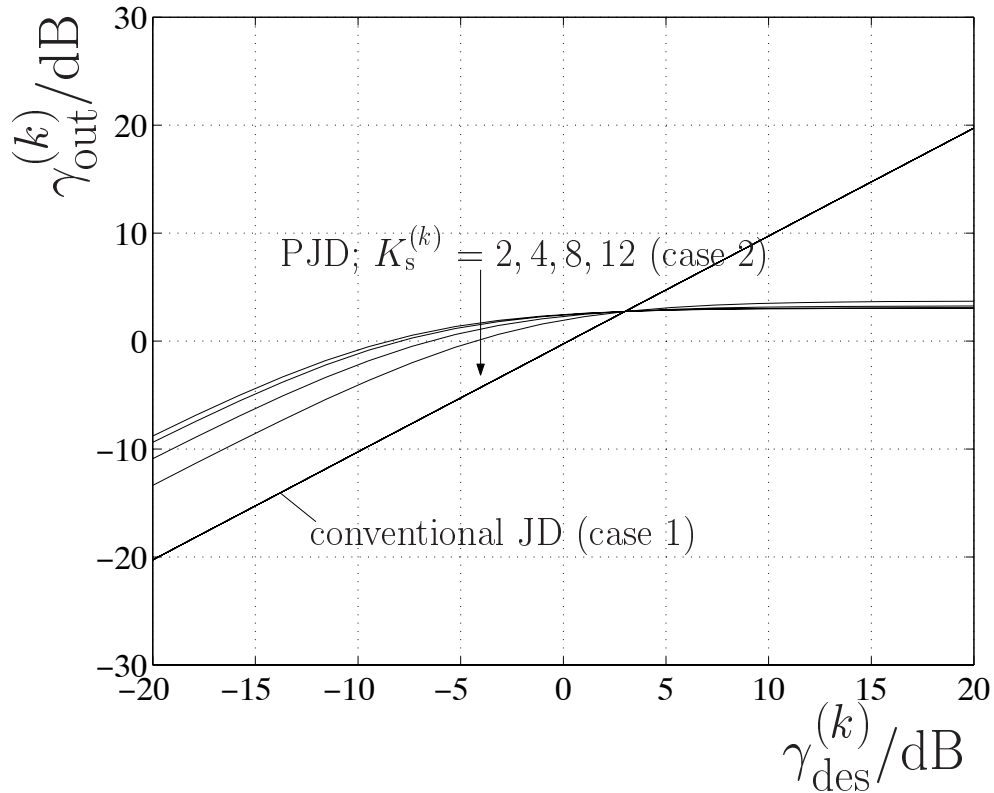
Fig. 4.12: $\gamma_{\text{out}}^{(k)}$ versus $\gamma_{\text{des}}^{(k)}$ of (4.72) for cases 1 and 2; $K_\text{s} = 16$, $Q = 16$, $r^{(k)} = 0.5$; parameter: $K_\text{s}^{(k)}$

with decreasing $r^{(k)}$ of (4.73). For a given value of $\gamma_{\text{des}}^{(k)}$ of (4.72), $\gamma_{\text{out}}^{(k)}$ of (4.80) for case 2 improves with decreasing $r^{(k)}$ of (4.73), which can be achieved by utilizing adaptive transmit antennas with increasing K_a. In the extreme situation of a vanishing $r^{(k)}$, i.e., $r^{(k)}$ equal to zero, $\gamma_{\text{out}}^{(k)}$ of (4.80) for case 2 is always approximately 9dB higher than $\gamma_{\text{out}}^{(k)}$ of (4.81) for case 1.

4.8 Efficient simulation concept

4.8.1 Introduction

As stated in Section 1.3, one of the standard performance criteria in mobile radio systems is the BER. Some data service applications require BERs not greater than 10^{-6}, whereas other applications such as digitized voice in mobile radio systems will tolerate BERs as high as 10^{-3}. The traditional method to investigate the BER performance of mobile radio systems is by means of computer simulations such as the well-known Monte-Carlo-Simulation [Naß95, Kle96]. As the main disadvantage of this method a large number of
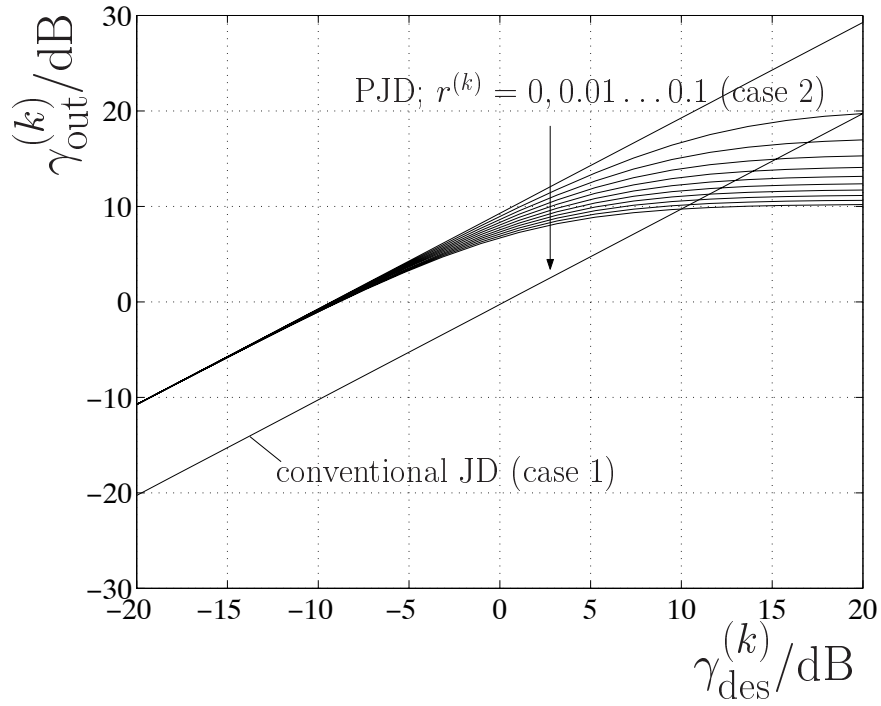
Fig. 4.13: $\gamma_{\text{out}}^{(k)}$ versus $\gamma_{\text{des}}^{(k)}$ of (4.72) for cases 1 and 2; $K_{\text{s}} = 16$, $Q = 16$, $K_{\text{s}}^{(k)} = 8$; parameter: $r^{(k)} = 0, 0.01 \ldots 0.1$
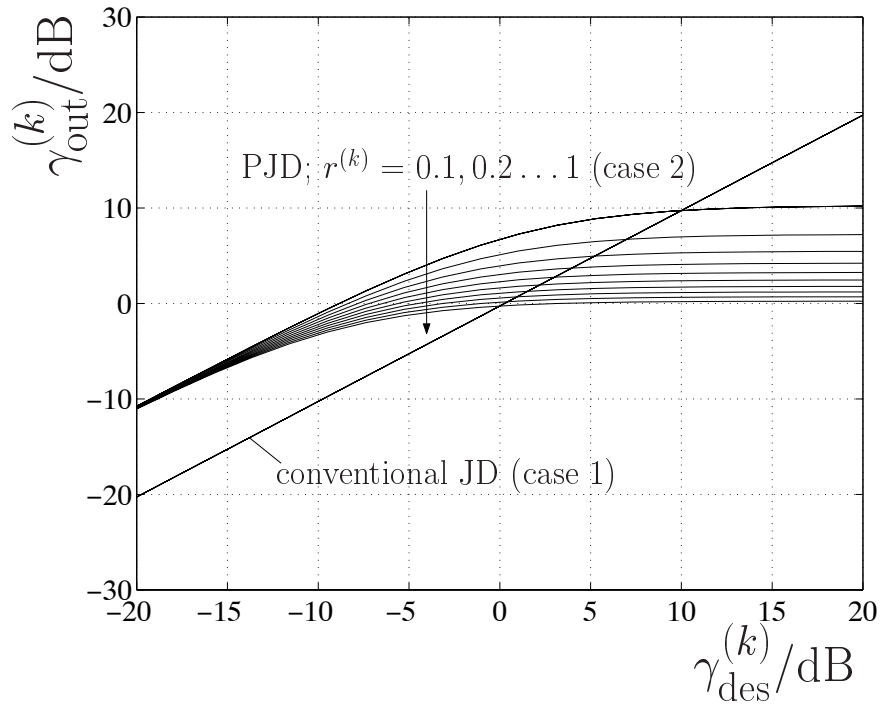
Fig. 4.14: $\gamma_{\text{out}}^{(k)}$ versus $\gamma_{\text{des}}^{(k)}$ of (4.72) for cases 1 and 2; $K_{\text{s}} = 16$, $Q = 16$, $K_{\text{s}}^{(k)} = 8$; parameter: $r^{(k)} = 0.1, 0.2 \ldots 1$

experiments should be accomplished, which require computationally expensive matrix calculations and inversions. In this section, an efficient simulation method for investigating the coded BER performance both for conventional JD and PJD in the TD-CDMA downlink utilizing a single omnidirectional transmit antenna or adaptive transmit antennas is introduced.

4.8.2   Estimating the coded BER for the case of using a single omnidirectional transmit antenna

When using a single omnidirectional transmit antenna at the BS in the TD-CDMA downlink no spatial selectivity is available. This means that the power of the transmitted CDMA signals not being of interest to a certain MS μ_k, $k = 1 \ldots K$, and received at this MS, cannot be reduced. Under the assumption that the undesired CDMA signals arrive at MS μ_k with nearly the same powers as compared with that of the desired CDMA signals, conventional JD has to be taken into account to perform data detection. The concept developed to efficiently estimate the coded BER in this case is summarized as follows:

- First, the SNR degradations $\delta^{(k,k_{\mathrm{s}})}$ of (4.47) valid for all CDMA signals k_{s} being of interest to MS μ_k are determined by utilizing

    - either the approximation given by (4.54), or
    - the exact expression given by (4.47).

- With the input SNRs $\gamma^{(k,k_{\mathrm{s}})}$ of (4.56) valid for all CDMA signals being of interest to MS μ_k and received at MS μ_k, the corresponding output SNRs

$$\gamma_{\mathrm{out}}^{(k,k_{\mathrm{s}})} = \frac{|\underline{\mathbf{b}}^{(k,k_{\mathrm{s}})}|^2}{2Q\sigma^{(k)2}} \frac{Q}{\delta^{(k,k_{\mathrm{s}})}} \tag{4.83}$$

  are calculated.

- As introduced in [Ste96], with T_{c}, B and M being the chip duration, the bandwidth of a partial frequency band and the size of the data symbol alphabet, the output SNRs $\gamma_{\mathrm{out}}^{(k,k_{\mathrm{s}})}$ of (4.83) can be converted into the bit related SNRs

$$(\frac{E_{\mathrm{b}}}{N_0})^{(k,k_{\mathrm{s}})} = \frac{T_{\mathrm{c}}B}{R_{\mathrm{c}}\log_2 M}\gamma_{\mathrm{out}}^{(k,k_{\mathrm{s}})}, \ k = 1 \ldots K, \ k_{\mathrm{s}} = 1 \ldots K_{\mathrm{s}}^{(k)}. \tag{4.84}$$

  Then, according to Friedrichs's formula [Fri96], the coded BER valid for each desired CDMA signal k_{s} related to CDMA code $\underline{\mathbf{c}}^{(k_{\mathrm{s}})}$, $k_{\mathrm{s}} = 1 \ldots K_{\mathrm{s}}^{(k)}$, of (4.5) received at MS μ_k can be calculated by

$$P_{\mathrm{b}}^{(k,k_{\mathrm{s}})} \approx \exp(-R_{\mathrm{c}}\frac{d_{\mathrm{f}}}{2}(\frac{E_{\mathrm{b}}}{N_0})^{(k,k_{\mathrm{s}})}), \ k = 1 \ldots K, \ k_{\mathrm{s}} = 1 \ldots K_{\mathrm{s}}^{(k)}, \tag{4.85}$$

  with R_{c} and d_{f} being the coding rate, the free distance of the utilized FEC encoder.

- Finally, with $\sum\limits_{\text{des}}$ of (4.71) the coded BER

$$\bar{P}_{\text{b}}^{(k)} = \frac{\sum\limits_{\text{des}} P_{\text{b}}^{(k,k_{\text{s}})}}{K_{\text{s}}^{(k)}}, \ k = 1 \dots K, \tag{4.86}$$

averaged over all CDMA signals associated with the CDMA codes $\underline{\mathbf{c}}^{(k_{\text{s}})}$, $k_{\text{s}} = 1 \dots K_{\text{s}}^{(k)}$, of (4.5) being of interest to MS μ_k and received at MS μ_k, is obtained.

In Section 4.9.5, the coded BER performance obtained by this simulation concept will be shown and compared with that obtained by conventional simulation method.

4.8.3 Estimating the coded BER for the case of using adaptive transmit antennas

On the whole, the efficient simulation concept to estimate the average coded BER $\bar{P}_{\text{b}}^{(k)}$ at MS μ_k when using adaptive transmit antennas is analogous to that when using a single omnidirectional transmit antennas at the BS as introduced in Section 4.8.2. However, when using adaptive transmit antennas PJD is considered to perform the data detection at MS μ_k, $k = 1 \dots K$, which results in an additional intracell interference, see Section 4.4. Therefore, in contrast to the simulation concept introduced in Section 4.8.2 for $K_{\text{a}} = 1$, when using adaptive transmit antennas, instead of the input SNRs $\gamma^{(k,k_{\text{s}})}$ of (4.56), the input SNIRs $\gamma^{(k,k_{\text{s}})}$ of (4.79) should be taken into account.

The estimation of the average coded BER $\bar{P}_{\text{b}}^{(k)}$ at MS μ_k when using adaptive transmit antennas at the BS is performed as follows:

- First, the signal separation ratio $r^{(k)}$ of (4.73) is determined and the input SNIRs $\gamma^{(k,k_{\text{s}})}$ of (4.79) are calculated.

- Then, the SNR degradations $\delta^{(k,k_{\text{s}})}$ are either estimated by the approximate formula, see (4.54), or calculated by using the exact expression (4.47).

- Next, with the $\gamma^{(k,k_{\text{s}})}$ of (4.79), the SNIRs

$$
\begin{aligned}
\gamma_{\text{out}}^{(k,k_{\text{s}})} &= \frac{\gamma^{(k,k_{\text{s}})}Q}{\delta^{(k,k_{\text{s}})}} \\
&= \frac{|\underline{\mathbf{b}}^{(k,k_{\text{s}})}|^2 Q}{2Q\sigma^{(k)2} + r^{(k)}(K_{\text{s}} - K_{\text{s}}^{(k)})(\sum\limits_{\text{des}}|\underline{\mathbf{b}}^{(k,k_{\text{s}})}|^2)/K_{\text{s}}^{(k)}}/\delta^{(k,k_{\text{s}})}
\end{aligned}
\tag{4.87}
$$

at the output of the JD at MS μ_k valid for the CDMA signals related to the CDMA codes $\underline{\mathbf{c}}^{(k_{\text{s}})}$, $k_{\text{s}} = 1 \dots K_{\text{s}}^{(k)}$, of (4.5) being of interest to this MS are calculated.

- Finally, using (4.85) the coded BER $P_{\mathrm{b}}^{(k,k_{\mathrm{s}})}$ valid for the CDMA signals related to the CDMA codes $\underline{\mathbf{c}}^{(k_{\mathrm{s}})}$, $k_{\mathrm{s}} = 1 \ldots K_{\mathrm{s}}^{(k)}$, of (4.5) being of interest to MS μ_k and received at MS μ_k, and using (4.86) the coded BER $\bar{P}_{\mathrm{b}}^{(k)}$ averaged over all CDMA signals being of interest to MS μ_k are obtained.

The introduced efficient simulation concept will be assessed in the next section.

4.9 Simulation results and discussions

4.9.1 Considered simulation parameters

In this section, comprehensive simulation results and discussions concerning link level considerations when using adaptive transmit antennas in the TD-CDMA downlink will be presented. The considered directional channel models are the modified 3GPP channel model derived from 3GPP channel model, see Section 2.3.1, and the scattering point based directional channel model, see Section 2.3.2. As stated in Section 1.4, the modified 3GPP channel model is suitable to investigate and analyze the effect of co-channel interference resulting from multi-user scenarios in link level simulations, whereas the scattering point based directional channel model is considered in link level simulations to study the concept CDMA code pooling. The remaining simulation parameters are described as follows:

- K_{s} equal to 16 real binary orthogonal codes $\mathbf{a}^{(k_{\mathrm{s}})}$ of dimension Q equal to 16 are generated by element wise multiplication of each of the 16 Walsh functions of length 16 by the same random sequence $(-1 - 1 \quad 1 \quad 1 \quad 1 - 1 \quad 1 - 1 \quad 1 - 1 \quad 1 - 1 \quad 1 - 1 - 1 - 1)^{\mathrm{T}}$. From the elements $a_q^{(k_{\mathrm{s}})}$, $q = 1 \ldots Q$, of $\mathbf{a}^{(k_{\mathrm{s}})}$ the Q elements of $\underline{\mathbf{c}}^{(k_{\mathrm{s}})}$ of (4.5) are obtained according to [3G99]

$$\underline{c}_q^{(k_{\mathrm{s}})} = (\mathrm{j})^q a_q^{(k_{\mathrm{s}})}, \; q = 1 \ldots Q. \tag{4.88}$$

- The same convolutional FEC encoder of coding rate

$$R_{\mathrm{c}} = \frac{1}{2} \tag{4.89}$$

and constraint length

$$K_{\mathrm{c}} = 5 \tag{4.90}$$

is used for each of the K_{s} CDMA signals. The corresponding generator polynome (octal) is $(23, 35)$.

- The data modulation is QPSK with the elements of the coded partial data vectors $\underline{\mathbf{d}}^{(k_\mathrm{s})}$, see Tab. 4.1, having magnitude one. Gray coding is used when mapping the binary output symbols of the FEC encoder on the QPSK symbols.

- The elements of the intercell interference vector $\underline{\mathbf{n}}^{(k)}$, see Tab. 4.1, are assumed to be independent complex Gaussian variables with variance $\sigma^{(k)^2}$ of their real and imaginary parts.

- The carrier frequency is

$$f_0 = 2 \text{ GHz}, \tag{4.91}$$

the chip rate is

$$f_\mathrm{c} = 1.28 \text{ MChip/s}, \tag{4.92}$$

and the bandwidth of the partial frequency band, see Fig. 1.1, is

$$B = 1.6 \text{ MHz}. \tag{4.93}$$

- Uniform linear arrays (ULA) are considered as the multi-element transmit antennas utilized at BSs. The distance between adjacent array elements is one half of the carrier wavelength λ.

The chosen value of the chip rate f_c of (4.92) corresponds to the low chip rate mode recently agreed upon by 3GPP [3G99]. However, the value of the chip rate f_c of (4.92) is of minor importance with respect to the basic investigations performed in this thesis.

In Section 4.9.2 the influence of the MC and MPCI algorithms for determining the antenna weight vectors $\underline{\mathbf{w}}^{(k_\mathrm{s})}$ of (4.7) and the other simulation parameters such as the angular spread β and the angular separation $\Delta\varphi$, see Section 2.3.1, on the generated antenna patterns is investigated. The signal separation effect enabled by utilizing adaptive transmit antennas is investigated in Section 4.9.3. Moreover, transmit power reduction achieved by adaptive transmit antennas is discussed in Section 4.9.4. Finally, the coded BER performance is investigated in Section 4.9.5. Tab. 4.3 brings an overview of the figures presenting simulation results.

4.9.2   Antenna patterns

For comparison purposes, the influence of the MC and MPCI algorithms introduced in Section 4.5, on the antenna patterns is investigated for an isolated cell. In the simulations,

Tab. 4.3: Overview of figures presenting simulation results

Investigated influence	Fig.
Antenna patterns	
Algorithm for determining antenna weight vectors $\underline{\mathbf{w}}^{(k_\mathrm{s})}$ of (4.7)	4.15 and 4.16
Angular spread β, see Fig. 2.2	4.17 and 4.18
Number K_a of transmit antenna elements	4.17, 4.19 and 4.20
Signal separation	
Angular separation $\Delta\varphi$, see Fig. 2.2	4.21
Angular spread β, see Fig. 2.2	4.22
Transmit power reduction	
Angular spread β, see Fig. 2.2	4.23

the number K_a of the transmit antenna elements is chosen equal to eight and the number K of the active MSs is eight. Furthermore, the modified 3GPP channel model, see Section 2.3.1, is considered. The angular spread β pertaining to each MS μ_k, $k = 1 \ldots 8$, see Fig. 2.2, is assumed to be $10°$. Figs. 4.15 and 4.16 show antenna patterns generated by the MC and MPCI algorithms, see Section 4.5. The eight MSs μ_k, $k = 1 \ldots 8$, are uniformly spaced over the angular domain Ω equal to $140°$ and $70°$ in the case of Fig. 4.15 and Fig. 4.16, respectively. In order to arrange the multi-user scenario symmetrically to the line vertically to the RD, see Fig. 2.2, the DOD towards the desired MS is set to be $80°$ in Fig. 4.15 and $85°$ in Fig. 4.16. From the figures the following conclusions can be drawn:

- In general, the signal separation effect offered by the MPCI algorithm is better than that offered by the MC algorithm.

- When applying the MPCI algorithm the main lobe may not exactly point towards the desired MS, see Fig. 4.16.

The influence of the angular spread β, see Section 2.3.1, on the antenna patterns generated by the MC algorithm is shown in dB in Figs. 4.17 and 4.18, respectively. The two MSs μ_1 and μ_2 are spaced with azimuths $80°$ and $100°$, respectively. Fig. 4.17 holds for $\beta = 10°$ and Fig. 4.18 for $\beta = 30°$. From the figures the following conclusions are obtained:

- In general, the signal separation effect becomes better with decreasing β.

- With increasing β the width of the main lobe towards the desired MS becomes larger and the main lobe is shifted away from the DOD of the desired MS.
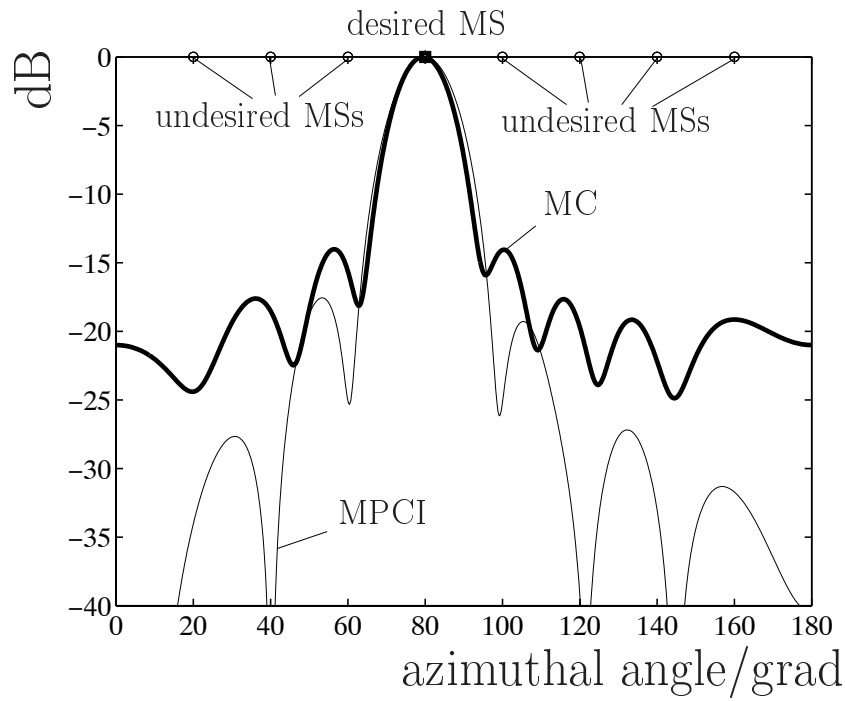
Fig. 4.15: Antenna patterns shown in dB when using the MC and MPCI algorithms; $K = 8$, $K_a = 8$ and $\Delta\varphi = 20°$
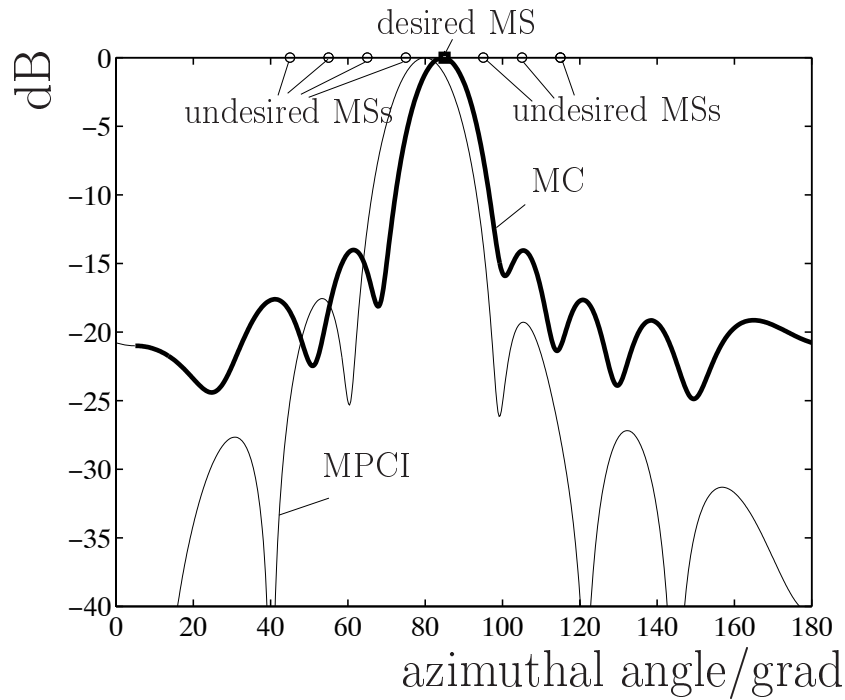
Fig. 4.16: Antenna patterns shown in dB when using the MC and MPCI algorithms; $K = 8$, $K_a = 8$ and $\Delta\varphi = 10°$
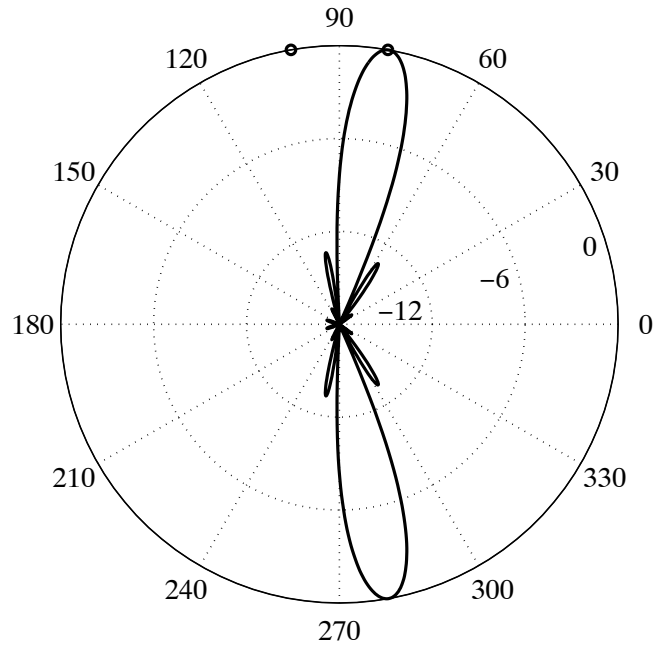
Fig. 4.17: Antenna pattern shown in dB when using the MC algorithm; $K_a = 8$, $K = 2$, $\varphi^{(1)} = 80°$, $\varphi^{(2)} = 100°$ and $\beta = 10°$
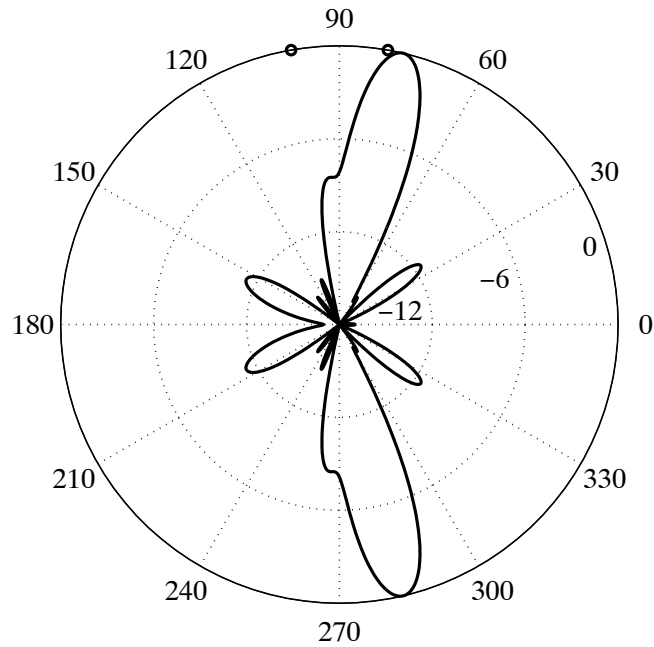
Fig. 4.18: Antenna pattern shown in dB when using the MC algorithm; $K_a = 8$, $K = 2$, $\varphi^{(1)} = 80°$, $\varphi^{(2)} = 100°$ and $\beta = 30°$
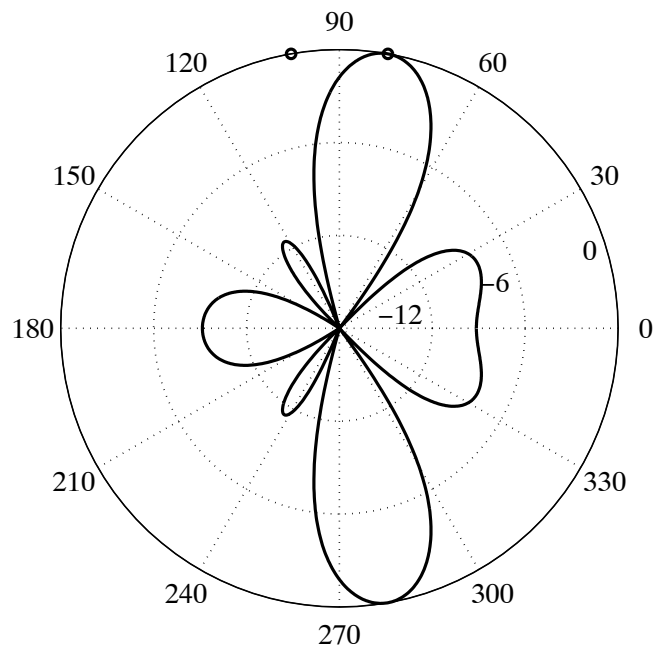
Fig. 4.19: Antenna pattern shown in dB when using the MC algorithm; $K_a = 4$, $K = 2$, $\varphi^{(1)} = 80°$, $\varphi^{(2)} = 100°$, $\beta = 10°$
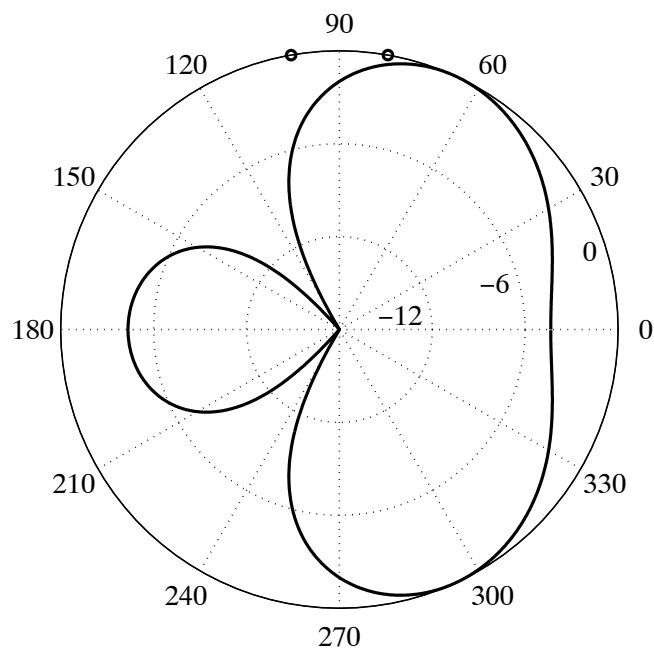
Fig. 4.20: Antenna pattern shown in dB when using the MC algorithm; $K_a = 2$, $K = 2$, $\varphi^{(1)} = 80°$, $\varphi^{(2)} = 100°$, $\beta = 10°$

- Additionally, the gains of the side lobes become larger with increasing β.

The reason for this is due to the overlaps of the associated directions in terms of $\varphi^{(k,k_e)}$ of (2.9) of the two MSs μ_1 and μ_2 when β increasing, see Section 2.3.1.

Now, the influence of K_a on the antenna patterns is investigated. With the same simulation parameters used in Fig. 4.17, the antenna patterns for $K_a = 4$ and $K_a = 2$ are shown in dB in Figs. 4.19 and 4.20, respectively. As compared with the antenna pattern for $K_a = 8$ shown in Fig. 4.17, the following conclusions can be drawn:

- In general, the signal separation effect becomes better with increasing K_a.

- With increasing K_a the width of the main lobe towards the desired MS and the gains of the side lobes become smaller.

4.9.3   Signal separation

In this section, the influence of the angular separation $\Delta\varphi$ and of the angular spread β, see Fig. 2.2, on the signal separation ratio $r^{(k)}$ of (4.73) are quantitatively investigated when using the MC algorithm.

First, the investigation focuses on $\Delta\varphi$. $r^{(1)}$ of (4.73) valid for MS μ_1 versus K_a with $\Delta\varphi$ as parameter is shown in Fig. 4.21. Following conclusions can be obtained from the figure:

- In general, $r^{(1)}$ of (4.73) becomes smaller with increasing K_a, if $\Delta\varphi$ is kept unchanged.

- $r^{(1)}$ of (4.73) becomes smaller with increasing $\Delta\varphi$.

Fig. 4.22 shows the influence of β on $r^{(1)}$ of (4.73) valid for MS μ_1. Following conclusions are obtained:

- In general, $r^{(1)}$ of (4.73) becomes smaller with increasing K_a, if β is kept unchanged.

- $r^{(1)}$ of (4.73) becomes smaller with decreasing β.

In summary, with increasing $\Delta\varphi$, and/or with decreasing β and/or with increasing K_a $r^{(k)}$ of (4.73) becomes smaller. Consequently, the powers of the undesired CDMA signals received at a certain MS μ_k decrease.
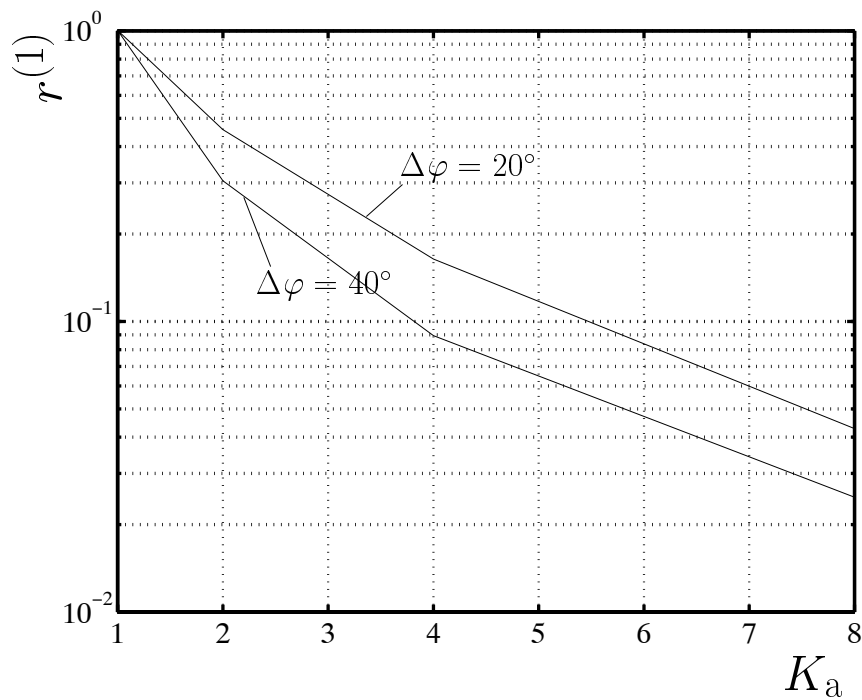
Fig. 4.21: $r^{(1)}$ of (4.73) versus K_a when using the MC algorithm; $K_s = 16$, $K = 2$ and $\beta = 10°$; parameter: $\Delta\varphi$
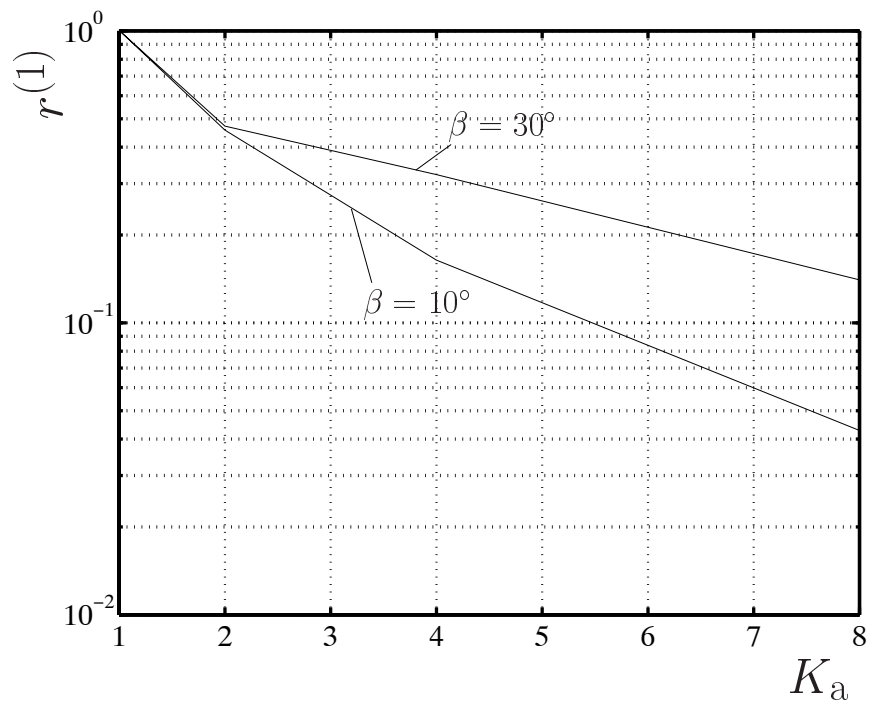
Fig. 4.22: $r^{(1)}$ of (4.73) versus K_a when using the MC algorithm; $K_s = 16$, $K = 2$ and $\Delta\varphi = 20°$; parameter: β

4.9.4   Transmit power reduction

As stated in Chapter 1, in addition to offering the signal separation, adaptive transmit antennas also tender the possibility of transmit power reduction, and consequently, reduce the total co-channel interference. This potential enabled by adaptive transmit antennas will be quantitatively studied in this section.

Obviously, in order to generate a certain desired power $R^{(k,k_\mathrm{s})}$ of (4.33) of CDMA signal k_s related to CDMA code $\underline{\mathbf{c}}^{(k_\mathrm{s})}$ of (4.5) and received at MS μ_k, a certain power $T^{(k_\mathrm{s})}$ of (4.32) associated with this CDMA code has to be transmitted by the BS. Let us assume that the term $T_0^{(k_\mathrm{s})}$ is the required transmit power associated with CDMA code $\underline{\mathbf{c}}^{(k_\mathrm{s})}$ of (4.5) used to generate the corresponding CDMA signal k_s to serve a certain MS μ_k, if a single omnidirectional antenna, i.e., $K_\mathrm{a} = 1$, is utilized at the BS. When applying CDMA code pooling, see Section 4.3, with the symbolism $\sum_\mathrm{des}$ of (4.71), the total transmit power

$$T_0^{(k)} = \sum_\mathrm{des} T_0^{(k_\mathrm{s})} \tag{4.94}$$

of the CDMA signals used to serve MS μ_k is given.

Similarly, with the term $T^{(k_\mathrm{s})}$ of (4.32) defining the required transmit power associated with CDMA code $\underline{\mathbf{c}}^{(k_\mathrm{s})}$ of (4.5) used to generate CDMA signal k_s to serve a certain MS μ_k when utilizing adaptive transmit antennas, the total transmit power

$$T^{(k)} = \sum_\mathrm{des} T^{(k_\mathrm{s})} \tag{4.95}$$

of the CDMA signals used to serve MS μ_k can be formed. Therefore, the ratio

$$\frac{T^{(k)}}{T_0^{(k)}} = \frac{\sum_\mathrm{des} T^{(k_\mathrm{s})}}{\sum_\mathrm{des} T_0^{(k_\mathrm{s})}} \tag{4.96}$$

is introduced.

The ratio $T^{(k)}/T_0^{(k)}$ of (4.96) versus K_a for $\beta = 10°$ and $\beta = 30°$ when using the MC algorithm is shown in Fig. 4.23. It is seen that,

- the required transmit power dramatically decreases with increasing K_a for both cases of $\beta = 10°$ and $\beta = 30°$, and

- the transmit power reduction effect becomes more and more explicit if β decreases.
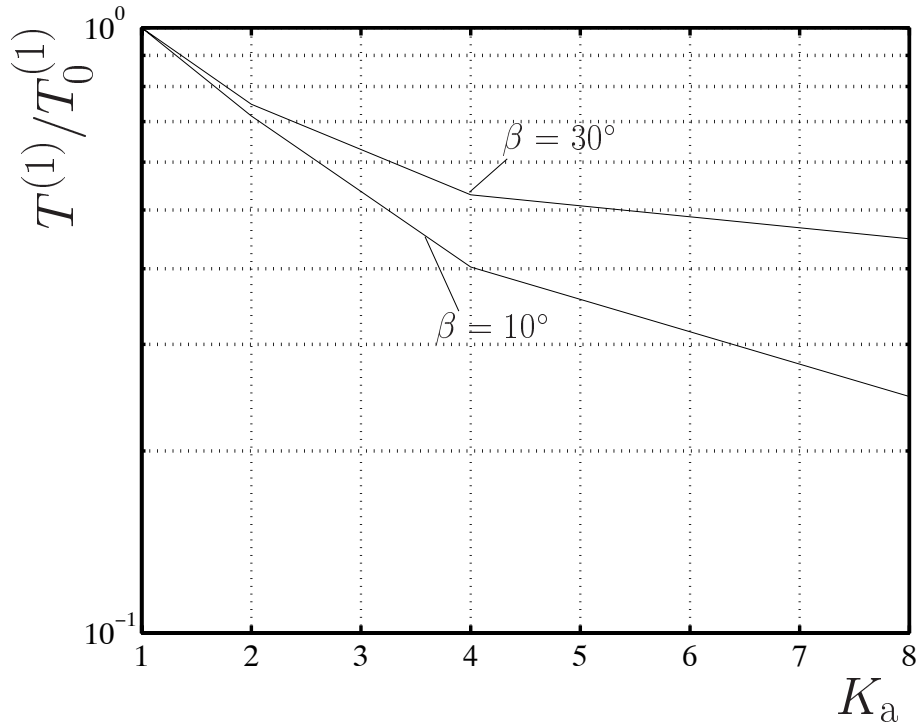
Fig. 4.23: $T^{(1)}/T_0^{(1)}$ of (4.96) at MS μ_1; $\varphi^{(1)} = 80°$ and $\varphi^{(2)} = 100°$; parameter: β

4.9.5 BER performance

The present section deals with investigating the system performance in terms of the average coded BER $\bar{P}_{\mathrm{b}}^{(k)}$ of (4.86) at MS μ_k.

First, $\bar{P}_{\mathrm{b}}^{(k)}$ of (4.86) is evaluated by the efficient simulation concept introduced in Section 4.8 and compared with that obtained by the conventional computer simulation method. Simulations are performed for both cases of using adaptive transmit antennas and a single omnidirectional antenna at the BS. If a single omnidirectional antenna is utilized at the BS, conventional JD introduced in Section 4.6.2 is considered as the data detection scheme. On the contrary, if adaptive transmit antennas are used at the BS, PJD case 2 introduced in Section 4.7.4 is taken into account. In the simulations, CDMA code pooling 2×8 is considered. This means that an isolated cell with one BS and two MSs μ_1 and μ_2 is taken into account. To each of the two MSs μ_1 and μ_2 eight CDMA codes are assigned. Without loss of the generality, it is further assumed that CDMA codes $\underline{c}^{(1)} \ldots \underline{c}^{(8)}$ are assigned to MS μ_1 and CDMA codes $\underline{c}^{(9)} \ldots \underline{c}^{(16)}$ to MS μ_2. The two MSs μ_1 and μ_2 are spaced in azimuth characterized by the angle $\varphi^{(1)} = 80°$ and $\varphi^{(2)} = 100°$, respectively, see Fig. 2.2. The angular spread β pertaining to each MS is assumed to be equal and is $10°$, see also Fig. 2.2. The SNR degradations $\delta^{(1,k_{\mathrm{s}})}$, $k_{\mathrm{s}} = 1 \ldots 8$, of (4.47), the SNR degradation $\delta^{(1)}$ averaged over $\delta^{(1,k_{\mathrm{s}})}$, $k_{\mathrm{s}} = 1 \ldots 8$, and the SNR degradation δ

of (4.48) at MS μ_1 for $K_a = 1$ for one snapshot of the modified 3GPP channel model, see Section 2.3.1, are shown in Tab. 4.4. It is seen that the estimated average SNR degradation δ of (4.48) is much larger than the simulated $\delta^{(1)}$ for this snapshot. This is due to the fact that the SNR degradation δ estimated by using (4.48) is an expectation of the SNR degradations obtained in different snapshots. The difference between $\delta^{(1)}$ and δ of (4.48) should become smaller, if a large number of different snapshots are taken into account in the simulations. Fig. 4.24 shows $\bar{P}_b^{(1)}$ of (4.86) obtained by applying the conventional simulation method and that obtained by applying the efficient simulation concept versus $\gamma_{\text{des}}^{(1)}$ of (4.72) at MS μ_1. The values of the SNR degradations utilized in the simulation are $\delta^{(1,k_s)}$ of (4.47) given in Tab. 4.4. From the figure it is seen that $\bar{P}_b^{(1)}$ of (4.86) obtained by applying the efficient simulation concept is very close to that obtained by applying the conventional simulation method. For instance, in order to achieve a given $\bar{P}_b^{(1)} = 10^{-3}$ at MS μ_1, the difference of the required $\gamma_{\text{des}}^{(1)}$ of (4.72) for the two different simulation methods is less than 0.5dB.

The efficient simulation concept is also investigated for the case of utilizing adaptive transmit antennas. The simulation environment is as same as that used for $K_a = 1$ mentioned above. The considered algorithm for determining the antenna weight vectors $\underline{\mathbf{w}}^{(k_s)}$ of (4.7) is the MC algorithm. Again, the SNR degradations $\delta^{(1,k_s)}$, $k_s = 1 \ldots 8$, of (4.47), the SNR degradation $\delta^{(1)}$ averaged over $\delta^{(1,k_s)}$, $k_s = 1 \ldots 8$, and the SNR degradation δ of (4.48) for one snapshot of the modified 3GPP channel model, see Section 2.3.1, are shown in Tabs. 4.5 and 4.6 for $K_a = 4$ and $K_a = 8$, respectively.

Tab. 4.4: SNR degradations for one snapshot of the modified 3GPP channel model, see Section 2.3.1; $K_a = 1$, $K = 2$ and $K_s = 16$

k_s	1	2	3	4	5	6	7	8
$\delta^{(1,k_s)}$/dB	8.01	7.69	9.30	7.75	7.85	7.66	7.87	8.46
$\delta^{(1)}$/dB	8.05							
δ/dB	12.30							

Tab. 4.5: SNR degradations for one snapshot of the modified 3GPP channel model, see Section 2.3.1; $K_a = 4$, $K = 2$ and $K_s = 16$

k_s	1	2	3	4	5	6	7	8
$\delta^{(1,k_s)}$/dB	2.95	1.73	2.98	2.16	1.87	2.26	2.39	1.91
$\delta^{(1)}$/dB	2.30							
δ/dB	2.76							

Tab. 4.6: SNR degradations for one snapshot of the modified 3GPP channel model, see Section 2.3.1; $K_{\mathrm{a}} = 8$, $K = 2$ and $K_{\mathrm{s}} = 16$

k_{s}	1	2	3	4	5	6	7	8
$\delta^{(1,k_{\mathrm{s}})}/\mathrm{dB}$	3.16	1.80	3.03	1.69	1.69	1.84	2.59	1.83
$\delta^{(1)}/\mathrm{dB}$	2.24							
δ/dB	2.76							

Comparing the SNR degradations shown in Tabs. 4.5 and 4.6 with those shown in Tab. 4.4, the following conclusions are obtained:

- The SNR degradation $\delta^{(1)}$ averaged over $\delta^{(1,k_{\mathrm{s}})}$, $k_{\mathrm{s}} = 1\ldots 8$, of (4.47) when using adaptive transmit antennas is smaller than that obtained when $K_{\mathrm{a}} = 1$. This is due to the fact that in the latter case conventional JD is utilized, which results in higher SNR degradation δ of (4.48), see Fig. 4.8.

- The SNR degradations $\delta^{(1,k_{\mathrm{s}})}$, $k_{\mathrm{s}} = 1\ldots 8$, of (4.47) for $K_{\mathrm{a}} = 4$ and $K_{\mathrm{a}} = 8$ do not attain the same value, although in both cases PJD case 2 is considered and the simulation environments are exactly identical. The reason is that, as mentioned in Section 4.4, the total system matrix $\underline{\mathbf{A}}^{(k)}$ of (4.21), $k = 1\ldots K$, depends on the choice of the antenna weight vectors $\underline{\mathbf{w}}^{(k_{\mathrm{s}})}$, $k_{\mathrm{s}} = 1\ldots 8$, of (4.7), consequently, the SNR degradations $\delta^{(1,k_{\mathrm{s}})}$, $k_{\mathrm{s}} = 1\ldots 8$, of (4.47) are also dependent of the antenna weigh vectors $\underline{\mathbf{w}}^{(k_{\mathrm{s}})}$ of (4.7), which are different for $K_{\mathrm{a}} = 4$ and $K_{\mathrm{a}} = 8$.

- The average SNR degradation $\delta^{(1)}$ are very close to the estimated SNR degradation δ of (4.48).

$\bar{P}_{\mathrm{b}}^{(1)}$ of (4.86) obtained by applying the conventional simulation method and by applying the efficient simulation concept versus $\gamma_{\mathrm{des}}^{(1)}$ of (4.72) at MS μ_1 are shown in Figs. 4.25 and 4.26 for $K_{\mathrm{a}} = 4$ and $K_{\mathrm{a}} = 8$, respectively. In order to achieve a target $\bar{P}_{\mathrm{b}}^{(1)}$, for example, 10^{-3}, the difference of the required $\gamma_{\mathrm{des}}^{(1)}$ of (4.72) for the two different simulation methods is less than 1dB. This means that the efficient simulation concept retains the accuracy of the conventional simulation method. The key advantage of applying the efficient simulation concept is that the simulation time can be reduced by more than 90% as compared with that of the conventional simulation concept. This computational reduction can be explained as follows:

- As shown in Section 4.6.2, when using the conventional simulation method the estimate total coded data vector $\underline{\hat{\mathbf{d}}}$ can be obtained by (4.44). In the simulations it
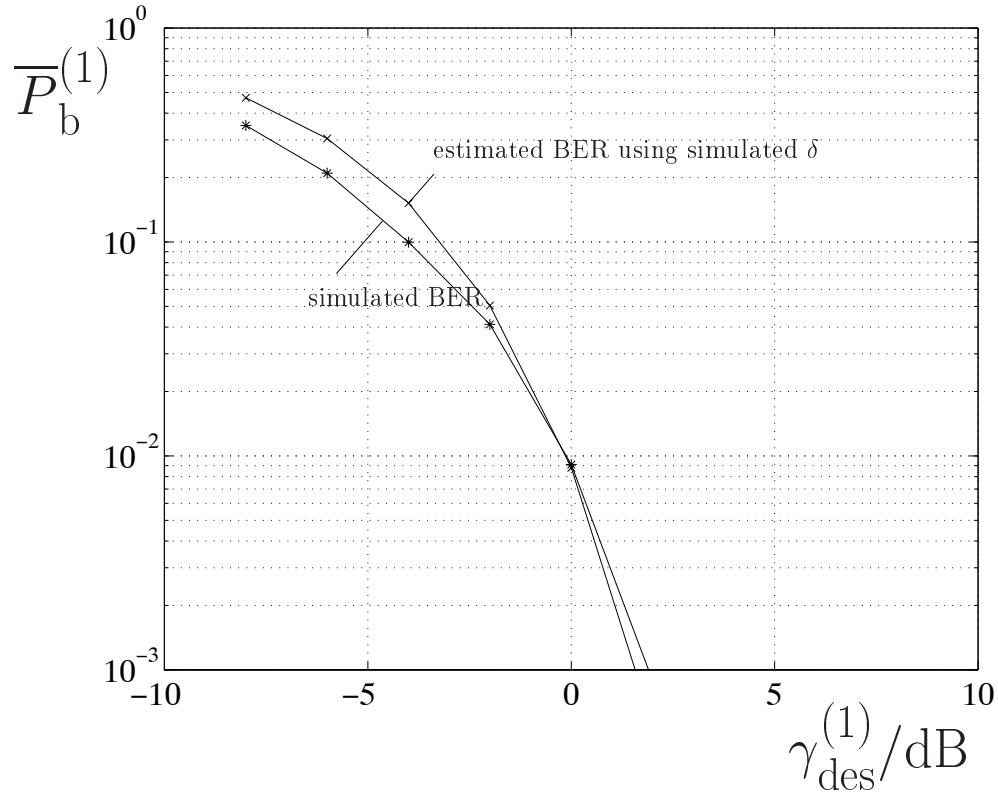
Fig. 4.24: Estimated and simulated $\bar{P}_{\text{b}}^{(1)}$ of (4.86) versus $\gamma_{\text{des}}^{(1)}$ of (4.72) at MS μ_1; $K_{\text{a}} = 1$, $K = 2$ and $K_{\text{s}} = 16$

is assumed that the covariance matrix $\underline{\mathbf{R}}_{\text{n}}^{(k)}$ in (4.44) is equal to $\sigma^{(k)^2}\mathbf{I}$, where $\sigma^{(k)^2}$ is the variance of the real and imaginary parts of the elements of $\underline{\mathbf{n}}^{(k)}$, see Tab. 4.1. Therefore, the computational complexity of the conventional simulation concept is given as follows:

- Matrix inverse complexity is $O((K_{\text{s}}^{(k)}N)^3)$.
- Multiplication operations are $K_{\text{s}}^{(k)}N(NQ + W - 1)(K_{\text{s}}^{(k)}N + 1)$ times.

• If the efficient simulation concept is applied, see Section 4.8, no matrix inverses, matrix-vector and matrix-matrix multiplications are required.

This observation associated with the simulation results shown in Figs. 4.25 and 4.26 demonstrates that the efficient simulation concept keeps the accuracy of the conventional simulation concept, and, simultaneously, dramatically reduces the required simulation time. Therefore, in what follows only the efficient simulation concept is taken into consideration to assess $\bar{P}_{\text{b}}^{(k)}$ of (4.86) at MS μ_k for both cases of utilizing adaptive transmit antennas and a single omnidirectional transmit antenna at the BS.
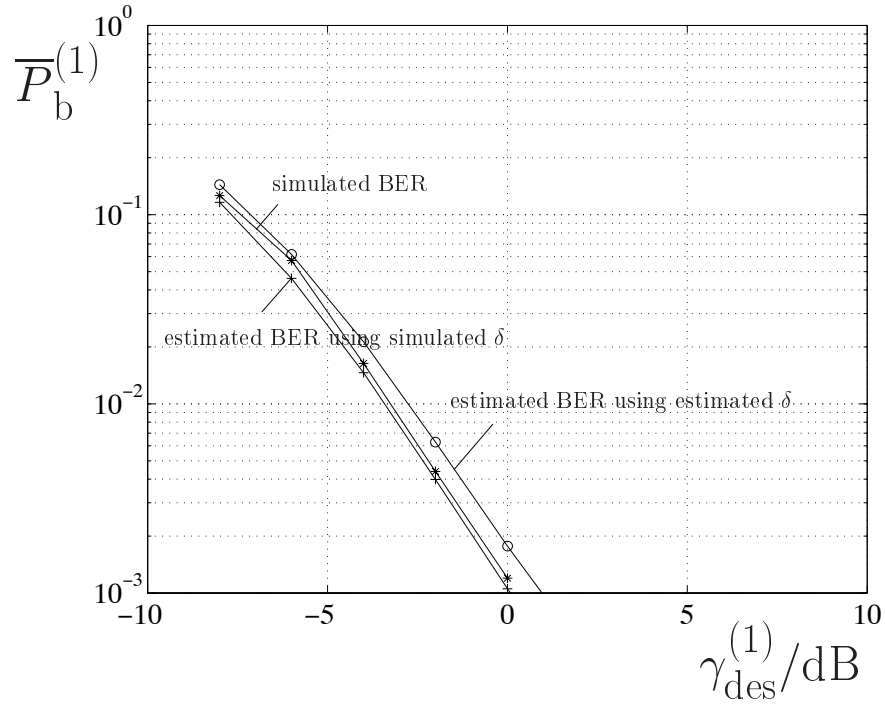
Fig. 4.25: Estimated and simulated $\bar{P}_{\mathrm{b}}^{(1)}$ of (4.86) versus $\gamma_{\mathrm{des}}^{(1)}$ of (4.72) at MS μ_1; $K_{\mathrm{a}} = 4$, $K = 2$ and $K_{\mathrm{s}} = 16$
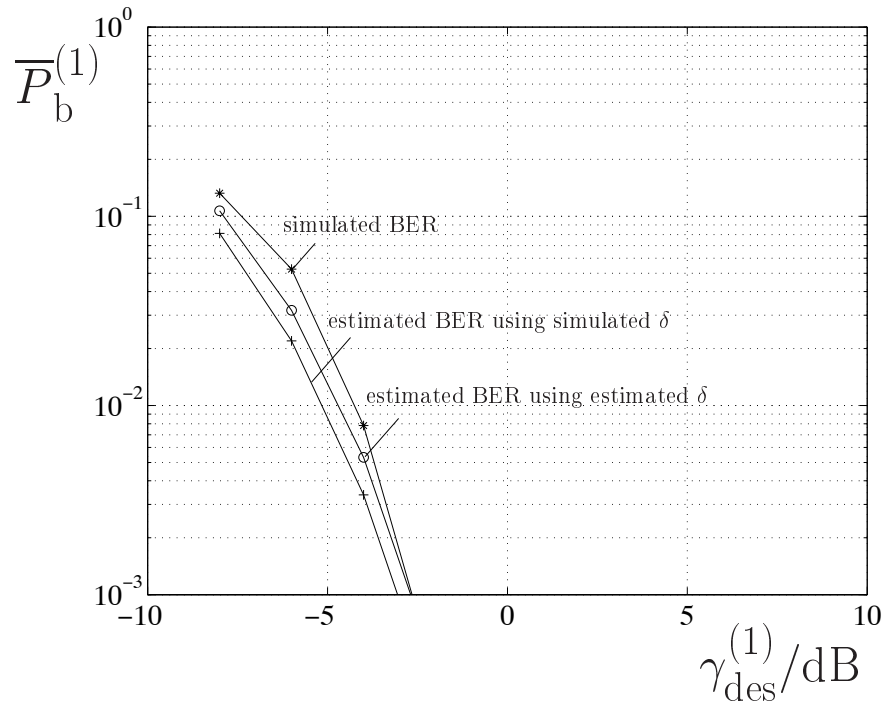
Fig. 4.26: Estimated and simulated $\bar{P}_{\mathrm{b}}^{(1)}$ of (4.86) versus $\gamma_{\mathrm{des}}^{(1)}$ of (4.72) at MS μ_1; $K_{\mathrm{a}} = 8$, $K = 2$ and $K_{\mathrm{s}} = 16$

Now, the data detection schemes, conventional JD and PJD introduced in Section 4.6, are investigated. In the simulations CDMA code pooling 2×8 is considered and the scattering point based directional channel model introduced in Section 2.3.2 is utilized. The angular separation between the two MSs μ_1 and μ_2 is $\Delta\varphi = 20°$, see Fig. 2.4. The algorithm for determining the antenna weight vectors $\underline{\mathbf{w}}^{(k_s)}$ of (4.7) is the MC algorithm, see Section 4.5.1. In Figs. 4.27 and 4.28 $\bar{P}_b^{(1)}$ of (4.86) is depicted versus K_a for $\gamma_{\mathrm{des}}^{(1)} = -6\mathrm{dB}$ and $\gamma_{\mathrm{des}}^{(1)} = -4\mathrm{dB}$, respectively. In the two figures, the upper curves hold for conventional JD and the lower curves for PJD. The most important results concerning the figures are the following:

- If conventional JD is applied, $\bar{P}_b^{(1)}$ of (4.86) virtually does not decrease with increasing K_a. The reason for this behaviour is that the conditioning of the total system matrix $\underline{\mathbf{A}}^{(1)}$ of (4.21) is not improved, and consequently, the SNR degradations $\delta^{(1,k_s)}$, $k_s = 1 \ldots K_s$, of (4.47) do not become smaller as K_a increases. This effect will be discussed more in detail in Section 6.4.3. When applying PJD, the run of the curves shows that $\bar{P}_b^{(1)}$ of (4.86) is significantly lower than that of conventional JD. This is especially true for larger values of K_a.

- Moreover, for $K_a = 1$, with increasing $\gamma_{\mathrm{des}}^{(1)}$ of (4.72), $\bar{P}_b^{(1)}$ of (4.86) obtained when applying PJD becomes worse than that obtained when performing conventional JD. This is due to the fact that $r^{(1)}$ of (4.73) is large for $K_a = 1$. As discussed in Section 4.7.4, the critical input SNR $\gamma_{\mathrm{crit}}^{(1)}$ of (4.82) decreases with increasing $r^{(1)}$ of (4.73). As a consequence, the corresponding $\gamma_{\mathrm{crit}}^{(1)}$ of (4.82) is smaller for $K_a = 1$.

Finally, $\bar{P}_b^{(1)}$ of (4.86) is investigated with different values of K_a, K, β and $\Delta\varphi$, see Fig. 2.2. In the simulations $K_s = 16$ CDMA codes $\underline{\mathbf{c}}^{(k_s)}$ of (4.5) and CDMA code pooling $K \times \dfrac{K_s}{K}$ are considered. The MC algorithm is applied for determining the antenna weight vectors $\underline{\mathbf{w}}^{(k_s)}$ of (4.7). $\bar{P}_b^{(1)}$ of (4.86) versus $\gamma_{\mathrm{des}}^{(1)}$ of (4.72) for $K_a = 1$, 2, 4, 8 and $K = 2$, 4, 8 are shown in Figs. 4.29 to 4.34. An overview of the simulation conditions is given in Tab. 4.7. The important results concerning the figures are as follows:

- $\bar{P}_b^{(1)}$ of (4.86) decreases with increasing K_a, if the other simulation conditions, such as β, $\Delta\varphi$ and K are kept unchanged. This is due to the fact that $r^{(1)}$ of (4.73) valid for MS μ_1 becomes smaller with increasing K_a, and consequently, the power of the intracell interfering CDMA signals excluded from PJD, see Section 4.4, decreases. This means that the beneficial effect arising from the PJD outweighs the detrimental effect, see Section 4.6.3.
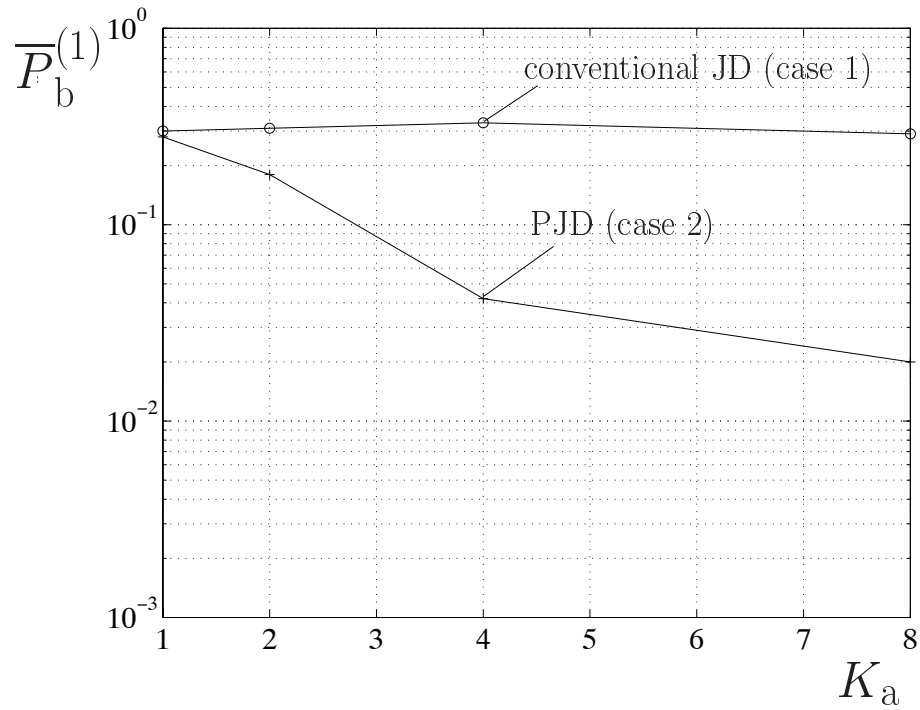
Fig. 4.27: $\bar{P}_{\mathrm{b}}^{(1)}$ versus K_{a} at MS μ_1 using scattering point based channel model; $\gamma_{\mathrm{des}}^{(1)} = -6\mathrm{dB}$, $K = 2$, $\beta = 10°$ and $\Delta\varphi = 20°$
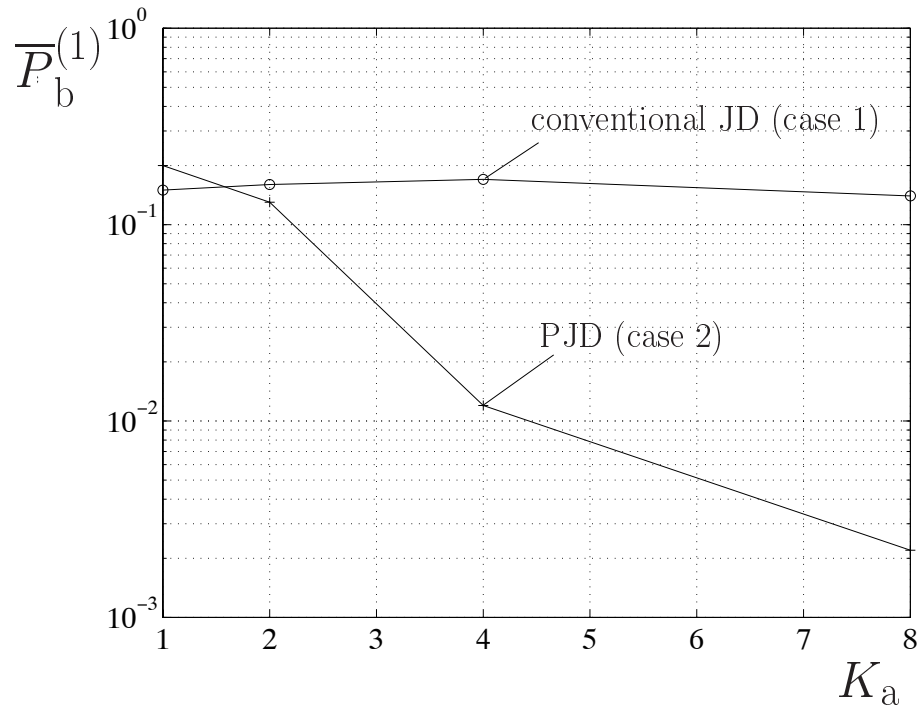
Fig. 4.28: $\bar{P}_{\mathrm{b}}^{(1)}$ versus K_{a} at MS μ_1 using scattering point based channel model; $\gamma_{\mathrm{des}}^{(1)} = -4\mathrm{dB}$, $K = 2$, $\beta = 10°$ and $\Delta\varphi = 20°$

Tab. 4.7: Overview of β, $\Delta\varphi$ and K considered in the simulations

	β	$\Delta\varphi$	K
Fig. 4.29	10°	20°	2
Fig. 4.30	10°	40°	2
Fig. 4.31	20°	20°	2
Fig. 4.32	10°	20°	4
Fig. 4.33	20°	20°	4
Fig. 4.34	10°	20°	8

- For $K_a = 2$, if $\gamma_{\text{des}}^{(1)}$ of (4.72) exceeds a certain value, $\bar{P}_b^{(1)}$ of (4.86) does not decrease with increasing $\gamma_{\text{des}}^{(1)}$ and becomes worse than that obtained for $K_a = 1$. This is because of the worse signal separation effect for $K_a = 2$, which results in a relative lower $\gamma_{\text{crit}}^{(1)}$ of (4.82) at MS μ_1 when performing PJD, see Section 4.7.4.

- $\bar{P}_b^{(1)}$ of (4.86) decreases with increasing $\Delta\varphi$, compare Fig. 4.29 and 4.30. For instance, in order to achieve $\bar{P}_b^{(1)} = 10^{-3}$, the required $\gamma_{\text{des}}^{(1)}$ of (4.72) for $K_a = 4$ when $\Delta\varphi = 40°$ is approximately 3dB lower than that when $\Delta\varphi = 20°$. However, the reduction of the required $\gamma_{\text{des}}^{(1)}$ of (4.72) for $K_a = 8$ becomes less than 1dB. Fig. 4.30 shows that $\bar{P}_b^{(1)}$ of (4.86) for $K_a = 8$ and $K_a = 4$ are very close to each other.

- $\bar{P}_b^{(1)}$ of (4.86) increases with increasing β, compare Fig. 4.29 and Fig. 4.31 as well as Fig. 4.32 and Fig. 4.33. For instance, in order to achieve $\bar{P}_b^{(1)} = 10^{-3}$, the required $\gamma_{\text{des}}^{(1)}$ of (4.72) for $K_a = 8$ and $K = 2$ when $\beta = 10°$ is approximately 3.5dB lower than that when $\beta = 20°$, and approximately 2.5dB lower than that when $\beta = 20°$ and $K = 4$. This is because the signal separation effect becomes better with decreasing β, see Section 4.9.3.

- From Figs. 4.29, 4.32 and 4.34, it can be seen that, with equal K_a, $\bar{P}_b^{(1)}$ of (4.86) decreases when K increases and the other simulation parameters are kept unchanged. For instance, in order to achieve $\bar{P}_b^{(1)} = 10^{-3}$, the required $\gamma_{\text{des}}^{(1)}$ for $K_a = 8$ with $K = 8$ is approximately 1dB lower than that with $K = 4$, which is approximately 1dB lower than that with $K = 2$. The reasons for that are explained as follows:

  - Although K increases, the total number K_s of CDMA codes does not change, and consequently, the total number of the physical channels in each burst is kept unchanged.

  - For $K = 2$, to each MS eight CDMA codes are assigned, whereas for $K = 8$, to each MS only two CDMA codes are assigned. Therefore, according to (4.54), when performing PJD at MS μ_1 the SNR degradation $\delta^{(1)}$ for $K = 8$ is lower than that for $K = 2$.

   – For $K = 2$, eight CDMA signals, which are utilized to serve MS μ_2 located with $\Delta\varphi = 20°$ related to MS μ_1, cause intracell interference at MS μ_1. For $K = 8$, only four CDMA signals are utilized to serve two MSs with the same $\Delta\varphi = 20°$ related to MS μ_1. The other 12 CDMA signals used to serve the other MSs result in lower intracell interference power at MS μ_1, because the signal separation effect becomes better with increasing $\Delta\varphi$ of these MSs related to MS μ_1, see Fig. 4.21. This means that, despite of the increasing K, the total intracell interference power at MS μ_1 does not increase. On the contrary, the total additional intracell interference power decreases when performing PJD at MS μ_1. Therefore, with the smaller $\delta^{(1)}$ and the smaller additional intracell interference power, $\bar{P}_{\mathrm{b}}^{(1)}$ of (4.86) decreases with increasing K when performing PJD.
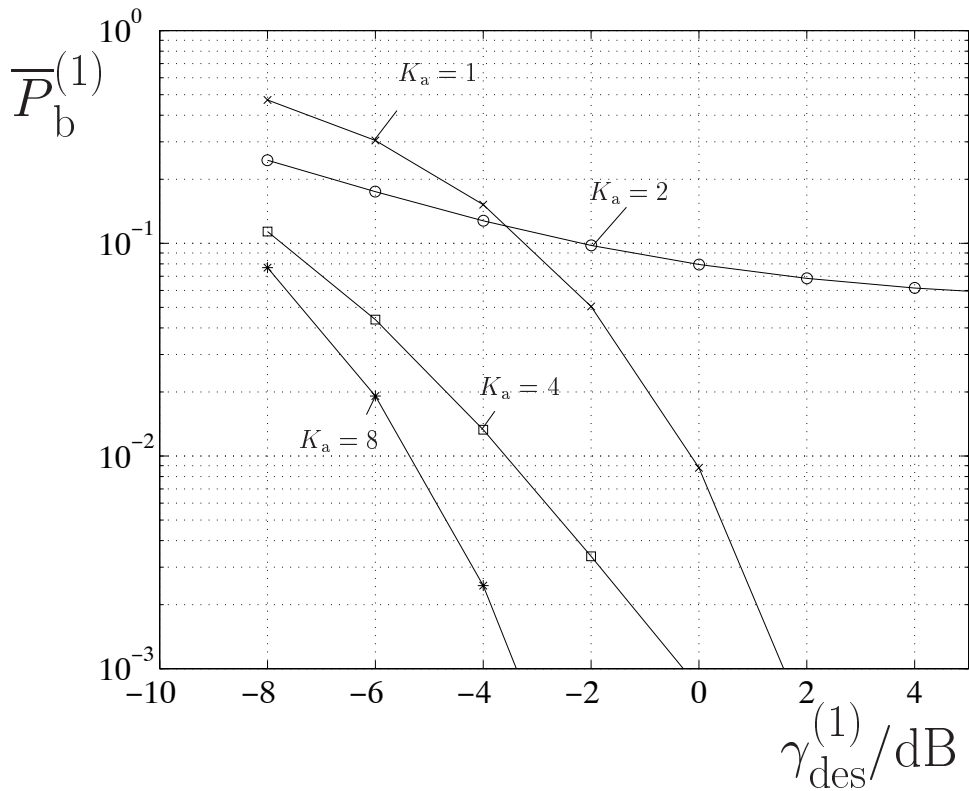
Fig. 4.29: $\bar{P}_{\mathrm{b}}^{(1)}$ of (4.86) versus $\gamma_{\mathrm{des}}^{(1)}$ of (4.72); modified 3GPP channel model; $K = 2$, $K_{\mathrm{s}} = 16$, $\beta = 10°$, $\Delta\varphi = 20°$, parameter: K_{a}
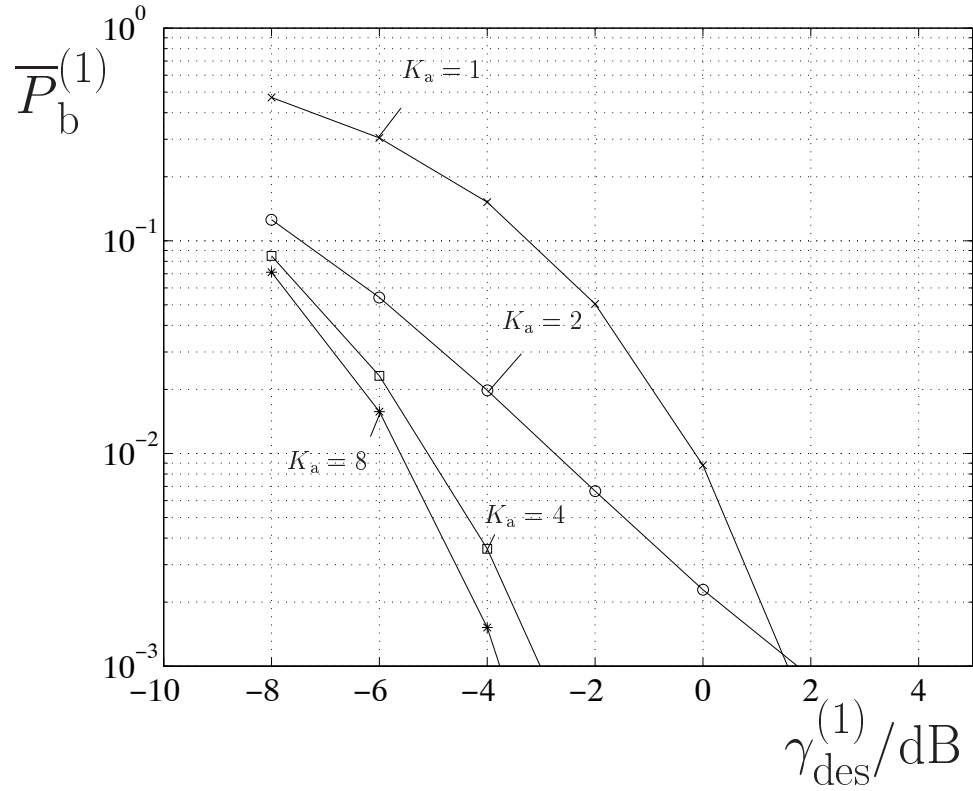
Fig. 4.30: $\bar{P}_b^{(1)}$ of (4.86) versus $\gamma_{\mathrm{des}}^{(1)}$ of (4.72); modified 3GPP channel model; $K = 2$, $K_s = 16$, $\beta = 10°$, $\Delta\varphi = 40°$; parameter: K_a
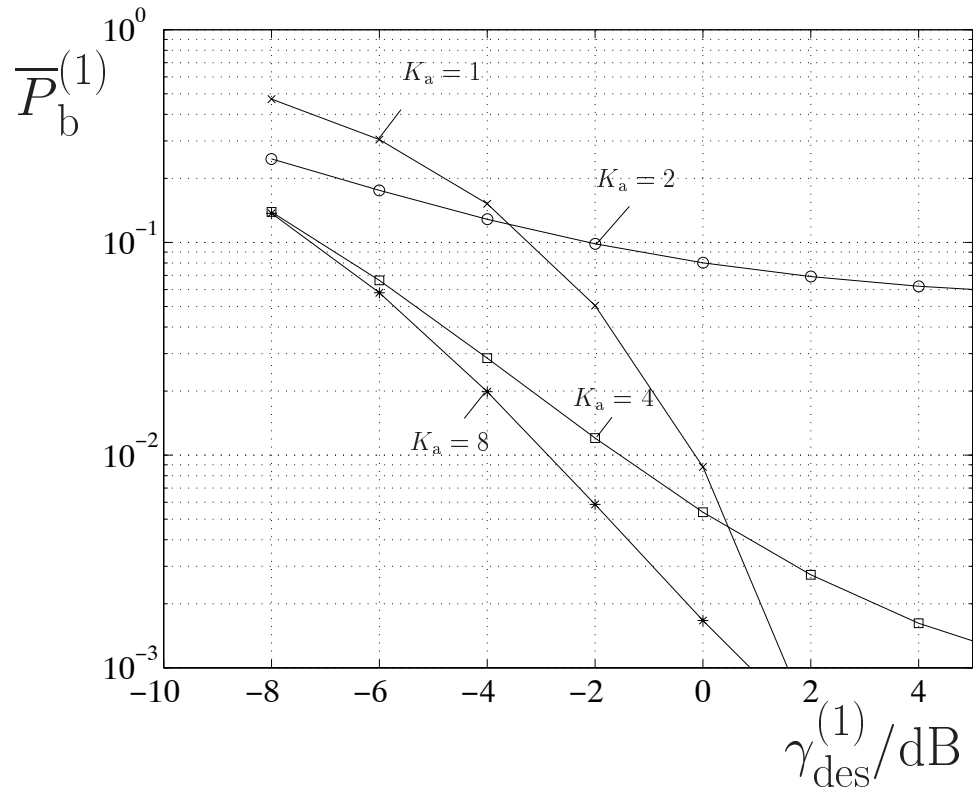
Fig. 4.31: $\bar{P}_b^{(1)}$ of (4.86) versus $\gamma_{\mathrm{des}}^{(1)}$ of (4.72); modified 3GPP channel model; $K = 2$, $K_s = 16$, $\beta = 20°$, $\Delta\varphi = 20°$; parameter: K_a
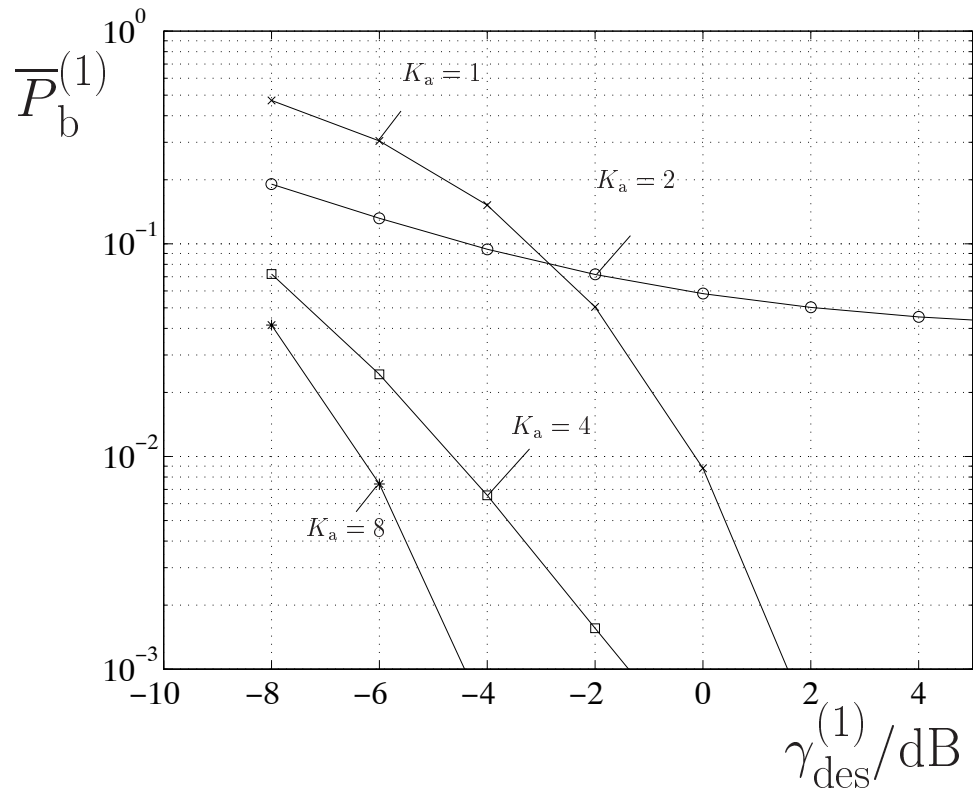
Fig. 4.32: $\bar{P}_{\mathrm{b}}^{(1)}$ of (4.86) versus $\gamma_{\mathrm{des}}^{(1)}$ of (4.72); modified 3GPP channel model; $K = 4$, $K_{\mathrm{s}} = 16$, $\beta = 10°$, $\Delta\varphi = 20°$; parameter: K_{a}
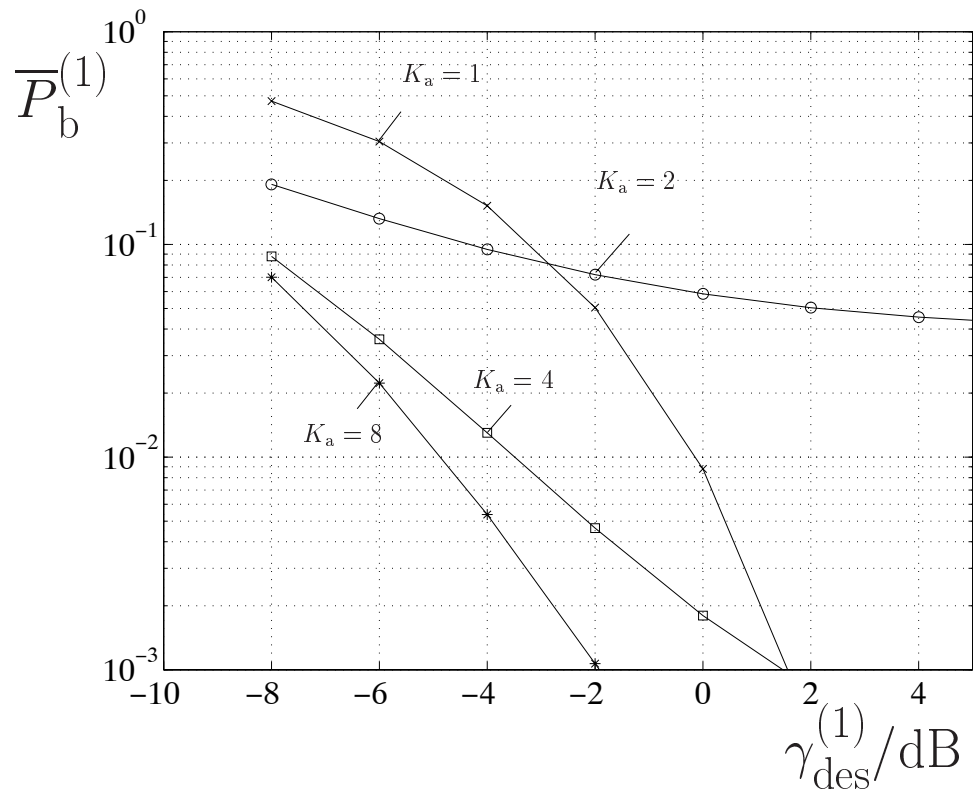
Fig. 4.33: $\bar{P}_{\mathrm{b}}^{(1)}$ of (4.86) versus $\gamma_{\mathrm{des}}^{(1)}$ of (4.72); modified 3GPP channel model; $K = 4$, $K_{\mathrm{s}} = 16$, $\beta = 20°$, $\Delta\varphi = 20°$; parameter: K_{a}
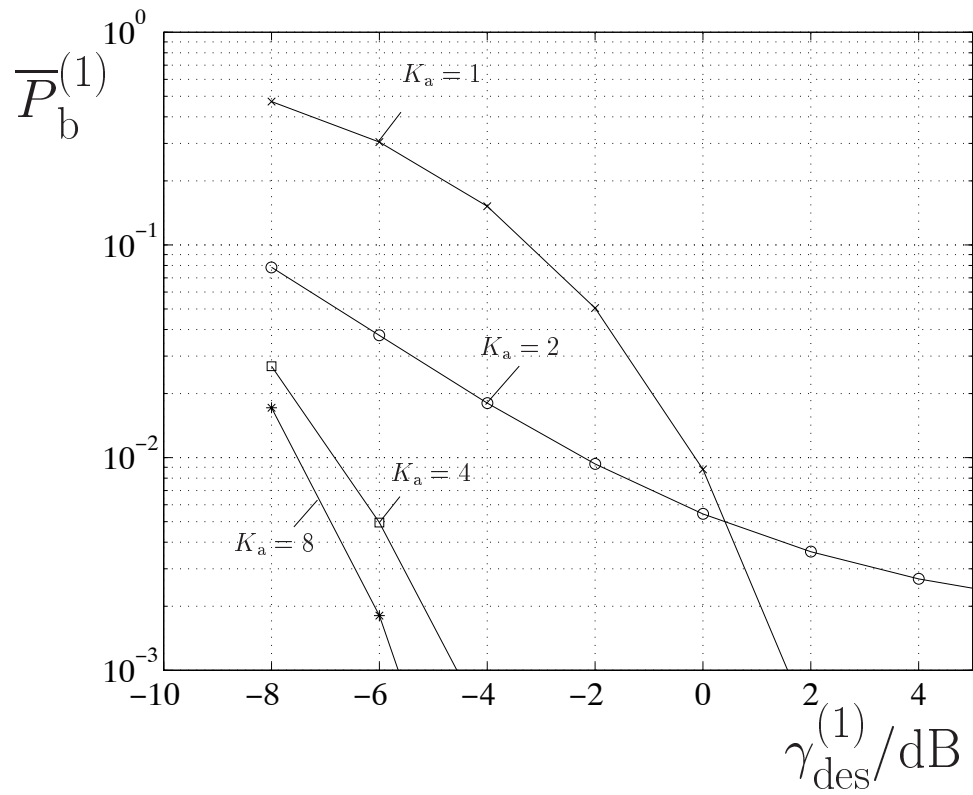
Fig. 4.34: $\bar{P}_{\mathrm{b}}^{(1)}$ versus $\gamma_{\mathrm{des}}^{(1)}$ of (4.72) using modified 3GPP channel model; $K = 8$, $K_{\mathrm{s}} = 16$, $\beta = 10°$, $\Delta\varphi = 20°$; parameter: K_{a}

Chapter 5

Blind channel estimation

5.1   Introduction

As shown in Chapter 4, if adaptive transmit antennas are applied at the BS, it can be achieved that the CDMA signals undesired at a MS μ_k arrive at this MS with a relatively low power as compared to the powers of the CDMA signals desired at this MS. Under certain conditions this situation can be exploited to perform blind channel estimation at the MSs based on subspace methods. The application of such methods to blind channel estimation is well known, see for instance [MDCM95, TP98]. In this chapter subspace based approaches to blind channel estimation will be adapted to the downlink of the transmission scheme TD-CDMA. In the case of blind channel estimation the channel information required for data detection is obtained mainly from the received data carrying signals so that the transmission of long training signals in the form of midambles, see Fig. 1.2, is no longer required. In principle, the transmission of a single training symbol would be sufficient which allows to tackle the phase and amplitude ambiguity of the channel impulse responses obtained by blind channel estimation. In conventional TD-CDMA the transmission of the midambles consume a significant portion of the transmission resources. Therefore, dispensing with the midambles would help to increase system capacity, which is especially attractive in the downlink. The considerations in this chapter are confined to the presentation of some basic ideas and of preliminary simulation results. In order to assess the potential of blind channel estimation in the TD-CDMA downlink, further research would be required which would be beyond the scope of this thesis.
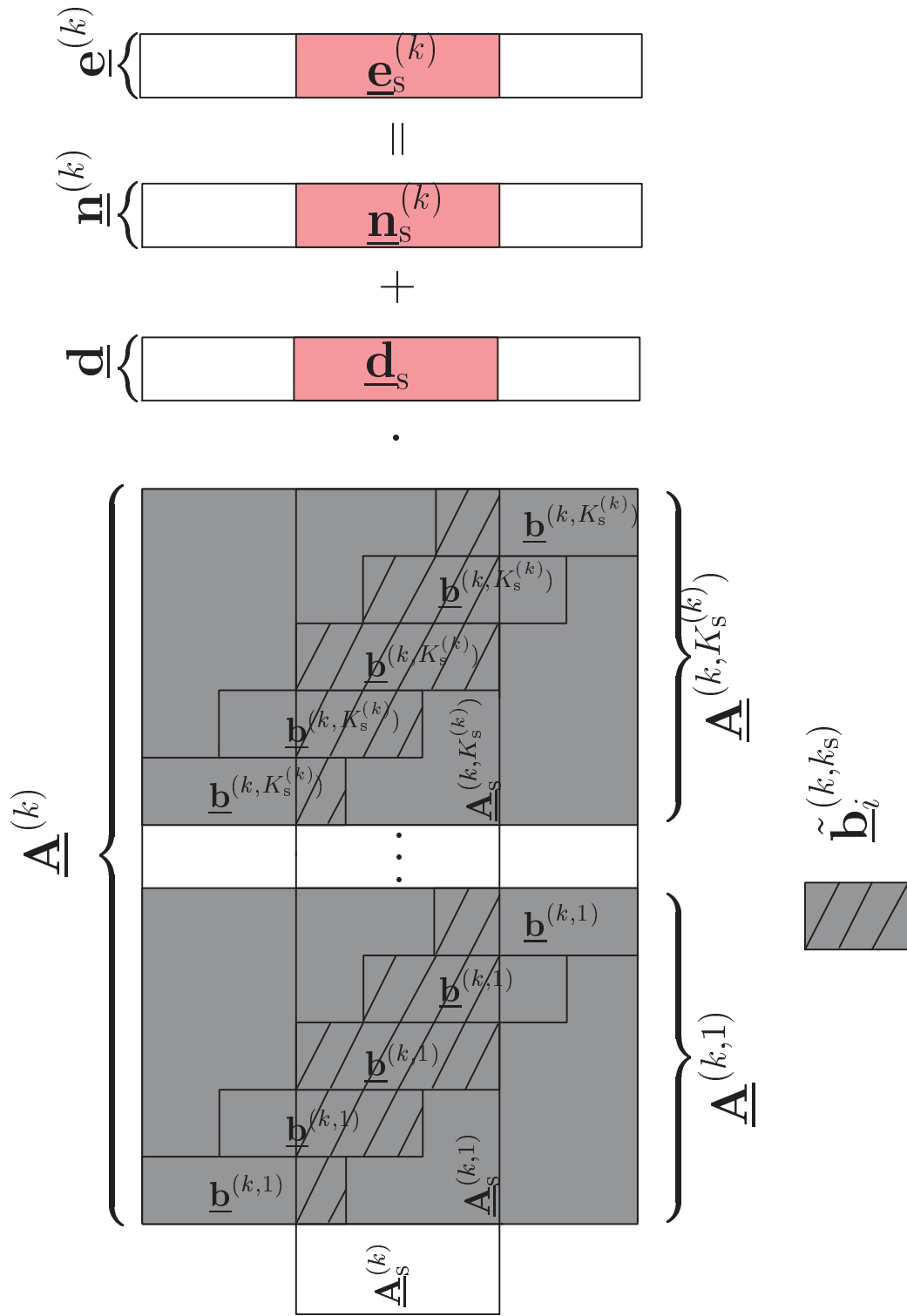
Fig. 5.1: Structure of the system matrix $\underline{\mathbf{A}}^{(k)}$ of (4.21), of the partial system matrix $\underline{\mathbf{A}}^{(k,k_{\mathrm{s}})}$ of (4.20) and of the partial system submatrix $\underline{\mathbf{A}}_{\mathrm{s}}^{(k,k_{\mathrm{s}})}$ of (5.2) responsible for the transmission of the desired CDMA signals $k_{\mathrm{s}} = 1 \ldots K_{\mathrm{s}}^{(k)}$ to MS μ_k

5.2 System submatrix

Fig. 5.1 once more shows the structure of the system matrix $\underline{\mathbf{A}}^{(k)}$ of (4.21) and of the partial system matrices $\underline{\mathbf{A}}^{(k,k_\mathrm{s})}$ of (4.20) responsible for the transmission of the desired CDMA signal $k_\mathrm{s} = 1 \ldots K_\mathrm{s}^{(k)}$ to MS μ_k. As indicated by hatching in Fig. 5.1, within the central part of the partial system matrix $\underline{\mathbf{A}}^{(k,k_\mathrm{s})}$ a partial system submatrix $\underline{\mathbf{A}}_\mathrm{s}^{(k,k_\mathrm{s})}$ can be defined, where the upper and lower boundaries of $\underline{\mathbf{A}}_\mathrm{s}^{(k,k_\mathrm{s})}$ within $\underline{\mathbf{A}}^{(k,k_\mathrm{s})}$ have to be chosen such that no fringing effects due to the head or tail of the burst fall into $\underline{\mathbf{A}}_\mathrm{s}^{(k,k_\mathrm{s})}$. Obviously, there exist a number of possibilities to place $\underline{\mathbf{A}}_\mathrm{s}^{(k,k_\mathrm{s})}$ within $\underline{\mathbf{A}}^{(k,k_\mathrm{s})}$ under these conditions. This number increases with the number of data symbols to be transmitted in the burst. With

$$I = \begin{cases} \dfrac{2(Q + W - 1)}{Q} - 1 & \text{for } \dfrac{Q + W - 1}{Q} \text{ integer,} \\ 2\mathrm{int}(\dfrac{Q + W - 1}{Q}) + 1 & \text{for } \dfrac{Q + W - 1}{Q} \text{ non integer} \end{cases} \tag{5.1}$$

$\underline{\mathbf{A}}_\mathrm{s}^{(k,k_\mathrm{s})}$ has the dimension $(Q + W - 1) \times I$. The I columns of $\underline{\mathbf{A}}_\mathrm{s}^{(k,k_\mathrm{s})}$ are termed $\tilde{\underline{\mathbf{b}}}_i^{(k,k_\mathrm{s})}$, $i = 1 \ldots I$, that is

$$\underline{\mathbf{A}}_\mathrm{s}^{(k,k_\mathrm{s})} = (\tilde{\underline{\mathbf{b}}}_1^{(k,k_\mathrm{s})} \ldots \tilde{\underline{\mathbf{b}}}_I^{(k,k_\mathrm{s})}). \tag{5.2}$$

The central column of $\underline{\mathbf{A}}_\mathrm{s}^{(k,k_\mathrm{s})}$ of (5.2) is equal to $\underline{\mathbf{b}}^{(k,k_\mathrm{s})}$ of (4.19), and the other columns are shifted and clipped versions of $\underline{\mathbf{b}}^{(k,k_\mathrm{s})}$ of (4.19), and, therefore, can be expressed by $\underline{\mathbf{b}}^{(k,k_\mathrm{s})}$. To this purpose the two acyclic shift operators $\mathcal{L}_m(\cdot)$ and $\mathcal{R}_m(\cdot)$ are introduced. Let us consider the vector

$$\mathbf{v} = (v_1 \ldots v_V)^\mathrm{T} \tag{5.3}$$

of dimension V and the $M \times M$-matrix

$$\mathbf{M} = (\mathbf{m}_1 \ldots \mathbf{m}_M). \tag{5.4}$$

Then,

$$\mathcal{L}_m(\mathbf{v}) = (v_{V-m} \ldots v_V \underbrace{0 \ldots 0}_{m \text{ zeros}})^\mathrm{T} \tag{5.5}$$

$$\mathcal{L}_m(\mathbf{M}) = (\mathbf{m}_{M-m} \ldots \mathbf{m}_M \underbrace{0 \ldots 0}_{m \text{ zeros}})^\mathrm{T} \tag{5.6}$$

$$\mathcal{R}_m(\mathbf{V}) = (\underbrace{0 \ldots 0}_{m \text{ zeros}} v_1 \ldots v_{V-m})^\mathrm{T} \tag{5.7}$$

$$\mathcal{R}_m(\mathbf{M}) = (\underbrace{0\ldots0}_{m \text{ zeros}}\mathbf{m}_1\ldots\mathbf{m}_{M-m})^{\mathrm{T}}. \tag{5.8}$$

With $\mathcal{L}_m(\cdot)$ and $\mathcal{R}_m(\cdot)$ and the identity matrix $\mathbf{I}$ the matrix

$$\mathbf{S}_m = \begin{cases} \mathcal{L}_m(\mathbf{I}) & \text{for } m > 0, \\ \mathbf{I} & \text{for } m = 0, \\ \mathcal{R}_m(\mathbf{I}) & \text{for } m < 0, \end{cases} \tag{5.9}$$

is introduced. Then,

$$\tilde{\underline{\mathbf{b}}}_i^{(k,k_{\mathrm{s}})} = \mathbf{S}_{Q(i-\frac{(I+1)}{2})}\underline{\mathbf{b}}^{(k,k_{\mathrm{s}})} \tag{5.10}$$

holds for the columns of $\underline{\mathbf{A}}_{\mathrm{s}}^{(k,k_{\mathrm{s}})}$ of (5.2).

Let us assume that, with $K_{\mathrm{s}}^{(k)} \leq K_{\mathrm{s}}$, only the CDMA signals k_{s}, $k_{\mathrm{s}} = 1\ldots K_{\mathrm{s}}^{(k)}$, arrive at MS μ_k with significant powers. The partial system submatrices $\underline{\mathbf{A}}_{\mathrm{s}}^{(k,k_{\mathrm{s}})}$ of (5.2) and (5.10) of these $K_{\mathrm{s}}^{(k)}$ CDMA signals can be stacked to form the system submatrix

$$\underline{\mathbf{A}}_{\mathrm{s}}^{(k)} = (\underline{\mathbf{A}}_{\mathrm{s}}^{(k,1)}\ldots\underline{\mathbf{A}}_{\mathrm{s}}^{(k,K_{\mathrm{s}}^{(k)})}) \tag{5.11}$$

of dimension $(Q + W - 1) \times K_{\mathrm{s}}^{(k)}I$. If the $K_{\mathrm{s}}^{(k)}I$ columns of $\underline{\mathbf{A}}_{\mathrm{s}}^{(k)}$ of (5.11) are linearly independent, then $\underline{\mathbf{A}}_{\mathrm{s}}^{(k)}$ of (5.11) has full rank, that is

$$\mathrm{rank}(\underline{\mathbf{A}}_{\mathrm{s}}^{(k)}) = \begin{cases} K_{\mathrm{s}}^{(k)}I & \text{if } K_{\mathrm{s}}^{(k)}I < Q + W - 1, \\ Q + W - 1 & \text{else.} \end{cases} \tag{5.12}$$

The following considerations are based on the assumptions that

$$K_{\mathrm{s}}^{(k)}I < Q + W - 1 \tag{5.13}$$

holds and $\underline{\mathbf{A}}_{\mathrm{s}}^{(k)}$ is of full rank $K_{\mathrm{s}}^{(k)}I$. Then, $\mathbf{I}$ in (5.9) has the dimension $(Q + W - 1) \times (Q + W - 1)$.

5.3   Singular value decomposition

In what follows the $(Q + W - 1) \times (Q + W - 1)$ covariance matrix

$$\underline{\mathbf{R}}_{\mathrm{a}}^{(k)} = \underline{\mathbf{A}}_{\mathrm{s}}^{(k)}\underline{\mathbf{A}}_{\mathrm{s}}^{(k)*\mathrm{T}} \tag{5.14}$$

of $\underline{\mathbf{A}}_{\mathrm{s}}^{(k)}$ of (5.11) plays a role. With the $Q + W - 1$ eigenvalues $\lambda_s^{(k)}$, $s = 1 \ldots Q + W - 1$, and the $Q + W - 1$ eigenvectors $\underline{\mathbf{u}}_s^{(k)}$, $s = 1 \ldots Q + W - 1$, of $\underline{\mathbf{R}}_{\mathrm{a}}^{(k)}$ of (5.14) the diagonal matrix

$$\Lambda^{(k)} = \begin{pmatrix} \lambda_1^{(k)} & 0 & \ldots & 0 \\ 0 & \lambda_2^{(k)} & \ldots & 0 \\ \vdots & \vdots & \ddots & \vdots \\ 0 & 0 & \ldots & \lambda_{Q+W-1}^{(k)} \end{pmatrix} \tag{5.15}$$

and the matrix

$$\underline{\mathbf{U}}^{(k)} = (\underline{\mathbf{u}}_1^{(k)} \ldots \underline{\mathbf{u}}_{Q+W-1}^{(k)}) \tag{5.16}$$

can be formed. With these two matrices, $\underline{\mathbf{R}}_{\mathrm{a}}^{(k)}$ of (5.14) can be expressed in the form

$$\underline{\mathbf{R}}_{\mathrm{a}}^{(k)} = \underline{\mathbf{U}}^{(k)} \Lambda^{(k)} \underline{\mathbf{U}}^{(k)^{*\mathrm{T}}}, \tag{5.17}$$

which is termed eigenvalue decomposition [Ste98, Dep88] of $\underline{\mathbf{R}}_{\mathrm{a}}^{(k)}$. Under the above made assumptions of $K_{\mathrm{s}}^{(k)} I < Q + W - 1$ and full rank $K_{\mathrm{s}}^{(k)} I$ of $\underline{\mathbf{A}}_{\mathrm{s}}^{(k)}$, a number of $Q + W - 1 - K_{\mathrm{s}}^{(k)} I$ eigenvalues of $\underline{\mathbf{R}}_{\mathrm{a}}^{(k)}$ of (5.14) are zero. The corresponding $Q + W - 1 - K_{\mathrm{s}}^{(k)} I$ eigenvectors are termed $\underline{\mathbf{u}}_{\mathrm{n},s}$, $s = 1 \ldots (Q + W - 1 - K_{\mathrm{s}}^{(k)} I)$ and span a space to which the columns $\underline{\tilde{\mathbf{b}}}_i^{(k,k_{\mathrm{s}})}$, $i = 1 \ldots I$, $k_{\mathrm{s}} = 1 \ldots K_{\mathrm{s}}^{(k)}$ of the system submatrix $\underline{\mathbf{A}}_{\mathrm{s}}^{(k)}$ of (5.11) are orthogonal. The eigenvectors $\underline{\mathbf{u}}_{\mathrm{n},s}$, can be compiled to the matrix

$$\underline{\mathbf{U}}_{\mathrm{n}}^{(k)} = (\underline{\mathbf{u}}_{\mathrm{n},1} \ldots \underline{\mathbf{u}}_{\mathrm{n},Q+W-1-K_{\mathrm{s}}^{(k)} I}) \tag{5.18}$$

of dimension $(Q + W - 1) \times (Q + W - 1 - K_{\mathrm{s}}^{(k)} I)$.

5.4 Blind determination of the channel impulse responses

The composite channel impulse response $\underline{\mathbf{b}}^{(k,k_{\mathrm{s}})}$ of (4.19) can be expressed by the signal specific channel impulse response $\underline{\mathbf{h}}^{(k,k_{\mathrm{s}})}$ of (4.9) and the CDMA code matrix $\underline{\mathbf{C}}^{(k_{\mathrm{s}})}$ of (4.18) as follows:

$$\underline{\mathbf{b}}^{(k,k_{\mathrm{s}})} = \underline{\mathbf{C}}^{(k_{\mathrm{s}})} \underline{\mathbf{h}}^{(k,k_{\mathrm{s}})}. \tag{5.19}$$

In what follows it is assumed that

$$\underline{\mathbf{h}}^{(k,k_{\mathrm{s}})^{*\mathrm{T}}} \underline{\mathbf{h}}^{(k,k_{\mathrm{s}})} = 1, \ k_{\mathrm{s}} = 1 \ldots K_{\mathrm{s}}, \ k = 1 \ldots K, \tag{5.20}$$

holds. Substituting $\underline{\mathbf{b}}^{(k,k_{\mathrm{s}})}$ of (5.19) into (5.10) yields

$$\underline{\tilde{\mathbf{b}}}_i^{(k,k_{\mathrm{s}})} = \mathbf{S}_{Q(i-\frac{(I+1)}{2})}\underline{\mathbf{C}}^{(k_{\mathrm{s}})}\underline{\mathbf{h}}^{(k,k_{\mathrm{s}})}, \ i = 1 \ldots I, \tag{5.21}$$

for the i-th column of the partial system submatrix $\underline{\mathbf{A}}_{\mathrm{s}}^{(k,k_{\mathrm{s}})}$ of (5.2). Each of the I vectors $\underline{\tilde{\mathbf{b}}}_i^{(k,k_{\mathrm{s}})}$ of (5.21) is orthogonal to all $Q + W - 1 - K_{\mathrm{s}}^{(k)}I$ columns $\underline{\mathbf{u}}_{\mathrm{n},s}$ of the matrix $\underline{\mathbf{U}}_{\mathrm{n}}^{(k)}$ of (5.18). Due to this an estimate $\underline{\hat{\mathbf{h}}}^{(k,k_{\mathrm{s}})}$ of the signal specific channel impulse response $\underline{\mathbf{h}}^{(k,k_{\mathrm{s}})}$ of (4.9) can be obtained by performing, with $\underline{\tilde{\mathbf{b}}}_i^{(k,k_{\mathrm{s}})}$ of (5.21) and $\underline{\mathbf{U}}_{\mathrm{n}}^{(k)}$ of (5.18), the minimization

$$
\begin{aligned}
\underline{\hat{\mathbf{h}}}^{(k,k_{\mathrm{s}})} &= \arg \min_{\underline{\mathbf{h}}^{(k,k_{\mathrm{s}})}} \left(\sum_{i=1}^{I} |\underline{\tilde{\mathbf{b}}}_i^{(k,k_{\mathrm{s}})\mathrm{T}} \underline{\mathbf{U}}_{\mathrm{n}}^{(k)}|^2 \right) \\
&= \arg \min_{\underline{\mathbf{h}}^{(k,k_{\mathrm{s}})}} \left(\sum_{i=1}^{I} \underline{\tilde{\mathbf{b}}}_i^{(k,k_{\mathrm{s}})\mathrm{T}} \underline{\mathbf{U}}_{\mathrm{n}}^{(k)} \underline{\mathbf{U}}_{\mathrm{n}}^{(k)*\mathrm{T}} \underline{\tilde{\mathbf{b}}}_i^{(k,k_{\mathrm{s}})*} \right) \\
&= \arg \min_{\underline{\mathbf{h}}^{(k,k_{\mathrm{s}})}} \left(\sum_{i=1}^{I} \underline{\mathbf{h}}^{(k,k_{\mathrm{s}})\mathrm{T}} \underline{\mathbf{C}}^{(k_{\mathrm{s}})\mathrm{T}} \mathbf{S}_{Q(i-\frac{(I+1)}{2})}^{\mathrm{T}} \underline{\mathbf{U}}_{\mathrm{n}}^{(k)} \underline{\mathbf{U}}_{\mathrm{n}}^{(k)*\mathrm{T}} \mathbf{S}_{Q(i-\frac{(I+1)}{2})}^{*} \underline{\mathbf{C}}^{(k_{\mathrm{s}})*} \underline{\mathbf{h}}^{(k,k_{\mathrm{s}})*} \right) \\
&= \arg \min_{\underline{\mathbf{h}}^{(k,k_{\mathrm{s}})}} \left(\underline{\mathbf{h}}^{(k,k_{\mathrm{s}})\mathrm{T}} \underbrace{\left(\sum_{i=1}^{I} \underline{\mathbf{C}}^{(k_{\mathrm{s}})\mathrm{T}} \mathbf{S}_{Q(i-\frac{(I+1)}{2})}^{\mathrm{T}} \underline{\mathbf{U}}_{\mathrm{n}}^{(k)} \underline{\mathbf{U}}_{\mathrm{n}}^{(k)*\mathrm{T}} \mathbf{S}_{Q(i-\frac{(I+1)}{2})}^{*} \underline{\mathbf{C}}^{(k_{\mathrm{s}})*} \right)}_{\underline{\mathbf{E}}^{(k)}} \underline{\mathbf{h}}^{(k,k_{\mathrm{s}})*} \right).
\end{aligned}
$$

$$\tag{5.22}$$

The desired signal specific channel impulse response estimate $\underline{\hat{\mathbf{h}}}^{(k,k_{\mathrm{s}})}$ is obtained as the eigenvector of the matrix $\underline{\mathbf{E}}^{(k)}$ introduced in (5.22) belonging to the smallest eigenvalue of $\underline{\mathbf{E}}^{(k)}$. This eigenvalue should be zero. If a single omnidirectional transmit antenna is utilized at the BS, all $K_{\mathrm{s}}^{(k)}$ signal specific channel impulse responses $\underline{\mathbf{h}}^{(k,k_{\mathrm{s}})}$ of (4.9) become the same. In this case, for instance an average over all $K_{\mathrm{s}}^{(k)}$ estimates $\underline{\hat{\mathbf{h}}}^{(k,k_{\mathrm{s}})}$ can be taken into account in further research.

In the case $K_{\mathrm{s}}^{(k)}$ equal to one, instead of determining $\underline{\hat{\mathbf{h}}}^{(k,1)}$, one can also determine an estimate $\underline{\hat{\mathbf{b}}}^{(k,1)}$ of the composite channel impulse response $\underline{\mathbf{b}}^{(k,1)}$. To this purpose (5.10) is substituted in (5.22) without resorting to (5.21). We then obtain

$$
\begin{aligned}
\underline{\hat{\mathbf{b}}}^{(k,1)} &= \arg \min_{\underline{\mathbf{b}}^{(k,1)}} \left(\sum_{i=1}^{I} \underline{\mathbf{b}}^{(k,1)\mathrm{T}} \mathbf{S}_{Q(i-\frac{(I+1)}{2})}^{\mathrm{T}} \underline{\mathbf{U}}_{\mathrm{n}}^{(k)} \underline{\mathbf{U}}_{\mathrm{n}}^{(k)*\mathrm{T}} \mathbf{S}_{Q(i-\frac{(I+1)}{2})}^{*} \underline{\mathbf{b}}^{(k,1)*} \right) \\
&= \arg \min_{\underline{\mathbf{b}}^{(k,1)}} \left(\underline{\mathbf{b}}^{(k,1)\mathrm{T}} \underbrace{\left(\sum_{i=1}^{I} \mathbf{S}_{Q(i-\frac{(I+1)}{2})}^{\mathrm{T}} \underline{\mathbf{U}}_{\mathrm{n}}^{(k)} \underline{\mathbf{U}}_{\mathrm{n}}^{(k)*\mathrm{T}} \mathbf{S}_{Q(i-\frac{(I+1)}{2})}^{*} \right)}_{\underline{\mathbf{E}}^{(k)}} \underline{\mathbf{b}}^{(k,1)*} \right).
\end{aligned}
\tag{5.23}
$$

The estimate $\underline{\hat{\mathbf{b}}}^{(k,1)}$ of $\underline{\mathbf{b}}^{(k,1)}$ is the eigenvector of the matrix $\underline{\mathbf{E}}^{(k)}$ introduced in (5.23) belonging to the smallest eigenvalue of $\underline{\mathbf{E}}^{(k)}$.

The estimates $\hat{\underline{\mathbf{h}}}^{(k,k_{\mathrm{s}})}$ and $\hat{\underline{\mathbf{h}}}^{(k,1)}$ of (5.22) and (5.23), respectively, are determined only up to an arbitrary complex factor. Therefore, the utilization of these estimates in the TD-CDMA downlink requires the transmission of at least one training symbol per CDMA code. These training symbols allow the resolution of the phase and amplitude ambiguities of the estimates $\hat{\underline{\mathbf{h}}}^{(k,k_{\mathrm{s}})}$ of (5.22) and $\hat{\underline{\mathbf{b}}}^{(k,1)}$ of (5.23), respectively.

5.5 Estimation of the covariance matrix of the system submatrix

Blind channel estimation as described in the previous Sections 5.1 to 5.4 requires the knowledge of the matrix $\underline{\mathbf{U}}_{\mathrm{n}}^{(k)}$ of (5.18). In this section it will be shown how this knowledge can be approximately obtained by evaluating the signal $\underline{\mathbf{e}}^{(k)}$ of (4.22) received at MS μ_k.

As explained in Section 5.2, a number of possibilities exist how to place $\underline{\mathbf{A}}_{\mathrm{s}}^{(k,k_{\mathrm{s}})}$ of (5.2) within $\underline{\mathbf{A}}^{(k,k_{\mathrm{s}})}$ of (4.20), and, consequently, how to place $\underline{\mathbf{A}}_{\mathrm{s}}^{(k)}$ of (5.11) within $\underline{\mathbf{A}}^{(k)}$ of (4.21). To each of these possibilities corresponds a subvector $\underline{\mathbf{e}}_{\mathrm{s}}^{(k)}$ of dimension $Q + W - 1$ of the total received signal $\underline{\mathbf{e}}^{(k)}$ of (4.22), see Fig. 5.1. With the corresponding subvectors $\underline{\mathbf{d}}_{\mathrm{s}}$ and $\underline{\mathbf{n}}_{\mathrm{s}}^{(k)}$ of the total data vector $\underline{\mathbf{d}}$ and the received intercell interference vector $\underline{\mathbf{n}}^{(k)}$ in (4.22), respectively, and with $\underline{\mathbf{A}}_{\mathrm{s}}^{(k)}$ of (5.11) $\underline{\mathbf{e}}_{\mathrm{s}}^{(k)}$ can be expressed as

$$\underline{\mathbf{e}}_{\mathrm{s}}^{(k)} = \underline{\mathbf{A}}_{\mathrm{s}}^{(k)}\underline{\mathbf{d}}_{\mathrm{s}} + \underline{\mathbf{n}}_{\mathrm{s}}^{(k)}. \tag{5.24}$$

By choosing different positions of $\underline{\mathbf{A}}_{\mathrm{s}}^{(k)}$ of (5.11) within $\underline{\mathbf{A}}^{(k)}$ of (4.21) a set of subvectors $\underline{\mathbf{e}}_{\mathrm{s}}^{(k)}$ can be obtained in each received burst. Averaging over the covariance matrices $\underline{\mathbf{e}}_{\mathrm{s}}^{(k)}\underline{\mathbf{e}}_{\mathrm{s}}^{(k)*\mathrm{T}}$ of these subvectors yields the covariance matrix

$$\underline{\mathbf{R}}_{\mathrm{e}}^{(k)} = \mathrm{E}\{\underline{\mathbf{e}}_{\mathrm{s}}^{(k)}\underline{\mathbf{e}}_{\mathrm{s}}^{(k)*\mathrm{T}}\} = \mathrm{E}\{(\underline{\mathbf{A}}_{\mathrm{s}}^{(k)}\underline{\mathbf{d}}_{\mathrm{s}} + \underline{\mathbf{n}}_{\mathrm{s}}^{(k)})(\underline{\mathbf{A}}_{\mathrm{s}}^{(k)}\underline{\mathbf{d}}_{\mathrm{s}} + \underline{\mathbf{n}}_{\mathrm{s}}^{(k)})^{*\mathrm{T}}\}. \tag{5.25}$$

Now the following assumptions are made concerning the covariance matrices of $\underline{\mathbf{d}}_{\mathrm{s}}$ and $\underline{\mathbf{n}}_{\mathrm{s}}^{(k)}$:

$$\underline{\mathbf{R}}_{\mathrm{d}} = \mathrm{E}\{\underline{\mathbf{d}}_{\mathrm{s}}\underline{\mathbf{d}}_{\mathrm{s}}^{*\mathrm{T}}\} = \mathbf{I}^{(K_{\mathrm{s}}^{(k)}I)\times(K_{\mathrm{s}}^{(k)}I)}. \tag{5.26}$$

$$\underline{\mathbf{R}}_{\mathrm{n}}^{(k)} = \mathrm{E}\{\underline{\mathbf{n}}_{\mathrm{s}}^{(k)}\underline{\mathbf{n}}_{\mathrm{s}}^{(k)*\mathrm{T}}\} = \sigma^2\mathbf{I}^{(Q+W-1)\times(Q+W-1)}. \tag{5.27}$$

Furthermore, it is assumed that $\underline{\mathbf{d}}_{\mathrm{s}}$ and $\underline{\mathbf{n}}_{\mathrm{s}}^{(k)}$ are uncorrelated, and that the set of subvectors $\underline{\mathbf{e}}_{\mathrm{s}}^{(k)}$ available in the received burst is sufficiently large. Then, with $\underline{\mathbf{R}}_{\mathrm{a}}^{(k)}$ of (5.14), $\underline{\mathbf{R}}_{\mathrm{e}}^{(k)}$ of (5.25) can be expressed as

$$\underline{\mathbf{R}}_{\mathrm{e}}^{(k)} = \underline{\mathbf{R}}_{\mathrm{a}}^{(k)} + \sigma^2\mathbf{I}. \tag{5.28}$$

If $\underline{\mathbf{R}}_{\mathrm{e}}^{(k)}$ of (5.28) is subject to eigenvalue decomposition, the smallest eigenvalues become $\sigma^{(k)2}$, and the corresponding eigenvectors constitute the matrix $\underline{\mathbf{U}}_{\mathrm{n}}^{(k)}$ of (5.18). Then, the estimation procedures of (5.22) and (5.23), respectively, can be performed. As the problems likely to occur in practical applications, the available number of subvectors $\underline{\mathbf{e}}^{(k)}$ per burst may be too small to obtain from (5.25) a covariance matrix $\underline{\mathbf{R}}_{\mathrm{e}}^{(k)}$ which complies sufficiently well with (5.28), and the channel impulse responses may change too much within the burst so that the assumption of that there is no impact of time variance within each burst would be no longer justified. In the latter case also conventional non-blind channel estimation would have problems.

5.6   Simulation results

In Section 5.6 the results of simulations performed to assess the blind channel estimation method developed in Sections 5.1 to 5.5 are presented. The simulations are performed for the multi-user scenario of Fig. 2.2 with $\Delta\varphi = 20°$ and $\beta = 10°$. The signal specific channel impulse responses $\underline{\mathbf{h}}^{(k,k_{\mathrm{s}})}$ of (4.9) are snapshots of the modified 3GPP channel model with $W = 19$, see Section 2.3.1. The simulation results are presented in Figs. 5.2 to 5.7. In Tab. 5.1 the simulation conditions are given in detail. Different values for the system parameters k, k_{s}, $K_{\mathrm{s}}^{(k)}$ and K_{a} are chosen, and both the case of exactly known and estimated matrix $\underline{\mathbf{U}}_{\mathrm{n}}^{(k)}$ of (5.18) is considered. When estimating $\underline{\mathbf{U}}_{\mathrm{n}}^{(k)}$, see Section 5.5, the number N of symbols per burst is set equal to 50.

Tab. 5.1: Overview of Figs. 5.2 to 5.7 presenting simulation results

Fig.	K	K_{s}	$K_{\mathrm{s}}^{(k)}$	K_{a}	$\underline{\mathbf{U}}_{\mathrm{n}}^{(k)}$ of (5.18)	presented function
5.2	1	1	1	1	exact	$\underline{\mathbf{b}}^{(k,1)}$
5.3	1	1	1	1	estimated	$\underline{\mathbf{b}}^{(k,1)}$
5.4	4	4	1	8	exact	$\underline{\mathbf{b}}^{(k,1)}$
5.5	4	4	1	8	estimated	$\underline{\mathbf{b}}^{(k,1)}$
5.6	2	8	4	8	exact	$\underline{\mathbf{h}}^{(k,1)}$
5.7	2	8	4	8	estimated	$\underline{\mathbf{h}}^{(k,1)}$

From Figs. 5.2 to 5.7 the following conclusions can be drawn:

- The estimation accuracy decreases with increasing K_{s} and unchanged $K_{\mathrm{s}}^{(k)}$, compare Figs. 5.3 and 5.5. This is due to the fact that the power of the additional intracell interference, i.e., the power of the CDMA signals not being of interest to MS μ_k, increases with increasing K_{s}.

- The estimation accuracy increases, if the knowledge of the noise subspace in terms of $\underline{\mathbf{U}}_{\mathrm{n}}^{(k)}$ of (5.18) is perfectly known, compare Figs. 5.3 and 5.2, Figs. 5.5 and 5.4, as well as Figs. 5.7 and 5.6.

- The estimation accuracy decreases with increasing $K_{\mathrm{s}}^{(k)}$, compare Figs. 5.3 a) and 5.7 a), as well as Figs. 5.3 b) and 5.7 b).
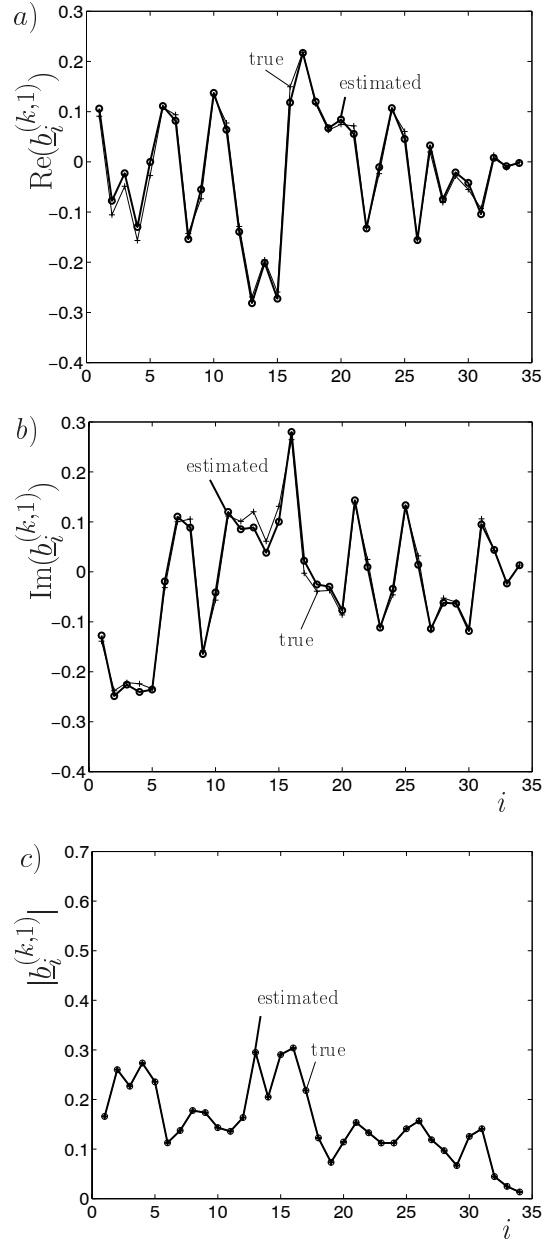
Fig. 5.2: $\underline{b}_i^{(k,1)}$, $i = 1 \ldots (Q + W - 1)$, and estimated $\hat{\underline{b}}_i^{(k,1)}$, $i = 1 \ldots (Q + W - 1)$, of (5.23); exact matrix $\underline{\mathbf{U}}_{\mathrm{n}}^{(k)}$ of (5.18); $K = 1$, $K_{\mathrm{s}} = 1$, $K_{\mathrm{s}}^{(k)} = 1$, $K_{\mathrm{a}} = 1$, $Q = 16$, $W = 19$, $\gamma_{\mathrm{des}}^{(k)} = 0\mathrm{dB}$, see (4.72); a) real part, b) imaginary part, c) magnitude
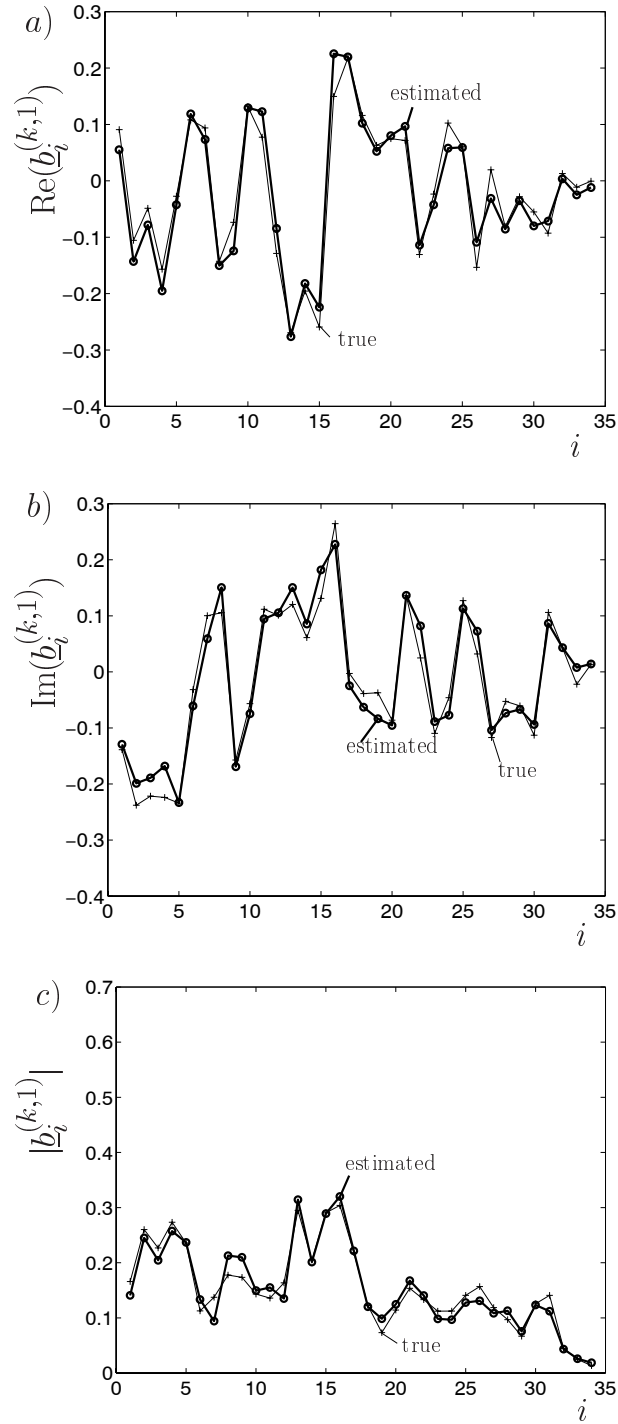
Fig. 5.3: $\underline{b}_i^{(k,1)}$, $i = 1 \ldots (Q + W - 1)$, and estimated $\hat{\underline{b}}_i^{(k,1)}$, $i = 1 \ldots (Q + W - 1)$, of (5.23); estimated matrix $\underline{\mathbf{U}}_n^{(k)}$ of (5.18); $K = 1$, $K_s = 1$, $K_s^{(k)} = 1$, $K_a = 1$, $Q = 16$, $W = 19$, $\gamma_{des}^{(k)} = 0$dB, see (4.72); a) real part, b) imaginary part, c) magnitude
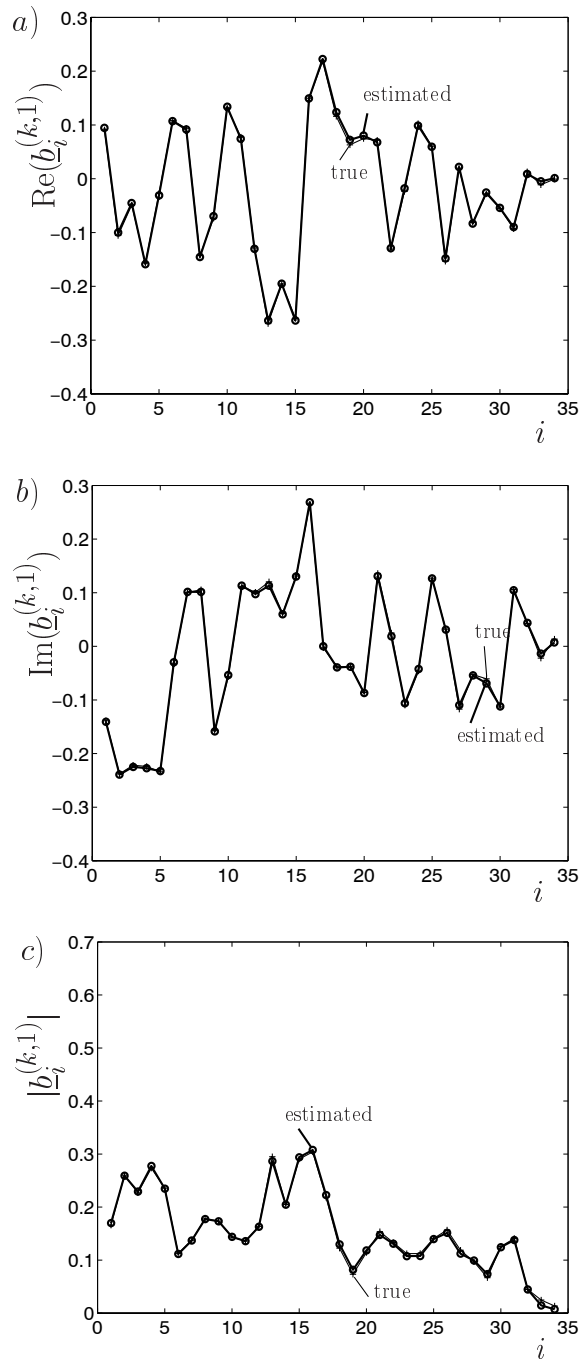
Fig. 5.4: $\underline{b}_i^{(k,1)}$, $i = 1 \ldots (Q + W - 1)$, and estimated $\hat{\underline{b}}_i^{(k,1)}$, $i = 1 \ldots (Q + W - 1)$, of (5.23); exact matrix $\underline{\mathbf{U}}_{\mathrm{n}}^{(k)}$ of (5.18); $K = 4$, $K_{\mathrm{s}} = 4$, $K_{\mathrm{s}}^{(k)} = 1$, $K_{\mathrm{a}} = 8$, $Q = 16$, $W = 19$, $\gamma_{\mathrm{des}}^{(k)} = 0$dB, see (4.72); a) real part, b) imaginary part, c) magnitude
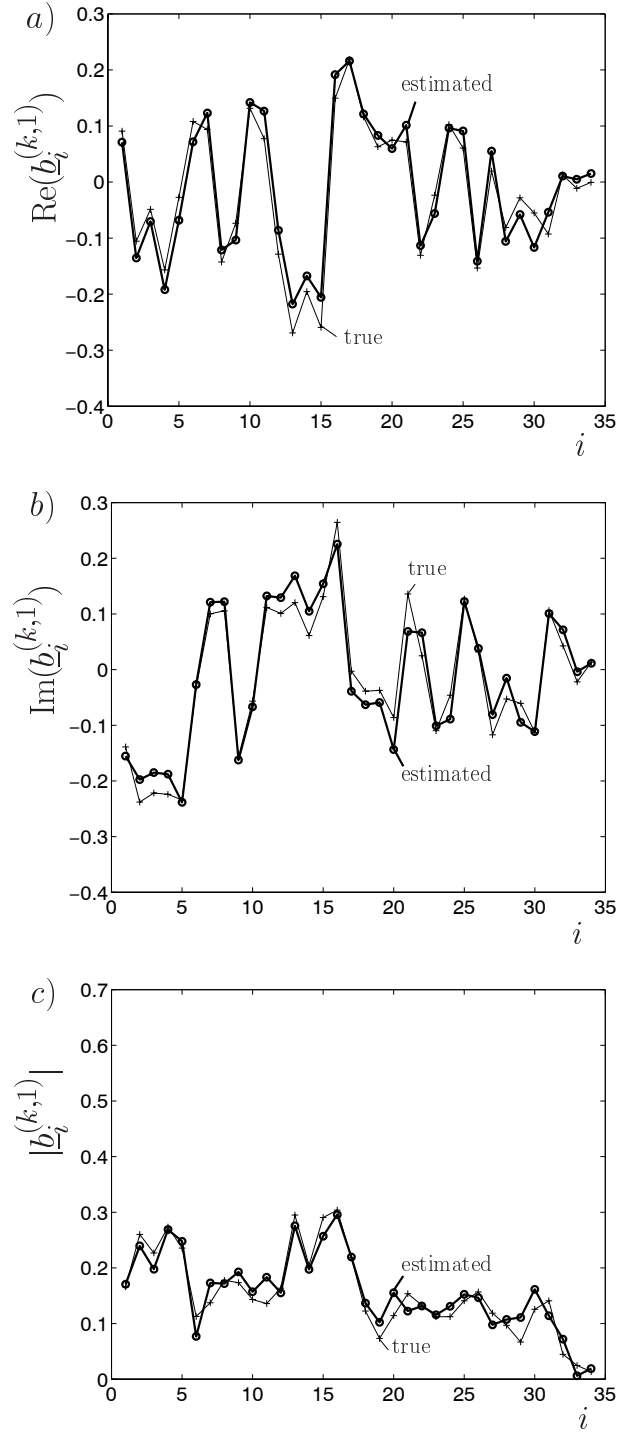
Fig. 5.5: $\underline{b}_i^{(k,1)}$, $i = 1 \ldots (Q + W - 1)$, and estimated $\hat{\underline{b}}_i^{(k,1)}$, $i = 1 \ldots (Q + W - 1)$, of (5.23); estimated matrix $\underline{\mathbf{U}}_{\mathrm{n}}^{(k)}$ of (5.18); $K = 4$, $K_{\mathrm{s}} = 4$, $K_{\mathrm{s}}^{(k)} = 1$, $K_{\mathrm{a}} = 8$, $Q = 16$, $W = 19$, $\gamma_{\mathrm{des}}^{(k)} = 0\mathrm{dB}$, see (4.72); a) real part, b) imaginary part, c) magnitude
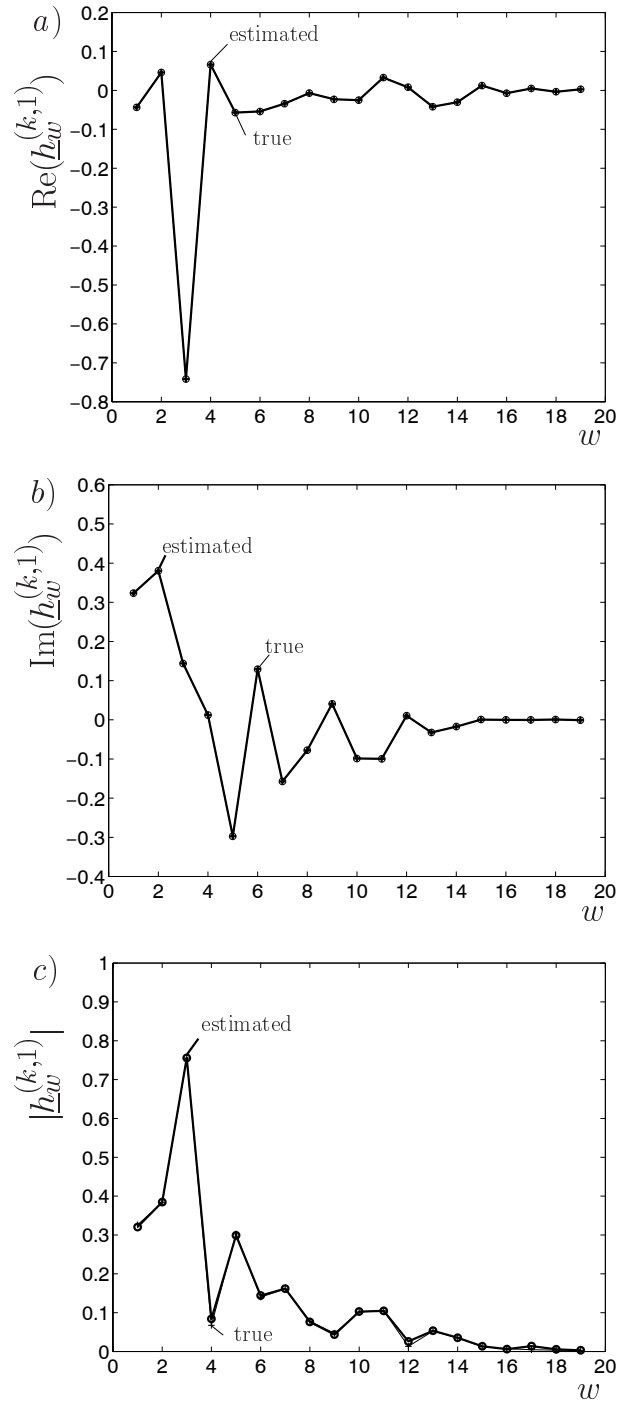
Fig. 5.6: $\underline{h}_w^{(k,1)}$, $w = 1 \ldots W$, and estimated $\underline{\hat{h}}_w^{(k,1)}$, $w = 1 \ldots W$, of (5.22); exact matrix $\underline{\mathbf{U}}_n^{(k)}$ of (5.18); $K = 2$, $K_s = 8$, $K_s^{(k)} = 4$, $K_a = 8$, $Q = 16$, $W = 19$, $\gamma_{\text{des}}^{(k)} = 10\text{dB}$, see (4.72); a) real part, b) imaginary part, c) magnitude)
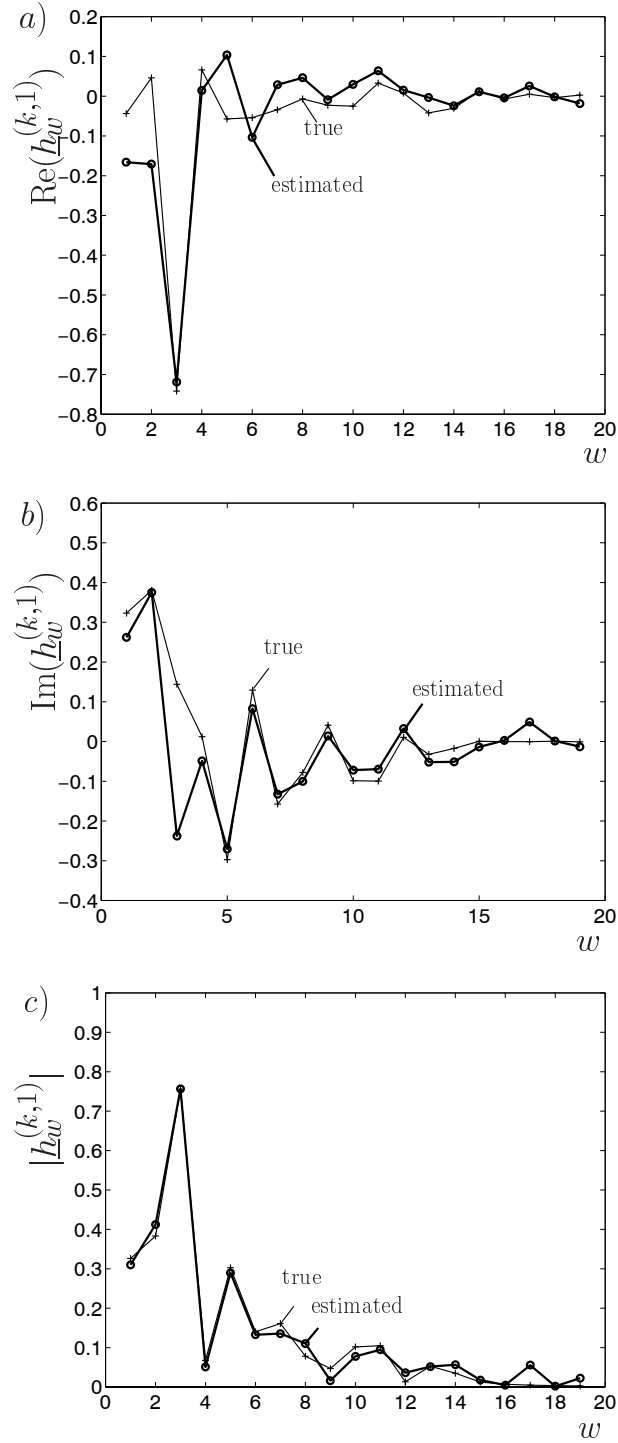
Fig. 5.7: $\underline{h}_w^{(k,1)}$, $w = 1 \ldots W$, and estimated $\hat{\underline{h}}_w^{(k,1)}$, $w = 1 \ldots W$, of (5.22); estimated matrix $\underline{\mathbf{U}}_n^{(k)}$ of (5.18); $K = 2$, $K_s = 8$, $K_s^{(k)} = 4$, $K_a = 8$, $Q = 16$, $W = 19$, $\gamma_{\mathrm{des}}^{(k)} = 10\mathrm{dB}$, see (4.72); a) real part, b) imaginary part, c) magnitude

Chapter 6

Multi-channel transmission in the TD-CDMA downlink

6.1 Introduction

In Section 4.3, CDMA code pooling is introduced as a method for supporting high user data rates in the TD-CDMA downlink. According to this concept, more than one burst signal are assigned to certain MSs μ_k in each partial frequency band B and time slot, see Section 1.1. Each of the K_s burst signals in the same partial frequency band B and time slot utilizes a specific CDMA code and is characterized as a physical channel. Therefore, CDMA code pooling leads to a multi-channel transmission model, which is treated in this chapter. In Section 6.2 this model is presented. For this model the maximal total channel capacity under the assumption of a constant average input SNR at the receiver of MS μ_k, $k = 1 \ldots K$, is investigated in Section 6.3. Section 6.4 discusses the CDMA-code/channel mismatch mentioned already in Section 1.3 and gives a mathematical analysis of the SNR degradation. Different methods for mitigating the impact of the CDMA-code/channel mismatch are provided in Section 6.5. Finally, an adaptive channel coding scheme is described in Section 6.6.

6.2 Multi-channel transmission model

In this section, a simplified AWGN multi-channel model including the signal transmission and data detection in the TD-CDMA downlink will be derived. In the following derivations only one MS is considered, to which K_s CDMA codes are assigned.

BS   MS μ_k
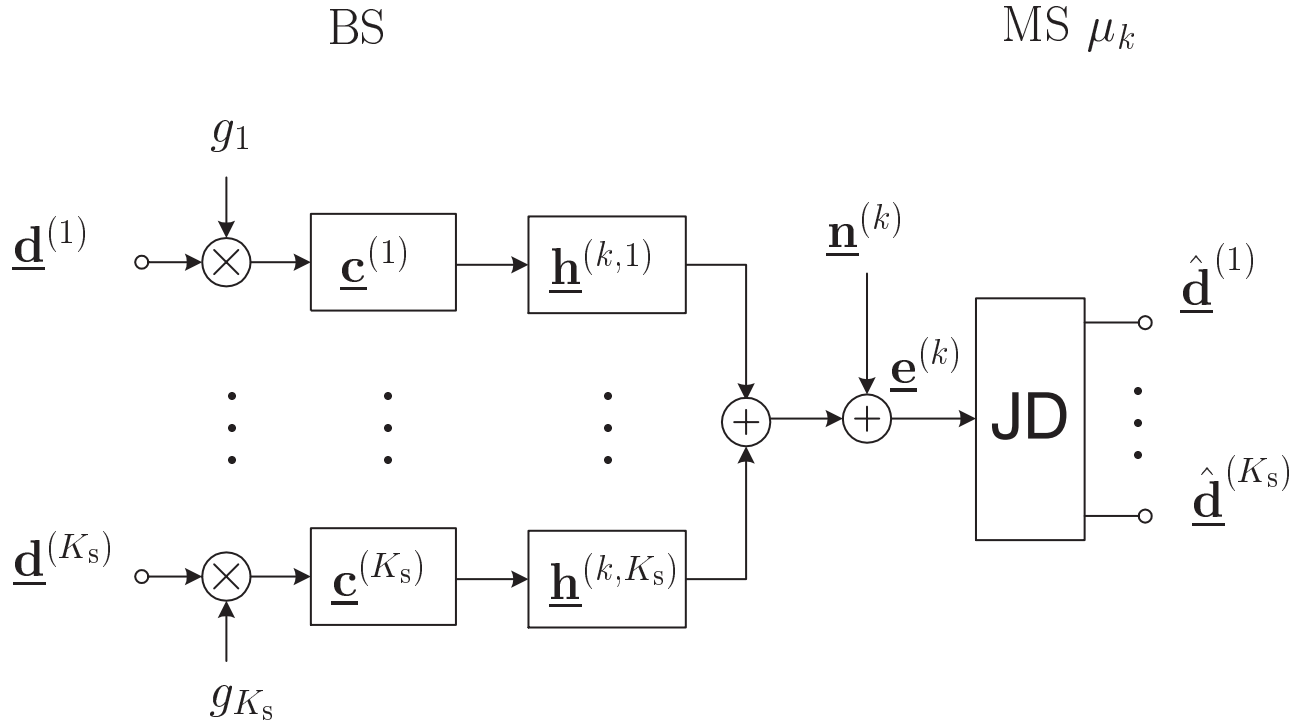
Fig. 6.1: Signal transmission between the BS and MS μ_k in the TD-CDMA downlink

A block diagram illustrating the signal transmission between the BS and MS μ_k, $k = 1 \ldots K$, in the TD-CDMA downlink is shown in Fig. 6.1. The BS transmitter simultaneously generates the K_{s} partial data vectors $\underline{\mathbf{d}}^{(k_{\mathrm{s}})}$, $k_{\mathrm{s}} = 1 \ldots K_{\mathrm{s}}$, of (4.6). To perform transmit power control, each of these K_{s} partial data vectors $\underline{\mathbf{d}}^{(k_{\mathrm{s}})}$ is weighted by a corresponding gain $g_{k_{\mathrm{s}}}$, $k_{\mathrm{s}} = 1 \ldots K_{\mathrm{s}}$. Then, the weighted partial data vectors $\underline{\mathbf{d}}^{(k_{\mathrm{s}})}$, $k_{\mathrm{s}} = 1 \ldots K_{\mathrm{s}}$, are spectrally spread by the CDMA codes $\underline{\mathbf{c}}^{(k_{\mathrm{s}})}$, $k_{\mathrm{s}} = 1 \ldots K_{\mathrm{s}}$, of (4.5) and transmitted over a mobile radio channel characterized by the signal specific channel impulse responses $\underline{\mathbf{h}}^{(k,k_{\mathrm{s}})}$, $k_{\mathrm{s}} = 1 \ldots K_{\mathrm{s}}$, of (4.9). As discussed in Section 4.2, see (4.9), the signal specific channel impulse responses $\underline{\mathbf{h}}^{(k,k_{\mathrm{s}})}$ depend on the antenna weight vectors $\underline{\mathbf{w}}^{(k_{\mathrm{s}})}$ of (4.7), if adaptive transmit antennas are used at the BS. If a single omnidirectional transmit antenna is utilized at the BS, $\underline{\mathbf{h}}^{(k,k_{\mathrm{s}})}$, $k_{\mathrm{s}} = 1 \ldots K_{\mathrm{s}}$, in the model of Fig. 6.1, is equal for all K_{s} channels. This means that the weighted and spectrally spread partial data vectors $\underline{\mathbf{d}}^{(k_{\mathrm{s}})}$, $k_{\mathrm{s}} = 1 \ldots K_{\mathrm{s}}$, are transmitted to MS μ_k over a common mobile radio channel. At MS μ_k, the received signal $\underline{\mathbf{e}}^{(k)}$, which is corrupted by the intercell interference vector $\underline{\mathbf{n}}^{(k)}$, see Tab. 4.1, is fed into the input of the joint detector. As introduced in Section 4.6.2, in order to perform JD at MS μ_k, the total system matrix $\underline{\mathbf{A}}^{(k)}$ of (4.21) is required, see (4.44). $\underline{\mathbf{A}}^{(k)}$ of (4.21) considered in Section 4.4 contains the composite channel impulse responses $\underline{\mathbf{b}}^{(k,k_{\mathrm{s}})}$, $k_{\mathrm{s}} = 1 \ldots K_{\mathrm{s}}$, see (4.19), (4.20) and (4.21). However, when performing JD in the model of Fig. 6.1 not only the composite channel impulse responses $\underline{\mathbf{b}}^{(k,k_{\mathrm{s}})}$, $k_{\mathrm{s}} = 1 \ldots K_{\mathrm{s}}$, of (4.19), but also the gains $g_{k_{\mathrm{s}}}$, $k_{\mathrm{s}} = 1 \ldots K_{\mathrm{s}}$, should be considered to form

$$\underline{\mathbf{n}}^{(k)}$$
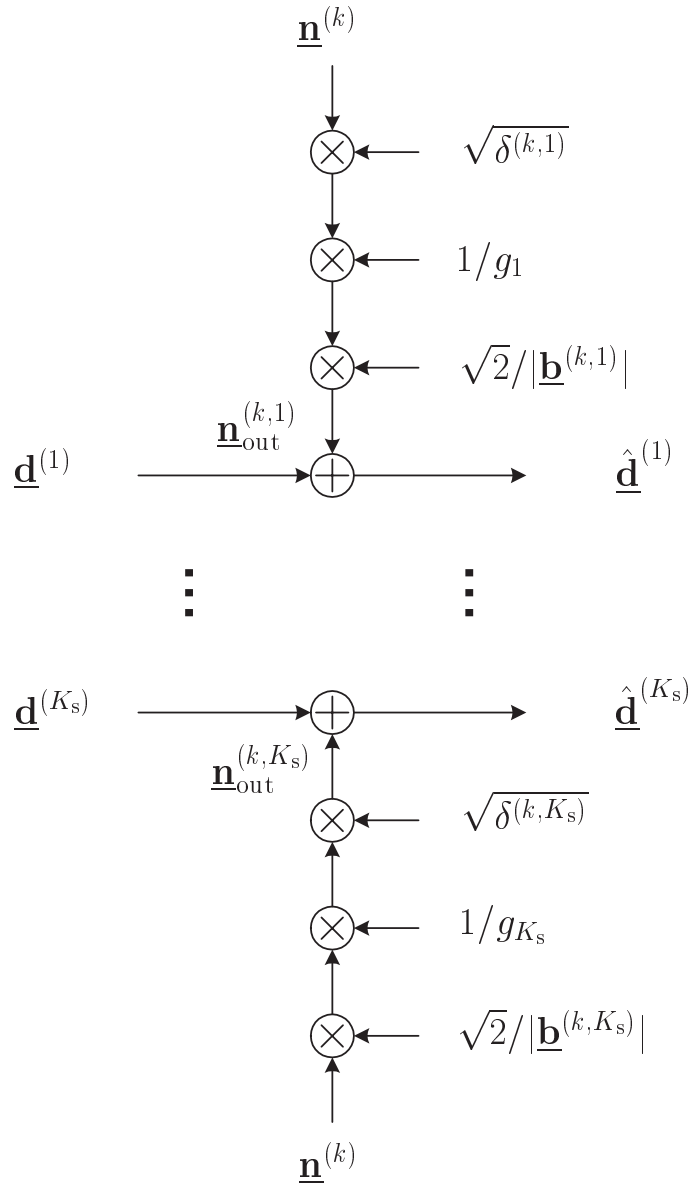
Fig. 6.2: Simplified multi-channel model equivalent to the model shown in Fig. 6.1

the total system matrix $\underline{\mathbf{A}}^{(k)}$. At the output of the joint detector the estimated partial data vectors $\hat{\underline{\mathbf{d}}}^{(k_\mathrm{s})}$, $k_\mathrm{s} = 1 \dots K_\mathrm{s}$, are obtained. With the gains g_{k_s}, $k_\mathrm{s} = 1 \dots K_\mathrm{s}$, see Fig. 6.1, and the composite channel impulse responses $\underline{\mathbf{b}}^{(k,k_\mathrm{s})}$, $k = 1 \dots K$, $k_\mathrm{s} = 1 \dots K_\mathrm{s}$, of (4.19), the SNRs $\gamma^{(k,k_\mathrm{s})}$ of (4.56) at the input of the joint detector become

$$\gamma^{(k,k_\mathrm{s})} = \frac{|\underline{\mathbf{b}}^{(k,k_\mathrm{s})}|^2 g_{k_\mathrm{s}}^2}{2Q\sigma^{(k)2}}, \quad k = 1 \dots K, \ k_\mathrm{s} = 1 \dots K_\mathrm{s}. \tag{6.1}$$

Moreover, with $\gamma^{(k,k_\mathrm{s})}$ of (6.1) and with the SNR degradations $\delta^{(k,k_\mathrm{s})}$, $k = 1 \dots K$, $k_\mathrm{s} = 1 \dots K_\mathrm{s}$, of (4.47), the SNRs

$$\gamma_{\mathrm{out}}^{(k,k_\mathrm{s})} = \frac{\gamma^{(k,k_\mathrm{s})}Q}{\delta^{(k,k_\mathrm{s})}} = \frac{|\underline{\mathbf{b}}^{(k,k_\mathrm{s})}|^2 g_{k_\mathrm{s}}^2}{2\sigma^{(k)2}\delta^{(k,k_\mathrm{s})}}, \quad k_\mathrm{s} = 1 \dots K_\mathrm{s}, \tag{6.2}$$

at the output of the joint detector are obtained. (6.1) and (6.2) show that the SNRs $\gamma^{(k,k_\mathrm{s})}$ and $\gamma_\mathrm{out}^{(k,k_\mathrm{s})}$, respectively, can be adjusted by setting the gains g_{k_s}.

As mentioned in Section 4.6.2, the JD process is transparent for the partial data vectors $\underline{\mathbf{d}}^{(k_\mathrm{s})}$, $k_\mathrm{s} = 1 \ldots K_\mathrm{s}$, transmitted by the BS. Following (4.44), we have

$$\hat{\underline{\mathbf{d}}}^{(k_\mathrm{s})} = \underline{\mathbf{d}}^{(k_\mathrm{s})} + \underline{\mathbf{n}}_\mathrm{out}^{(k,k_\mathrm{s})}, \quad k_\mathrm{s} = 1 \ldots K_\mathrm{s}, \tag{6.3}$$

where $\underline{\mathbf{n}}_\mathrm{out}^{(k,k_\mathrm{s})}$ depends on the matrix $\underline{\mathbf{M}}^{(k)}$ and the intercell interference vector $\underline{\mathbf{n}}^{(k)}$ in (4.44). Now, under the assumption that each transmitted symbol of the partial data vectors $\underline{\mathbf{d}}^{(k_\mathrm{s})}$, $k_\mathrm{s} = 1 \ldots K_\mathrm{s}$, has the magnitude one, the variance

$$\sigma^{(k,k_\mathrm{s})2} = \frac{2\sigma^{(k)2}\delta^{(k,k_\mathrm{s})}}{|\underline{\mathbf{b}}^{(k,k_\mathrm{s})}|^2 g_{k_\mathrm{s}}^2} \tag{6.4}$$

of the real and imaginary parts of the components of $\underline{\mathbf{n}}_\mathrm{out}^{(k,k_\mathrm{s})}$ in (6.3) can be obtained following (6.3) and (6.2). According to (6.3) and (6.4), a simplified multi-channel model, which is equivalent to the signal transmission model shown in Fig. 6.1, can be developed. This model is shown in Fig. 6.2, see also [Pap00]. It is observed from Fig. 6.2 that each of the K_s channels can be treated as an AWGN channel. Based on this observation, the concept for maximizing the total channel capacity of the multi-channel transmission is given in the next section.

6.3 Maximizing the total channel capacity with constant average input SNR

6.3.1 Concept

The input SNRs $\gamma^{(k,k_\mathrm{s})}$ of (6.1) have the average

$$\gamma^{(k)} = \frac{1}{K_\mathrm{s}} \sum_{k_\mathrm{s}=1}^{K_\mathrm{s}} \gamma^{(k,k_\mathrm{s})}. \tag{6.5}$$

With $\gamma^{(k,k_\mathrm{s})}$ of (6.1) and $\gamma_\mathrm{out}^{(k,k_\mathrm{s})}$ of (6.2) each of the K_s channels in the structures of Figs. 6.1 and 6.2 has a channel capacity [Fis97]

$$R^{(k,k_\mathrm{s})} = \mathrm{ld}(1 + \gamma_\mathrm{out}^{(k,k_\mathrm{s})}) = \mathrm{ld}(1 + \gamma^{(k,k_\mathrm{s})} \frac{Q}{\delta^{(k,k_\mathrm{s})}}), \tag{6.6}$$

and the total channel capacity of all K_s channels is

$$R^{(k)} = \sum_{k_\mathrm{s}=1}^{K_\mathrm{s}} R^{(k,k_\mathrm{s})} = \sum_{k_\mathrm{s}=1}^{K_\mathrm{s}} \mathrm{ld}(1 + \gamma^{(k,k_\mathrm{s})} \frac{Q}{\delta^{(k,k_\mathrm{s})}}) = \mathrm{ld} \prod_{k_\mathrm{s}=1}^{K_\mathrm{s}} (1 + \gamma^{(k,k_\mathrm{s})} \frac{Q}{\delta^{(k,k_\mathrm{s})}}). \tag{6.7}$$

The idea proposed in this section consists in keeping $\gamma^{(k)}$ of (6.5) at a fixed value and choosing the gains g_{k_s} in (6.1) in such a way that $R^{(k)}$ of (6.7) is maximized. It can be seen from (6.7) that maximizing $R^{(k)}$ is equivalent to maximizing the term $\prod_{k_\mathrm{s}=1}^{K_\mathrm{s}} (1 + \gamma^{(k,k_\mathrm{s})} \frac{Q}{\delta^{(k,k_\mathrm{s})}})$ on the right side of (6.7). According to Lagrange's extreme value theorem [BS80], with Lagrange factor μ and with (6.5) and (6.7) the Lagrange function

$$\mathcal{L} = \prod_{k_\mathrm{s}=1}^{K_\mathrm{s}} (1 + \gamma^{(k,k_\mathrm{s})} \frac{Q}{\delta^{(k,k_\mathrm{s})}}) - \mu \left(\frac{1}{K_\mathrm{s}} \sum_{k_\mathrm{s}=1}^{K_\mathrm{s}} \gamma^{(k,k_\mathrm{s})} - \gamma^{(k)} \right) \tag{6.8}$$

can be formed. By substituting zero in the partial derivation of (6.8) with respect to $\gamma^{(k,k_\mathrm{s})}$,

$$\begin{aligned}
\frac{\partial \mathcal{L}}{\partial \gamma^{(k,k_\mathrm{s})}} &= \prod_{\substack{k_\mathrm{s}'=1 \\ k_\mathrm{s}' \neq k_\mathrm{s}}}^{K_\mathrm{s}} (1 + \gamma^{(k,k_\mathrm{s}')} \frac{Q}{\delta^{(k,k_\mathrm{s}')}}) \frac{\partial}{\partial \gamma^{(k,k_\mathrm{s})}} (1 + \gamma^{(k,k_\mathrm{s})} \frac{Q}{\delta^{(k,k_\mathrm{s})}}) - \frac{\mu}{K_\mathrm{s}} \\
&= \prod_{\substack{k_\mathrm{s}'=1 \\ k_\mathrm{s}' \neq k_\mathrm{s}}}^{K_\mathrm{s}} (1 + \gamma^{(k,k_\mathrm{s}')} \frac{Q}{\delta^{(k,k_\mathrm{s}')}}) \frac{Q}{\delta^{(k,k_\mathrm{s})}} - \frac{\mu}{K_\mathrm{s}} \overset{!}{=} 0
\end{aligned} \tag{6.9}$$

holds. The linear system of equations

$$\begin{aligned}
\gamma^{(k,2)} &= \gamma^{(k,1)} - \frac{\delta^{(k,2)} - \delta^{(k,1)}}{Q}, \\
\gamma^{(k,3)} &= \gamma^{(k,1)} - \frac{\delta^{(k,3)} - \delta^{(k,1)}}{Q}, \\
&\vdots \\
\gamma^{(k,K_\mathrm{s})} &= \gamma^{(k,1)} - \frac{\delta^{(k,K_\mathrm{s})} - \delta^{(k,1)}}{Q}
\end{aligned} \tag{6.10}$$

can be obtained by describing (6.9) in detail. The desired values $\gamma^{(k,k_\mathrm{s})}$, $k_\mathrm{s} = 1 \ldots K_\mathrm{s}$, which maximize $R^{(k)}$ of (6.7) at MS μ_k, can be found by solving the system of equations given by (6.5) and (6.10). For instance, for $K_\mathrm{s} = 2$ we obtain

$$\gamma^{(k,1)} = \gamma^{(k)} + \frac{\delta^{(k,2)} - \delta^{(k,1)}}{2Q}, \qquad \gamma^{(k,2)} = \gamma^{(k)} - \frac{\delta^{(k,2)} - \delta^{(k,1)}}{2Q}. \tag{6.11}$$

In the case $\gamma^{(k)} \gg 1$

$$\gamma^{(k,k_\mathrm{s})} = \gamma^{(k)} \tag{6.12}$$

Tab. 6.1: SNR degradations $\delta^{(1,k_{\mathrm{s}})}$, $k_{\mathrm{s}} = 1\ldots16$, of (4.47) at MS μ_1 sorted in ascending order with respect to their values for one snapshot of the modified 3GPP channel model, see Section 4.6.3

k_{s}	1	2	3	4	5	6	7	8
$\delta^{(1,k_{\mathrm{s}})}$/dB	6.81	7.01	7.04	7.05	7.22	7.57	7.66	7.69
k_{s}	9	10	11	12	13	14	15	16
$\delta^{(1,k_{\mathrm{s}})}$/dB	7.75	7.76	7.85	7.87	8.01	8.08	8.46	9.30

holds for all K_{s} values $\gamma^{(k,k_{\mathrm{s}})}$. The corresponding gains $g_{k_{\mathrm{s}}}$, $k_{\mathrm{s}} = 1\ldots K_{\mathrm{s}}$, can be obtained by resolving (6.1) and substituting the values $\gamma^{(k,k_{\mathrm{s}})}$:

$$g_{k_{\mathrm{s}}} = \frac{\sqrt{2Q\sigma^{(k)2}\gamma^{(k,k_{\mathrm{s}})}}}{|\underline{\mathbf{b}}^{(k,k_{\mathrm{s}})}|}, \ \ k_{\mathrm{s}} = 1\ldots K_{\mathrm{s}}. \tag{6.13}$$

6.3.2 Results

As stated in Section 6.2, in the simulations presented in this section, only one MS, i.e., MS μ_1 is considered and to this MS all $K_{\mathrm{s}} = 16$ CDMA codes are assigned. The different properties of the utilized CDMA codes $\underline{\mathbf{c}}^{(k_{\mathrm{s}})}$ of (4.5) result in different SNR degradations $\delta^{(1,k_{\mathrm{s}})}$ of (4.47) for each of the K_{s} CDMA signals arriving at MS μ_1. For one snapshot of the modified 3GPP channel model, see Section 4.6.3, the SNR degradations $\delta^{(1,k_{\mathrm{s}})}$, $k_{\mathrm{s}} = 1\ldots K_{\mathrm{s}}$, of (4.47) take the values shown in Tab. 6.1, where the subscripts k_{s} are chosen such that $\delta^{(1,k_{\mathrm{s}})}$ increases as k_{s} increases. The difference between the smallest SNR degradation $\delta^{(1,1)}$ and the largest SNR degradation $\delta^{(1,16)}$ amounts to approximately 2.5dB in this case. With the SNR degradations $\delta^{(1,k_{\mathrm{s}})}$, $k_{\mathrm{s}} = 1\ldots16$, of (4.47) shown in Tab. 6.1, the input SNRs $\gamma^{(1,k_{\mathrm{s}})}$, $k_{\mathrm{s}} = 1\ldots16$, of (6.1) maximizing the total channel capacity $R^{(k)}$ of (6.7) can be obtained by solving the system of equations given by (6.5) and (6.10) as explained above. Fig. 6.3 shows the ratio $\gamma^{(1,k_{\mathrm{s}})}/\gamma^{(1)}$ in dB versus k_{s}. The curves in Fig. 6.3 show that $\gamma^{(1,k_{\mathrm{s}})}$ goes down as $\delta^{(1,k_{\mathrm{s}})}$ decreases. However, as already stated, see (6.12), all K_{s} values $\gamma^{(1,k_{\mathrm{s}})}$ approach $\gamma^{(1)}$ for $\gamma^{(1)} \gg 1$.
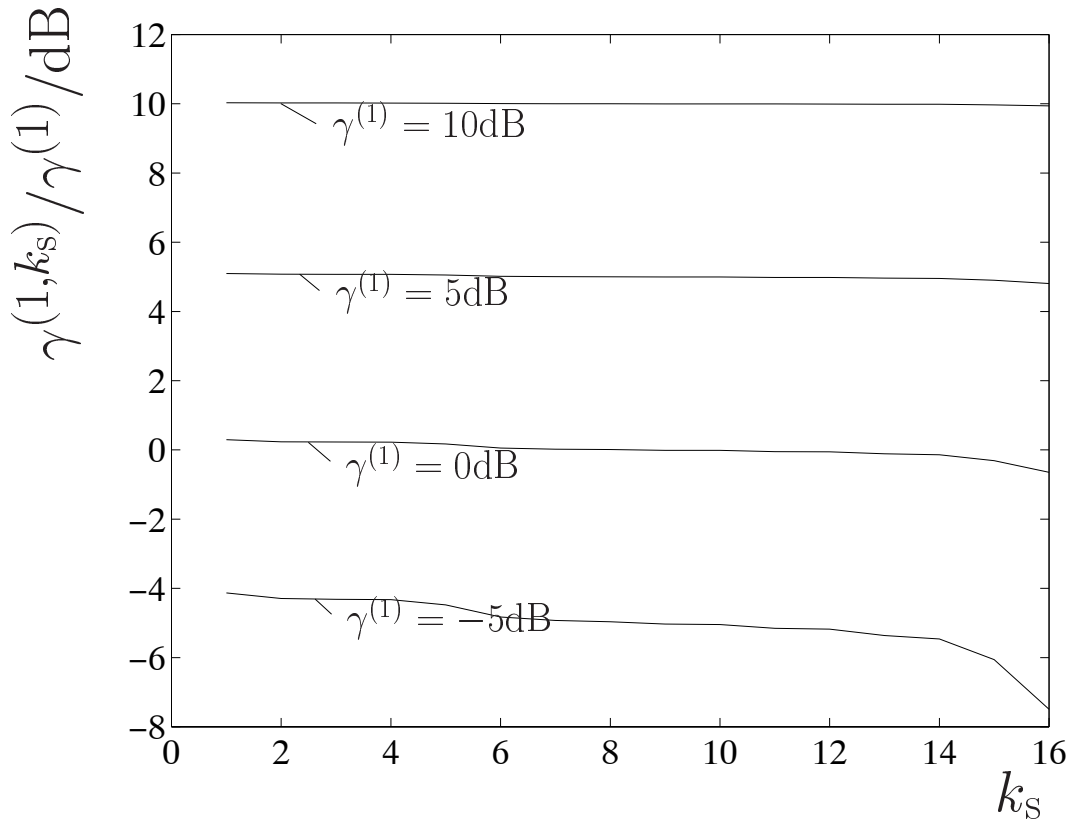
Fig. 6.3: $\gamma^{(1,k_\text{s})}/\gamma^{(1)}$ in dB versus k_s; parameter: $\gamma^{(1)}$

6.4 CDMA-code/channel mismatch

6.4.1 Introduction

As shown in Tab. 6.1, each of the K_s CDMA signals arriving at MS μ_1 attains an individual SNR degradation $\delta^{(1,k_\text{s})}$ of (4.47). This means, even if the gains g_{k_s}, $k_\text{s} = 1 \ldots K_\text{s}$, in the model of Fig. 6.1, are adjusted in order that the input SNRs $\gamma^{(1,k_\text{s})}$, $k_\text{s} = 1 \ldots K_\text{s}$, of (6.1) take the same value, the output SNRs $\gamma_\text{out}^{(1,k_\text{s})}$, $k_\text{s} = 1 \ldots K_\text{s}$, of (6.2) at MS μ_1 differ from one CDMA signal to another CDMA signal. The differences of the SNR degradations $\delta^{(1,k_\text{s})}$ of (4.47) and of the output SNRs $\gamma_\text{out}^{(1,k_\text{s})}$ of (6.2) can be interpreted as a mismatch between the CDMA codes $\underline{\mathbf{c}}^{(k_\text{s})}$, $k_\text{s} = 1 \ldots K_\text{s}$, of (4.5) and the signal specific channel impulse responses $\underline{\mathbf{h}}^{(1,k_\text{s})}$, $k_\text{s} = 1 \ldots K_\text{s}$, of (4.9). As already stated in Section 1.3, this mismatch is termed CDMA-code/channel mismatch [Pap00]. In this section, the SNR degradations $\delta_i^{(k)}$, $i = 1 \ldots K_\text{s}N$, $k = 1 \ldots K$, of (4.46) under consideration of both single- and multi-direction channel models are studied.

6.4.2 SNR degradation under consideration of single-direction channel models

As stated in Section 4.4, the total system matrix $\underline{\mathbf{A}}^{(k)}$, $k = 1 \ldots K$, of (4.21) depends on the choice of the antenna weight vectors $\underline{\mathbf{w}}^{(k_s)}$ of (4.7). Consequently, the covariance matrix

$$\underline{\mathbf{A}}^{(k)^*\mathrm{T}} \underline{\mathbf{A}}^{(k)} = \begin{pmatrix} \underline{\mathbf{A}}^{(k,1)^*\mathrm{T}} \underline{\mathbf{A}}^{(k,1)} & \cdots & \underline{\mathbf{A}}^{(k,1)^*\mathrm{T}} \underline{\mathbf{A}}^{(k,K_s)} \\ \vdots & \vdots & \vdots \\ \underline{\mathbf{A}}^{(k,K_s)^*\mathrm{T}} \underline{\mathbf{A}}^{(k,1)} & \cdots & \underline{\mathbf{A}}^{(k,K_s)^*\mathrm{T}} \underline{\mathbf{A}}^{(k,K_s)} \end{pmatrix} \tag{6.14}$$

and the corresponding SNR degradations $\delta_i^{(k)}$, $i = 1 \ldots K_s N$, of (4.46) also depend on $\underline{\mathbf{w}}^{(k_s)}$. In the following without loss of generality it is assumed that there are only two MSs, μ_1 and μ_2, in an isolated cell. MS μ_1 is served by CDMA code $\underline{\mathbf{c}}^{(1)}$ and MS μ_2 by CDMA code $\underline{\mathbf{c}}^{(2)}$. The locations of the two MSs μ_1 and μ_2 are characterized by the azimuth angles $\varphi^{(1)}$ and $\varphi^{(2)}$, respectively, related to RD as shown in Fig. 2.2. Since the single-direction channel model is considered, the antenna weight vectors $\underline{\mathbf{w}}^{(k_s)}$, $k_s = 1$, 2, of (4.7) are simply chosen as the complex conjugate of the steering vector $\mathbf{a}^{(k)}$, $k = 1 \ldots K$, of (4.2):

$$\underline{\mathbf{w}}^{(k_s)} = \mathbf{a}^{(k)^*}, \ k_s = k = 1, \ 2. \tag{6.15}$$

Following (6.15), we obtain

$$\sum_{k_a=1}^{K_a} \underline{w}_{k_a}^{(2)} \underline{a}_{k_a}^{(1)} = \sum_{k_a=1}^{K_a} \underline{a}_{k_a}^{(2)^*} \underline{a}_{k_a}^{(1)} = \underline{r} \tag{6.16}$$

and

$$\sum_{k_a=1}^{K_a} \underline{w}_{k_a}^{(1)} \underline{a}_{k_a}^{(1)} = \sum_{k_a=1}^{K_a} \underline{a}_{k_a}^{(1)^*} \underline{a}_{k_a}^{(1)}. \tag{6.17}$$

Let us assume that

$$\underline{a}_{k_a}^{(1)^*} \underline{a}_{k_a}^{(1)} = 1, \ k_a = 1 \ldots K_a, \tag{6.18}$$

holds, (6.17) becomes

$$\sum_{k_a=1}^{K_a} \underline{w}_{k_a}^{(1)} \underline{a}_{k_a}^{(1)} = K_a. \tag{6.19}$$

According to (4.31), the total system matrix

$$\underline{\mathbf{A}}_1^{(1)} = \begin{pmatrix} \tilde{\underline{\mathbf{H}}}^{(1,1)} \tilde{\underline{\mathbf{C}}}^{(1)} & \tilde{\underline{\mathbf{H}}}^{(1,1)} \tilde{\underline{\mathbf{C}}}^{(2)} \end{pmatrix} \tag{6.20}$$

valid for MS μ_1 when using a single omnidirectional transmit antenna at the BS is formed with the subscript 1 on the left side of (6.20) denoting the number K_a of transmit antenna elements. Similarly, the total system matrix

$$\mathbf{\underline{A}}_{K_a}^{(1)} = \sum_{k_a=1}^{K_a} \left(\ \mathbf{\underline{\tilde{H}}}^{(1,1)} \mathbf{\underline{\tilde{C}}}^{(1)} \underline{w}_{k_a}^{(1)} \underline{a}_{k_a}^{(1)} \quad \mathbf{\underline{\tilde{H}}}^{(1,1)} \mathbf{\underline{\tilde{C}}}^{(2)} \underline{w}_{k_a}^{(2)} \underline{a}_{k_a}^{(1)} \ \right) \tag{6.21}$$

valid for MS μ_1 when using adaptive transmit antennas with K_a transmit antenna elements at the BS is given. Substituting (6.16) and (6.17) into (6.21) yields

$$\mathbf{\underline{A}}_{K_a}^{(1)} = \left(\ K_a \mathbf{\underline{\tilde{H}}}^{(1,1)} \mathbf{\underline{\tilde{C}}}^{(1)} \quad r \mathbf{\underline{\tilde{H}}}^{(1,1)} \mathbf{\underline{\tilde{C}}}^{(2)} \ \right). \tag{6.22}$$

According to (4.46), in order to determine the SNR degradations $\delta_i^{(1)}$, $i = 1 \ldots K_s N$, of (4.46) valid for MS μ_1 the covariance matrices $\mathbf{\underline{A}}_1^{(1)*T} \mathbf{\underline{A}}_1^{(1)}$ and $\mathbf{\underline{A}}_{K_a}^{(1)*T} \mathbf{\underline{A}}_{K_a}^{(1)}$, as well as the inverse matrices $(\mathbf{\underline{A}}_1^{(1)*T} \mathbf{\underline{A}}_1^{(1)})^{-1}$ and $(\mathbf{\underline{A}}_{K_a}^{(1)*T} \mathbf{\underline{A}}_{K_a}^{(1)})^{-1}$ must be calculated. Following (6.20) and (6.21), in the case of $K_a = 1$ the covariance matrix

$$
\begin{aligned}
\mathbf{\underline{A}}_1^{(1)*T} \mathbf{\underline{A}}_1^{(1)} &= \begin{pmatrix} \mathbf{\underline{\tilde{C}}}^{(1)*T} \mathbf{\underline{\tilde{H}}}^{(1,1)*T} \\ \mathbf{\underline{\tilde{C}}}^{(2)*T} \mathbf{\underline{\tilde{H}}}^{(1,1)*T} \end{pmatrix} \begin{pmatrix} \mathbf{\underline{\tilde{H}}}^{(1,1)} \mathbf{\underline{\tilde{C}}}^{(1)} & \mathbf{\underline{\tilde{H}}}^{(1,1)} \mathbf{\underline{\tilde{C}}}^{(2)} \end{pmatrix} \\[2em]
&= \begin{pmatrix} \underbrace{\mathbf{\underline{\tilde{C}}}^{(1)*T} \mathbf{\underline{\tilde{H}}}^{(1,1)*T} \mathbf{\underline{\tilde{H}}}^{(1,1)} \mathbf{\underline{\tilde{C}}}^{(1)}}_{\mathbf{\underline{F}}_1} & \underbrace{\mathbf{\underline{\tilde{C}}}^{(1)*T} \mathbf{\underline{\tilde{H}}}^{(1,1)*T} \mathbf{\underline{\tilde{H}}}^{(1,1)} \mathbf{\underline{\tilde{C}}}^{(2)}}_{\mathbf{\underline{F}}_2} \\ \underbrace{\mathbf{\underline{\tilde{C}}}^{(2)*T} \mathbf{\underline{\tilde{H}}}^{(1,1)*T} \mathbf{\underline{\tilde{H}}}^{(1,1)} \mathbf{\underline{\tilde{C}}}^{(1)}}_{\mathbf{\underline{F}}_2^{*T}} & \underbrace{\mathbf{\underline{\tilde{C}}}^{(2)*T} \mathbf{\underline{\tilde{H}}}^{(1,1)*T} \mathbf{\underline{\tilde{H}}}^{(1,1)} \mathbf{\underline{\tilde{C}}}^{(2)}}_{\mathbf{\underline{F}}_3} \end{pmatrix} \\[2em]
&= \begin{pmatrix} \mathbf{\underline{F}}_1 & \mathbf{\underline{F}}_2 \\ \mathbf{\underline{F}}_2^{*T} & \mathbf{\underline{F}}_3 \end{pmatrix}
\end{aligned} \tag{6.23}
$$

and in the case of using adaptive transmit antennas with K_a transmit antenna elements the covariance matrix

$$
\begin{aligned}
\mathbf{\underline{A}}_{K_a}^{(1)*T} \mathbf{\underline{A}}_{K_a}^{(1)} &= \begin{pmatrix} K_a \mathbf{\underline{\tilde{C}}}^{(1)*T} \mathbf{\underline{\tilde{H}}}^{(1,1)*T} \\ r^* \mathbf{\underline{\tilde{C}}}^{(2)*T} \mathbf{\underline{\tilde{H}}}^{(1,1)*T} \end{pmatrix} \begin{pmatrix} K_a \mathbf{\underline{\tilde{H}}}^{(1,1)} \mathbf{\underline{\tilde{C}}}^{(1)} & r \mathbf{\underline{\tilde{H}}}^{(1,1)} \mathbf{\underline{\tilde{C}}}^{(2)} \end{pmatrix} \\[1em]
&= \begin{pmatrix} K_a^2 \mathbf{\underline{F}}_1 & r K_a \mathbf{\underline{F}}_2 \\ r^* K_a \mathbf{\underline{F}}_2^{*T} & |r|^2 \mathbf{\underline{F}}_3 \end{pmatrix}
\end{aligned} \tag{6.24}
$$

can be formed. The inverse matrices $(\mathbf{\underline{A}}_1^{(1)*T} \mathbf{\underline{A}}_1^{(1)})^{-1}$ of the covariance matrix $\mathbf{\underline{A}}_1^{(1)*T} \mathbf{\underline{A}}_1^{(1)}$ of (6.23) and $(\mathbf{\underline{A}}_{K_a}^{(1)*T} \mathbf{\underline{A}}_{K_a}^{(1)})^{-1}$ of the covariance matrix $\mathbf{\underline{A}}_{K_a}^{(1)*T} \mathbf{\underline{A}}_{K_a}^{(1)}$ of (6.24) can be obtained by using the partitioned matrix inversion lemma [Wha71]. Let the matrices $\underline{\Lambda}_1^{-1}$, $\underline{\Gamma}_1^{-1}$, $\underline{\Theta}_1^{-1}$ and $\underline{\Delta}_1^{-1}$ be the partitioned matrices of $(\mathbf{\underline{A}}_1^{(1)*T} \mathbf{\underline{A}}_1^{(1)})^{-1}$, the inverse matrix

$$(\mathbf{\underline{A}}_1^{(1)*T} \mathbf{\underline{A}}_1^{(1)})^{-1} = \begin{pmatrix} \underline{\Lambda}_1^{-1} & \underline{\Gamma}_1^{-1} \\ \underline{\Theta}_1^{-1} & \underline{\Delta}_1^{-1} \end{pmatrix} \tag{6.25}$$

of the covariance matrix $\underline{\mathbf{A}}_1^{(1)*\mathrm{T}}\underline{\mathbf{A}}_1^{(1)}$ of (6.23) is given, where

$$\underline{\Lambda}_1 = \underline{\mathbf{F}}_1 - \underline{\mathbf{F}}_2\underline{\mathbf{F}}_3^{-1}\underline{\mathbf{F}}_2^{*\mathrm{T}} \tag{6.26}$$

and

$$\underline{\Delta}_1 = \underline{\mathbf{F}}_3 - \underline{\mathbf{F}}_2^{*\mathrm{T}}\underline{\mathbf{F}}_1^{-1}\underline{\mathbf{F}}_2 \tag{6.27}$$

as explained in [Wha71]. Analogously, let the matrices $\underline{\Lambda}_{K_\mathrm{a}}^{-1}$, $\underline{\Gamma}_{K_\mathrm{a}}^{-1}$, $\underline{\Theta}_{K_\mathrm{a}}^{-1}$ and $\underline{\Delta}_{K_\mathrm{a}}^{-1}$ be the partitioned matrices of $(\underline{\mathbf{A}}_{K_\mathrm{a}}^{(1)*\mathrm{T}}\underline{\mathbf{A}}_{K_\mathrm{a}}^{(1)})^{-1}$, the inverse matrix

$$(\underline{\mathbf{A}}_{K_\mathrm{a}}^{(1)*\mathrm{T}}\underline{\mathbf{A}}_{K_\mathrm{a}}^{(1)})^{-1} = \begin{pmatrix} \underline{\Lambda}_{K_\mathrm{a}}^{-1} & \underline{\Gamma}_{K_\mathrm{a}}^{-1} \\ \underline{\Theta}_{K_\mathrm{a}}^{-1} & \underline{\Delta}_{K_\mathrm{a}}^{-1} \end{pmatrix} \tag{6.28}$$

of the covariance matrix $\underline{\mathbf{A}}_{K_\mathrm{a}}^{(1)*\mathrm{T}}\underline{\mathbf{A}}_{K_\mathrm{a}}^{(1)}$ of (6.24) is obtained, where

$$\begin{aligned} \underline{\Lambda}_{K_\mathrm{a}} &= K_\mathrm{a}^2\underline{\mathbf{F}}_1 - \underline{r}K_\mathrm{a}\underline{\mathbf{F}}_2(|\underline{r}|^2\underline{\mathbf{F}}_3)^{-1}\underline{r}^*K_\mathrm{a}\underline{\mathbf{F}}_2^{*\mathrm{T}} \\ &= K_\mathrm{a}^2(\underline{\mathbf{F}}_1 - \underline{\mathbf{F}}_2\underline{\mathbf{F}}_3^{-1}\underline{\mathbf{F}}_2^{*\mathrm{T}}) \\ &= K_\mathrm{a}^2\underline{\Lambda}_1 \end{aligned} \tag{6.29}$$

and

$$\begin{aligned} \underline{\Delta}_{K_\mathrm{a}} &= |\underline{r}|^2\underline{\mathbf{F}}_3 - \underline{r}^*K_\mathrm{a}\underline{\mathbf{F}}_2^{*\mathrm{T}}\frac{1}{K_\mathrm{a}^2}\underline{\mathbf{F}}_1^{-1}\underline{r}K_\mathrm{a}\underline{\mathbf{F}}_2 \\ &= |\underline{r}|^2(\underline{\mathbf{F}}_3 - \underline{\mathbf{F}}_2^{*\mathrm{T}}\underline{\mathbf{F}}_1^{-1}\underline{\mathbf{F}}_2) \\ &= |\underline{r}|^2\underline{\Delta}_1 \end{aligned} \tag{6.30}$$

as shown in [Wha71]. According to (4.46) the SNR degradations $\delta_{1,i}^{(1)}$, $i = 1\ldots K_\mathrm{s}N$, valid for MS μ_1 when using a single omnidirectional transmit antenna at the BS and $\delta_{K_\mathrm{a},i}^{(1)}$, $i = 1\ldots K_\mathrm{s}N$, valid for MS μ_1 when using adaptive transmit antennas with K_a transmit antenna elements at the BS can be obtained from (6.23), (6.24), (6.29) and (6.30), respectively. The results are:

- The SNR degradation

$$\begin{aligned} \delta_{1,i}^{(1)} &= (\underline{\mathbf{A}}_1^{(1)*\mathrm{T}}\underline{\mathbf{A}}_1^{(1)})_{i,i}(\underline{\mathbf{A}}_1^{(1)*\mathrm{T}}\underline{\mathbf{A}}_1^{(1)})_{i,i}^{-1} \\ &= \begin{cases} (\underline{\mathbf{F}}_1)_{i,i}(\underline{\Lambda}_1^{-1})_{i,i} & i = 1\ldots\dfrac{K_\mathrm{s}N}{2}, \\ (\underline{\mathbf{F}}_3)_{i-\frac{K_\mathrm{s}N}{2},i-\frac{K_\mathrm{s}N}{2}}(\underline{\Delta}_1^{-1})_{i-\frac{K_\mathrm{s}N}{2},i-\frac{K_\mathrm{s}N}{2}} & i = \dfrac{K_\mathrm{s}N}{2}+1\ldots K_\mathrm{s}N, \end{cases} \end{aligned} \tag{6.31}$$

is valid for MS μ_1 when using a single omnidirectional transmit antenna at the BS.

- The SNR degradation

$$
\begin{aligned}
\delta_{K_a,i}^{(1)} &= (\underline{\mathbf{A}}_{K_a}^{(1)^{*\mathrm{T}}}\underline{\mathbf{A}}_{K_a}^{(1)})_{i,i}(\underline{\mathbf{A}}_{K_a}^{(1)^{*\mathrm{T}}}\underline{\mathbf{A}}_{K_a}^{(1)})_{i,i}^{-1} \\
&= \begin{cases} (K_a^2\underline{\mathbf{F}}_1)_{i,i}(\underline{\Lambda}_{K_a}^{-1})_{i,i} \\ (|\underline{r}|^2\underline{\mathbf{F}}_3)_{i,i}(\underline{\Lambda}_{K_a}^{-1})_{i-\frac{K_s N}{2},i-\frac{K_s N}{2}} \end{cases} \\
&= \begin{cases} K_a^2(\underline{\mathbf{F}}_1)_{i,i}\frac{1}{K_a^2}(\underline{\Lambda}_1^{-1})_{i,i} \\ |\underline{r}|^2(\underline{\mathbf{F}}_3)_{i,i}\frac{1}{|\underline{r}|^2}(\underline{\Lambda}_{K_a}^{-1})_{i-\frac{K_s N}{2},i-\frac{K_s N}{2}} \end{cases} \\
&= \begin{cases} (\underline{\mathbf{F}}_1)_{i,i}(\underline{\Lambda}_1^{-1})_{i,i} & i = 1\dots\frac{K_s N}{2}, \\ (\underline{\mathbf{F}}_3)_{i-\frac{K_s N}{2},i-\frac{K_s N}{2}}(\underline{\Lambda}_1^{-1})_{i-\frac{K_s N}{2},i-\frac{K_s N}{2}} & i = \frac{K_s N}{2}+1\dots K_s N, \end{cases}
\end{aligned}
\tag{6.32}
$$

is valid for MS μ_1 when using adaptive transmit antennas with K_a transmit antenna elements at the BS.

Comparing (6.31) with (6.32), we have

$$
\delta_{1,i}^{(1)} = \delta_{K_a,i}^{(1)}, \ i = 1\dots K_s N.
\tag{6.33}
$$

(6.33) indicates that the SNR degradation $\delta_i^{(k)}$, $k = 1\dots K$, $i = 1\dots K_s N$, of (4.46) is independent of the number K_a of transmit antenna elements, if single-direction channel models are taken into consideration for the data transmission between the BS and the MSs.

6.4.3 SNR degradation under consideration of multi-direction channel models

In Section 6.4.2, it is shown that the SNR degradations $\delta_i^{(k)}$, $i = 1\dots K_s N$, of (4.46) are independent of K_a for single-direction channel models. Unfortunately, no closed analytical way is available to determine whether the SNR degradations $\delta_i^{(k)}$, $i = 1\dots K_s N$, of (4.46) are also independent of K_a for multi-direction channel models. In what follows the SNR degradations $\delta^{(k,k_s)}$, $k_s = 1\dots16$, of (4.47) are simulated with $K_a = 1$ and $K_a = 4$ for one snapshot of the scattering point based channel model, see Section 2.3.2. The SNR degradations $\delta^{(1,k_s)}$, $k_s = 1\dots16$, of (4.47) are shown in Tab. 6.2. It can be seen that the SNR degradations $\delta^{(1,k_s)}$, $k_s = 1\dots16$, for $K_a = 4$ are not equal to those for $K_a = 1$.

In contrast to single-direction channel models, in multi-direction channel models the SNR degradations $\delta^{(k,k_s)}$ of (4.47) generally depend on the number K_a of transmit antenna elements.

Tab. 6.2: SNR degradations $\delta^{(1,k_s)}$ of (4.47) with $K_a = 1$ and $K_a = 4$ for one snapshot of the scattering point based channel model, see Section 2.3.2; $K = 1$

k_s	$\delta^{(1,k_s)}$/dB							
k_s	1	2	3	4	5	6	7	8
$K_a = 1$	9.09	9.91	8.17	7.10	7.23	9.48	7.40	7.99
$K_a = 4$	12.65	12.86	11.07	12.57	13.69	13.42	12.37	12.04
k_s	9	10	11	12	13	14	15	16
$K_a = 1$	10.62	11.14	10.73	6.59	9.34	10.45	8.29	11.02
$K_a = 4$	14.91	15.03	14.81	10.17	13.06	14.69	12.12	12.19

6.5 Concepts for overcoming the CDMA-code/channel mismatch

6.5.1 CDMA code interleaving

As stated in Section 1.4, in order to mitigate the impact of the CDMA-code/channel mismatch on the system performance, CDMA code interleaving is considered, which is treated in this section. In addition, two different power control rationales for improving the system performance in the presence of CDMA-code/channel mismatch are studied in Section 6.5.2.

In order to clarify the CDMA code interleaving concept in connection with CDMA code pooling, let us start with the consideration of CDMA code pooling without CDMA code interleaving. Suppose that the total data vector $\underline{\mathbf{d}}$ containing K_s partial data vectors $\underline{\mathbf{d}}^{(k_s)}$, $k_s = 1 \ldots K_s$, see Tab. 4.1, will be transmitted from the BS to MS μ_1. If CDMA code interleaving is not considered, each of the K_s partial data vectors $\underline{\mathbf{d}}^{(k_s)}$ of dimension N is row wise read into a register at the transmitter as shown in Fig. 6.4. The register in Fig. 6.4 has K_s rows and N columns. Each of the K_s rows contains a partial data vector $\underline{\mathbf{d}}^{(k_s)}$, $k_s = 1 \ldots K_s$. The coded data symbols $\underline{d}_n^{(k_s)}$, $n = 1 \ldots N$, $k_s = 1 \ldots K_s$, in each of the K_s rows of the register will be spectrally spread by a corresponding CDMA code $\underline{\mathbf{c}}^{(k_s)}$, $k_s = 1 \ldots K_s$, of (4.5) and transmitted to MS μ_1. At MS μ_1, JD is performed with the received data vector $\underline{\mathbf{e}}^{(1)}$ of (4.22), see Fig. 6.5. Each of the K_s estimated partial data vectors $\underline{\hat{\mathbf{d}}}^{(k_s)}$ of (4.44) is decoded by an individual FEC decoder. Therefore, K_s coded BERs $P_b^{(1,k_s)}$, $k_s = 1 \ldots K_s$, of (4.85) are obtained. Finally, we have the coded BER $\bar{P}_b^{(1)}$ of (4.86) averaged over all K_s CDMA signals at MS μ_1.
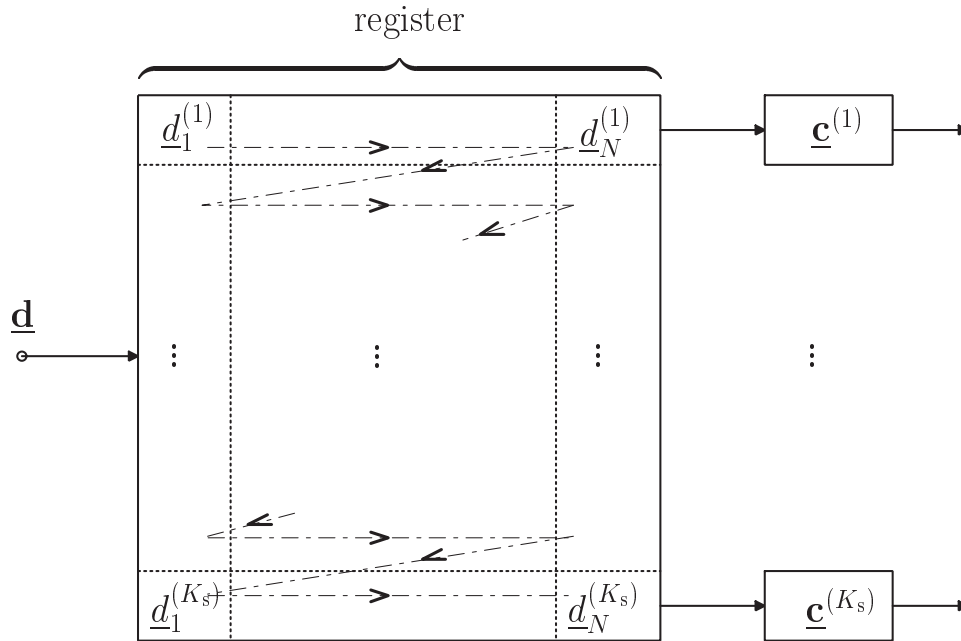
Fig. 6.4: Block diagram of the transmitter when utilizing CDMA code pooling without CDMA code interleaving
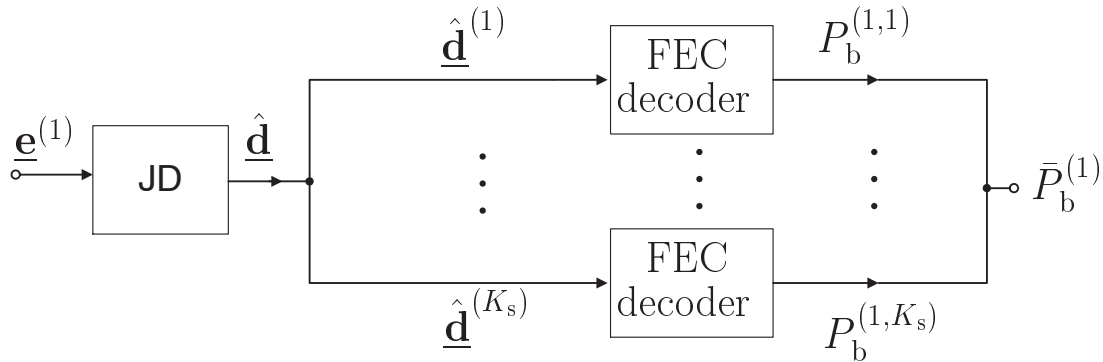
Fig. 6.5: Block diagram of the receiver when utilizing CDMA code pooling without CDMA code interleaving

On the contrary, in the case of utilizing CDMA code interleaving in connection with CDMA code pooling, each of the K_s partial data vectors $\underline{\mathbf{d}}^{(k_s)}$ is column wise read into the register at the transmitter, see Fig. 6.6. The coded data symbols in each of the K_s rows will be spectrally spread by a corresponding CDMA code $\underline{\mathbf{c}}^{(k_s)}$, $k_s = 1 \ldots K_s$, of (4.5) and transmitted to MS μ_1. After performing JD and CDMA code deinterleaving at MS μ_1, the total estimated data vector $\hat{\underline{\mathbf{d}}}$ will be decoded by only one FEC decoder as shown in Fig. 6.7. The coded BER $\bar{P}_b^{(1)}$ of (4.86) averaged over all K_s CDMA signals at MS μ_1 for CDMA code pooling with and without CDMA code interleaving will be compared in Section 6.5.3.
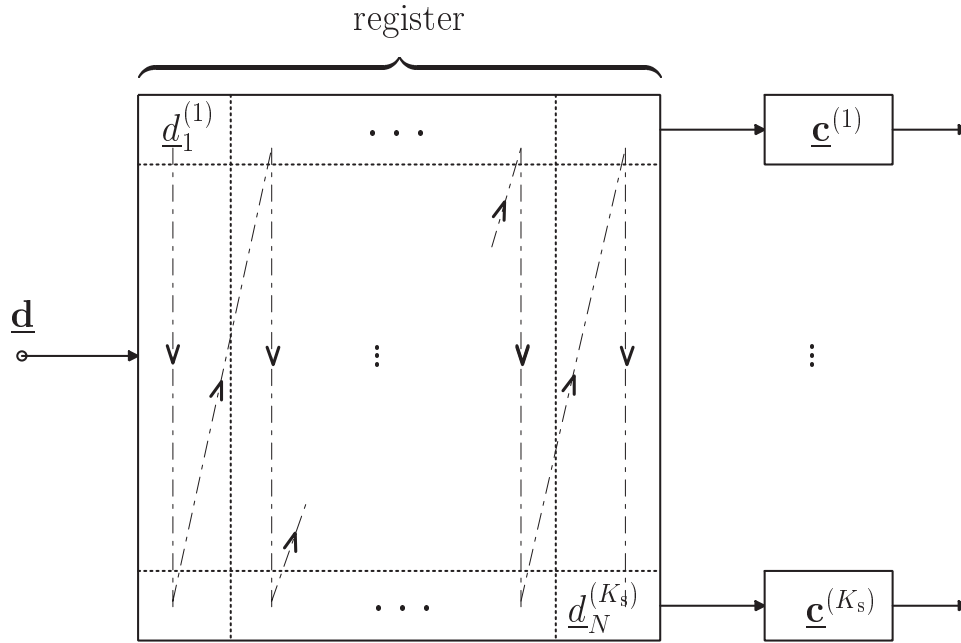
Fig. 6.6: Block diagram of the transmitter when utilizing CDMA code pooling with CDMA code interleaving
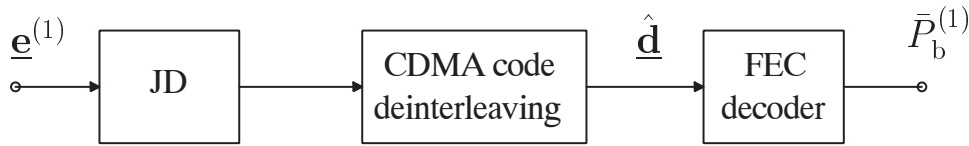
Fig. 6.7: Block diagram of the receiver when utilizing CDMA code pooling with CDMA code interleaving

6.5.2 Power control rationales

Utilizing CDMA code interleaving in connection with CDMA code pooling to mitigate the impact of the CDMA-code/channel mismatch on the system performance is introduced in Section 6.5.1. To the same purpose, two power control rationales are discussed in this section.

For a given average input SNR $\gamma^{(k)}$ of (6.5) at MS μ_k, two different power control rationales can be followed by choosing the gains g_{k_s}, $k_s = 1 \ldots K_s$, see Fig. 6.1, correspondingly:

1. The input SNRs $\gamma^{(k,k_s)}$, $k_s = 1 \ldots K_s$, of (6.1) are made equal for all K_s CDMA signals, that is,

$$\gamma^{(k,k_s)} = \gamma^{(k)}, \ k_s = 1 \ldots K_s. \tag{6.34}$$

2. The output SNRs $\gamma_{\text{out}}^{(k,k_\text{s})}$, $k_\text{s} = 1 \ldots K_\text{s}$, of (6.2) are made equal for all K_s CDMA signals, that is,

$$\gamma_{\text{out}}^{(k,k_\text{s})} = \gamma_{\text{out}}^{(k)}, \quad k_\text{s} = 1 \ldots K_\text{s}. \tag{6.35}$$

In the case of power control rationale 1, following (6.1), (6.5) and (6.34), the gains become

$$g_{k_\text{s}} = \frac{\sigma^{(k)}}{|\underline{\mathbf{b}}^{(k,k_\text{s})}|} \sqrt{2Q\gamma^{(k)}}, \quad k_\text{s} = 1 \ldots K_\text{s}. \tag{6.36}$$

In the case of power control rationale 2, following (6.2), (6.5) and (6.35), the gains become

$$g_{k_\text{s}} = \frac{\sigma^{(k)}}{|\underline{\mathbf{b}}^{(k,k_\text{s})}|} \sqrt{2\delta^{(k,k_\text{s})}\gamma_{\text{out}}^{(k)}}, \quad k_\text{s} = 1 \ldots K_\text{s}. \tag{6.37}$$

According to (6.5), (6.36) and (6.37), the knowledge of the variance $\sigma^{(k)^2}$ of the real and imaginary parts of the intercell interference characterized by $\underline{\mathbf{n}}^{(k)}$, see Tab. 4.1, at MS μ_k and the composite channel impulse responses $\underline{\mathbf{b}}^{(k,k_\text{s})}$, $k_\text{s} = 1 \ldots K_\text{s}$, of (4.19) are necessary for determining the gains g_{k_s} for both power control rationales. Moreover, power control rationale 2 additionally needs the knowledge of the SNR degradations $\delta^{(k,k_\text{s})}$, $k_\text{s} = 1 \ldots K_\text{s}$, of (4.47). Therefore, the implementation complexity of power control rationale 2 is higher than that of power control rationale 1.

6.5.3   Simulation results

The average coded BERs $\bar{P}_\text{b}^{(1)}$ of (4.86) versus the average input SNR $\gamma^{(1)}$ of (6.5) at MS μ_k for the two power control rationales 1 and 2 and CDMA code interleaving are shown in Figs. 6.8 to 6.11. In the simulations, when a single omnidirectional transmit antenna is utilized at the BS, only one MS, i.e., MS μ_1 is considered. To this MS $K_\text{s} = 16$ CDMA codes are assigned. For the case of using adaptive transmit antennas at the BS, two MSs μ_1 and μ_2 are considered. To each of the two MSs μ_1 and μ_2 eight CDMA codes are assigned. Both the modified 3GPP channel model, see Section 2.3.1 and the scattering point based directional channel model, see 2.3.2, are considered.

According to the curves shown in Figs. 6.8 to 6.11, the average coded BER $\bar{P}_\text{b}^{(1)}$ of (4.86) for the case of CDMA code interleaving is better than that obtained when using power control rationale 2, whose performance is better than that obtained when using power control rationale 1. To get a given $\bar{P}_\text{b}^{(1)}$ of (4.86), the reduction of the required $\gamma^{(1)}$ of (6.5) allowed by CDMA code interleaving instead of using power control rationale 1 is getting smaller when adaptive transmit antennas are used. This is because that the available number of the CDMA codes for performing CDMA code interleaving in the case of using adaptive transmit antennas becomes smaller.
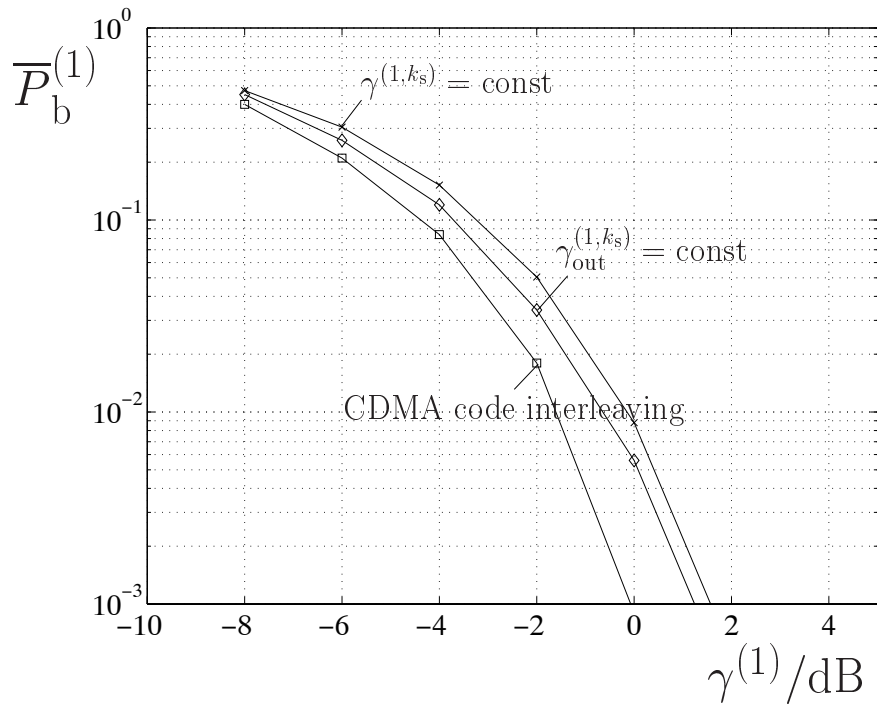
Fig. 6.8: $\bar{P}_b^{(1)}$ of (4.86) versus $\gamma^{(1)}$ of (6.5); $K_a = 1$, $K = 1$, $K_s = 16$, $\beta = 10°$, $\Delta\varphi = 20°$, modified 3GPP channel model
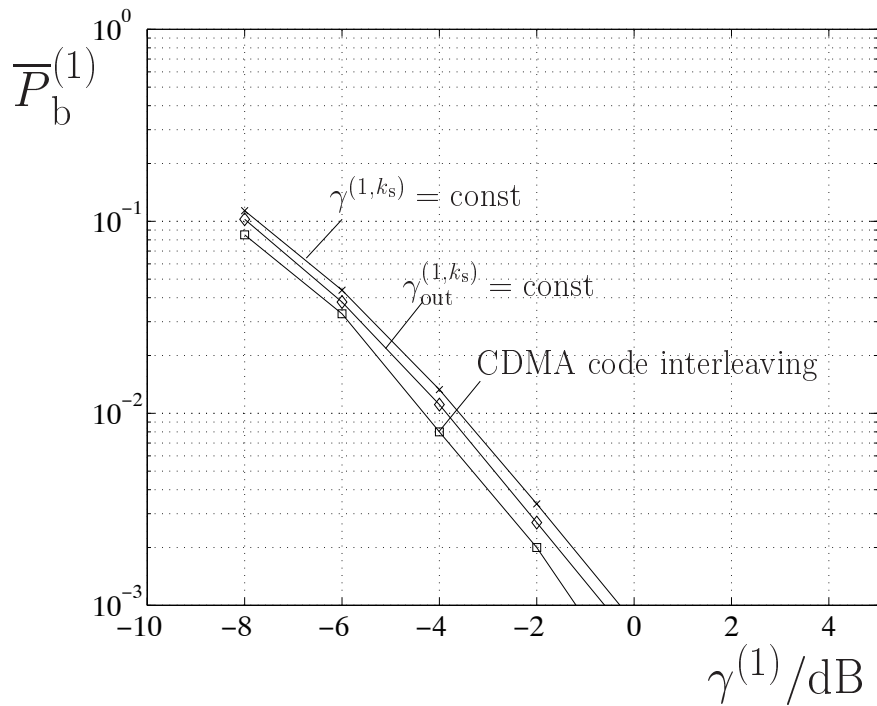
Fig. 6.9: $\bar{P}_b^{(1)}$ of (4.86) versus $\gamma^{(1)}$ of (6.5); $K_a = 4$, $K = 2$, $K_s = 16$, $\beta = 10°$, $\Delta\varphi = 20°$, modified 3GPP channel model
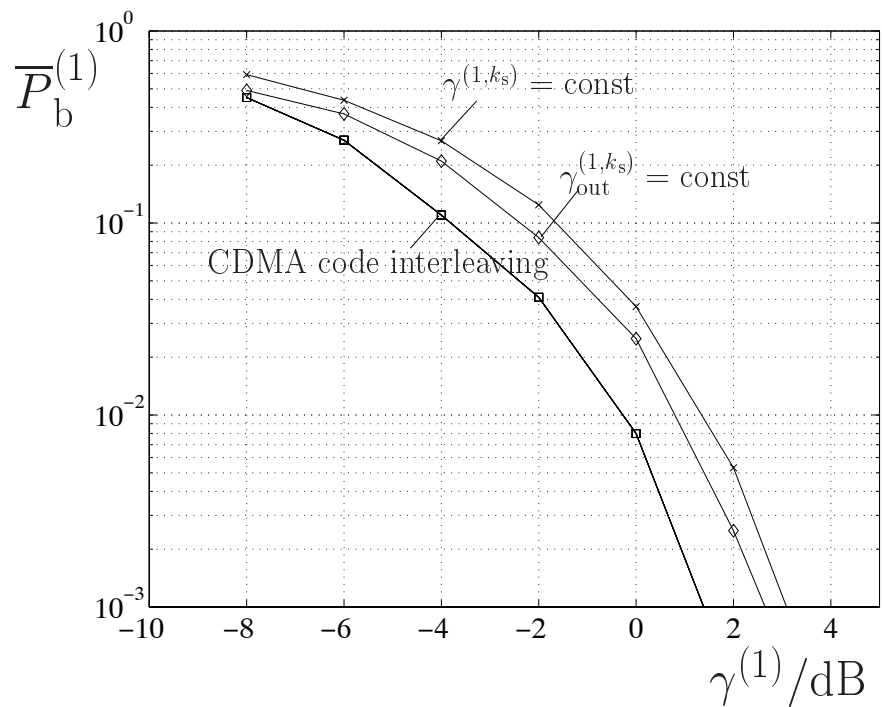
Fig. 6.10: $\bar{P}_{\mathrm{b}}^{(1)}$ of (4.86) versus $\gamma^{(1)}$ of (6.5); $K_{\mathrm{a}} = 1$, $K = 1$, $K_{\mathrm{s}} = 16$, $\Delta\varphi = 30°$, scattering point based channel model
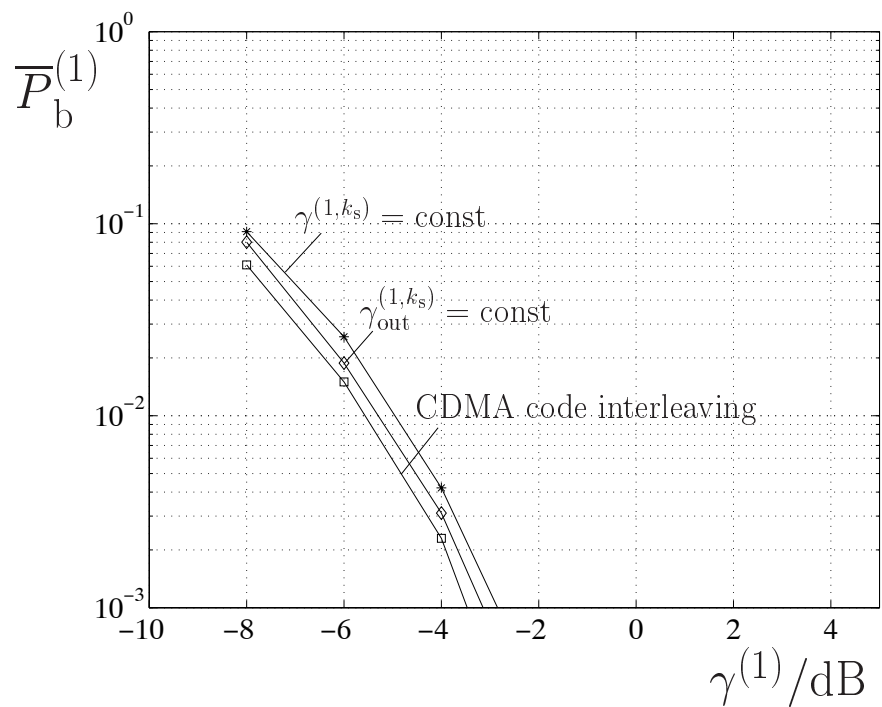
Fig. 6.11: $\bar{P}_{\mathrm{b}}^{(1)}$ of (4.86) versus $\gamma^{(1)}$ of (6.5); $K_{\mathrm{a}} = 8$, $K = 2$, $K_{\mathrm{s}} = 16$, $\Delta\varphi = 30°$, scattering point based channel model

6.6 Adaptive channel coding

6.6.1 Introduction

Adaptive channel coding schemes are of interest for improving the performance of data transmission over mobile radio channels with time variant SNR due to fading and time variant interference. As already stated in Section 1.4, in the case of FEC coded transmission the information data rate can be adapted by properly choosing the modulation scheme and/or the FEC channel coding rate. In this thesis it is assumed that the modulation scheme is always QPSK and the FEC channel coding rate R_c is varying. The aim of the adaptive channel coding scheme discussed in this section is not to describe a channel coding with variable coding rate R_c, as for example, punctured convolutional coding. For contributions to channel coding with variable coding rate R_c see [CCG79, YKH84, Yas83, Hag88]. In this section we assume that a set of channel codes with different coding rates R_c is already available. The question to be answered is which coding rate R_c should be chosen according to the channel quality in terms of $\gamma_{\text{out}}^{(k,k_s)}$, $k = 1 \ldots K$, $k_s = 1 \ldots K_s$, of (6.2) in order to achieve the required $P_b^{(k,k_s)}$ of (4.85) or the lowest possible $\bar{P}_b^{(k)}$ of (4.86). In what follows the required $P_b^{(k,k_s)}$ is termed $P_{b,\text{des}}$. Section 6.6.2 focuses on the channel coding rate adaptation for single-channel transmission models to achieve the required $P_{b,\text{des}}$. The channel coding rate adaptation for multi-channel transmission models proposed in Section 6.2 is discussed in Section 6.6.3 to achieve the lowest possible $\bar{P}_b^{(k)}$ of (4.86).

6.6.2 Channel coding rate adaptation for single-channel transmission

Suppose that convolutional encoders with different coding rates R_c equal to 1/4, 1/3, 1/2, 2/3 and 3/4 are available in the adaptive channel coding scheme. These five coding rates constitute the set

$$\mathbb{R}_c = \{R_{c,1}\ R_{c,2}\ R_{c,3}\ R_{c,4}\ R_{c,5}\} = \{1/4\ 1/3\ 1/2\ 2/3\ 3/4\}. \tag{6.38}$$

According to [Pro95] the corresponding free distances d_f are 17, 12, 7, 4, 3, respectively. These fives free distances constitute the set

$$\mathbb{D}_f = \{d_{f,1}\ d_{f,2}\ d_{f,3}\ d_{f,4}\ d_{f,5}\} = \{17\ 12\ 7\ 4\ 3\}. \tag{6.39}$$

Tab. 6.3: γ_i, $i = 1 \ldots 5$, in dB for voice and data transmission

	$P_{\mathrm{b,des}}$	γ_1	γ_2	γ_3	γ_4	γ_5
voice transmission	10^{-3}	5.1198	5.3831	5.9630	7.1440	7.8818
data transmission	10^{-6}	8.1301	8.3934	8.9733	10.1543	10.8921

Let us assume that the channel qualities in terms of $\gamma_{\mathrm{out}}^{(k,k_{\mathrm{s}})}$, $k = 1 \ldots K$, $k_{\mathrm{s}} = 1 \ldots K_{\mathrm{s}}$, of (6.2) are known at the BS. Based on $\gamma_{\mathrm{out}}^{(k,k_{\mathrm{s}})}$, a channel coding rate $R_{\mathrm{c}}^{(k,k_{\mathrm{s}})}$ should be selected from the elements $R_{\mathrm{c},i}$, $i = 1 \ldots 5$, of the set $\mathbb{R}_{\mathrm{c}}$ of (6.38) in order to achieve the desired coded BER $P_{\mathrm{b,des}}$. Following (4.84) and (4.85), with the given required coded BER $P_{\mathrm{b,des}}$, for each pair $(R_{\mathrm{c},i}, d_{\mathrm{f},i})$, $i = 1 \ldots 5$, of the sets $\mathbb{R}_{\mathrm{c}}$ of (6.38) and $\mathbb{D}_{\mathrm{f}}$ of (6.39) a corresponding γ_i, $i = 1 \ldots 5$, can be determined by

$$\gamma_i \approx -\frac{2 \log_2 M}{d_{\mathrm{f},i} T_{\mathrm{c}} B} \ln(P_{\mathrm{b,des}}), \ \ i = 1 \ldots 5. \tag{6.40}$$

If the channel quality in terms of $\gamma_{\mathrm{out}}^{(k,k_{\mathrm{s}})}$ is below γ_i of (6.40), the required $P_{\mathrm{b,des}}$ cannot be satisfied by utilizing the corresponding channel coding with $(R_{\mathrm{c},i}, d_{\mathrm{f},i})$, $i = 1 \ldots 5$. Suppose that $P_{\mathrm{b,des}}$ in (6.40) for voice and data transmission is 10^{-3} and 10^{-6}, respectively. Then, the required γ_i, $i = 1 \ldots 5$, of (6.40) take the values shown in Tab. 6.3. Now, following Tab. 6.3, the channel coding rate

$$R_{\mathrm{c}}^{(k,k_{\mathrm{s}})} = \begin{cases} 1/4 & \text{if } \gamma_1 \le \gamma_{\mathrm{out}}^{(k,k_{\mathrm{s}})} < \gamma_2, \\ 1/3 & \text{if } \gamma_2 \le \gamma_{\mathrm{out}}^{(k,k_{\mathrm{s}})} < \gamma_3, \\ 1/2 & \text{if } \gamma_3 \le \gamma_{\mathrm{out}}^{(k,k_{\mathrm{s}})} < \gamma_4, \\ 2/3 & \text{if } \gamma_4 \le \gamma_{\mathrm{out}}^{(k,k_{\mathrm{s}})} < \gamma_5, \\ 3/4 & \text{if } \gamma_{\mathrm{out}}^{(k,k_{\mathrm{s}})} \ge \gamma_5 \end{cases} \tag{6.41}$$

can be chosen depending on $\gamma_{\mathrm{out}}^{(k,k_{\mathrm{s}})}$.

6.6.3 Channel coding rate adaptation for multi-channel transmission

The aim of the channel coding rate adaptation in the multi-channel transmission case is to achieve the lowest possible average coded BER $\bar{P}_{\mathrm{b}}^{(k)}$ of (4.86) under the assumption that

$$R_{\mathrm{c}}^{(k)} = \frac{1}{K_{\mathrm{s}}} \sum_{k_{\mathrm{s}}=1}^{K_{\mathrm{s}}} R_{\mathrm{c}}^{(k,k_{\mathrm{s}})}, \ \ k = 1 \ldots K, \tag{6.42}$$

averaged over all K_{s} channel coding rates $R_{\mathrm{c}}^{(k,k_{\mathrm{s}})}$ is kept unchanged. The free distance related to each of the K_{s} channel coding rates $R_{\mathrm{c}}^{(k,k_{\mathrm{s}})}$ of the convolutional encoders is termed $d_{\mathrm{f}}^{(k,k_{\mathrm{s}})}$. In what follows the average channel coding rate $R_{\mathrm{c}}^{(k)}$ of (6.42) is assumed to be $1/2$.

For the sake of illustration, a simple two-channel transmission scheme is considered. The channel quality of each channel is characterized by $\gamma_{\mathrm{out}}^{(k,k_{\mathrm{s}})}$, $k_{\mathrm{s}} = 1$, 2. Furthermore, let us assume that

$$\gamma_{\mathrm{out}}^{(k,1)} \geq \gamma_{\mathrm{out}}^{(k,2)} \tag{6.43}$$

holds. (6.43) means that the channel quality of channel 1 is equal or better than that of channel 2. The channel quality difference between channels 1 and channel 2 can be characterized by

$$\Delta\gamma_{\mathrm{out}} = \gamma_{\mathrm{out}}^{(k,1)} - \gamma_{\mathrm{out}}^{(k,2)}. \tag{6.44}$$

Since the average channel coding rate $R_{\mathrm{c}}^{(k)}$ of (6.42) is $1/2$, with the available five channel coding rates introduced in Section 6.6.2 the possible combinations $(R_{\mathrm{c}}^{(k,1)}, R_{\mathrm{c}}^{(k,2)})$ of the channel coding rates valid for these two transmission channels are $(1/2, 1/2)$, $(2/3, 1/3)$ or $(3/4, 1/4)$. Now, the question is, which of the three combinations should be chosen according to the channel qualities $\gamma_{\mathrm{out}}^{(k,k_{\mathrm{s}})}$, $k_{\mathrm{s}} = 1$, 2, in order to achieve the lowest possible $\bar{P}_{\mathrm{b}}^{(k)}$.

As shown in Section 4.8.2, according to (4.85) and (4.84), the coded BER

$$\bar{P}_{\mathrm{b}}^{(k)} \approx \frac{1}{2}\sum_{k_{\mathrm{s}}=1}^{2} \exp(-R_{\mathrm{c}}^{(k,k_{\mathrm{s}})}\frac{d_{\mathrm{f}}^{(k,k_{\mathrm{s}})}}{2}(\frac{E_{\mathrm{b}}}{N_0})^{(k,k_{\mathrm{s}})}) = \frac{1}{2}\sum_{k_{\mathrm{s}}=1}^{2} \exp(-\frac{d_{\mathrm{f}}^{(k,k_{\mathrm{s}})}}{2}(\frac{T_{\mathrm{c}}B}{\log_2 M})\gamma_{\mathrm{out}}^{(k,k_{\mathrm{s}})}) \tag{6.45}$$

averaged over the two transmission channels 1 and 2 is obtained. Following (6.44) and (6.45), the combination $(R_{\mathrm{c}}^{(k,1)}, R_{\mathrm{c}}^{(k,2)})$ of the channel coding rates valid for the two transmission channels 1 and 2 can be determined to achieve the lowest possible $\bar{P}_{\mathrm{b}}^{(k)}$ at MS μ_k by simulation and is given by

$$(R_{\mathrm{c}}^{(k,1)}, R_{\mathrm{c}}^{(k,2)}) = \begin{cases} (1/2, 1/2) & \text{if } \Delta\gamma_{\mathrm{out}} < 2.434\mathrm{dB}, \\ (2/3, 1/3) & \text{if } 2.434\mathrm{dB} \leq \Delta\gamma_{\mathrm{out}} < 6.020\mathrm{dB}, \\ (3/4, 1/4) & \text{if } 6.020\mathrm{dB} \leq \Delta\gamma_{\mathrm{out}} < 9.046\mathrm{dB}. \end{cases} \tag{6.46}$$

When more than K_{s} equal to two transmission channels are taken into account in the multi-channel transmission scheme, the channel coding rate adaptation can be implemented as follows:

- The channel qualities in terms of $\gamma_{\text{out}}^{(k,k_{\text{s}})}$ are arranged in descending order with respect to their values.

- The simple two-channel transmission scheme introduced above can be formed by the combination of the i-th and the $(K_{\text{s}} - i + 1)$-th transmission channels.

- According to the differences

$$\Delta\gamma_{\text{out}} = \gamma_{\text{out}}^{(k,i)} - \gamma_{\text{out}}^{(k,K_{\text{s}}-i+1)}, \ \ i = 1 \ldots K_{\text{s}}/2, \tag{6.47}$$

of the channel qualities and with (6.46), the combinations $(R_{\text{c}}^{(k,i)}, R_{\text{c}}^{(k,K_{\text{s}}-i+1)})$ of the channel coding rate valid for the i-th and the $(K_{\text{s}} - i + 1)$-th transmission channels can be determined.

Chapter 7

Spectrum efficiency

7.1 Definition of spectrum efficiency

In order to be able to determine how efficient a mobile radio system concept is with respect to economical spectrum utilization and to be able to compare concepts, a performance measure termed spectrum efficiency η is introduced in [Lee89, Ste96, Bla98, Pap00]. η is defined as a ratio of the total available information rate R_{tot} in a single cell of the cellular network to the total available system bandwidth B_{sys}. η is measured in bit/(sHz) and is given by

$$\eta = \frac{R_{\mathrm{tot}}}{B_{\mathrm{sys}}}. \tag{7.1}$$

In what follows, the determination of the spectrum efficiency η of the TD-CDMA downlink considered in this thesis follows [Ste96, Bla98, Pap00].

As shown in Fig. 1.1, the total available system bandwidth B_{sys} is divided into N_{par} partial frequency bands B, see FDMA-feature in Fig. 1.1. With the cluster size r, the number of the available partial frequency band becomes N_{par}/r. According to the TDMA-feature in Fig. 1.1, the frame duration T_{fr} is divided into N_{fr} time slots of duration T_{bu}. Suppose that there are K_{s} burst signals in each partial frequency band B and each time slot. With R being the information rate the total transmission data rate

$$R_{\mathrm{tot}} = RK_{\mathrm{s}}N_{\mathrm{fr}}\frac{N_{\mathrm{par}}}{r} \tag{7.2}$$

per cell is obtained. Then, with

$$N_{\mathrm{par}} = \frac{B_{\mathrm{sys}}}{B} \tag{7.3}$$

and

$$N_{\mathrm{fr}} = \frac{T_{\mathrm{fr}}}{T_{\mathrm{bu}}} \tag{7.4}$$

the spectrum efficiency η of (7.1) takes the form

$$\eta = \frac{K_{\mathrm{s}} R T_{\mathrm{fr}}}{r B T_{\mathrm{bu}}}. \tag{7.5}$$

The spectrum efficiency η of (7.5) depends on K_{s} and r, when R, T_{fr}, T_{bu}, and B are fixed. r should be chosen as small as possible to make η large. However, the smaller r is, the more severe the impact of MAI becomes. The minimal possible value of r is one. By increasing K_{s} the value of η of (7.5) can be made arbitrarily large. However, the larger K_{s} is, the larger the SNR degradation δ of (4.48) becomes when performing JD, see Section 4.4. This means that, in order to maximize η of (7.5), the values of K_{s} and r should be simultaneously taken into account.

A quality of service (QoS) criterion to quantify the performance of mobile radio systems is introduced in [Bla98, Pap00] and is defined in what follows. The QoS criterion is fulfilled if $\bar{P}_{\mathrm{b}}^{(k)}$ of (4.86) valid for MS μ_k, $k = 1 \ldots K$, exceeds a given bound $P_{\mathrm{b}}^{\mathrm{M}}$ with a probability not greater than a given value $P_{\mathrm{o}}^{\mathrm{M}}$. It is obvious that the QoS is determined by the values $P_{\mathrm{b}}^{\mathrm{M}}$ and $P_{\mathrm{o}}^{\mathrm{M}}$, which are typical 10^{-3} and $5 \cdot 10^{-2}$ for the speech system, respectively. For each pair (r, K_{s}), a CDF $\mathrm{Prob}(\bar{P}_{\mathrm{b}}^{(k)} \leq \Gamma)$ holds. Therefore, the outage probability

$$P_{\mathrm{o}}^{(k)} = P_{\mathrm{o}}^{(k)}(\Gamma) = \mathrm{Prob}(\bar{P}_{\mathrm{b}}^{(k)} > \Gamma) = 1 - \mathrm{Prob}(\bar{P}_{\mathrm{b}}^{(k)} \leq \Gamma) \tag{7.6}$$

valid for MS μ_k, $k = 1 \ldots K$, can be defined. The following decision rule is applied [Bla98, Pap00]:

$$\begin{aligned} P_{\mathrm{o}}^{(k)}(P_{\mathrm{b}}^{\mathrm{M}}) > P_{\mathrm{o}}^{\mathrm{M}} : & \quad \text{QoS criterion not fulfilled,} \\ P_{\mathrm{o}}^{(k)}(P_{\mathrm{b}}^{\mathrm{M}}) \leq P_{\mathrm{o}}^{\mathrm{M}} : & \quad \text{QoS criterion fulfilled.} \end{aligned} \tag{7.7}$$

The above described procedure to determine η of (7.5) cannot be performed in closed analytical form [BBS97, Bla98, Pap00]. Therefore, computer simulations are required. In what follows the simulation method to determine η of (7.5) is presented according to [Ste96, Bla98, Pap00]:

- In step 1 the statistic of the interference in terms of the CDF of C/I is investigated on the system level, see Chapter 3.

- Data transmission between BS and MSs in an isolated cell is simulated on the link level in step 2, see Chapter 4. In link level simulations, both the co-channel intercell interference, which is modeled as white Gaussian noise, and the intracell interference are taken into consideration. In this step $\bar{P}_{\mathrm{b}}^{(k)}$ of (4.86) depending on $\gamma_{\mathrm{des}}^{(k)}$ of (4.72) at MS μ_k, $k = 1 \ldots K$, is determined, see Chapter 4.
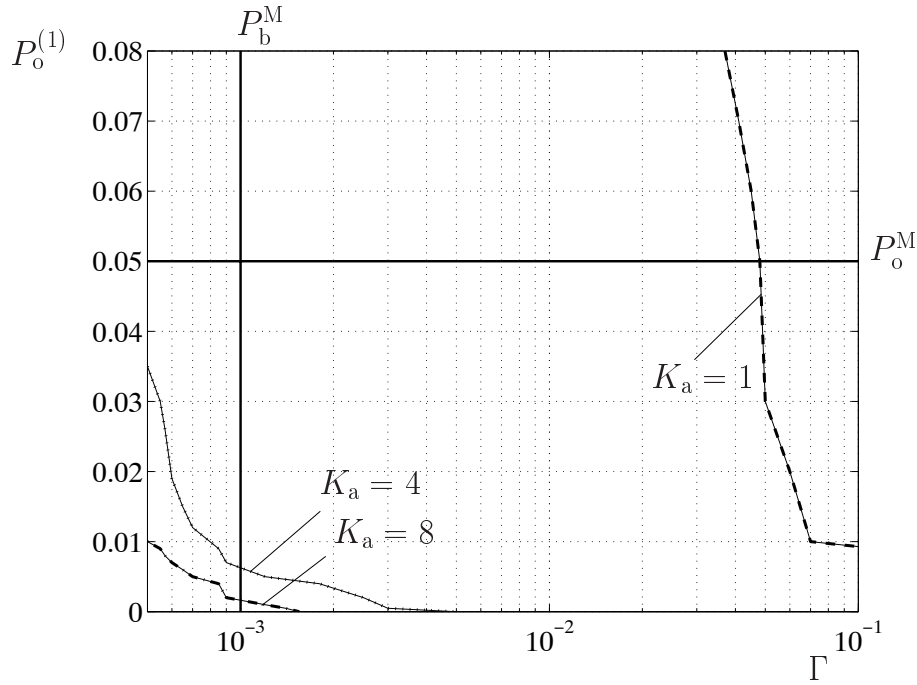
Fig. 7.1: $P_{\mathrm{o}}^{(1)}$ versus Γ, see (7.6); modified 3GPP channel model, $K_{\mathrm{s}} = 16$, $K = 2$, $\beta = 10°$, $\Delta\varphi = 20°$; parameter: K_{a}

- From the CDF of C/I obtained in step 1 and $\bar{P}_{\mathrm{b}}^{(k)}$ of (4.86) versus $\gamma_{\mathrm{des}}^{(k)}$ of (4.72) obtained in step 2, the spectrum efficiency η of (7.5) can be determined.

7.2   Simulation results

In this section the simulation results are presented in terms of the outage probability. The aim of the investigation is to demonstrate the potential of the use of adaptive transmit antennas compared with the use of a single omnidirectional transmit antenna at the BS.

The simulation results for the outage probability $P_{\mathrm{o}}^{(1)}(\Gamma)$ of (7.6) valid for MS μ_1 are shown in Figs. 7.1 and 7.2 for the following simulation parameters:

- modified 3GPP channel model,

- $\beta = 10°$, see Fig. 7.1, and $\beta = 30°$, see Fig. 7.2,

- $K_{\mathrm{s}} = 16$, $K = 2$ and $\Delta\varphi = 20°$.
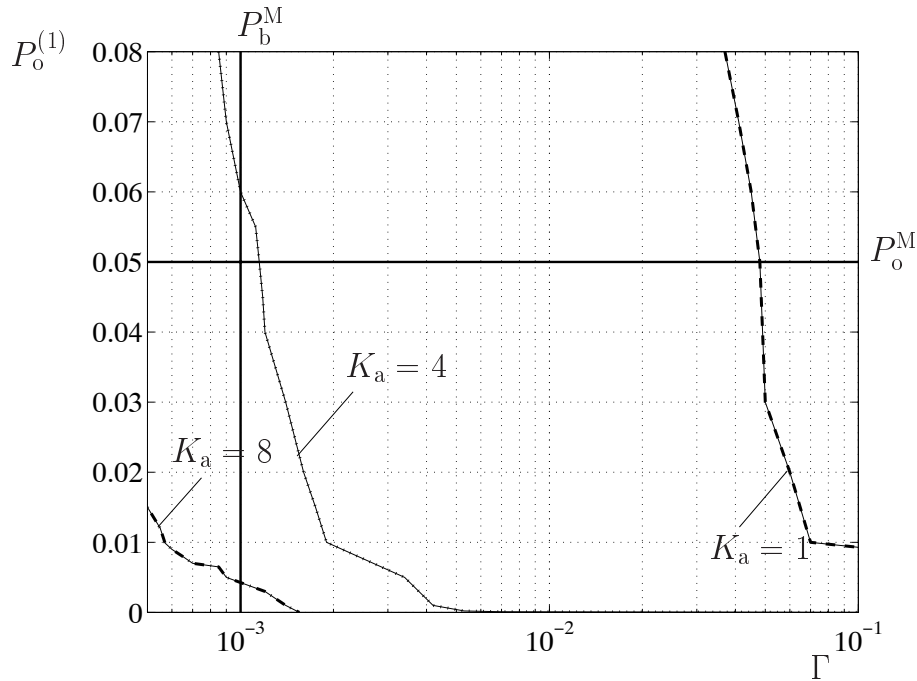
Fig. 7.2: $P_\mathrm{o}^{(1)}$ versus Γ, see (7.6); modified 3GPP channel model, $K_\mathrm{s} = 16$, $K = 2$, $\beta = 30°$, $\Delta\varphi = 20°$; parameters: K_a

As a QoS criterion, P_o^M and P_b^M are chosen to be $5 \cdot 10^{-2}$ and 10^{-3}, respectively. P_o^M and P_b^M are represented by straight lines in Figs. 7.1. and 7.2. The simulation results for $P_\mathrm{o}^{(1)}(\Gamma)$ which fulfill the QoS criterion do not simultaneously mean that the spectrum efficiency η of (7.5) is maximized. From the figures the following results are observed:

- Figs. 7.1 and 7.2 show that the QoS cannot be fulfilled when using a single omnidirectional transmit antenna at the BS.

- Fig. 7.1 shows that the QoS can be fulfilled, if adaptive transmit antennas with $K_\mathrm{a} = 4$ transmit antenna elements is utilized at the BS.

- Fig. 7.2 shows that the QoS can not be fulfilled, even if adaptive transmit antennas with $K_\mathrm{a} = 4$ transmit antenna elements is utilized at the BS.

The results demonstrate the potential of using adaptive transmit antennas in the downlink to improve the spectrum efficiency η of (7.5). Moreover, it is seen that the smaller the angular spread β is, the higher the value of the spectrum efficiency η of (7.5) becomes, when adaptive transmit antennas with the same number K_a of transmit antenna elements are used.

Chapter 8

Summary

8.1 English

TD (Time Division)-CDMA is one of the partial standards adopted by 3GPP (3rd Generation Partnership Project) for 3rd Generation (3G) mobile radio systems. An important issue when designing 3G mobile radio systems is the efficient use of the available frequency spectrum, that is the achievement of a spectrum efficiency as high as possible. It is well known that the spectrum efficiency can be enhanced by utilizing multi-element antennas instead of single-element antennas at the base station (BS). Concerning the uplink of TD-CDMA, the benefits achievable by multi-element BS antennas have been quantitatively studied to a satisfactory extent. However, corresponding studies for the downlink are still missing. This thesis has the goal to make contributions to fill this lack of information. For near-to-reality directional mobile radio scenarios TD-CDMA downlink utilizing multi-element antennas at the BS are investigated both on the system level and on the link level. The system level investigations show how the carrier-to-interference ratio can be improved by applying such antennas. As the result of the link level investigations, which rely on the detection scheme Joint Detection (JD), the improvement of the bit error rate by utilizing multi-element antennas at the BS can be quantified. Concerning the link level of TD-CDMA, a number of improvements are proposed which allow considerable performance enhancement of TD-CDMA downlink in connection with multi-element BS antennas. These improvements include

- the concept of partial joint detection (PJD), in which at each mobile station (MS) only a subset of the arriving CDMA signals including those being of interest to this MS are jointly detected,

- a blind channel estimation algorithm,

- CDMA code pooling, that is assigning more than one CDMA code to certain connections in order to offer these users higher data rates,

- maximizing the Shannon transmission capacity by an interleaving concept termed CDMA code interleaving and by advantageously selecting the assignment of CDMA codes to mobile radio channels,

- specific power control schemes, which tackle the problem of different transmission qualities of the CDMA codes.

As a comprehensive illustration of the advantages achievable by multi-element BS antennas in the TD-CDMA downlink, quantitative results concerning the spectrum efficiency for different numbers of antenna elements at the BS conclude the thesis.

8.2 German

TD (Time Division)-CDMA ist einer der Teilstandards, die von 3GPP (3rd Generation Partnership Project) für Mobilfunksysteme der dritten Generation (3G-Systeme) geschaffen wurden. Ein wichtiger Gesichtspunkt beim Entwurf von 3G-Systemen ist die möglichst effiziente Benutzung der zugeteilten Frequenzbänder, d.h. das Erzielen einer möglichst hohen spektralen Effizienz. Es ist bekannt, daß die spektrale Effizienz dadurch gesteigert werden kann, daß man an den Basisstationen (BS) anstelle von Einelement-Antennen Mehrelement-Antennen verwendet. Für die TD-CDMA-Aufwärtsstrecke gibt es inzwischen befriedigend viele Arbeiten, aus denen der mit solchen Antennen erzielbare Nutzen quantitativ hervorgeht. Für die TD-CDMA-Abwärtsstrecke fehlen allerdings noch entsprechende Untersuchungen. Die vorliegende Arbeit hat das Ziel, Beiträge zum Schließen dieser Kenntnislücke zu leisten. TD-CDMA-Abwärtsstrecken mit Mehrelement-Antennen an der BS werden sowohl auf System- als auch auf Verbindungsebene untersucht. Die Untersuchungen auf Systemebene zeigen, in welchem Maß das Träger-zu-Interferenz-Verhältnis durch solche Antennen verbessert werden kann. Als Ergebnis der Untersuchungen auf Verbindungsebene, die auf der Verwendung des Detektionsschemas Joint Detection (JD) basieren, wird die mit Multielement-Antennen an der BS erzielbare Verringerung der Bitfehlerrate quantitativ beschrieben. Für die Verbindungsebene wird eine Reihe von Verbesserungen vorgeschlagen, die zu erheblichen Performanz-Verbesserungen der TD-CDMA-Abwärtsstrecke in Verbindung mit Multi-Element-Antennen an der BS führen. Diese Verbesserungen umfassen

- Das Konzept Partial Joint Detection (PJD), bei dem an jeder Mobilstation (MS) zum Verringern der JD-typischen Rauscherhöhung nur eine Untermenge der ankommenden CDMA-Signale inklusive der an der betreffenden MS interessierenden Signale gemeinsam detektiert wird.

- Einen Algorithmus zur blinden Kanalschätzung auf der Grundlage eines Unterraumverfahrens.

- CDMA-Code-Pooling, d.h. Zuweisung von mehr als einem einzigen CDMA-Code zu gewissen MSen mit dem Ziel, diesen MSen eine höhere Datenrate zu ermöglichen.

- Maximieren der Shannonschen Kanalkapazität durch eine auf die Zuweisung der CDMA-Codes an die zu übertragenden Datensymbole angewandtes Interleaving-konzept und durch günstige Zuweisung der CDMA-Codes an die entsprechenden Mobilfunkkanäle.

- Spezielle Verfahren der senderseitigen Leistungsregelung, die das Problem der unterschiedlichen CDMA-Code-spezifischen Übertragungsqualitäten mildern.

Als eine gesamtheitliche Veranschaulichung der mit Multi-Element-Antennen an der BS in der TD-CDMA-Abwärtsstrecke erzielbaren Vorteile werden Werte der mit unterschiedlichen Anzahlen von Antennenelementen erzielbaren spektralen Effizienz präsentiert.

Chapter A

List of frequently used acronyms and symbols

A.1 Acronyms

2G	2nd Generation
3G	3rd Generation
3GPP	3G Partnership Project
AWGN	Additive White Gaussian Noise
ATM	Asynchronous Transfer Mode
BER	Bit Error Rate
BS	Base Station
CDF	Cumulative Distribution Function
CDMA	Code Division Multiple Access
COST	European Cooperation in the Field of Scientific and Technical Research
CPC	Centralized Power Control
DFT	Discrete Fourier Transformation
DL	Downlink
DOA	Direction of Arrival
DOD	Direction of Departure
DS	Direct Sequence
ETSI	European Telecommunications Standards Institute
FDD	Frequency Division Duplex
FDMA	Frequency Division Multiple Access
FEC	Forward Error Correction

GPRS	General Packet Radio Service
GSM	Global System for Mobile Communications
HIC	Hybrid Interference Cancellation
IC	Interference Cancellation
IMT-2000	International Mobile Telecommunications 2000
ISI	Intersymbol Interference
ITU	International Telecommunications Union
JD	Joint Detection
LOS	Line of Sight
MAI	Multiple Access Interference
ML	Maximum Likelihood
MLSE	Maximum Likelihood Sequence Estimation
MMSE	Minimum Mean Square Error detector
MS	Mobile Station
MUD	Multi-user Detection
pdf	probability density function
PIC	Parallel Interference Cancellation
QoS	Quality of Service
PJD	Partial Joint Detection
RD	Reference Direction
RL	Reference Line
RP	Reference Point
SA	Scattering Area
SDMA	Space Division Multiple Access
SIC	Successive Interference Cancellation
SNR	Signal-to-Noise Ratio
SNIR	Signal-to-Noise-plus-Interference Ratio
SUD	Single-user Detection
SVD	Singular Value Decomposition
TDD	Time Division Duplex
TDMA	Time Division Multiple Access
UL	Uplink
ULA	Uinform Linear Array
UMTS	Universal Mobile Telecommunications System
URA	Uinform Rectangular Array
UTRA	UMTS Terrestrial Radio Access
UTRAN	UMTS Terrestrial Radio Access Network
WCDMA	Wideband Code Division Multiple Access
ZF–BLE	Zero Forcing Block Linear Equalizer

A.2   Symbols

α	attenuation coefficient
$\alpha^{(k,k_{\mathrm{s}})}$	coefficient assigned to CDMA code $\underline{\mathbf{c}}^{(k_{\mathrm{s}})}$ being the basis for CDMA signal k_{s} undesired at MS μ_k, $k = 1\ldots K$, $k_{\mathrm{s}} = 1\ldots K_{\mathrm{s}}$
$\underline{a}_m$	amplitude of the signal transmitted by BS $\beta_{z(m)}$ to serve MS μ_m, $m = 1\ldots|\mathbb{M}|$
$\underline{a}_{m,k_{\mathrm{a}}}$	amplitude of the weighted signal transmitted by BS $\beta_{z(m)}$ from the k_{a}–th transmit antenna element to MS μ_m, $m = 1\ldots|\mathbb{M}|$, $k_{\mathrm{a}} = 1\ldots K_{\mathrm{a}}$
$a^{(k_{\mathrm{a}})}$	azimuthal angle of the k_{a}–th transmit antenna element related to RP, $k_{\mathrm{a}} = 1\ldots K_{\mathrm{a}}$
$a_q^{(k_{\mathrm{s}})}$	element of $\mathbf{a}^{(k_{\mathrm{s}})}$, $q = 1\ldots Q$, $k_{\mathrm{s}} = 1\ldots K_{\mathrm{s}}$
$\mathbf{a}^{(k_{\mathrm{s}})}$	vector presenting the real binary orthogonal codes of length Q, $k_{\mathrm{s}} = 1\ldots K_{\mathrm{s}}$
$\underline{\mathbf{a}}^{(k,k_{\mathrm{d}})}$	steering vector valid for the k_{d}–th DOD from BS to MS μ_k, $k = 1\ldots K$, $k_{\mathrm{d}} = 1\ldots K_{\mathrm{d}}$
$\underline{\mathbf{A}}^{(k)}$	total system matrix of the considered TDMA burst valid for MS μ_k, $k = 1\ldots K$
$\underline{\mathbf{A}}^{(k,k_{\mathrm{s}})}$	partial system matrix valid for CDMA signal k_{s}, $k_{\mathrm{s}} = 1\ldots K_{\mathrm{s}}$, and MS μ_k, $k = 1\ldots K$
$\underline{\mathbf{A}}_{\mathrm{s}}^{(k)}$	system submatrix containing $\underline{\mathbf{A}}_{\mathrm{s}}^{(k,k_{\mathrm{s}})}$ used for blind channel estimation, $k = 1\ldots K$
$\underline{\mathbf{A}}_{\mathrm{s}}^{(k,k_{\mathrm{s}})}$	partial system submatrix used for blind channel estimation, $k = 1\ldots K$, $k_{\mathrm{s}} = 1\ldots K_{\mathrm{s}}$
β	angular spread, i.e., the angular range around the LOS from the BS to the MS
β_b	the b-th base station considered on the system level, $b = 1\ldots|\mathbb{B}|$
B	width of the partial frequency band
B_{sys}	width of the total available frequency band
$\underline{\mathbf{b}}^{(k,k_{\mathrm{s}})}$	vector presenting the composite channel impulse response valid for CDMA signal k_{s}, $k_{\mathrm{s}} = 1\ldots K_{\mathrm{s}}$, and MS μ_k, $k = 1\ldots K$
$\underline{\hat{\mathbf{b}}}^{(k,k_{\mathrm{s}})}$	vector presenting the estimated composite channel impulse response valid for CDMA signal k_{s}, $k_{\mathrm{s}} = 1\ldots K_{\mathrm{s}}$, and MS μ_k, $k = 1\ldots K$
$\underline{\tilde{\mathbf{b}}}_i^{(k,k_{\mathrm{s}})}$	vector presenting the shifted and clipped versions of $\underline{\mathbf{b}}^{(k,k_{\mathrm{s}})}$ for blind channel estimation, $i = 1\ldots I$, $k_{\mathrm{s}} = 1\ldots K_{\mathrm{s}}$, $k = 1\ldots K$
$|\mathbb{B}|$	number of BSs considered on the system level
$\chi_{b,m}$	logarithmic shadowing factor of the propagation path from BS β_b, $b = 1\ldots|\mathbb{B}|$, to MS μ_m, $m = 1\ldots|\mathbb{M}|$
C	carrier power

C_m	carrier power of the signal transmitted by BS $\beta_{z(m)}$ to serve MS μ_m, $m = 1 \ldots |\mathbb{M}|$
$\underline{\mathbf{c}}^{(k_\mathrm{s})}$	vector with the user specific CDMA code, $k_\mathrm{s} = 1 \ldots K_\mathrm{s}$
$\underline{\mathbf{C}}^{(k_\mathrm{s})}$	matrix containing $\underline{\mathbf{c}}^{(k_\mathrm{s})}$, $k_\mathrm{s} = 1 \ldots K_\mathrm{s}$
$\underline{\tilde{\mathbf{C}}}^{(k_\mathrm{s})}$	matrix containing $\underline{\mathbf{c}}^{(k_\mathrm{s})}$, $k_\mathrm{s} = 1 \ldots K_\mathrm{s}$
$\mathbb{C}$	set containing all available CDMA codes $\underline{\mathbf{c}}^{(k_\mathrm{s})}$, $k_\mathrm{s} = 1 \ldots K_\mathrm{s}$
$\mathbb{C}^{(k)}$	set containing CDMA codes $\underline{\mathbf{c}}^{(k_\mathrm{s})}$ assigned to MS μ_k, $k = 1 \ldots K$
$\overline{\mathbb{C}^{(k)}}$	set containing CDMA codes $\underline{\mathbf{c}}^{(k_\mathrm{s})}$ not assigned to MS μ_k, $k = 1 \ldots K$
δ	approximated SNR degradation
$\delta_i^{(k)}$	SNR degradation valid for the i–th element of $\underline{\mathbf{d}}$, $i = 1 \ldots K_\mathrm{s}N$, at MS μ_k, $k = 1 \ldots K$
$\delta^{(k,k_\mathrm{s})}$	maximal SNR degradation valid for the CDMA signal k_s related to the CDMA code $\underline{\mathbf{c}}^{(k_\mathrm{s})}$, $k_\mathrm{s} = 1 \ldots K_\mathrm{s}$, and received at MS μ_k, $k = 1 \ldots K$
ΔT_m	difference between the adjacent transmit powers contained in vector $\mathbf{t}$
$\Delta T_m'$	modified difference between the adjacent transmit powers contained in vector $\mathbf{t}$
$\Delta \tilde{T}_m$	compression unit
$\Delta \varphi$	angular separation in azimuth between two adjacent MSs
d	distance between BS and MS
d_f	free distance of the convolutional encoder
$d_\mathrm{f}^{(k,k_\mathrm{s})}$	free distance of the convolutional encoder valid for CDMA signal k_s used to serve MS μ_k
$\underline{\mathbf{d}}$	total coded data vector obtained by stacking the K_s coded data vectors $\underline{\mathbf{d}}^{(k_\mathrm{s})}$, $k_\mathrm{s} = 1 \ldots K_\mathrm{s}$.
$\underline{\hat{\mathbf{d}}}$	estimated total coded data vector
$\underline{\mathbf{d}}^{(k_\mathrm{s})}$	partial coded data vector conveyed by means of CDMA code $\underline{\mathbf{c}}^{(k_\mathrm{s})}$, $k_\mathrm{s} = 1 \ldots K_\mathrm{s}$
$\underline{\mathbf{d}}_\mathrm{s}$	subvector used for blind channel estimation
$\mathbb{D}_\mathrm{f}$	set containing the free distances of the corresponding convolutional encoders
η	spectrum efficiency
E_b	average received energy per transmitted bit
$\underline{\mathbf{e}}^{(k)}$	vector presenting the total received signal at MS μ_k, $k = 1 \ldots K$
$\underline{\mathbf{e}}_\mathrm{s}$	subvector used for blind channel estimation
f	frequency
f_c	carrier frequency
$f_\mathrm{D}^{(k,k_\mathrm{e})}$	Doppler frequency of propagation path k_e from the BS to MS μ_k, $k = 1 \ldots K$, $k_\mathrm{e} = 1 \ldots K_\mathrm{e}$
$\gamma^{(k)}$	input SNR at MS μ_k averaged over $\gamma^{(k,k_\mathrm{s})}$, $k = 1 \ldots K$

$\gamma^{(k,k_\mathrm{s})}$	input SNR valid for the CDMA signal k_s associated with CDMA code $\underline{c}^{(k_\mathrm{s})}$, $k_\mathrm{s} = 1 \ldots K_\mathrm{s}$, and received at MS μ_k, $k = 1 \ldots K$
$\gamma^{(k)}_\mathrm{crit}$	critical input SNR at MS μ_k, $k = 1 \ldots K$
$\gamma^{(k)}_\mathrm{des}$	input SNR averaged over $K^{(k)}_\mathrm{s}$ CDMA signals received at MS μ_k and being of interest to MS μ_k, $k = 1 \ldots K$
γ_m	C/I valid for MS μ_m, $m = 1 \ldots |\mathbb{M}|$
$\gamma^{(k)}_\mathrm{out}$	output SNR at MS μ_k averaged over $\gamma^{(k,k_\mathrm{s})}_\mathrm{out}$, $k = 1 \ldots K$
$\gamma^{(k,k_\mathrm{s})}_\mathrm{out}$	output SNR valid for CDMA signal k_s, $k_\mathrm{s} = 1 \ldots K_\mathrm{s}$, received at MS μ_k and being of interest to MS μ_k, $k = 1 \ldots K$
$g_{b,m}$	propagation gain for the propagation path from BS β_b to MS μ_m, $b = 1 \ldots |\mathbb{B}|$, $m = 1 \ldots |\mathbb{M}|$
g_{k_s}	gain related to CDMA signal k_s for power control purpose, $k_\mathrm{s} = 1 \ldots K_\mathrm{s}$
$g_{\mathrm{mod},z(m),m}$	modified propagation gain for the propagation path from BS $\beta_{z(m)}$ to MS μ_m, $m = 1 \ldots |\mathbb{M}|$
$g_{\mathrm{mod},z(\tilde{m}),m}$	modified propagation gain for the propagation path from BS $\beta_{z(\tilde{m})}$ to MS μ_m, $\tilde{m} = 1 \ldots |\mathbb{M}|$, $m = 1 \ldots |\mathbb{M}|$
$h_\mathrm{d}^{(k,k_\mathrm{e})}(\tau, t, \varphi)$	non-bandlimited directional channel impulse response corresponding to the k_e–th propagation path from the BS to MS μ_k, $k = 1 \ldots K$, $k_\mathrm{e} = 1 \ldots K_\mathrm{e}$
$\underline{h}^{(k,k_\mathrm{s})}$	vector presenting the signal specific channel impulse response between the input port k_s and the single output port of the network shown in Fig. 4.5, $k = 1 \ldots K$, $k_\mathrm{s} = 1 \ldots K_\mathrm{s}$
$\hat{\underline{h}}^{(k,k_\mathrm{s})}$	vector presenting the estimated signal specific channel impulse response between the input port k_s and the single output port of the network shown in Fig. 4.5, $k = 1 \ldots K$, $k_\mathrm{s} = 1 \ldots K_\mathrm{s}$
$\underline{h}_\mathrm{a}^{(k,k_\mathrm{a})}$	vector presenting the antenna element specific channel impulse response between the input of the k_a–th transmit antenna element and the output of the receive antenna at MS μ_k, $k = 1 \ldots K$, $k_\mathrm{a} = 1 \ldots K_\mathrm{a}$
$\underline{h}_\mathrm{d}^{(k,k_\mathrm{d})}$	vector presenting the directional channel impulse response corresponding to the k_d–th DOD from the BS to MS μ_k shown in Fig. 4.5, $k = 1 \ldots K$, $k_\mathrm{d} = 1 \ldots K_\mathrm{d}$
$\underline{H}_\mathrm{a}^{(k)}$	antenna element specific channel impulse matrix related to MS μ_k, $k = 1 \ldots K$
$\tilde{\underline{H}}^{(k,k_\mathrm{s})}$	channel impulse response matrix containing $\underline{h}^{(k,k_\mathrm{s})}$, $k = 1 \ldots K$, $k_\mathrm{s} = 1 \ldots K_\mathrm{s}$
I	interference power
I_m	cumulative interference power at MS μ_m, $m = 1 \ldots |\mathbb{M}|$
$\mathbf{I}^{(M \times M)}$	$M \times M$ identity matrix

$\mathbb{I}_m$	set containing all MSs $\mu_{\tilde{m}}$, $\tilde{m} = 1 \ldots |\mathbb{M}|$, with $\beta_{z(\tilde{m})}$ being an interfering BS for MS μ_m, $m = 1 \ldots |\mathbb{M}|$
j	imaginary unit
K	number of MSs active in a time slot
$\bar{K}$	average number of MSs active per cell in a time slot
K_{a}	number of transmit antenna elements at the BS
K_{d}	number of DODs
K_{e}	number of scattering points considered to generate directional channel models
K_{s}	total number of CDMA codes
$K_{\mathrm{s}}^{(k)}$	number of CDMA codes assigned to MS μ_k when applying CDMA code pooling, $k = 1 \ldots K$
$\tilde{K}_{\mathrm{s}}^{(k)}$	number of CDMA signals included in the PJD process at MS μ_k, $k = 1 \ldots K$
λ	wavelength
Λ	diagonal matrix containing the reciprocal values of $1/\gamma$
l	inter-element distance of ULA of K_{a} transmit antenna elements
l_{a}	number of propagation paths introduced in non-directional 3GPP channel model
$l^{(k_{\mathrm{a}})}$	distance between the k_{a}–th transmit antenna element to the RP, $k_{\mathrm{a}} = 1 \ldots K_{\mathrm{a}}$
L_{g}	dimension of the guard interval of a time slot
L_{m}	dimension of the midamble section of a time slot
$\mathcal{L}_m(\cdot)$	acyclic left shift operator
μ	Lagrange factor
μ_k	the k-th MS used on the link level, $k = 1 \ldots K$
μ_m	the m-th MS used on the system level, $m = 1 \ldots |\mathbb{M}|$
M	size of the data symbol alphabet
$|\mathbb{M}|$	number of MSs considered on the system level
$\underline{\mathbf{M}}^{(k)}$	matrix determined by $\underline{\mathbf{A}}^{(k)}$ and $\underline{\mathbf{R}}_{\mathrm{n}}^{(k)}$, $k = 1 \ldots K$
N	number of symbols per data block in a time slot
$N^{(k)}$	normalized effective noise plus interference power at the receiver input of MS μ_k, $k = 1 \ldots K$
$N^{(k)'}$	effective noise plus interference power at the receiver input of MS μ_k, $k = 1 \ldots K$
N_0	spectrum density of the additive white Gauschen distributed noise
N_{fr}	number of time slots per TDMA frame
$N_{\mathrm{in}}^{(k)}$	noise plus interference power at the receiver input of MS μ_k, $k = 1 \ldots K$
N_{par}	number of partial frequency bands

$\underline{\mathbf{n}}^{(k)}$	vector presenting intercell interference plus thermal noise at MS μ_k, $k = 1 \ldots K$
$\underline{\mathbf{n}}_{\text{out}}^{(k,k_{\text{s}})}$	output intercell MAI vector valid for CDMA signal k_{s}, $k_{\text{s}} = 1 \ldots K_{\text{s}}$ at MS μ_k, $k = 1 \ldots K$
$\underline{\mathbf{n}}_{\text{out}}^{(k)}$	output intercell MAI vector at MS μ_k, $k = 1 \ldots K$
$\underline{\mathbf{n}}_{\text{s}}^{(k)}$	subvector used for blind channel estimation, $k = 1 \ldots K$
Ω	angular domain
$P_{\text{b,des}}$	desired coded BER used to determine the channel coding rate
$P_{\text{b}}^{(k,k_{\text{s}})}$	coded BER valid for CDMA signal k_{s} related to CDMA code $\underline{\mathbf{c}}^{(k_{\text{s}})}$, $k_{\text{s}} = 1 \ldots K_{\text{s}}$, received at MS μ_k, $k = 1 \ldots K$
$\bar{P}_{\text{b}}^{(k)}$	coded BER averaged over all $K_{\text{s}}^{(k)}$ CDMA signals being of interest to MS μ_k, $k = 1 \ldots K$
$P_{\text{o}}^{(k)}$	outage probability valid for MS μ_k, $k = 1 \ldots K$
P_{b}^{M}	upper bound for the coded BER
P_{o}^{M}	maximal allowable outage probability
$\psi_{z(m),\tilde{m},k_{\text{a}}}$	phase advance between the signal transmitted from the k_{a}–th transmit antenna element and the signal transmitted from a fictitious transmit antenna element at the RP at BS $z(m)$ to MS μ_m, $m = 1 \ldots |\mathbb{M}|$
Q	dimension of CDMA code $\underline{\mathbf{c}}^{(k_{\text{s}})}$, $k_{\text{s}} = 1 \ldots K_{\text{s}}$
$\rho_{b,m}$	geometrical length of the propagation path from BS β_{b} to MS μ_m, $b = 1 \ldots |\mathbb{B}|$, $m = 1 \ldots |\mathbb{M}|$
r	cluster size
$r_1^{(k,k_{\text{e}})}$	distance between BS and the k_{e}–th scattering point, $k = 1 \ldots K$, $k_{\text{e}} = 1 \ldots K_{\text{e}}$
$r_2^{(k,k_{\text{e}})}$	distance between MS μ_k and the k_{e}–th scattering point, $k = 1 \ldots K$, $k_{\text{e}} = 1 \ldots K_{\text{e}}$
$r^{(k)}$	ratio of the average energies of the composite channel impulse responses related to the CDMA signals not being of and being of interest to MS μ_k, $k = 1 \ldots K$, which is termed signal separation ratio
$R^{(k)}$	total channel capacity observed at MS μ_k, $k = 1 \ldots K$
$R^{(k,k_{\text{s}})}$	energy of $\underline{\mathbf{b}}^{(k,k_{\text{s}})}$ observed at the receiver input at MS μ_k, $k = 1 \ldots K$
$R^{(k_{\text{s}})}$	channel capacity of the k_{s}–th channel, $k_{\text{s}} = 1 \ldots K_{\text{s}}$
R_{c}	channel coding rate
$R_{\text{c}}^{(k)}$	channel coding rate averaged over $R_{\text{c}}^{(k,k_{\text{s}})}$ valid for MS μ_k, $k = 1 \ldots K$
$R_{\text{c}}^{(k,k_{\text{s}})}$	channel coding rate of the convolutional encoder valid for CDMA signal k_{s} used to serve MS μ_k, $k = 1 \ldots K$
$R_{z(m),\tilde{m}}$	power of the signal transmitted by BS $\beta_{z(m)}$ and received at MS $\mu_{\tilde{m}}$, $m = 1 \ldots |\mathbb{M}|$, $\tilde{m} = 1 \ldots |\mathbb{M}|$
R_{tot}	total available information rate per cell

$\underline{\mathbf{R}}_{\mathrm{a}}^{(k)}$	covariance matrix of $\underline{\mathbf{A}}_{\mathrm{s}}^{(k)}$, $k = 1 \ldots K$
$\underline{\mathbf{R}}_{\mathrm{d}}$	covariance matrix of $\underline{\mathbf{d}}$
$\underline{\mathbf{R}}_{\mathrm{e}}^{(k)}$	covariance matrix of $\underline{\mathbf{e}}^{(k)}$, $k = 1 \ldots K$
$\underline{\mathbf{R}}_{\mathrm{n}}^{(k)}$	covariance matrix of $\underline{\mathbf{n}}^{(k)}$, $k = 1 \ldots K$
$\mathbb{R}_{\mathrm{c}}$	set containing the channel coding rates of the corresponding convolutional encoders
$\mathcal{R}_m(\cdot)$	acyclic right shift operator
$\sigma^{(k)^2}$	intercell interference plus thermal noise power, which is assumed to be equal for all elements of $\underline{\mathbf{n}}^{(k)}$, $k = 1 \ldots K$
τ	delay parameter
t	time
$\mathbf{t}$	vector containing the transmit powers for all MSs $\mu_m, m = 1 \ldots |\mathbb{M}|$
$\mathbf{t}'$	vector containing the constraint transmit powers for all MSs $\mu_m, m = 1 \ldots |\mathbb{M}|$
$T^{(k_{\mathrm{s}})}$	power transmitted by the BS due to feeding CDMA signal k_{s} related to CDMA code $\underline{\mathbf{c}}^{(k_{\mathrm{s}})}$ into port k_{s} of the network shown in Fig. 4.5, $k_{\mathrm{s}} = 1 \ldots K_{\mathrm{s}}$
$T^{(k)}$	total transmit power of the CDMA signals used to serve MS μ_k, $k = 1 \ldots K$
$T_0^{(k)}$	total transmit power of the CDMA signals used to serve MS μ_k, if a single omnidirectional transmit antenna is utilized at the BS, $k = 1 \ldots K$
$T_0^{(k_{\mathrm{s}})}$	transmit power associated with CDMA code $\underline{\mathbf{c}}^{(k_{\mathrm{s}})}$ used to generate the corresponding CDMA signal k_{s} to serve a certain MS μ_k, if a single omnidirectional transmit antenna is utilized at the BS, $k_{\mathrm{s}} = 1 \ldots K_{\mathrm{s}}$
T_{bu}	duration of a time slot
T_{c}	chip duration
T_{fr}	duration of a TDMA frame
T_{g}	duration of the guard interval
T_{m}	power of the signal transmitted from the K_{a}–th transmit antenna element at BS $\beta_{z(m)}$ to serve MS μ_m, $m = 1 \ldots |\mathbb{M}|$
$T_{\max}$	maximum bound of the transmit powers of $\mathbf{t}'$
$T_{\min}$	minimum bound of the transmit powers of $\mathbf{t}'$
$\tilde{T}_{\max}$	maximum bound of the transmit powers of $\mathbf{t}$
$\tilde{T}_{\min}$	minimum bound of the transmit powers of $\mathbf{t}$
T_{s}	symbol duration
$\underline{\mathbf{u}}_{\mathrm{n},s}$	the s–th column of matrix $\underline{\mathbf{U}}_{\mathrm{n}}^{(k)}$
$\underline{\mathbf{U}}_{\mathrm{n}}^{(k)}$	matrix used for blind channel estimation, $k = 1 \ldots K$
$\varphi^{(k)}$	azimuthal angle presenting the LOS between the BS and MS μ_k on the link level, $k = 1 \ldots K$

$\varphi_{\mathrm{e}}^{(k,k_{\mathrm{e}})}$	azimuthal angle between the x–axis and the k_{e}–th propagation path at BS, $k = 1 \ldots K$, $k_{\mathrm{e}} = 1 \ldots K_{\mathrm{e}}$
$\varphi_{\mathrm{s}}^{(k,k_{\mathrm{e}})}$	azimuthal angle between the x–axis and the k_{e}–th propagation path at MS μ_k, $k = 1 \ldots K$, $k_{\mathrm{e}} = 1 \ldots K_{\mathrm{e}}$
$\varphi_{\mathrm{v}}^{(k)}$	azimuthal angle presenting move direction of MS μ_k, $k = 1 \ldots K$
$\varphi_{z(m),\tilde{m}}$	azimuthal angle presenting the LOS from BS $\beta_{z(m)}$ to MS $\mu_{\tilde{m}}$ on the system level, $m = 1 \ldots |\mathbb{M}|$, $\tilde{m} = 1 \ldots |\mathbb{M}|$
$\mathbf{V}$	matrix containing the modified propagation gains $g_{\mathrm{mod},z(m),m}$ of the carrier
$\underline{\mathbf{w}}^{(k_{\mathrm{s}})}$	antenna weight vector associated with CDMA code $\underline{\mathbf{c}}^{(k_{\mathrm{s}})}$ used on the link level, $k_{\mathrm{s}} = 1 \ldots K_{\mathrm{s}}$
$\underline{\mathbf{w}}_{b,m}$	antenna weight vector for MS μ_m served by BS β_b used on the system level, $b = 1 \ldots |\mathbb{B}|$, $m = 1 \ldots |\mathbb{M}|$
W	length of signal specific channel impulse response $\underline{\mathbf{h}}^{(k,k_{\mathrm{s}})}$
$\mathbf{W}$	matrix containing the modified propagation gains $g_{\mathrm{mod},z(\tilde{m}),m}$ of the interferers
$\xi_{b,m}$	log-normal distributed random variable, $b = 1 \ldots |\mathbb{B}|$, $m = 1 \ldots |\mathbb{M}|$
$y(k_{\mathrm{s}})$	relation which uniquely assigns CDMA code $\underline{\mathbf{c}}^{(k_{\mathrm{s}})}$ to MS $\mu_{y(k_{\mathrm{s}})}$, $k_{\mathrm{s}} = 1 \ldots K_{\mathrm{s}}$
$z(m)$	relation which uniquely assigns MS μ_m to BS $\beta_{z(m)}$, $m = 1 \ldots |\mathbb{M}|$

Bibliography

[3G99]   3GPP, "About the Trird Generation Partnership Project (3GPP)", published in the Internet under the URL http://www.3gpp.org, 1999.

[AC99]   U. Amin, S. Chennakeshu: The evolution of TDMA to 3G. *IEEE Personal Communications*, vol. 6, 1999, pp. 6–7.

[AMVW91] S. Anderson, M. Millnert, M. Viberg, B. Wahlberg: An adaptive array for mobile radio communication systems. *IEEE Transactions on Vehicular Technology*, vol. 40, 1991, pp. 230–236.

[BA94]   M. Barrett, R. Arnott: Adaptive antennas for mobile communications. *Electron. Commun. Eng. J.*, vol. 6, 1994, pp. 203–214.

[BBNS94]   P.W. Baier, J.J. Blanz, M.M. Naßan, A. Steil: Realistic simulations of a CDMA mobile radio system using joint detection and coherent receiver antenna diversity. *Proc. IEE Colloquium on Spread Spectrum Techniques for Radio Communication Systems*, London, 1994, pp. 1/1–1/5.

[BBS97]   P.W. Baier, J.J. Blanz, R. Schmalenberger: Fundamentals of smart antennas for mobile radio applications. S.G. Glisic, P.A. Leppänen (Hrsg.): *Wireless Communications, TDMA versus CDMA*. pp. 345–376. Boston: Kluwer Academic Publishers, 1997.

[BKNS94]   J.J. Blanz, A. Klein, M.M. Naßhan, A. Steil: Performance of a cellular hybrid C/TDMA mobile radio system applying joint detection and coherent receiver antenna diversity. *IEEE Journal on Selected Areas in Communications*, vol. 12, 1994, pp. 568–579.

[Bla98]   J.J. Blanz: *Empfangsantennendiversität in CDMA-Mobilfunksystemen mit gemeinsamer Detektion der Teilnehmersignale*. Fortschrittberichte VDI, Reihe 10, Nr. 535. Düsseldorf: VDI-Verlag, 1998.

[BN99]   R.M. Buehrer, S.P. Nicoloso: Comments on partial interference cancellation on CDMA. *IEEE Transactions on Communications*, vol. 47, 1999, pp. 658–661.

[BS80]   I.N. Bronstein, K.A. Semendjajew: *Taschenbuch der Mathemathik*. Moskau: Nauka, 1980.

[BS92a]   P. Balaban, J. Salz: Optimum diversity combining and equlization in digital data transmission with application to cellular mobile radio – Part I: theoretical considerations. *IEEE Transactions on Communications*, vol. 40, 1992, pp. 885–894.

[BS92b]   P. Balaban, J. Salz: Optimum diversity combining and equlization in digital
           data transmission with application to cellular mobile radio – Part II: nu-
           merical results. *IEEE Transactions on Communications*, vol. 40, 1992, pp.
           895–907.

[BSP97]   J.J. Blanz, R. Schmalenberger, A. Papathanassiou: Smart antenna concepts
           for time-slotted CDMA. *Proc. IEEE 47th Vehicular Technology Conference
           (VTC'97)*, Phoenix, 1997, pp. 11–15.

[BWW99]   P.W. Baier, T. Weber, M. Weckerle: Spreading techniques, a far-reaching
           technology. Francis Swarts, Pieter van Rooyan, Ian Oppermann, Michiel P.
           Lötter (Hrsg.): *CDMA-Techniques for Third Generation Mobile Systems*.
           Kap. 1, pp. 1–22. Boston: Kluwer Academic Publishers, 1999.

[CCG79]   J.B. Cain, G.C. Clark, J.M. Geist: Punctured convolutional codes of rate
           $(N-1)/N$ and simplified maximum likelihood decoding. *IEEE Transactions
           on Information Theory*, vol. IT-24, 1979, pp. 97–100.

[COS89]   *COST 207*. Digital land mobile radio communications, Office for Official
           Publications of the European Communities, Luxembourg, 1989.

[Dep88]   Ed. F. Deprettere: *SVD and signal processing: Algorithms, Application and
           Architectures*. Amsterdam: North-Holland, 1988.

[DGE92]   P. Dent, B. Gudmundson, M. Ewerbring: A novel code division multiple
           access scheme based on inteference cancellation. *Proc. IEEE 3rd Interna-
           tional Symposium on Personal, Indoor and Mobile Radio Communications
           (PIMRC'92)*, Boston, 1992, pp. 411–415.

[DSR98]   D. Disalar, M.K. Simon, D. Raphaeli: Improved parallel interference can-
           cellation for CDMA. *IEEE Transactions on Communications*, vol. 46, 1998,
           pp. 258–268.

[FCB93]   J. Fernandez, I.R. Corden, M. Barrett: An adaptive array for mobile radio
           communication systems. *Proc. Inst. Elect. Eng. Int. Conf. Antennas Propa-
           gation*, Edinburgh, 1993, pp. 983–986.

[Fis97]   R. Fischer: *Mehrkanal- und Mehrträgerverfahren für die schnelle digitale
           Übertragung im Ortsanschlußleitungsnetz*. Aachen: Shaker, 1997.

[Fri96]   B. Friedrichs: *Kanalcodierung: Grundlagen und Anwendungen in modernen
           Kommunikationssystemen*. Berlin: Springer-Verlag, 1996.

[Fuh97]   J. Fuhl: *Smart antennas for second and third generation mobile radio com-
           munications systems*. Technical University of Vienna: PhD Dissertation,
           1997.

[GC81]   L.C. Godara, A. Cantoni: Uniqueness and linear independence of steering
           vectors in array space. *IEEE J. Acoust. Soc. Amer.*, vol. 70, 1981, pp. 467–
           475.

[GF97]   J. Goldberg, J.R. Fonollosa: Downlink beamforming for cellular mobile com-
           munications. *Proc. IEEE 47th Vehicular Technology Conference (VTC'97)*,
           Phoenix, 1997, pp. 632–636.

[God97a]   L.C. Godara: Applications of antenna arrays to mobile communications,
            Part I: performance improvement, feasibility, and system considerations.
            IEEE Proceedings, vol. 85, 1997, pp. 1032–1060.

[God97b]   L.C. Godara: Applications of antenna arrays to mobile communications,
            Part II: beam-forming and direction-of-arrival considerations.   *IEEE Pro-
            ceedings*, vol. 85, 1997, pp. 1195–1245.

[GVGZ94]   S.A. Grandhi, R. Vijavan, D.J. Goodman, J. Zander: Distributed power
            control in cellular radio systems.   *Proc. IEEE 44th Vehicular Technology
            Conference (VTC'94)*, Stockholm, 1994, pp. 824–828.

[Haa00]   M. Haart: Radio interface concepts for UTRA TDD. *Proc. IEEE 9th Inter-
            national Symposium on Personal, Indoor and Mobile Radio Communications
            (PIMRC2000)*, London, 2000, pp. 1210–1215.

[Hag88]   J. Hagenauer: Rate-compatible punctured convolutional codes (RCPC
            codes) and their applications.   *IEEE Transactions on Communications*,
            vol. 36, 1988, pp. 389–400.

[HWB00]   J.F. Huber, D. Weiler, H. Brand: UMTS, the mobile multimedia vision
            for IMT-2000: A focus on standardization. *IEEE Communications*, vol. 38,
            2000, pp. 129–136.

[IK96]   N. Ishi, R. Kohno: Spatially and temporally joint transmitter-reciever using
            an adaptive array antenna. *IEICE Transactions on Communications*, vol.
            E79-B, 1996, pp. 361–367.

[ITU98]   *The ETSI UMTS Terrestrial Radio Access (URTA) ITU-R RTT Candidate
            Submission.* http://www.itu.int, 1998.

[KA98]   H.R. Karimi, N.W. Anderson: A novel efficient solution to block-based joint-
            detection using approximate Cholesky factorization. *Proc. IEEE 9th Inter-
            national Symposium on Personal, Indoor and Mobile Radio Communications
            (PIMRC'98)*, vol. 3, Boston, 1998, pp. 1340–1345.

[KA00]   D. Koulakiotis, A.H. Aghvami: Data detection techniques for DS/CDMA
            mobile systems: A review. *IEEE Personal Communications*, vol. June, 2000,
            pp. 24–34.

[KB93]   A. Klein, P.W. Baier: Linear unbiased data estimation in mobile radio sys-
            tems applying CDMA. *IEEE Journal on Selected Areas in Communications*,
            vol. 11, 1993, pp. 1058–1066.

[KKB93]   A. Klein, K. Kaleh, P.W. Baier: Zero forcing and minimum mean square
            error equalization for multi-user detection in code division multiple access.
            IEEE Transactions on Vehicular Technology, vol. 35, 1993, pp. 461–468.

[KKB94]   A. Klein, K. Kaleh, P.W. Baier: Equalizers for multi-user detection in code
            division multiple access mobile radio systems. *Proc. IEEE 44th Vehicular
            Technology Conference (VTC'94)*, vol. 2, Stockholm, 1994, pp. 762–766.

[KKB96]   A. Klein, K.G. Kawas, P.W. Baier: Zero forcing and minimum mean-square-
            error equalization for multiuser detection in code-division multiple-access
            channels. *IEEE Transactions on Vehicular Technology*, vol. 45, 1996, pp.
            276–287.

[Kle96]   A. Klein: *Multi-user detection of CDMA signals – algorithms and their application to cellular mobile radio.* Fortschrittberichte VDI, Reihe 10, Nr. 423. Düsseldorf: VDI-Verlag, 1996.

[KMT⁻96]   A. Klein, W. Mohr, R. Thomas, P. Weber, B. Wirth: Direction-of-arrival of partial waves in wideband mobile radio channels for intelligent antenna concepts. *Proc. IEEE 46th Vehicular Technology Conference (VTC'96)*, Atlanta, 1996, pp. 849–853.

[Koh94]   R. Kohno: Spatial and temporal filtering for co-channel interference in CDMA. *Proc. IEEE 2th International Symposium on Spread Spectrum Techniques & Applications (ISSSTA'94)*, Oulu, 1994, pp. 51–60.

[LB00a]   Y. Lu, P.W. Baier: Adaptive antennas for the TD-CDMA downlink under special consideration of high data rate services. *Proc. IEEE 9th International Symposium on Personal, Indoor and Mobile Radio Communications (PIMRC2000)*, London, 2000, pp. 55–61.

[LB00b]   Y. Lu, P.W. Baier: Performance of adaptive antennas for the TD-CDMA downlink under special consideration of multi-directional channels and CDMA code pooling. *AEÜ International Journal of Electronics and Communications*, vol. 54, 2000, pp. 249–258.

[LCL99]   Y.C. Liang, F.P.S. Chin, K.J.R. Liu: Downlink beamforming for DS-CDMA mobile radio with multimedia services. *Proc. IEEE 49th Vehicular Technology Conference (VTC'99)*, Amsterdam, 1999, pp. 632–636.

[Lee89]   W.C.Y. Lee: *Mobile cellular telecommunications systems.* New York: McGraw-Hill, 1989.

[LR99]   J.C. Liberti, T.S. Rappaport: *Smart antennas for wireless communications.* Englewood Cliffs, NJ: Prentice-Hall, 1999.

[May99]   J. Mayer: *Signalisierungsprotokolle und Verkehrskapazität eines Mobilfunksystems der dritten Generation.* Fortschrittberichte VDI, Reihe 10. Düsseldorf: VDI-Verlag, 1999.

[MDCM95]   E. Moulines, P. Duhamel, J. Cardoso, S. Mayrargue: Subspace methods for blind identification of multichannel FIR filters. *IEEE Transactions on Signal Processing*, vol. 43, 1995, pp. 516–525.

[Min88]   H. Minc: *nonnegative matrices.* New York: John Wiley & Sons, 1988.

[MM80]   R.A. Monzingo, W.T. Miller: *Introduction to adaptive arrays.* New York: Wiley & Sons, Inc., 1980.

[MO94]   M. Mizuno, T. Ohgane: Application of adaptive array antennas to radio communications. *Electron. Commun. Japan*, vol. 77, 1994, pp. 48–59.

[MS99]   M. Meurer, R. Schmalenberger: System level modeling and simulation of mobile radio scenarios including terminal mobility. *Proc. IEEE 9th International Symposium on Personal, Indoor and Mobile Radio Communications (PIMRC'99)*, Osaka, 1999, pp. 332–336.

[Naß95]   M.M. Naßhan: *Realitätsnahe Modellierung und Simulation nachrichten-
            technischer Systeme, gezeigt am Beispiel eines CDMA-Mobilfunksystems.*
            Fortschrittberichte VDI, Reihe 10, Nr. 384. Düsseldorf: VDI-Verlag, 1995.

[NPK94]   A. Naguib, A. Paulraj, T. Kailath: Capacity improvement with base-station
            antenna arrays in cellular CDMA. *IEEE Transactions on Vehicular Techno-
            logy*, vol. 43, 1994, pp. 691–698.

[Ost01]   J. Oster: *Ein Beitrag zur Interzellinterferenzreduktion in zeitgeschlitzten
            CDMA-Systemen.* Universität Kaiserslautern: PhD Dissertation, 2001.

[Pap00]   A. Papathanassiou: *Adaptive antennas for mibile radio systems using Time
            Division CDMA and joint detection.* Forschungsberichte Mobilecommunika-
            tion Band 6, Nr. 386. Universität Kaiserslautern: 2000.

[PFBB99]   A. Papathanassiou, I. Furio, J.J. Blanz, P.W. Baier: Smart antennas with
            two-dimensional array configurations for performance enhancement of a joint
            detection CDMA mobile radio system. *Wireless Personal Communications*,
            vol. 11, 1999, pp. 89–108.

[PH93]   P. Putel, J.M. Holtzman: Analysis of a DS/CDMA successive interference
            cancellation scheme using correlations. *IEEE GLOBECOM'93*, Huston, TX,
            1993, pp. 76–80.

[PH94a]   P. Putel, J.M. Holtzman: Analysis of simple successive interference cancel-
            lation scheme in a DS/CDMA system. *IEEE Journal on Selected Areas in
            Communications*, vol. 12, 1994, pp. 796–807.

[PH94b]   P. Putel, J.M. Holtzman: Performance comparison of a DS/CDMA sys-
            tem using successive interference cancellation (IC) scheme and a parallel IC
            scheme under fading. New Orleans, 1994, pp. 510–514.

[Pro95]   J.G. Proakis: *Digital Communications.* 3. Auflage. New York: McGraw-Hill,
            1995.

[PV97]   H.V. Poor, S. Verdu: Probability of error in MMSE multiuser detection.
            IEEE Transactions on Information Theory, vol. 43, 1997, pp. 858–871.

[RB98]   P.B. Rapajic, D.K. Borah: An adaptive maximum likelihood receiver for
            asynchronous CDMA systems. *Proc. IEEE 5th International Symposium on
            Spread Spectrum Techniques & Applications (ISSSTA'98)*, Sun City, South
            Africa, 1998, pp. 671–675.

[SB97]   R. Schmalenberger, J.J. Blanz: Multi antenna C/I balancing in the downlink
            of digital cellular mobile radio systems. *Proc. IEEE 47th Vehicular Techno-
            logy Conference (VTC'97)*, Phoenix, 1997, pp. 607–611.

[SBEM90]   S.C. Swales, M.A. Beach, D.J. Edwards, J.P. McGeeham: The performance
            enhancement of multibeam adaptive base-station antennas for cellular land
            mobile radio systems. *IEEE Transactions on Vehicular Technology*, vol. 39,
            1990, pp. 56–67.

[Sch01]   R. Schmalenberger: *Modell und Simulation der Abwärtsstrecke eines CDMA
            Mobilfunksystems mit gemeinsamer Detektion der Teilnehmersignale und
            adaptiven Sendeantennen.* Forschungsberichte Mobilecommunikation Band
            7, Nr. 386. Universität Kaiserslautern: 2001.

[SOY⁻99] Y.R. Senhaji, H. Okada, T. Yamazato, M. Katayama, A. Ogawa: Perfor-
mance improvements applying an adaptive array antenna at both base and
mobile stations in celluar CDMA. *Proc. IEEE 9th International Symposium
on Personal, Indoor and Mobile Radio Communications (PIMRC'99)*, Osaka,
1999, pp. 982–986.

[Ste95] B. Steiner: *Ein Beitrag zur Mobilfunk-Kanalschätzung unter besonderer
Berücksichtigung synchroner CDMA-Mobilfunksysteme mit Joint Detection.*
Fortschrittberichte VDI, Reihe 10, Nr. 337. Düsseldorf: VDI-Verlag, 1995.

[Ste96] A. Steil: *Spektrale Effizienz digitaler CDMA–Mobilfunksysteme mit gemein-
samer Detektion.* Fortschrittberichte VDI, Reihe 10, Nr. 437. Düsseldorf:
VDI-Verlag, 1996.

[Ste98] G.W. Stewart: *Matrix algorithms Volume I: Basic Decompositions.* Philadel-
phia: Society for industrial and applied mathematics, 1998.

[Sun98] S. Sun: A hybrid interference cancellation in CDMA. *Proc. IEEE 5th
International Symposium on Spread Spectrum Techniques & Applications
(ISSSTA'98)*, Sun City, 1998, pp. 150–154.

[THGM99] J.S. Thompson, J.E. Hudson, P.M. Grant, B. Mulgrew: CDMA downlink
beamforming for frequency selective channels. *Proc. IEEE 9th Interna-
tional Symposium on Personal, Indoor and Mobile Radio Communications
(PIMRC'99)*, Osaka, 1999, pp. 233–237.

[TP98] L. Tong, S. Perreau: Multichannel blind identification: From subspace to
maximum Likelihood methods. *Proceeding of the IEEE*, vol. 86, 1998, pp.
1951–1968.

[VA90] M.K. Varanasi, B. Aazhang: Multistage detection in asnchronous code-
division multiple-access communications. *IEEE Transactions on Communi-
cations*, vol. 38, 1990, pp. 509–519.

[Ver86] S. Verdu: Minimum probability of error for asynchronous gaussian multiple-
access channels. *IEEE transactions on Information Theory*, vol. 32, 1986,
pp. 85–96.

[Vit90] A.J. Viterbi: Very low convolution codes for maximun theoretical perfor-
mance of spread-spectrum multiple-access channels. *IEEE Journal on Se-
lected Areas in Communications*, vol. 8, 1990, pp. 641–649.

[WBOW00] T. Weber, P.W. Baier, J. Oster, M. Weckerle: Performance enhancement
of Time Division CDMA TD-CDMA systems by Multi-Step joint detection.
Proc. 7th International Conference on Telecommunications (ICT2000), Aca-
pulco, 2000, pp. 1038–1044.

[Web00] T. Weber: *Signalverarbeitungskonzepte für Mobilfunksysteme der
dritten Generation, gezeigt am Beispiel eines JD-CDMA-Mobilfunksystems.*
Forschungsberichte Mobilecommunikation Band 4, Nr. 386. Universität
Kaiserslautern: 2000.

[Wha71] A.D. Whalen: *Detection of Signals in Noise.* New York: Academic Press,
1971.

[Win84]   J.H. Winters: Optimum combining in digital mobile radio with co-channel in-
            terference. *IEEE Journal on Selected Areas in Communications*, vol. SAC-2,
            1984, pp. 528–539.

[WOWB01]   T. Weber, J. Oster, M. Weckerle, P.W. Baier: Turbo multiuser detection for
            TD-CDMA. *Accepted for publication in Archiv für Elektronik und Übertra-
            gungstechnik AEÜ*, 2001.

[Yas83]   Y. Yasuda: Development of variable-rate Viterbi decoder and its performance
            characteristics. *Proc. 6th Int. Conf. Digit. Satellite Commun.*, Phoenix, 1983,
            pp. XII–24–XII–31.

[YKH84]   Y. Yasuda, K. Kashiki, Y. Hirata: High rate punctured convolutional codes
            for soft decision Viterbi decoding. *IEEE Transactions on Communications*,
            vol. COM-32, 1984, pp. 315–319.

[YKI93]   Y.C. Yoon, R. Kohno, H. Imai: A spread-spectrum multiaccess system
            with cochannel interference cancellation for multipath fading channels. *IEEE
            Journal on Selected Areas in Communications*, vol. 11, 1993, pp. 1067–1075.

[Zet86]   P. Zetterberg: A comparison of two systems for downlink communication
            with base station antenna arrays. *IEEE Transactions on Vehicular Techno-
            logy*, vol. 48, 1986, pp. 1356–1370.

[ZF84]   R. Zurmühl, S. Falk: *Matrizen und ihre Anwendungen (Teil I: Grundlagen)*.
            Berlin Heidelberg New York Tokyo: Springer-Verlag, 1984.

[ZO95]   P. Zetterberg, B. Ottersten: The spectrum efficiency of a base station an-
            tenna array system for spatially selective transmission. *IEEE Transactions
            on Vehicular Technology*, vol. 44, 1995, pp. 651–660.

Tabellarischer Lebenslauf

Name: Yang Lu
Adresse: Trippstadter–Straße 121
                               67663 Kaiserslautern
Geburtsdatum: 27. Januar 1968
Familienstand: verheiratet
Staatsangehörigkeit: Chinesisch

Schulausbildung: September 1974 – Juni 1979 Grundschule in Shanghai
                               September 1979 – Juni 1984 Gymnasium in Shanghai
Hochschulaufnahmenprüfung: Juli 1984

1. Studium: September 1984 – Juli 1988
                               Studium der Elektrotechnik
                               an der Eisenbahn Universität Shanghai
Studienabschluß: Bachelor

2. Studium: Oktober 1994 – März 1999
                               Studium der Elektrotechnik/Nachrichtentechnik
                               an der Universität Kaiserslautern
Studienabschluß: Diplom

Berufstätigkeit: August 1988 – Februar 1994
                               Elektronikingenieur beim Shanghai Eisenbahn Büro

                               seit April 1999
                               wissenschaftlicher Mitarbeiter
                               am Lehrstuhl für hochfrequente Signalübertragung
                               und –verarbeitung der Universität Kaiserslautern